

Université du Québec
Institut National de la Recherche Scientifique
Énergie, Matériaux et Télécommunications

**INVESTIGATIONS ON SEMICONDUCTOR MATERIAL SYNTHESIS
AND ON MORPHOLOGY MANIPULATION TOWARDS HIGH
EFFICIENCY AND STABLE SOLAR TECHNOLOGIES**

Par
Long Tan

Thèse présentée pour l'obtention du grade de
Philosophiae doctor (Ph.D.)
en sciences de l'énergie et des matériaux

Jury d'évaluation

Président du jury et examineur interne	Ana Tavares INRS-EMT
Examineur externe	Clara Santato École Polytechnique de Montréal
Examineur externe	Armand Soldera Université de Sherbrooke
Directeur de recherche	Dongling Ma INRS-EMT
Codirecteur de recherche	Mohamed Chaker INRS-EMT

ABSTRACT

Solar cells, which harvest renewable solar energy via the photovoltaic (PV) effect, have been considered as one of the cleanest and most promising technologies to address the press energy crisis and environmental issues. In order to make solar cells the feasible and best replacement of fossil fuels, the concept of the third-generation PV devices based on inorganic nanomaterials, dye molecules, conjugated polymers and perovskite materials was proposed to largely decrease the cost of the solar cell devices, at the same time maintaining comparable or even achieving higher power conversion efficiency (PCE) compared to that of the existing ones. Additionally, luminescent solar concentrators (LSCs), which convert a wide range of photons into concentrated light in a specific range, are another potential approach to achieve these goals by reducing the use of expensive PV materials. In principle, the development of both PV and LSC devices depends on the material chemistry and device engineering, which are the two main directions to optimise the performance of these solar technologies. In this thesis, the work performed focuses on the synthesis of near infrared (NIR) absorbing quantum dots (QDs), their characterizations, and solar-related applications, as well as morphology optimisation of the photoactive film of polymer solar cells (PSCs), leading to enhanced PCE and stabilities.

In the first part, we successfully synthesized high-quality NIR PbS QDs in very small sizes using PbCl_2 and elemental sulfur (S) as lead and sulfur precursor, respectively, by introducing tributylphosphine (TBP) into the reaction. This route is much “greener” and facile as compared to the glove-box-involved method using toxic bis(trimethylsilyl)sulfide as sulfur precursor. Afterwards, the synthesis mechanism of very small QDs and their optical properties, morphology, dispersity, surface properties and LSC application were systematically investigated. In detail, this work can be divided into three sections (I-III): two sections are related to the PbS QDs synthesis, and the last section is about LSC application based on these synthesized QDs.

In section I, the S-oleylamine (OLA) solution was mixed with different contents of TBP prior to its injection into the pre-heated PbCl_2 -OLA solution. For the TBP-free reaction, the shortest absorption wavelength of synthesized PbS QDs was limited to ~ 1056 nm. With increasing the TBP content to $40 \mu\text{L}$, the first-excitonic absorption peak of obtained PbS QDs was gradually blue-shifted to ~ 705 nm, due to the decreased QD size. Further increasing the contents of TBP,

no QDs could be collected. The key factor leading to the blue-shifted first-excitonic absorption peak and final disappearance of QDs with increasing TBP content is the formation of strong bond between S and TBP. The S-TBP could have participated into the QD growth process, which prevented the QDs further growing to larger size with TBP as a type of rigid ligands on the surface. However, the stable S-TBP itself was not able to start the nucleation reaction with the lead precursor, then failed to form the QD once the S-OLA concentration was below a critical point. In addition to decreasing the size of QDs, as extra ligands located at the S sites on the QD surface (rather than on the Pb site as OLA ligands), TBP could change the QD surface composition, morphology and dispersity, and benefit its optical properties. In brief, TBP-assisted synthesis of PbS QDs shows narrow QD size distributions without any QD aggregation and demonstrates high photoluminescent quantum yield (PL QY) in the range of 60–90%, depending on the QD size. All of these results underline that this route is convenient for synthesis of high-quality PbS QDs in very small sizes.

Different from that of section I, a two-step injection synthesis is introduced in section II. For instance, large amounts of TBP were first injected into the preheated lead precursor, followed by the sulfur precursor solution. Based on this synthesis, the first-excitonic peak of the PbS QDs can be largely extended to ~780 nm (corresponding to diameter ~2.5 nm) as compared to that of the TBP-free reaction. The resulted PbS QDs show excellent dispersity without any aggregation and high PL QY around 80%. Moreover, the TBP chemical was revealed to assist the transformation of $\text{PbCl}_2\text{-OLA}$ into more reactive Pb(OH)Cl , that can directly participate into the nucleation process, yielding ultrasmall PbS QDs. It indicates that Pb(OH)Cl can be potentially applied for synthesis of other lead-based small size QDs as a new precursor.

In section III, LSC devices using PbS and PbS/CdS QDs as the phosphor were fabricated, respectively, and their performance of concentrating the wide range of photons into a specific range of light was also tested. The high performance is mainly attributed to their high PL QY, wide separation of absorption and PL spectrum and good photo-stability. Clearly, ultrasmall PbS QDs are promising for LSC application. More specifically, the LSC device showed optical efficiency around 1.2% at a geometric factor of 50 (10 cm in length) by using the 2.5 nm QDs with a 0.1 nm CdS shell, which is record-high compared to other QD-based LSCs. The devices using pure PbS QDs and PbS/CdS QDs with thick shell were also fabricated and tested, and all

of them showed promising results. Over all, these results confirmed the high quality of our synthesized QDs via TBP involved synthetic route, which is promising for large-area LSCs application and has high potential for other NIR-related applications.

In the second part, we focused on improving the air-stability of the PSCs using the blend of Poly(3-hexylthiophene-2,5-diyl) (P3HT) and phenyl-C₆₁-butyric acid methyl ester (PCBM) as the research system. To do so, the inorganic NIR QDs were selected as a stabilizer, which extended the photoresponse of the device to the NIR range in the same time. Considering the energy level alignment of P3HT and PCBM, PbS QDs sample with an average diameter of ~3.3 nm was preferred, which can facilitate the charge transfer processes in the device. Moreover, further surface treatments of QDs were performed before applying them for PV application. First, a thin CdS shell (0.1 nm) on the surface of PbS QDs was formed by cation-exchange reaction. It can significantly improve the air-stability of QDs as well as their thermo- and photo-stability, without blocking charge carrier transport. Second, large amounts of insulating, long-chain oleic acid ligands (OA⁻) on the QD surface were replaced by short inorganic Cl⁻ via metal halide treatment. The atomic Cl⁻ ligands can form a dense “ligand shell” on the surface and reach the mid-gap trap states, which can’t be achieved by the long-chain ligands, due to the “steric effect”. Therefore, the QD stability can be further enhanced and the density of trap states can be effectively reduced, which makes these ligand-exchanged QDs suitable for PV application. It is worth mentioning that the surface ligand manipulation also affected the morphology of the P3HT:PCBM:QDs film, which played a significant role in device stability. As evidenced by the images obtained from atomic force microscopy (AFM) measurements, the QDs with Cl⁻ ligands formed continuous QD-networks in the P3HT:PCBM film, whereas QDs without Cl⁻ ligands were homogeneously distributed in the film. Importantly, PSCs device based on the film with the unusual QD-networks showed excellent long-term stability under relative high humidity air (50-60%), while accomplishing over 3% of PCE simultaneously. After 30 days storage without any encapsulation, around 91% of the pristine PCE can be retained. It was a remarkable improvement as compared to that of the devices based on pure P3HT:PCBM film (~53%). We verified that such improvement was attributed to the prevention of PCBM aggregation and oxidation of the thiophene ring in P3HT. Furthermore, the presence of QD-networks efficiently improved the thermal stability of the device as well by suppressing the thermal stress/oxidation under relative high humidity air. Around 60% of pristine PCE was retained after 12 h thermal treatment at

85 °C, which was more than twice higher than that of the device without QD networks. To the best of our knowledge, this work represents the first unambiguous demonstration of the formation of QD networks in the photoactive layer and of their important contribution to stability of PSCs. This strategy is highly promising for other fullerene based PSCs, and opens a new avenue towards achieving PSCs with high PCE and excellent stability.

The third part was focused on morphology manipulation of the P3HT:PCBM blend, in order to improve the PCE of the PSCs. The key point is to control the mobility of the film components in the fabrication process. To do so, butylamine was introduced as an additive into the P3HT:PCBM solution with dichlorobenzene as the solvent. It was confirmed that PCBM has a higher solubility than P3HT in butylamine. As a result of different solubilities, the addition of butylamine improved the accumulation of P3HT and PCBM at the top and bottom of the blend film, respectively, leading to a P3HT-enriched top surface and buried abundance of PCBM as evidenced by the results from AFM and X-ray photoelectron spectroscopy characterizations. Then, solar cell devices with the configuration of ITO/ZnO/P3HT:PCBM/MoO₃/Ag were fabricated to evaluate the effect of resulted morphology change by butylamine on the performance of device. The butylamine affected device showed largely enhanced fill factor (FF: ~70%) and PCE (~4.03%) compared to the standard device, which can be attributed to the improved charge transport in the P3HT:PCBM film and enhanced electrode selectivity. The formation of such morphology offers a possibility to further optimize the thickness of the active layer in order to absorb more light, without prohibiting charge transport. In other words, it is possible to further enhance the PCE by increasing the short-circuit current (J_{sc}) without significantly sacrificing the FF, if the same preferable bicontinuous interpenetrating morphology can also be achieved in a thicker film. Therefore, we further fabricated devices based on thicker P3HT:PCBM film by doubling the concentration of precursor solution. The results from the current-voltage measurement indicate that FF of ~63% was obtained for the butylamine involved device, which is even higher than that of the standard device based on relatively thin film. In the same time, the J_{sc} was also largely enhanced due to the increased thickness of the active layer, leading to a high PCE of 4.61%, among the best efficiencies of P3HT:PCBM-based devices. Over all, these results well confirmed that butylamine as an additive can effectively improve the performance of P3HT:PCBM device. Besides, it has the advantages of free of malodorousness

and halogen ions compared to commonly applied alkane dithiols and halogen additives, which makes it promising for the use in large scale fabrication of PSCs in the future.

ACKNOWLEDGEMENTS

First, I would like to express my deeply gratitude to my supervisor Prof. Dongling Ma for offering me a precious opportunity to perform my Ph.D. study in INRS-EMT and for her continuous support. Her invaluable advices and immense knowledge helped me in all the time of carrying out my research work, writing of paper and completing my thesis. I learned a lot from her, and I believe what I have learned will continue to help me in my future career.

I also would like to extend my sincerely appreciation to my co-supervisor Prof. Mohamed Chaker for his constant support during my Ph.D. study. His kindness, invaluable suggestions and motivations helped me a lot in my research work. I benefitted greatly from the discussions with him.

I am grateful to Prof. Ricardo Izquierdo for kindly allowing me to work in his laboratory, Prof. Federico Rosei for letting me collaborate with his group members, and the contributions from Prof. Joëlle Margot.

It is my pleasure to acknowledge the assistance of Dr. Haiguang Zhao, Dr. Shun Li and Dr. Gaixia Zhang during my Ph.D. study. I learned a lot from them with respect to the scientific research and handling troubles in my daily life.

I thank Christophe Chabanier at INRS-EMT, Alexandre Robichaud and Gwenaëlle Chamoulaud at UQAM for giving me training and their patience in helping me using the instruments. I would like to thank Jean-Philippe Masse at Ecole Polytechnique and Alexandre Arnold at UQAM for carrying out the TEM and NMR measurement, respectively.

I would like to say thanks to the departmental and technical staff at INRS-EMT.

I would like to thank the present and previous group members in Prof. Ma's group for their help throughout the work. These people include Dr. Mee Rahn Kim, Dr. Fuqiang Ren, Dr. Jiujun Deng, Fan Yang, Deepak Thrithamarassery Gangadharan, Qingzhe Zhang, Yanlong Liu, Pandeng Li, Shengyun Huang, Dr. Hongyang Liang and Dr. Guozhu Chen. They altogether created hardworking and inspiring group, and I am grateful to be part of this group. I am grateful to Mohamed Cherif for his help in the French translation.

Contents

CHAPTER 1	INTRODUCTION	1
1.1	Basic theory of solar cells	2
1.2	Overview of solar cell development.....	3
1.3	Classification of the third generation solar cells	5
1.3.1	Dye-sensitized solar cells (DSSCs)	5
1.3.2	Quantum dot solar cells (QDSCs).....	6
1.3.3	Perovskite solar cells (PVSCs)	8
1.3.4	Polymer solar cells (PSCs).....	10
1.3.5	Hybrid solar cells (HySCs).....	11
1.4	Luminescent solar concentrators (LSCs)	12
1.5	Thesis Objectives and Organization.....	13
1.5.1	Objectives	13
1.5.2	Thesis Organization	14
CHAPTER 2	LITERATURE REVIEW ON SYNTHESIS AND SURFACE ENGINEERING OF NIR QDS, AND MORPHOLOGY MANIPULATION OF ACTIVE LAYER OF PSCs	16
2.1	Introduction	16
2.2	QD synthesis via hot-injection method	17
2.3	Stabilities Related to Near-Infrared Quantum Dot-Based Solar Cells: The Role of Surface Engineering	20
2.4	Morphology control of the active layer of PSCs.....	59
CHAPTER 3	EXPERIMENTAL.....	65
3.1	Chemicals and Materials	65
3.2	PbS QD Synthesis	65
3.2.1	One-step injection of TBP route	65

3.2.2	Two-step injection of TBP route.....	66
3.2.3	TMS route	66
3.3	PbS/CdS QD Synthesis	66
3.3.1	PbS/CdS QD synthesis by microwave-assisted method.....	67
3.3.2	PbS/CdS QD synthesis by oil-bath method	67
3.3.3	Metal halide treatment	67
3.4	Device Fabrication	68
3.4.1	Fabrication of LSC devices.....	68
3.4.2	Fabrication of solar cell devices	68
3.5	QD concentration calculation.....	69
3.6	Characterizations.....	70
CHAPTER 4	RESULTS	72
4.1	Ultrasmlal PbS Quantum Dots: A Facile and Greener Synthetic Route and Their High Performance in Luminescent Solar Concentrators.....	72
4.2	Enhanced Long-term and Thermal Stability of Polymer Solar Cells in Air at High Humidity with the Formation of Unusual Quantum Dot Networks.....	107
4.3	Towards Enhancing Solar Cell Performance: An Effective and “Green” Additive	139
CHAPTER 5	CONCLUSIONS AND PERSPECTIVES.....	154
5.1	Conclusions	154
5.2	Perspectives.....	156
Reference	159
RÉSUMÉ	170

LIST OF FIGURES

Figure 1.1 Cumulative PV capacity in megawatts globally and trend of the price change of a solar panel per watt from 1975 to 2015.[2]

Figure 1.2 (a) The equivalent circuit of a solar cell and (b) the typical I-V curve of a silicon solar cell. (The graphs were taken from internet: https://en.wikipedia.org/wiki/Theory_of_solar_cells and <http://www.alternative-energy-tutorials.com/energy-articles/solar-cell-i-v-characteristic.html>)

Figure 1.3 Evolution of record PCE values of different generations of solar cells since 1976, retrieved from <https://www.nrel.gov/pv/assets/images/efficiency-chart.png>.

Figure 1.4 Schematic diagram of a dye sensitized solar cell.[14]

Figure 1.5 TEM images of (a) optimized nanowire network device, and (b) a planar device.[35]

Figure 1.6 Figure 1.6 The perovskite crystal structure with the general form ABX_3 , in which A^+ is confined within a cage determined by the octahedral coordination of B^{2+} with X^- anions. The sizes of the spheres are given by the ionic radii of $CH_3NH_3^+$, Pb^{2+} , and I^- . The most common cations and anions that have been used in each position within the 3D halide perovskites are listed.[39]

Figure 1.7 Conventional (a) and inverted (b) structure of polymer solar cells.

Figure 1.8 Energy levels of PbS QDs according to their diameter and LUMO/HOMO values of conjugated polymers widely used as electron donors in polymer BHJ solar cells. PBDTTT-CF is poly[4,8-bis-substitutedbenzo [1,2-b:4,5-b0]dithiophene-2,6-diyl-alt-4-substituted-thieno [3,4-b]thiophene-2,6-diyl], PCDTBT is poly[N-90-hepta-decanyl-2,7-carbazole-alt-5,5-(40,70-di-2-thienyl-20,10,30-benzothiadiazole)], and PBSDTBT is poly[9,9-dioctyl-2,7-dibenzosilole-co-alt-5,5-(40,70-di-2-thienyl-20,10,30-benzothiadiazole)].[47]

Figure 1.9 Configuration of the LSC device, retrieved from <https://www.spie.org/>.

Figure 2.1 (a) Absorption spectra spanning the range of the tunable sizes.[74] (b) Absorption and photoluminescence spectra of ultras-small PbS QDs dispersed in tetrachloroethylene.[29] (c) Typical absorbance spectra of PbS QD suspensions. Full lines are QDs synthesized with TOP, dotted lines without TOP.[21]

Figure 2.2 The normalized S 2p XPS spectra of the air surface and the buried interface in the photoactive layers prepared in a) DCB:OT and b) DCB. All spectra were normalized to the C 1s intensity. c) Schematic morphologies of the P3HT:PCBM films prepared in DCB and DCB:OT, as reconstructed from the results of the SIMS, TEMT, and XPS investigations. The purple lines are P3HT nanocrystals and the yellow circles are pure PCBM phases.[77]

Figure 2.3 AFM topography (left) and phase (right) images for RR-P3HT:PCBM films fabricated using different processing conditions. The spin-coating times are (a,b) 30 s and (c,d) 80 s. (e) Effect of solvent annealing on the absorption and PL spectra of RR-P3HT:PCBM films with 4:1 and 1:2 weight ratios of the components. (f) J - V characteristics of RR-P3HT:PCBM (4:1 squares, 2:1 circles, and 1:2 triangles) solar cells with (solid symbols, 30 s) and without (hollow symbols, 80 s) solvent annealing. The differences in device performance become more pronounced for higher PCBM loading fractions.[85]

Figure 2.4 Optical microscopy images of P3HT:PCBM matrix. Blend ratio was varied from 1:1 to 1:4. Annealing time was kept constant at 5 min at temperatures of 125, 150, and 175 °C.[93]

Figure 2.5 (a) Relationship between boiling point, difference in solubility parameter and device PCE of the different additive systems. 15 × 15 mm scanning transmission X-ray microscopy (STXM) images taken at 285 eV for P3HT:PC₆₁BM blends processed with: (a) NDT and (b) HDT.[96]

Figure 3.1 Scheme illustration of QD synthesis.[99]

Figure 3.2 Scheme illustration of CdS-shell coating

Figure 3.3 Scheme illustration of ligand-exchange.

Figure 3.4 ITO substrate pattern and process of PSC devices fabrication.

LIST OF CHEMICAL COMPOUNDS, ABBREVIATIONS AND SYMBOLS

Chemical Compounds

Ag	silver
Al	aluminum
C	carbon
CdS	cadmium sulfide
CdO	cadmium oxide
CH ₃ OCH ₂ CH ₂ OH	2-methoxyethanol
MoO ₃	molybdenum oxide
N ₂	nitrogen gas
NH ₂ CH ₂ CH ₂ OH	ethanolamine
PbCl ₂	lead (II) chloride
Pb(OAc) ₂ ·3H ₂ O	lead acetate trihydrate
Pb(OH)Cl	laurionite
PbS	lead sulfide
S	sulfur
ZnO	zinc oxide
Zn(CH ₃ COO) ₂ ·2H ₂ O	zinc acetate dehydrate

Abbreviations

AFM	atomic force microscopy
D	dimensional
D/A	donor/acceptor
DSSC(s)	dye sensitized solar cell(s)
EDS	energy dispersive X-ray spectroscopy
EQE	external quantum efficiency
FF	fill factor
FTIR	Fourier transform infrared spectroscopy
FWHM	full width at half maximum
G	geometric
HOMO	highest occupied molecular orbital
HR TEM	high resolution transmission electron microscopy
ICP-AES	Inductively coupled plasma/atomic emission spectrometry
IQE	internal quantum efficiency
ITO	indium tin oxide
J-V	current-voltage
LSC(s)	luminescence solar concentrator(s)
NIR	near infrared
NMR	nuclear magnetic resonance
OA	oleic acid
ODE	1-octadecene

OLA	oleylamine
PCBM	phenyl-C61-butyric acid methyl ester
PCE	power conversion efficiency
PEDOT:PSS	poly(3,4-ethylenedioxythiophene):polystyrene sulfonate
PL	photoluminescence
PSC(s)	polymer solar cell(s)
PVSC(s)	perovskite solar cell(s)
PV	photovoltaic
P3HT	poly (3-hexylthiophene)
QD(s)	quantum dot(s)
QDSC(s)	quantum dot solar cell(s)
QY	quantum yield
RMS	root-mean-square roughness
TBP	tributylphosphine
TMS	bis(trimethylsilyl) sulfide
TOP	trioctylphosphine
UV	ultraviolet
Vis	visible
VPS	vertical phase segregation
XPS	X-ray photoelectron spectroscopy
XRD	X-ray diffraction

Symbols

μ	micro
J_{sc}	short circuit current
V_{oc}	open circuit voltage
R_{sh}	shunt resistance
R_s	series resistance
Ω	Ohm
η_{opt}	optical efficiency
η_{quan}	quantum efficiency
θ	diffraction angle
λ	wave length
K_{rad}	radiative recombination rates
K_{nr}	nonradiative recombination rates
I_{sc}	short circuit photocurrent from the Si diode coupled with a LSC
I_{LSC}	short circuit photocurrent from the Si diode under AM 1.5G
T_g	glass transition temperature
I_{sc}^{Abs}	short circuit photocurrent from the Si diode under the illumination of light absorbed by quantum dots

LIST OF PUBLICATIONS AND CONFERENCE CONTRIBUTIONS

Journal Publications

- 1) **L. Tan**, *P. Li, R. Izquierdo et al.* Towards enhancing solar cell performance: an effective and “green” additive. Submitted.
- 2) **L. Tan**, *F. Yang, M. R. Kim et al.* Enhanced long-term and thermal stability of polymer solar cells in air at high humidity with the formation of unusual quantum dot networks. *ACS Appl. Mater. Interfaces*, 2017, **9**, 26257–26267.
- 3) **L. Tan**, *Y. Zhou, F. Ren, D. Benetti et al.* Ultrasmall PbS quantum dots: a facile and greener synthetic route and their high performance in luminescent solar concentrators. *J. Mater. Chem. A*, 2017, **5**, 10250–10260.
- 4) **L. Tan**, *P. Li, B. Sun et al.* Stabilities related to near infrared quantum dot-based solar cells: the role of surface engineering. *ACS Energy Lett.*, 2017, **2**, 1573–1585.
- 5) **L. Tan**, *P. Li, B. Sun et al.* Development of photovoltaic devices based on near infrared quantum dots and conjugated polymers. *ChemNanoMat*, 2016, **2**, 601–615.
- 6) *F. Ren, S. A. Lindley, H. Zhao, L. Tan et al.* Towards understanding unusual photoluminescence intensity variation of ultrasmall colloidal PbS quantum dots with the formation of thin CdS shell. *Phys. Chem. Chem. Phys.*, 2016, **18**, 31828–31835.
- 7) *M. R. Kim, H. A. Hafez, X. Chai, L. V. Besteiro, L. Tan et al.* Covellite CuS nanocrystals: realizing rapid microwave-assisted synthesis in air and unraveling the disappearance of their plasmon resonance after coupling with carbon nanotubes. *Nanoscale*, 2016, **8**, 12946–12957.
- 8) *X. Tong, H. Liang, Y. Liu, L. Tan et al.* Anisotropic optical properties of oriented silver nanorice and nanocarrot in stretched polymer films. *Nanoscale*, 2015, **7**, 8858–8863.

Conference Presentations

1) Long Tan, Fuqiang Ren, Mohamed Chaker and Dongling Ma, A facile route towards synthesizing ultra-small near infrared quantum dots, Centre québécois sur les matériaux fonctionnels (CQMF)/Centre for Self-Assembled Chemical Structures (CSACS). 1100, rue Notre-Dame Ouest, Montréal(Québec), May 3-4, 2016. (*Poster Presentation*)

2) Long Tan, Haiguang Zhao, Yufeng Zhou, Daniele Benetti, Fuqiang Ren, Fan Yang, Federic Rosei, Mohamed Chaker and Dongling Ma, Investigations on greener route synthesized small near infrared quantum dots in application of luminescent solar concentrator, Centre Québécois sur les Matériaux Fonctionnels (CQMF). 1100, rue Notre-Dame Ouest, Montréal(Québec), November 24-25, 2016. (*Poster Presentation*)

CHAPTER 1 INTRODUCTION

Nowadays, human being has become more and more dependent on electricity that makes our life convenient and comfortable. As a consequence, the electricity consumption in the world has increased rapidly. For instance, an increment of 60.9% (13,174 to 21,191 TeraWatt Hour) from the year 2000 to 2016 was reported.[1] However, the electricity generation is mainly relying on the use of fossil fuels such as coal, natural gas, *etc.* In addition to finite reserves, burning of fossil fuels is associated with the emission of CO₂ and SO₂ into the atmosphere, resulting in global warming and acid rain. Therefore, it is emergent to develop clean and sustainable resources as alternative. Among various types of renewable energy sources (such as solar energy, wind, biomass, geo-electric *etc.*), the solar energy with advantages of infinite abundance and easy utilization is most attractive. In addition to being commonly used in human being's life everywhere for heating, drying and so on, for a long history, the solar energy becomes a popular energy source for end-use electricity conversion by a designed device, called a solar cell. It represents one of the most effective, cheap, clean and renewable ways to supply the electricity in the future, which has attracted many attentions in research and real applications. For decades, the electricity supply from solar energy conversion is gradually growing year by year as evidenced by increased solar panel installations (Figure 1.1). On the other hand, the cost of photovoltaics (PV) electricity dramatically decreased from \$101.5 per watt in 1975 to \$0.61 in 2015.[2] However, more work should be devoted to improve solar technologies in terms of higher efficiency, better stability and lower cost.

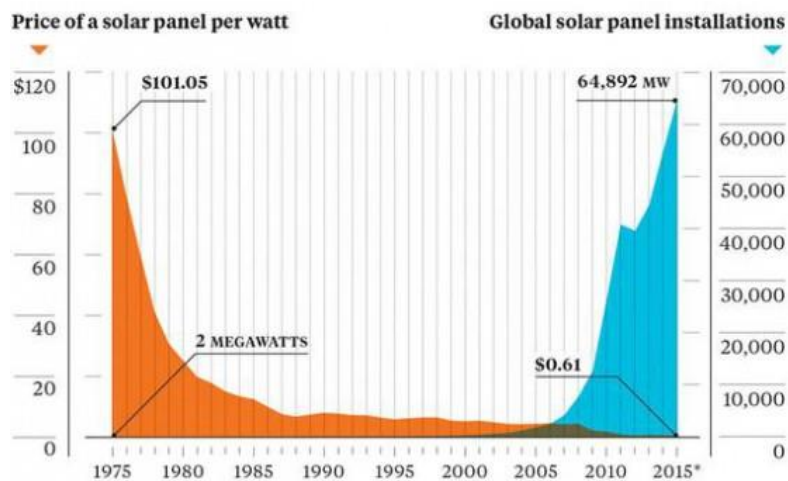


Figure 1.1 Cumulative PV capacity in megawatts globally and trend of the price change of a solar panel per watt from 1975 to 2015.[2]

1.1 Basic theory of solar cells

A solar cell is a device that directly converts the sunlight into electrical energy by the photovoltaic effect. This effect was discovered by Edmond Becquerel in 1839, but the first real solar cell on this basis was only created 50 years later by Charles Fritts in 1883.[3] It is composed of a selenium film together with a thin layer of gold (Au). In this structure, the combination of selenium and Au forms a Schottky contact, which is known as a potential barrier at the metal-semiconductor contact due to the difference of their Fermi energy and has rectifying characteristics, suitable for solar cell application. Briefly, the semiconductor selenium serves as a photo-active material, generating excitons (electron-hole pairs) by absorbing the sunlight. The formed built-in electric field due to the Schottky contact benefits the “exciton separation” and electron transport towards the cathode, while preventing the hole hopping in the same direction. Devices with such working mechanism are called Schottky junction solar cell, which is the simplest PV device. The performance of this type of solar cells is limited due to serious recombination of photo-generated charge carriers because the minority carriers from the illumination side (opposite to the Schottky junction) must travel the entire semiconductor film to reach the destination electrode.[4] To date, various advanced device architectures have been developed to address the problem. Most of them involve the use of both P-type and N-type materials, which form a P-N junction as the crucial part of the device.

Basically, the P-N junction solar cells work in several steps: I. the active material absorbs photons of the sunlight, generating electron/hole pairs (excitons); II. the excitons move to the interface between the P- and N-type materials, where a band offset drives the separation of excitons into free electrons and holes; III. the electrons and holes are then transported to cathode and anode of the cell, respectively; IV. at last, these charge carriers can be collected by electrodes, and directed to the outer circuit. A solar cell device with maximum light absorption and minimal charge carrier recombination is thus largely pursued to achieve the best performance.

The electronic behavior of solar cells can be modeled by an equivalent circuit composed of some discrete ideal electrical components (Figure 1.2 (a)). According to the equivalent circuit, a solar cell under illumination produces current (I) equal to the sum of photo-generated current (I_L) and the current (in a negative sign) passing through the diode (I_D) and shunt resistor (I_{SH}). The performance of a solar cell can be characterized by current-voltage measurements, and the typical curve is shown in Figure 1.2 (b). From this curve, the power conversion efficiency (PCE) of a solar cell can be determined. It is given by the equation: $PCE = (J_{sc} \times V_{oc} \times FF \times A) / P_{incident}$, where J_{sc} is short-circuit current density, V_{oc} is open-circuit voltage, FF is fill factor, A is device area and $P_{incident}$ is the incident optical power.

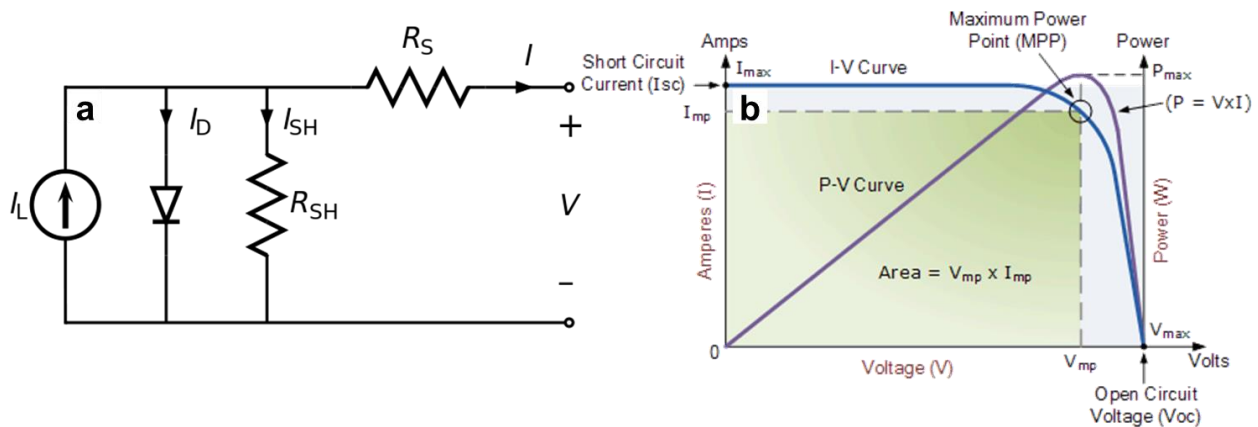


Figure 1.2 (a) The equivalent circuit of a solar cell, and (b) the typical I-V curve of a silicon solar cell. (The graphs were taken from internet: https://en.wikipedia.org/wiki/Theory_of_solar_cells and <http://www.alternative-energy-tutorials.com/energy-articles/solar-cell-i-v-characteristic.html>)

1.2 Overview of solar cell development

Traditionally, solar cell technologies can be classified into three generations. The first-generation solar cells mainly include wafer silicon-based (single-/multi-crystalline) silicon solar cells, which are still dominating the market, due to their high PCE (typically: 15-20%) and good stability as well.[5-6] However, high energy consumption technology is necessary to obtain pure, defect-free silicon materials, leading to the high cost of Si solar cell production.

As compared to the first-generation ones, the price of the second-generation solar cells (also called thin film solar cells) is relatively lower by avoiding use of silicon wafer. Nevertheless, the PCE is also decreased. For example, the amorphous silicon, $CuInGaSe_2$ and $CdTe$ based thin

film solar cells show typical PCE of 10-15% [7]. Further considering their high-energy consumption fabrication, there is scarce probability for the second generation solar cells to fully replace the first-generation ones.

Based on the development of material chemistry and device engineering, the third-generation solar cell was proposed one decade ago with the purpose of reducing the cost and achieving high PCE at the same time. The third generation solar cell can be divided into several categories, depending on the type of photo-active materials, such as dyes, quantum dots (QDs), conjugated polymers and perovskites.[8-11] The active film of all these materials can be fabricated by solution-processable technique (*e.g.* roll-to-roll process *etc.*), which is cost-effective and comfortable with large scale device fabrication. Furthermore, the high temperature and vacuum treatment commonly required in the fabrication of the first and second generation solar cells can be avoided, reducing the energy consumption. The performance of these solar cells has been largely improved from the beginning to present, especially for their PCE with remarkable improvement (Figure 1.3), by mainly focusing on the optimization of device configuration and material innovation. Additionally, each of these solar cells has their own advantages. For example, the three dimensional (3D) perovskite solar cell (single junction) shows the best PCE of ~22.1%[12] under 1 sun irradiation, whereas the QD-based device shows better air stability and reasonably high PCE (11.28%)[13] at the same time. Over all, there is still large space for these types of solar cells to improve their overall performance and reduce the cost with the purpose of realizing widespread application. More details about these types of solar cells will be introduced in the later section.

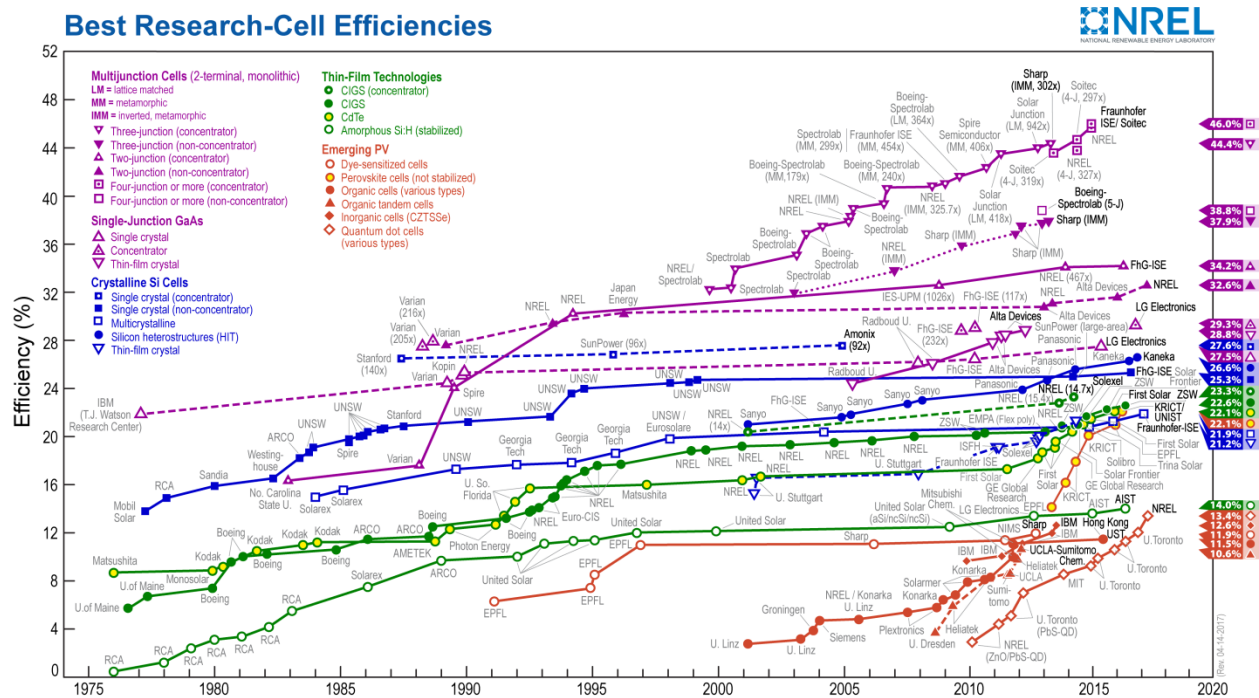


Figure 1.3 Evolution of record PCE values of different generations of solar cells since 1976, retrieved from <https://www.nrel.gov/pv/assets/images/efficiency-chart.png>.

1.3 Classification of the third generation solar cells

1.3.1 Dye-sensitized solar cells (DSSCs)

In a representative DSSC as illustrated in Figure 1.4 [14], the anode consisting of sintered semiconducting nanoparticles (mainly TiO_2) is deposited on a transparent conductive glass, a monolayer of organic dyes serves as a photo-sensitizer; and a redox couple such as $3\text{I}/\text{I}_3^-$ dissolved in an organic solvent acts as electrolyte, while platinum (Pt) serves as a counter electrode and catalyst simultaneously. Under working conditions, photons excite the organic dyes from their ground state to the excited state, the excited electrons subsequently inject into the conduction band of TiO_2 , and turn dyes into their oxidized form. Oxidized dyes are regenerated by acquiring electrons from I^- ions, which are converted into I_3^- . These I_3^- ions diffuse toward the Pt electrode and then they are reduced to I^- , finishing the circuit.

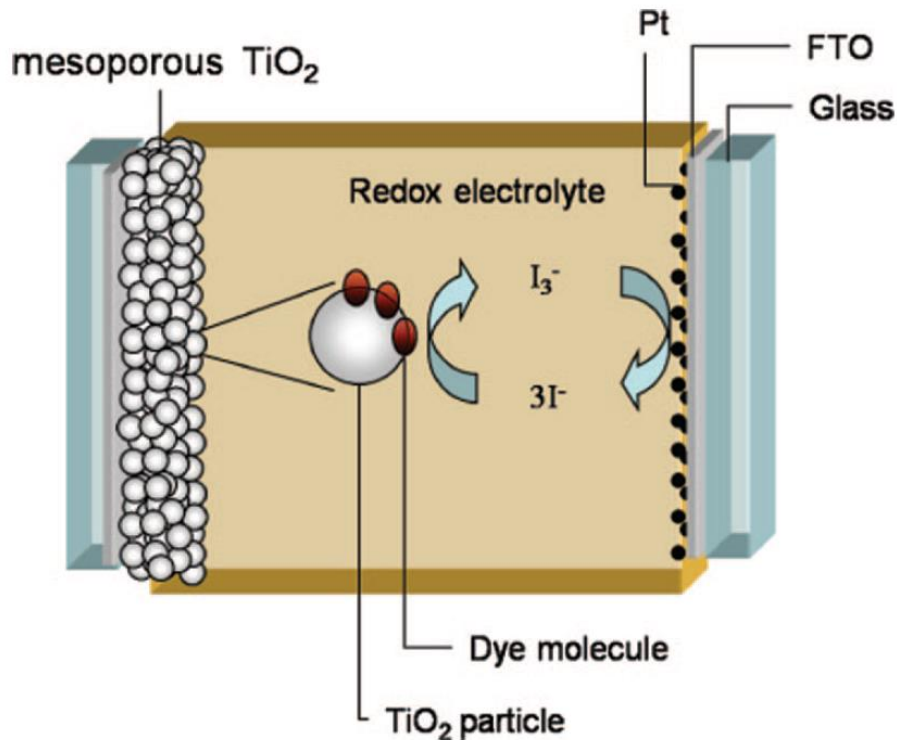


Figure 1.4 Schematic diagram of a dye sensitized solar cell.[14]

Compared to the silicon-based solar cells, DSSCs have the advantage of the simple fabrication and the use of low-cost materials. For instance, TiO_2 is a common material used in white pigment paint, and there are versatile dyes available in nature. In addition, there are some more merits as follows,[14] light weight, good flexibility, different color options, short energy pay-back time (<1 year), working in low-light conditions, *etc.* which make DSSCs a promising candidate for the next generation solar cells. However, the utilization of liquid electrolyte causes the stability issues. For instance, it can lead to Pt electrode corrosion and desorption of dye molecules from the TiO_2 surface.[15] Additionally, when they are operated at a very low temperature, the electrolyte can be frozen, leading to power cutting off and even physical damage. Future work can be progressed by taking the advantage of vast types of dyes in nature, investigating the tandem solar cell configuration and solid-state electrolytes.

1.3.2 Quantum dot solar cells (QDSCs)

QDs are semiconductor nanocrystals, whose size is smaller than the Bohr radius (distance between the electron and hole in an exciton) of the bulk material. As a consequence, excitons are

squeezed in the nanocrystals, due to the quantum confinement effect. With the development of materials chemistry, many types of QDs have been synthesized, such as II-VI (CdSe, HgTe, CdS)[16-18], III-V (InP, InAs)[19-20], IV-VI (PbS, PbSe, PbTe)[9, 21-24], I-III-VI₂ (InCuS₂)[25], and II₃-V₂ (Cd₃P₂, Cd₃As₂)[26-27] QDs. These QDs have the unique size-tunable optical properties over the spectral range from visible to infrared. Taking CdSe QDs (Bohr radius: ~5 nm) as an example, their absorption can cover the full visible range, when their size is tuned between about 2 and 5 nm.[28] For PbS QDs (Bohr radius: ~18 nm), the first-excitonic peak ranging from ~480 to 2100 nm has been achieved by tuning their size from ~1.5 to 10 nm.[21, 29] Therefore, it is promising to apply these QDs as the light absorbing material in solar cells, especially the near infrared (NIR) QDs, which are able to capture photons in a wider range than that of visible ones. Moreover, the PbS and PbSe QDs have been reported to be capable of generating multi-excitons by absorbing single solar photons with energy more than their band gaps.[23, 30-32] They hold the possibility of breaking the Shockley–Queisser limit.

QDSCs can be classified into QD sensitized solar cells (QDSSCs) and solid state QDSC. Like the DSSCs, QDs are immobilized on metal oxide (*e.g.*: TiO₂) film as sensitizers in QDSSCs. The certified highest PCE of this type of solar cells reached 11.61% by using the Zn–Cu–In–Se alloyed QDs.[33] Their excellent performance is derived from increased conduction band edge and the suppressed charge recombination at photoanode/electrolyte interfaces, resulting in higher photocurrent and photo-voltage as compared to that of the Cu–In–Se QD based device (9.54% in PCE). However, it is still a challenge to address the stability issues of this type of solar cells.[34]

The solid state QDSC (Figure 1.5) has a compact QD film, which is normally combined with another layer of N-type materials to form a heterojunction, considered as the efficient configuration for electricity generation. At the interface, a depleted region is responsible for the exciton separation and charge transport. The liquid electrolyte is not necessary for this type of QDSC, allowing them to work more safely and stably. The key factor of achieving good performance is the fabrication of a dense QD film, which mainly relies on surface treatments of the QDs via solution phase or solid phase method. Until now, the certified champion PCE (11.28%) was achieved by Sargent's group.[13] More contents are reviewed in chapter 2.

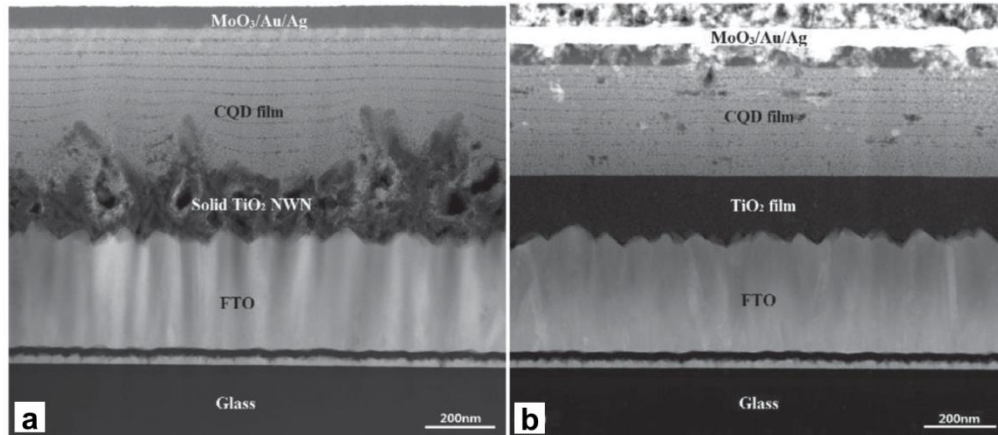


Figure 1.5 Transmission electron microscopy (TEM) images of (a) optimized nanowire network device, and (b) a planar device.[35]

1.3.3 Perovskite solar cells (PVSCs)

PVSC is a rising star in the PV field owing to its boosted PCE (over 20%) in several years (from 2009 to present). In this field, the most commonly investigated perovskite materials have a general formula of ABX_3 (Figure 1.6), where A represents a monovalent cation, B a divalent cation and X a monovalent anion. Depending on the radius of the selected component ions, the crystal structure of the perovskite materials varies, which can be estimated by calculating the Goldschmidt tolerance factor (t), $t = \frac{R_X + R_A}{\sqrt{2}(R_X + R_B)}$, where R_A , R_B and R_X is the radius of A, B and X ions, respectively.[36] As reported, a cubic structure was formed when $0.9 \leq t \leq 1$, while hexagonal/tetragonal or orthorhombic/rhombohedral structures can be formed with $t > 1$ or $0.71 \leq t \leq 0.9$, respectively.[37-38] Also, the optoelectrical properties of the perovskite materials change by varying their compositions. For example, the $CH_3NH_3PbI_3$ perovskite material (band gap: 1.55 eV) has the photo-response limited to ≤ 800 nm, while it decreases to ~ 550 nm when I ions are fully replaced by Br^- ($CH_3NH_3PbBr_3$, band gap: 2.2 eV).

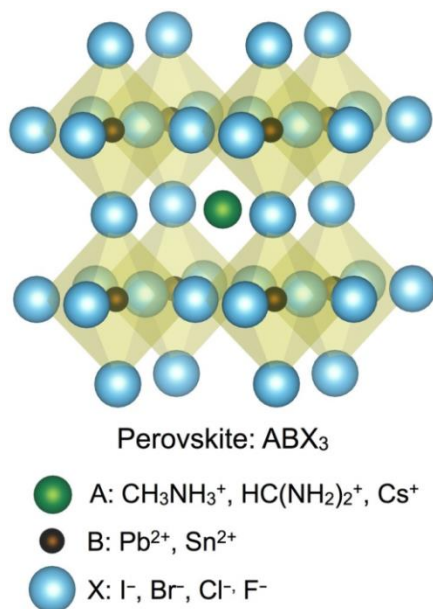


Figure 1.6 The perovskite crystal structure with the general form ABX_3 , in which A^+ is confined within a cage determined by the octahedral coordination of B^{2+} with X^- anions. The sizes of the spheres are given by the ionic radii of $CH_3NH_3^+$, Pb^{2+} , and I^- . The most common cations and anions that have been used in each position within the 3D halide perovskites are listed.[39]

Compared to other types of the third-generation solar cells, the excitons generated in perovskite material layer have loosely bonded energy between electrons and holes, which facilitates the separation of electron-hole pairs into free charges at the cost of a minimal driving force. Therefore, it allows the fabrication of a thick layer of perovskite materials to fully utilize the photons and avoid recombination at the same time. As a matter of fact, the photocurrent over 20 mA cm^{-2} has been reported for the 3D PVSCs, and a certified high PCE of 22.1% has been achieved close to the theoretical value for single-junction devices (26 - 27%)[40-41], by combing with other efforts on the optimisation of device configuration, interface effect, *etc.*[11]

Although a high-PCE record was achieved by PVSC devices, the reproducibility of perovskite film in high quality (pinhole-free, large crystal grains and rough-border-free) needs to be addressed. Additionally, it is still challenging to fabricate high performance devices in large area, and the high performance device based on 3D perovskite materials is commonly sensitive to O_2 and humidity, leading to rapid degradation of PCE. The future direction of PVSCs research can be focused on the stability of the PVSCs.

1.3.4 Polymer solar cells (PSCs)

With the potential advantages of abundant material, environment benign, light weight and good flexibility, PSC becomes one of the best candidates for the next-generation solar cells. Unlike inorganic materials, the charge mobility of organic materials is rather low ($10^{-3} \text{ cm}^2\text{V}^{-1}\text{s}^{-1}$), because the inter-molecular charge transport is difficult.[42] It means that a limited thickness of the active film is allowed to use in PSCs to avoid serious charge recombination. Fortunately, the organic chromophores have relatively high absorption coefficient, which allows a very thin layer (~100 – 200 nm) of semiconductor materials to capture most of the photons within their absorption ranges.[10] Additionally, due to the low dielectric constant of organic materials, the binding energy of electron-hole pairs is rather high (0.3 – 1 eV), resulting in short lifetime of these excitons.[43] Therefore, a typical PSC has the active film composed of a mixture of electron donor (conjugated polymer) and acceptor (such as fullerene derivatives), which enables the excitons to reach the donor/acceptor (D/A) interface in a short distance for charge carrier separation, without necessarily sacrificing the thickness of the photo-active layer. Afterwards, the band offset at the donor and acceptor interface drives the electron-hole pair to separate into free charges to be transported to respective electrodes. In the bulk film, the conjugated polymer and fullerene derivatives perform as the hole and electron transport material, respectively.

There are two types of the configuration of PSCs: conventional and inverted structure. In conventional PSCs demonstrated in Figure 1.7 (a), the generated free electrons/holes in the active film are directed to the Al cathode and indium tin oxide (ITO) anode, respectively. However, the highly acidic poly(3,4-ethylenedioxythiophene):polystyrene sulfonate (PEDOT:PSS) as a hole transport layer is detrimental to the ITO electrode and is hydrophilic. Additionally, the Al electrode is air sensitive, which can be easily oxidized.[44] All of these aspects can lead to the performance degradation of PSCs. As for inverted PSCs (Figure 1.7 (b)), the natural of charge collection is reversed, and at the same time the PEDOT:PSS hole transport material and Al electrode are replaced by MoO_3 and Ag, respectively. In this case, the stability of PSCs is largely improved. The future work can be focused on the stability of the active layer by avoiding the aggregation of PCBM and the degradation of polymers, new polymer materials design to extend the photo-response range and improve their $\text{H}_2\text{O}/\text{O}_2$ sensitivity, and green solvent development.

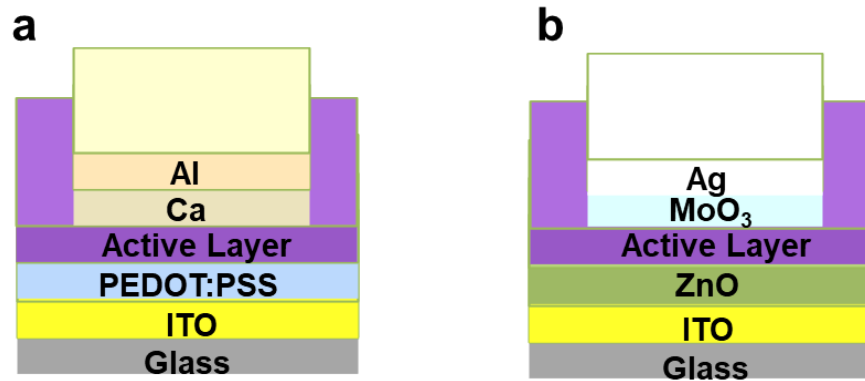


Figure 1.7 Conventional (a) and inverted (b) structure of polymer solar cells

1.3.5 Hybrid solar cells (HySCs)

A PV device based on the combination of organic conjugated polymer and inorganic QDs as the active layer can be called HySC. Considering the properties of the involved active materials, a device based on this concept is expected to have the advantages of good mechanical flexibility, low specific weight, strong light absorption over a wide spectral range and excellent photostability.[45-46] In designing a HySC device, several aspects need to be taken into considerations[45]: I) the surface ligands of the QDs; the as-prepared QDs are normally capped by insulating, long-chain ligands, which stabilize the QDs suspended in a solvent. These insulating ligands should be replaced by short ones to reduce the inter-dot and QD-organic material distance, facilitating the charge transport; II) the morphology of the photo-active layer, which largely determines exciton-separation and charge-transport processes, and thus directly influence the performance of solar cell devices. Ideally, the interpenetrating electron and hole transporting phases in the composite should be at the nanoscale to ensure that short-lived excitons can efficiently reach the D/A interface before any considerable electron-hole recombination [45]; and III) the band alignment of QDs and polymer. As for the exciton dissociation in a binary system made of QDs and polymers, a type II band alignment structure is required. Following charge separation, the QD is usually used to transport electrons, and the polymer holes due to its higher hole mobility. Thus, their band structures should be aligned in such a way to favor the transfer of photogenerated electrons from polymers to QDs and the transfer of photogenerated holes from NIR QDs to polymers [45]. Figure 1.8 shows the band alignment of some popular polymers and PbS QDs with different size [47].

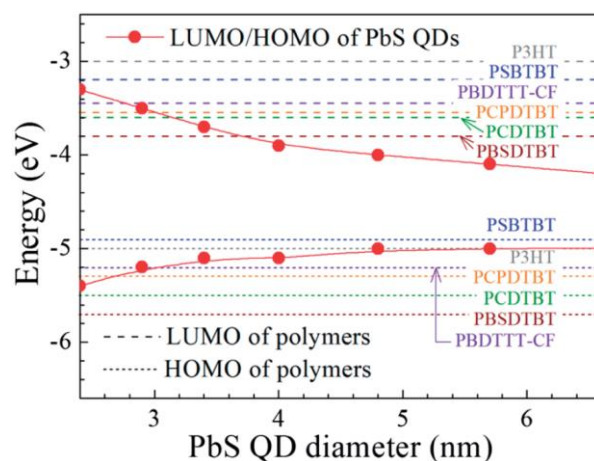


Figure 1.8 Energy levels of PbS QDs according to their diameter and LUMO/HOMO values of conjugated polymers widely used as electron donors in polymer BHJ solar cells. PBDTTT-CF is poly[4,8-bis-substitutedbenzo [1,2-b:4,5-b0]dithiophene-2,6-diyl-alt-4-substituted-thieno [3,4-b]thiophene-2,6-diyl], PCDTBT is poly[N-90-hepta-decanyl-2,7-carbazole-alt-5,5-(40,70-di-2-thienyl-20,10,30-benzothiadiazole)], and PBSDTBT is poly[9,9-dioctyl-2,7-dibenzosilole-co-alt-5,5-(40,70-di-2-thienyl-20,10,30-benzothiadiazole)].[47]

Over all, the HYSCs still suffer from low PCEs as compared to the other third-generation solar cells. However, the discovery of charge transferring from the “dark” triplet generated in organic semiconductor pentacene and tetracene to PbSe and PbS QDs would stimulate more interests on the hybrid system.[48-49]

1.4 Luminescent solar concentrators (LSCs)

LSCs are devices that are able to convert photons over a wide range of the solar spectrum into concentrated light in a specific range. They mainly consist of a fluorophore as light absorber/emitter and a polymer matrix acting as the wave guide of reemitted photons. Compared to the PV devices, the LSCs can be produced in low cost considering their constituent materials and fabrication process. It enables the large-scale implementation of solar technologies by combining the cheap LSC device in large-area with expensive PV device in small area. Therefore, the total cost of the solar technologies can be reduced without decreasing the PCE. Based on this concept, the LSC device with a big area of top surface and small side edge should be fabricated (Figure 1.9) to maximize the light absorption and output.

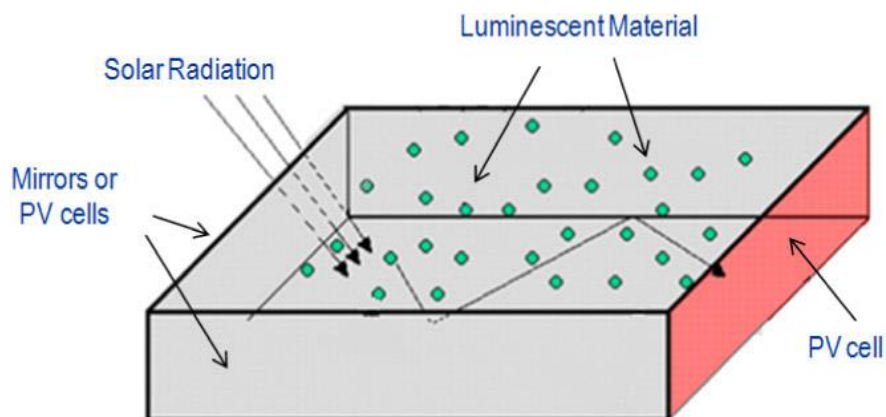


Figure 1.9 Configuration of LSC devices, retrieved from <https://www.spie.org/>.

In a LSC device, the fluorophore material is the most crucial factor of determining the device performance. From early stage to present, some organic dyes include rhodamines[50-51], coumarins[52], cyanines[53] and perylenebismides derivatives[54-55] *etc.* have been commonly applied in LSC application. These dyes have emission wavelengths mainly in the visible range, and show high photoluminescence quantum yield (PL QY) in solution. However, there are serious reabsorptions in dye-based LSC devices, due to the large overlap between their absorption and emission spectra. Additionally, the PL QY of dyes significantly decreases when they are immobilized in the polymer matrices.

Inorganic QDs with the advantages of high PL QY, wide-range of size-tunable optical properties and good chemical-/photostability are promising for LSC application. Taking the PbS QDs as an example, PL QY up to 90% has been achieved when the diameter of QDs was decreased to ~3.0 nm [21]. Moreover, metal ion doping and shell coating have been reported as the effective strategies to separate the absorption and emission spectrum of QDs. Depending on the QD types, the resulted QDs by these treatments can retain reasonable high or even better PL QY. They include Mn-doped ZnSe, CdSe/CdS, PbS/CdS, PbSe/PbS and so on.[56-63]

1.5 Thesis Objectives and Organization

1.5.1 Objectives

Part I: Investigations on QDs synthesis, characterization, mechanism and solar application

PbS QDs are promising for various applications in the NIR range, due to their tunable optical properties which are mainly relying on the QD synthesis. Among diverse synthetic routes, the method based on the use of PbCl_2 and elemental S as the precursors is a facile, safe and “green” way to synthesize high quality PbS QDs. However, this method normally yields QDs in a limited absorption range of 1200-1600 nm, corresponding to the size of 4.2-6.4 nm.[22] Although the trioctylphosphine (TOP) chemical as an additive has been employed to extend the size tunable range of QDs from this route, the product yield of the reaction is limited.[21] Additionally, their work was mainly focused on synthesizing large size QDs with the first-excitonic peak over 1600 nm, while it is still challenging to synthesize very small PbS QDs. As we know, the small QDs normally have higher PL QY and optical constant, and better stability than large ones. Therefore, we aim to realize the synthesis of very small PbS QDs via developing a convenient route by introducing a new additive in the reaction. The surface properties of resultant QDs are examined, which are correlated to their optical properties. The reaction mechanism, scale-up reaction and QD application are further systematically investigated.

Part II: Performance enhancement of PSCs

Although high PCE over 10% has been achieved for PSCs, the investigations on device stability and “green solvent” processable fabrication are limited, which impede the commercialization of PSCs. To address the device stability issue, two main factors should be taken into consideration [4]: 1) chemical degradations of polymer materials and electrode by reacting with $\text{O}_2/\text{H}_2\text{O}$; 2) physical degradations due to the morphology change of the active layer. Based on these considerations, we aim to improve the long-term and thermal stability of PSCs by involving the inorganic quantum dots into the active layer as a stabilizer of the film, and at the same time to scavenge $\text{O}_2/\text{H}_2\text{O}$ and prevent them from attacking the polymer material. The $\text{O}_2/\text{H}_2\text{O}$ sensitivity of QDs themselves and the morphology effect are two aspects to be focused in my thesis work.

As for “green processing”, the effect of a relatively “green” additive on the morphology, structure and performance are systematically investigated. This non-halogenated additive can be potentially used as a co-solvent together with the “green” polar solvents, which are normally insoluble for fullerene derivative materials, for high performance solar cell fabrication.

1.5.2 Thesis Organization

This thesis includes five chapters which are organized as follows:

Chapter 1 Introduction: This chapter briefly introduces the basic knowledge and development of solar cells, especially for the third-generation solar cells.

Chapter 2 Literature Review: synthesis and surface engineering of NIR QDs and morphology control of the active layer of PSCs are reviewed.

Chapter 3 Experimental: The experimental chapter describes the details of materials synthesis, such as PbS QD synthesized in different routes followed by surface treatments. Additionally, the LSC and solar cell device fabrications are also included. Finally, the characterizations of obtained materials, active film and devices are presented.

Chapter 4 Results: This chapter is divided into three parts. The first part demonstrates the very small PbS QDs synthesis via PbCl_2 -S based route, for the first-time, by introducing tributylphosphine (TBP) into the reaction. Material characterizations, reaction mechanism, reaction scale-up and materials application are also included. In the second part, NIR QDs are incorporated into the active film to improve the stability of PSC based on P3HT:PCBM, and simultaneously extend the photo-response of device to the NIR range. The morphology effect on the performance is also discussed. The third part presents the enhancement of device performance via addition of butylamine in the blend solution. The effect of butylamine on the nanoscale morphology and structure of film are investigated.

Chapter 5 Conclusion and Perspective: Main conclusions are presented based on the results and analysis, and potential work in this research direction in the future is proposed.

In this thesis, most of the work was completed by Long Tan, except for the LSC device fabrication/characterization, Pb/S ratio measurement of PbS QDs and the Fourier transform infrared spectroscopy (FTIR) characterization of P3HT:PCBM blend. To be specific, the LSC application of our synthesized QDs was conducted by Dr. Haiguang zhao, Yufeng Zhou and Daniele Benetti in Prof. Federico Rosei's group. Dr. Fuqiang Ren and Fan Yang assisted me on the Pb/S ratio measurement and FTIR characterization, respectively.

CHAPTER 2 LITERATURE REVIEW ON SYNTHESIS AND SURFACE ENGINEERING OF NIR QDS, AND MORPHOLOGY MANIPULATION OF ACTIVE LAYER OF PSCs

In this chapter, a literature survey on synthesis and surface engineering of NIR QDs is presented. The morphology manipulations of active layer of PSCs are also briefly summarized. Some contents of this chapter were published in a review article by our group very recently.[64]

2.1 Introduction

To date, substantial progress has been achieved for the third-generation solar cells, thanks to the development of material chemistry and device engineering. Except for HySCs, the record-high PCE for each type of the third-generation solar cells already reach the value of the commercialization criterion (over 10%). For LSCs, the development of material chemistry also provides space to design novel devices with improved performance stability, expanded light utilization range and tunable range of emission photons, than the widely reported device with dyes as fluorophores.[65-67] In other words, the material chemistry and device engineering played a significant role in determining the development of solar technologies, which are thus two major research directions to continue improve the performance of solar technologies towards actual application.

This chapter is divided into three parts. In the first part, we focus on introducing the hot-injection synthesis of NIR QDs, by which the optical properties of the QDs can be conveniently tuned. It is closely related to the light utilization and device design considering the band alignment of different materials in solar cells. Also, the synthesis method bears significant meaning to the quality of obtained QDs, which determines the final performance of devices under operation. The second part reviews the effect of the surface engineering of QDs on the performance of solar cells, which mainly includes two sections: ligand exchange and shell coating. Their effects on the properties of QDs themselves are also presented [64]. In the last part of this chapter, we summarize the ways of effectively controlling the morphology of the active film, and their

effects on performance of PSCs. The following aspects are introduced: solvent selection, solvent/thermal annealing, additive manipulation and interface effect.

2.2 QD synthesis via hot-injection method

The performance of QD-based solar technologies is highly relying on the quality of QDs, which is represented by their average size, PL QY, size distribution, morphology, *etc.*[68] To the best of our knowledge, the so-called hot-injection method is most popular for obtaining QDs with tunable size, high PL QY, narrow distribution and uniform shape, which is also more efficient and has the advantage of low-cost as compared to the physical synthesis route.[69] In brief, this wet chemistry method involves the swift injection of one (or multiple) precursor solution to another preheated precursor solution followed by rapid temperature decrease. The crucial point to tailor the size of QDs is to control the nucleation and growth processes. In the synthesis, the nucleation occurs upon injection of large amounts of precursor, and both injection temperature and precursor concentration play a significant role in this process.[70] With dramatic temperature drop or precursor concentration below a critical point, ideally the nucleation completely stops, while the growth starts. The growth process has been modeled based on the two competing effects: focusing and defocusing.[71-72] For the focusing effect, the QD growth is diffusion controlled with a constant number of particles during the process (theoretically), and the growth rate of QDs is inversely proportional to their radius. Therefore, QDs with narrow size distribution can be obtained via this effect, if a secondary nucleation process can be avoided. Normally, this effect dominates the QD growth at the early stage. However, the defocusing effect, well known as the Ostwald ripening,[73] prevails once the average QD size exceeds a critical point, meanwhile the precursor concentration is low. In this stage, the smaller particles are prone to dissolve owing to their high chemical potential, while the larger ones continue to grow, and together they lead to the decrease of particle numbers and size broadening. Moreover, the QDs can further grow to larger size by adding fresh precursor into the reaction. In this case, the precursor concentration should be taken into consideration to avoid the size broadening of QD induced by the secondary nucleation.

PbS QDs with a wide range of tunable optical properties in the NIR range are more stable than other types of QDs such as PbSe, CdSe and CuInZnS QDs, and their synthesis has been

extensively studied. To date, there are two typical routes to synthesize PbS QDs based on the use of different chemicals. The first route can be called the Hines synthesis, which uses PbO, bis(trimethylsilyl)sulfide (TMS), oleic acid (OA) and octadecene (ODE).[74] This method typically results in PbS QDs with the first-excitonic peak between 825 to 1750 nm (Figure 2.1(a)), corresponding to the diameter of 2.6 – 7.2 nm. By decreasing the lead to oleic acid ratio and controlling the temperature of nucleation and growth process, PbS QDs with the first-excitonic peak wavelength as short as 480 nm (Figure 2.1(b)) were synthesized by H. Choi *et al.* using the same method, which is the smallest PbS QDs ever reported.[29] The second route is processed based on the use of PbCl₂, elemental sulfur and OLA.[22] As demonstrated by the authors, the heterogeneous nature of PbCl₂-OLA complex in the reaction and the high ratio of Pb:S prolong the focusing process, which plays a significant role in obtaining high quality, uniform PbS QDs. Compared with the Hine synthesis, this route is much “greener” by using the elemental S to replace toxic TMS. However, the QDs synthesized from this route have a narrower photo-response range (1200 – 1600 nm) due to the limited reactivity of elemental S compared to that of TMS. Although Moreels *et al.* further extended the tunable range of absorption peak to 925 – 2100 nm by introducing TOP in the reaction (Figure 2.1(c)), the synthesis yield seemed to be low (20 – 30%).[21] In addition to these two commonly used routes, Hendricks *et al.* developed a new route to synthesize gram-scale PbS QDs recently.[75] They claimed that the size and product yield of PbS QDs can be precisely controlled by tuning the kinetics of precursor being converted into the monomer. In this case, a full conversion of precursors can be realized, rather than that in the above mentioned two methods with excess Pb precursor. The reported tunable absorption peak for this method is in the range of 850 – 1800 nm.

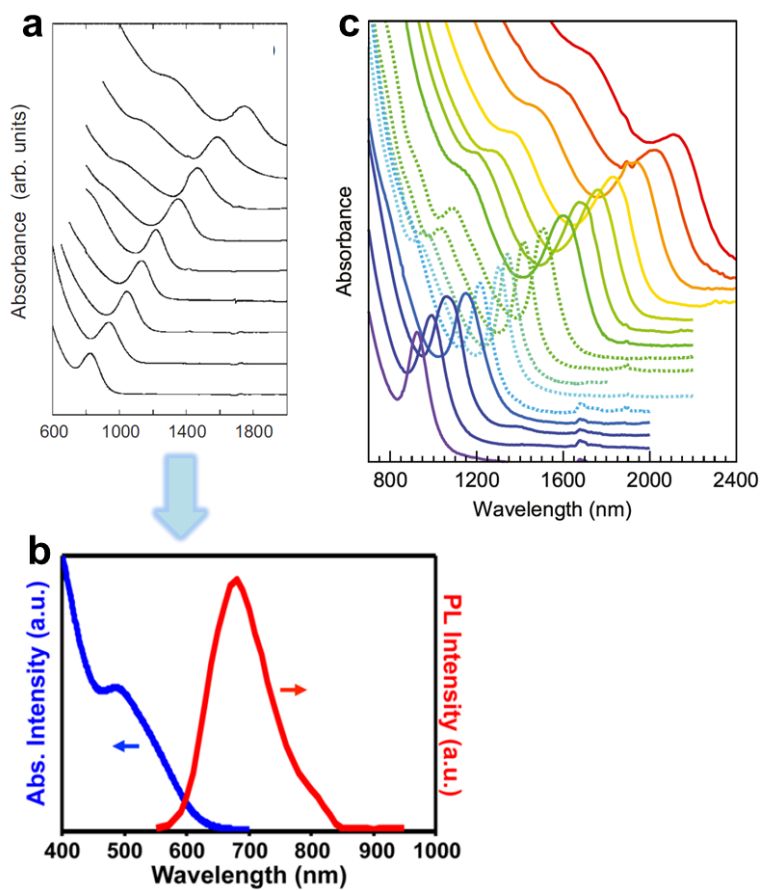


Figure 2.1 (a) Absorption spectra spanning the range of the tunable sizes.[74] (b) Absorption and photoluminescence spectra of ultrasmall PbS QDs dispersed in tetrachloroethylene.[29] (c) Typical absorbance spectra of PbS QD suspensions. Full lines are QDs synthesized with TOP, dotted lines without TOP.[21]

2.3 Stabilities Related to Near-Infrared Quantum Dot-Based Solar Cells: The Role of Surface Engineering

Long Tan, Pandeng Li, Baoquan Sun, Mohamed Chaker, and Dongling Ma

ACS Energy Lett. 2 (2017) 1573–1585.

Owing to the small particle size of QDs, their surface area to volume ratio is much higher than that of bulk materials, which lead to different properties between surface and interior atoms. It is significant to understand and control the surface properties of QDs, which influence the optoelectric properties of QDs and the performance of corresponding devices.

In this section, the surface engineering and its effect on the performance of QD-based solar cells are reviewed and discussed. It is mainly focused on the NIR QDs such as PbS and PbSe.

In this review, I wrote the first draft of introduction, contents related to ligand engineering and the perspective section, with the first draft of other parts (ink stability and core/shell QDs) being written by Pandeng Li.

Stabilities Related to Near Infrared Quantum Dot-based Solar Cells: the Role of Surface Engineering

*Long Tan⁺, Pandeng Li⁺, Baoquan Sun, Mohamed Chaker, Dongling Ma**

Énergie, Matériaux et Télécommunications, Institut National de la Recherche Scientifique (INRS), 1650 Boul. Lionel-Boulet, Varennes, Québec J3X 1S2, Canada

Institute of Functional Nano & Soft Materials (FUNSOM), Soochow University, 199 Ren'ai Road, Suzhou, Jiangsu 215123, P.R. China

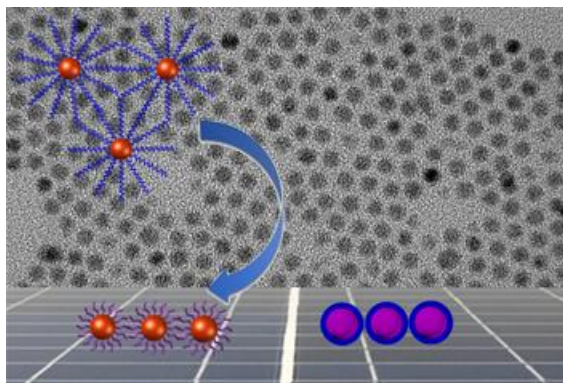
AUTHOR INFORMATION

Corresponding Author

*E-mail: ma@emt.inrs.ca. Website: <http://www.inrs.ca/dongling-ma/>.

ABSTRACT: As compared to the great effort made on improving the power conversion efficiency of quantum dot (QD) solar cells, investigations on relevant stability, regarded as another crucial factor for their widespread implementation, are still limited. In this perspective, we discuss the stability of QD solar cells from different aspects, all highly relying on the surface chemistry of QDs. Specifically, three types of stabilities, closely relevant to the realization of the actual application of QD solar cells, are presented: i) air-processability, which allows QDs to be processed in air with high batch-to-batch reproducibility; ii) long-term stability of QD solar cells, directly related to their performance degradation in the long run; and iii) QD ink stability that is concerned with the storage lifetime of QDs in solution and is compatible with low-cost solution processing techniques. Both air processability and excellent QD ink stability are critical for achieving the desired low-cost, large-scale roll-to-toll manufacturing of solar cells.

TOC GRAPHICS



Harvesting solar energy via the photovoltaics (PV) effect has been considered to be one of the cleanest and most promising ways in addressing both the energy crisis and environmental issues. In order to significantly increase the use of solar electricity globally, the concept of third-generation solar cells, based on the vast experience achieved on the first and second generations, was proposed about more than one decade ago, with the purpose of reducing cost yet achieving high power conversion efficiency (PCE), two most important ones among all the factors being considered for solar cells. In this research stream, quantum dot (QD)-based solar cells have

attracted extensive research interests and their different configurations have been explored.¹⁻⁶ QDs are semiconductor nanocrystals that are smaller than the Bohr radii, such as ~18 nm in bulk lead sulfide (PbS) and ~5 nm in bulk cadmium selenide (CdSe), to exhibit the quantum confinement effect. As a result, they show unique size-tunable absorption and energy levels, which allows tuning of charge transfer at interfaces and realization of better energy level matching between donor and acceptor materials as well as better spectral matching to the solar spectrum. Both of them are crucial to improve the performance of solar cells.⁷⁻¹¹ They also hold huge potential of multiple exciton generation from single absorbed photons.^{12,13} Quantum efficiencies over 100% at certain wavelengths have recently been achieved by harnessing this exceptional feature.¹⁴ Also importantly, owing to their small sizes, the surface area to volume ratio of QDs is much higher than that of bulk materials, with a significant portion of atoms situated on the surface of QDs. On one hand, the presence of under-coordinated atoms with dangling bonds on the QD surface leads to high chemical reactivity and a large number of trap states, which can cause instability and poor performance of QD solar cells. The effects can be twofold. On the other hand, owing to the high surface area to volume ratio, the surface of QDs plays a dominant role in various physical and chemical processes, which offers a large latitude for dramatically improving and tuning their properties via surface engineering.¹⁵⁻¹⁷ As a matter of fact, largely benefiting from surface engineering, considered as one of the most effective strategies, the PCE of QD-based solar cells has significantly enhanced from less than 1% to over 11%.¹⁸⁻²¹ Nevertheless, in a clear contrast to the rapid progress in PCE, only quite limited investigations on the stability issue, encountered during the solar cell fabrication process or observed in the performance degradation of QD solar cells, have been conducted, which clearly requires more intense attention.

Moving forward on the way towards the actual applications of QD solar cells, it is time to examine the stability issue seriously and improve the stability as much as possible by taking advantage of recently developed effective strategies from synthesis to surface engineering and of advances on theoretical calculations as well as by using a variety of characterization tools. Three important types of stabilities should be taken into consideration: air processability allowing simple and reproducible fabrication of solar cells in air; long-term stability of QD solar cells that determines device lifetime; and colloidal QD ink stability enabling facile and low cost solution

processing. Both air processability and ink stability are closely related to the large-scale roll-to-roll (RTR) manufacturing process and thus directly affect the cost of QD-based solar cell technology. Certain challenges need to be addressed in order to meet the requirements of these stabilities. They include, for example, the degradation of QDs with time owing to their interactions with oxygen/moisture, especially under extended illumination.²² As a consequence, the exciton generation/charge transfer in the QD layer and the exciton separation/charge collection at the interfaces of the QD layer and other materials can be deteriorated, which accounts for the device long-term instability. The way to obtain highly stable QD ink which has long shelf life and can be fabricated into the ultimate, functional QD film in a single film deposition step without involving solid-state ligand exchange that is incompatible with the large-scale fabrication, deserves more in-depth investigations. Although for long-term colloidal stability, long alkyl chain organic ligands usually behave better due to their steric effect, shorter and conductive ligands are absolutely preferred in light of the excellent performance of QD solar cells.^{16,20,23-25}

All these stabilities are closely related to the surface chemistry of QDs and thus can be tuned by surface engineering. For instance, the interactions of QD surface with ligands can be varied, depending on QD sizes, the nature and length of ligands, *etc.*, resulting in different surface coverage and binding strength of ligands.^{17,26,27} In a different vein, forming an epitaxial, robust inorganic shell around QDs to obtain the so-called core/shell QDs also permits the manipulation of the QD surface. All these factors can affect the reactivity of QDs with the external environment and thereby their stability. They also influence the distribution of defects and trap states, the presence of which in most of the circumstances is believed to cause the recombination of photogenerated charge carriers, being considered as the main obstacle for achieving a high PCE. In this perspective, we start with elaborating the surface chemistry of QDs from two entangled aspects, the surface structure of QDs themselves and the passivation layer comprising ligands or a robust inorganic shell. We explain how the surface chemistry is related to the stability and solar cell performance. We then introduce some recent advances in air processability, long-term QD solar cell stability and QD inks by using certain examples. Finally, promising research topics in this research theme are proposed. We would like to point out that in this perspective, we focus most of our discussions on PbS and lead selenide (PbSe) QDs, which

represent two types of the most prominent near infrared (NIR) QDs being investigated, and their solar cells involving a photoactive, compact layer of QDs.

General remarks on QD surface chemistry and its effects on solar cell performance

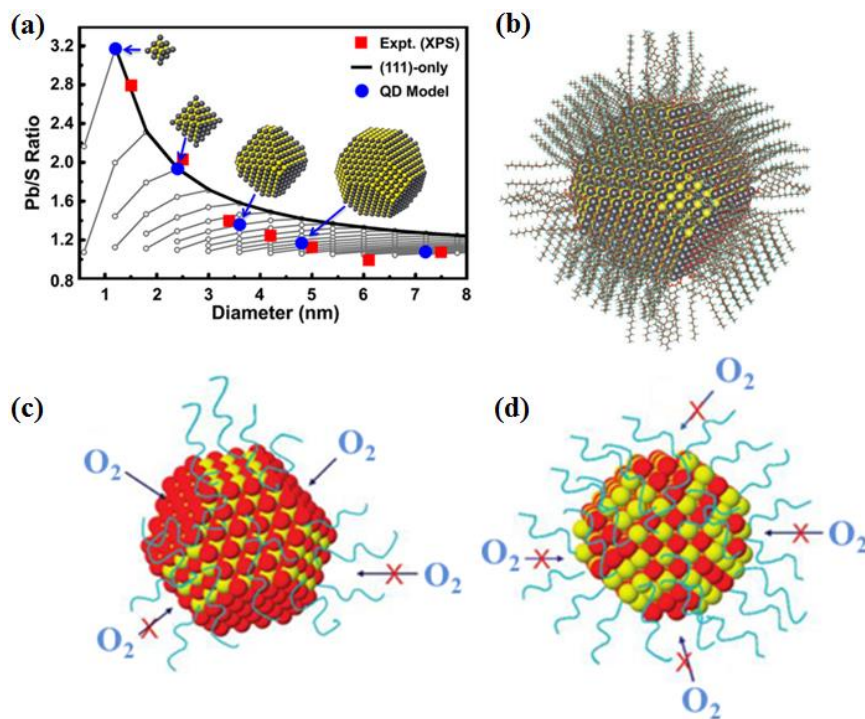


Figure 1 (a) Pb/S ratio of octahedral and cuboctahedral PbS QD models as a function of diameter (D), compared with the XPS data. (111)-only octahedral QDs show a deviation from experimental data at $D \approx 3$ nm. Proposed QD models are shown in the inset data, marked with blue circle. Reprinted from ref 27. Copyright 2013 American Chemical Society. (b) Calculated atomic structure of a 5-nm-diameter PbS QDs passivated with OA^- and OH^- (red) ligands. Reprinted from ref 31. Copyright 2014 American Association for the Advancement of Science. Schematic illustration of oxidation for large (c) and small (d) PbS QDs. Large PbS QDs are faceted and small ones are spherical. The red spheres, yellow spheres, and cyan tails are dedicated to sulfur atoms, lead atoms in PbS QDs, and surface ligands, respectively. (c) and (d) reprinted from ref 43. Copyright 2010 American Chemical Society.

The significance of surface chemistry increases with the drastically increasing surface to bulk atom ratio. Taking the well-studied CdSe material as an example, a 1.2 nm nanocrystal will have 88% of surface atoms, and an 8.5 nm crystal consists of 20% atoms on surface. Additionally, the surface atoms are more unstable compared to the bulk atoms. Altogether make it possible to precisely manipulate the properties of nanostructures via surface chemistry. For QDs, the

surface chemistry is fundamentally important for various properties. It can involve two major aspects. One aspect is related to the structure and atomic arrangement of the surface of QDs themselves. The other one is passivation layer since in most of the cases the surface of QDs is capped by other molecules or materials.^{26,28} The surface structure, enriched with dangling bonds, edges, corner sites and facets, is complicated and even dynamic (varying with the surrounding environment), and thus hard to analyze and quantitatively describe. The presence of dangling bonds causes the colloidal and chemical instability of QDs. It is also associated with charge carrier traps and mid-gap states, which explains that surface passivation is indispensable for QDs application.²⁹ Depending on the methods of preparation, exact synthesis parameters, and their sizes, QDs can display different facets exhibiting different patterns of surface atoms. Specifically for lead chalcogenide QDs, they are prone to exposing non-polar (100) and polar (111) facets,^{27,30,31} with the latter having higher surface energy and thus higher chemical reactivity if not passivated.^{27,32} The atomic arrangements on these two sets of facets are distinctly different, the (100) facet being stoichiometric, while the (111) facet being lead rich. Related to these arrangements, the ligand passivation can be different, determined by surface atom-ligand interactions. Altogether, they suggest that lead chalcogenide QDs display different chemical reactivity, thereby, different resistance to oxidative degradation correlated with the nature of exposed facets. Also due to the possibility of having different facets and stoichiometry variation on the exterior of the QDs, the overall composition of binary QDs can be different. These differences can be measured by chemical analysis tools, such as X-ray photoelectron spectroscopy (XPS). It was found that the Pb/S ratio of oleic acid (OA) capped PbS QDs, determined by XPS, varied significantly from ~1.1 to 2.8 when QD diameter altered from 7.5 to 1.5 nm (**Figure 1a**).²⁷ By correlating experimental results with density functional theory (DFT) calculation ones, the authors proposed that small PbS QDs tended to exhibit more (111) facets than larger ones. In addition, PbS QDs with a diameter less than 4 nm exhibited only the (111) facets on the external surface. Although the (111) facet is well-passivated by OA, the (100) facet is not, which adds another variable in terms of surface properties. Using combined experimental/theoretical approaches, it was found that depending on the synthesis method, the OH⁻ and Cl⁻ ions can be present with organic ligands on the (111) facet and stabilize it (**Figure 1b** as one example).³¹ With all the different surface features, it can be understood that the QDs with different sizes can have quite various stabilities. Such interesting findings reveal the

complexity of the surface of tiny QDs and also underline the importance of combining empirical and theoretical approaches in probing and understanding the QD surface.

High quality NIR QDs, mostly synthesized from wet chemical approach, are almost exclusively covered by long-chain ligands as a passivation layer. These ligands serve as stabilizers, rendering QDs colloidal stability in solution so as to avoid their agglomeration.³¹ In addition, because ligands passivate QD surface atoms and remove dangling bonds, they can decrease the chemical reactivity of QDs and increase their resistance against the chemical attack by the surrounding environment.^{17,33} Depending on the size and nature of ligands, their surface coverage on QDs and binding affinity to QDs are different, which directly modulate QD properties.^{17,34} In general, smaller and shorter ligands can pack more densely on the QD surface. For instance, n-alkylthiolate ligands pack two times denser on the CdSe QD surface than that of bulky tert-butylthiolate ligands at assumed full coverage.^{35,36} On the other hand, strong binding ligands allow higher coverage density being retained after solvent treatment in fabrication process and increase the “inertness” of QDs to the surrounding environment. As an example, for PbS QDs, OA has higher binding affinity than oleylamine (OLA) and I⁻ binds stronger than Cl⁻.^{17,34} In principle, the denser and tighter-binding the passivation layer is, the more stable the QDs will be.

The surface chemistry of QDs themselves and ligand arrangement in the passivation layer cannot be separated; they are entangled. For instance, the strong interaction of ligands with atoms on the QD surface can affect the way QD surface atoms are arranged.^{31,37} Conversely, the QD surface can dictate ligand arrangement. Different ratios of surface atoms lead to different ligand coverage because usually one type of ligand can only bind with one type of surface atoms (for example, OA only binds with Pb sites, but not S sites).³ In addition, it is found that the radius of nanoparticles curvature highly depends on their size, which directly and appreciably influences the surface coverage of molecules.³⁸⁻⁴⁰ The surface density of molecules tends to be higher for smaller nanoparticles and the trend holds true until the nanoparticle size approaches a critical value, after which the surface coverage remains nearly constant. Although detailed investigations on this point have not been reported for lead chalcogenide QDs, it is reasonable to expect that the QD surface curvature will also affect the accessibility of ligands to QDs and therefore their coverage density on the QD surface, especially for larger size ligands. As for the chemical nature of the interactions between the QD surface and ligands, Owen *et al.* proposed three classes of

metal-ligand interactions, L-type, X-type and Z-type, adapted from the classical concept developed originally for metal coordination complexes. Readers are referred to references for more details.^{26,41} Determining the exact and complete picture of the QD surface and the ligand layer is a tough task, which however can help to elucidate observed optical and electrical properties (for example, exciton dynamics) and ultimate device performance.⁴²

With such basic understanding, there is no surprise that multiple aspects demand attention when the QD stability issue is approached. QDs degradation starts from their surface and mainly proceeds through oxidation in most of the cases, in particular for NIR QDs discussed herein. The composition change of the QD surface can be readily detected by XPS technique.⁴³ In one case, both PbSO_4 and PbSO_3 were found to be present on the surface, depending on PbS QD size. Smaller QDs seemed to be more stable than larger ones and primarily PbSO_3 was identified as oxidized species on their surface, while for larger QDs, PbSO_4 was the principal oxidation product.⁴³ As mentioned above, smaller QDs tended to have more lead-rich (111) facets. As compared to the stoichiometric (100) facets, the lead-terminated (111) facets were more stable because most of the surface sites could be well passivated by forming strong bonding with ligands used in that study. It is to say the lead-rich (111) facets had a denser ligand shell (**Figure 1c and 1d**). This provides spatial hindrance to oxygen diffusion and thus repulsion to the surface oxidation and explains why smaller QDs are more stable. For the same reason of better surface passivation and less space available for oxygen diffusion, mainly PbSO_3 was generated on the surface of small QDs, which represented a relative lower level of oxidation. Similar results were reported for PbSe QDs, in the sense that smaller ones were more Pb-rich and more stable than large ones, which were mainly enclosed by the (100) facets.^{30,44,45} In the presence of oxygen, PbSe QDs could form PbO , SeO_2 and PbSeO_3 on the surface.^{46,47} Since Se is more reactive than S, the oxidation degradation of PbSe QDs could occur rapidly in a few hours. Halide ligand passivation so far appears most effective to stabilize PbSe QDs.^{48,49} Although the oxidation of QDs may be reversed by remediating the oxidative species in some special conditions,^{50,51} it is favorable to prevent the oxidation by producing and using stable QDs. In order to gain higher stability, appropriate manipulation of both QDs and ligands is needed. In particular, strong binding ligands and mixed ligands, which can provide more complete surface passivation, are preferred.⁵²

Oxidized species on the QD surface have immediate consequences to electronic properties, which are directly associated with the production of defect states and solar cell performance.⁴³ In partially oxidized PbS QDs, PbSO₃ can generate shallow trap states located in the bandgap near the conduction band (depth: ~0.1 eV), which actually contributed to the enhanced device performance by extending the effective lifetime of charge carriers.⁴³ In clear contrast, PbSO₄ presented on the surface of larger PbS QDs (e.g. $E_g = 0.8$ eV) are believed to produce mid-gap trap states (depth: ~0.3 eV),⁴³ acting as the detrimental recombination centers of the charge carriers. It reduces the excited state lifetime and the effective carrier mobility, which caused catastrophic loss of performance of the solar cell.⁵³ It should be noted that even before producing oxidization products, adsorbed oxygen can already have negative impact on electrical processes. Scanning probe based spectroscopic analysis and DFT calculations revealed that detrimental in-gap states are highly likely dominated by molecular oxygen introduced during the post-synthesis processes rather than in the material synthesis.⁵⁴ Less passivated QD surface tends to have more adsorbed oxygen molecules. This finding highlights once again the importance of attaining completely passivated QDs by making good use of surface engineering concepts. Both appreciable oxygen adsorption and subsequent uncontrolled post-synthesis oxidation that deteriorate device performance should be avoided.

Specifically for the manipulation of ligands in QD solar cells, ligand exchange process has to be mentioned, which has been a key factor for achieving not only the improved stability, but also the high efficiency of QD solar cells. As prepared QDs are normally capped by long insulating alkyl chain organic ligands, which are very effective to disperse and stabilize QDs in solution. The long ligands also improve the QD chemical stability and optical properties by occupying the trap states caused by unsaturated dangling bonds. Nonetheless, for solar cell applications especially those relying on the compact QD layer, these ligands can lead to very poor device performance by increasing the inter-QDs spacing in the solid state and acting as insulating barriers for charge carriers. With their relatively large size, they are also less capable of passivating the mid-gap trap states as compared to shorter ligands. These factors make ligand exchange, either in solid state or in solution phase, a very important process in solar cell fabrication.^{52,55} For the purpose of reducing the inter-dot distance and improving the electronic coupling between QDs, organic ligands with shorter chains, such as mercaptopropionic acid

(MPA) and 1,2-ethanedithiol (EDT), are favored and have been demonstrated very helpful in improving the charge carrier mobility of QD films.^{4,56} These thiol ligands have strong binding to the QD surface, facilitating efficient ligand exchange. Besides these short organic ligands, atomic inorganic ligands such as Cl⁻, Br⁻, I⁻ are also introduced as exchanging ligands in the PbS or PbSe QDs layer.^{16,30} With the smallest size (~0.1 nm vs EDT: ~0.5 nm), halide ligands are accessible to surface sites that are otherwise inaccessible to most of the organic ligands and can provide better coverage and coordinate with the deep mid-gap trap states as well, in comparison to organic ligands. An even better strategy, known as hybrid ligand passivation, involves the use of mixed inorganic ligands (*e.g.*, halides) and organic crosslinkers (*e.g.*, MPA) during the ligand exchange to achieve both excellent passivation and highly efficient charge transport in the QD layer.⁵² Such hybrid passivated QDs showed the lowest density of states, $2 \times 10^{16} \text{ cm}^{-3} \text{ eV}^{-1}$, in the band gap based on transient photovoltage measurements.⁵² This value was several times lower than those in the cases where organic or inorganic ligands were used alone. Interestingly, ligands are found to be able to tune the band energy levels and even the electronic nature of QDs.^{17,55} Such tunability enables the design and construction of different device architectures (such as p-n homojunction), offering an alternative way to improve the performance of QD solar cells that will be discussed in the later text. Meanwhile, the doping level can also be varied.⁵⁷ In most of the cases, the doping process with ligands can be well explained by a charge transfer process between QDs and ligands. All these interesting findings pinpoint that comprehensive considerations have to be taken in selecting appropriate ligands for achieving both stability and high PCE of QD-based solar cells.

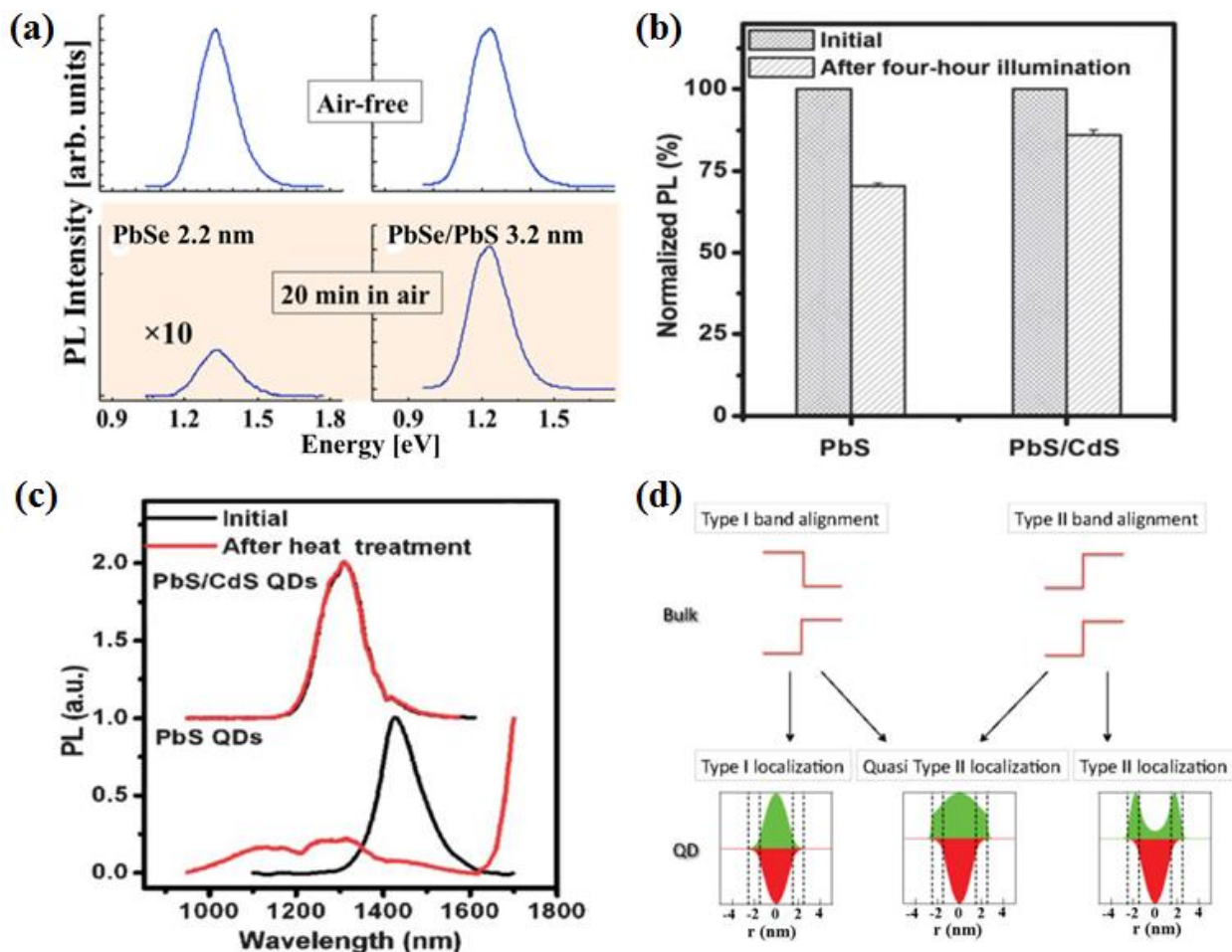


Figure 2. (a) Comparison of the PL spectra of 2.2 nm PbSe and 3.2 nm PbSe/PbS QDs recorded at room temperature under air-free conditions and after air exposure for 20 min. Reprinted from ref 61. Copyright 2014 American Chemical Society. (b) Variation in the PL intensity of PbS and PbS/CdS QDs in octadecene after 4 h of continuous illumination. (c) PL spectra of PbS and PbS/CdS QDs before and after heat treatment (PbS: 100 °C for 5 min in octadecene; PbS/CdS: 150 °C for 30 min in octadecene). (b) and (c) reprinted from ref 60. Copyright 2011 Royal Society of Chemistry. (d) Core/shell QDs can be divided in three types, depending on the localization of the electron and hole wave function. In type-I, electron and hole are confined in the same region (either core or shell), in type-II, they are spatially separated. In a quasi-type-II one carrier is fully delocalized over the entire volume and one is localized in one region. Reprinted from ref 62. Copyright 2011 American Chemical Society.

The passivation layer can also be made of an epitaxial, robust inorganic shell. In this case, QDs have a core/shell structure. NIR core/shell QDs have been largely explored in many fields, such as bioimaging and biosensing, but so far their use in NIR QD solar cells is limited. Although QD surface engineering made tremendous progress during past five years, constituting one of the

most important contributions to the PCE improvement of QD solar cells, it has been mainly focused on ligand passivation/exchange. However, the ligand layer may deteriorate from initial good passivation with time, leaving new surface defects that act as charge carrier traps. Moreover, during the solid-state ligand exchange process, incomplete ligand coverage and degraded passivation of the QD surface may occur due to ligand loss, generating new trap states. It is also highly desired to simultaneously passivate both cationic and anionic surface sites of QDs from both solar cell PCE and stability points of view. In this context, the core/shell structure, as an alternative effective way, was recently proposed to improve the passivation of the QD surface by simultaneously removing both the anionic and cationic dangling bonds and greatly enhance the chemical-/photo-stability of QDs through forming a robust, epitaxial shell.⁵⁸⁻⁶⁰ As shown in **Figure 2a**, after 20 min of air-exposure the photoluminescence (PL) intensity of the PbSe QDs was decreased by 30-fold and the peak was blue-shifted by 20 meV, indicating the formation of trapping sites due to surface oxidation.⁶¹ In clear contrast, the core/shell PbSe/PbS QDs were rather stable with PL intensity and emission peak position remaining nearly unchanged. As for photo-/thermal stability, enhancement was also observed for PbS/CdS core/shell QDs with respect to PbS QDs (**Figure 2b** and **2c**).⁶⁰ All these enhancements are highly important for the actual application of QDs in solar cells.

Depending on the relative energy levels of core and shell semiconductor materials and thereby the confinement region of electrons and holes, the core/shell QDs can be mainly divided to type I, type II and quasi-type II structures (**Figure 2d**).⁶² PbS/CdS and PbSe/PbS, two kinds of the most commonly reported NIR core/shell QDs have been identified to exhibit the quasi-type II band alignment, in which at least one type of charge carrier is localized in core or shell while the other one is delocalized in the entire core/shell volume.^{58,61,63} For solar cell applications, both electrons and holes should be extracted from individual QDs. Our group has studied in detail the charge transfer behavior of PbS/CdS core/shell QDs of different core sizes and shell thickness using electron and hole scavengers.⁵⁸ It was found that as long as the shell thickness is not too thick and the core QDs and scavengers can form appropriate energy level alignment, both electrons and holes can be efficiently transferred. Along with enhanced stability, these core/shell QDs are promising as stable photoactive materials for solar cell applications. Additionally, it gets more attractive to combine this strategy with the ligand exchange process to achieve even better

stability.⁶⁴ In most of the cases, NIR QDs with a relative thin shell are more appropriate for solar cell application. In a special condition, the situation can be changed in order to take advantage of the carrier multiplication effect by forming a thick shell.⁶⁵

Air-processability and Long-term Stability of NIR QD Solar Cells

With the recent tremendous progress of surface engineering, more and more NIR QDs with better air-stability have successfully been synthesized, which is highly beneficial for the air-processable fabrication and long-term running of NIR QD solar cells. Steadily increasing attention has now been drawn towards achieving air-processable, stable QD solar cells. Having that said, the relevant reports in the literature, although very useful, remain limited. In addition, more in depth analysis of the fundamental reasons of improved stability is needed. It should also be noted since the stability was studied under different conditions, cautions need to be taken in making direct comparison in some cases.

In general, surface ligand engineering can assist with solar cell PCE, air processibility and long-term stability in three ways: i) providing better surface passivation to prevent QD degradation; ii) varying the QD energy levels to allow the optimization of device structure and iii) changing the nature of doping to permit the formation of an n-type air stable QD layer and QD-homojunction solar cells, different from the most common QD-based heterojunction solar cells.

Attempts to investigate and enhance stability have been made with several types of ligands, from relatively weak-binding to strong-binding short organic ligands, further to ultrasmall, strong-binding inorganic halide ligands. For example, strongly bound benzenedithiol can offer better surface passivation and therefore stability than weakly bound butylamine.³³ As shown in **Figure 3a**, the benzenedithiol-treated PbSe QD Schottky junction devices exhibited considerably better long-term stability in air than that of the devices based on PbS QDs with butylamine as passivation ligands stored in nitrogen, although PbS QDs are usually considered to be more stable than PbSe QDs. The former retained ~80% of their PCE over 48 h when stored in air, while in clear contrast, the latter almost completely lost its performance within 40 h under nitrogen protection. The interaction of butylamine with the top metal contact was considered as another reason for the lower stability. It may be noted that the spin-coating process of the QD active layer before ligand exchange was carried out in a glovebox, the air-processability of these

QDs may be further improved. The PCE of 1.1% was achieved under simulated solar illumination with a high PCE obtained under NIR illumination (**Figure 3a**). As aforementioned, smaller QDs are more stable than larger ones. The use of relatively small PbS QDs (with a ~930 nm bandgap) and strongly bound EDT allowed the entire fabrication of the Schottky junction devices to be carried out in ambient environment yet leading to a higher PCE (>2%).⁴³ The device was tested in air under continuous simulated solar illumination without encapsulation for 63 h, and was able to maintain 87% of the initial PCE, which represented one of the best stability performance at that time. In addition to the role of ligands, the contribution from the unique surface feature of small QDs to enhanced device stability was well explained (**Figure 1c and 1d**), which provide a method for improving stability. Although above strong bound and short organic ligands were effective for device stability to a certain extent. The dangling bonds still existed on the QD surface. Further improvement of the ligand surface coverage of QDs is a key for achieving excellent stability.

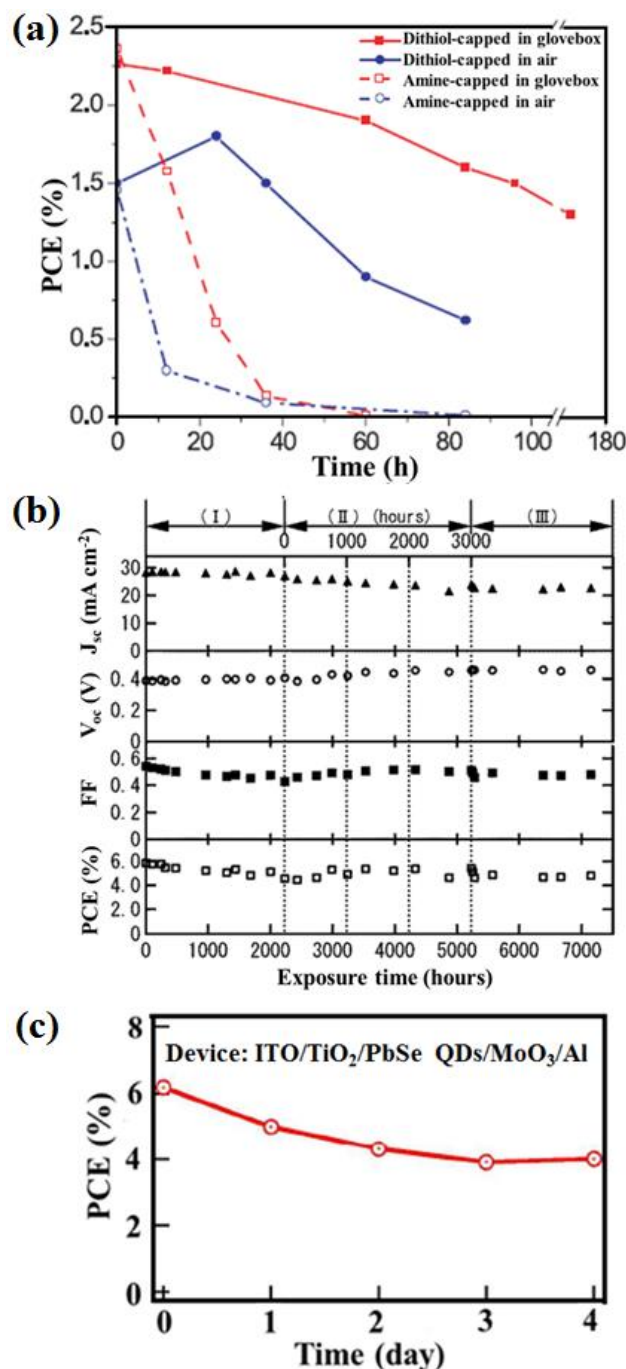


Figure 3. (a) PCE stability comparison of benzenedithiol-treated PbSe devices with previously reported amine-capped devices stored in air and in inert atmosphere. The reported PCE values were taken under 12 mW cm⁻² at 975 nm. Reprinted from ref 33. Copyright 2008 American Chemical Society. (b) Time course of the performance of Br⁻ capped PbS QD-based solar cells during long-term stability tests. The solar cell was stored under ambient atmosphere for the first 2200 h (I: pre-air stability test), then exposed to a Xe lamp with an AM1.5G filter (100 mW cm⁻²) for 3000 h (II: continuous light soaking test), and thereafter stored

under ambient atmosphere (III: post-air stability test). Reprinted from ref 66. Copyright 2014 Wiley-VCH.
(c) PCE evolutions of a hybrid passivated PbSe QD-based solar cell when it was stored in air. Reprinted from ref 48. Copyright 2014 American Chemical Society.

Considering better surface passivation, the use of ultrasmall, strongly bound monovalent halide anions (Cl^- , Br^- , I^-) represent a more effective strategy for achieving improved stability, which means that the small halide anions narrow the distance between QDs compared with above organic ligands. For example, the film of Br^- capped PbS QDs has been formed under ambient atmosphere and the resulting PbS/ TiO_2 bilayer heterojunction solar cells showed a record high PCE up to 6% at that time, significantly higher than that of organic ligand passivated QD devices.¹⁶ Good stability was also achieved, with 80% of pristine PCE being retained after storage in air for six days.¹⁶ In this study, surface S anions were also capped following the CdCl_2 treatment in solution, further improving the surface coverage of PbS QDs. In another study, with only Br^- capping, excellent long-term stability was achieved in PbS/ ZnO -nanowire-array bulk heterojunction solar cells during both air storage and under continuous simulated solar illumination without any device encapsulation.^{66,67} No obvious PV performance degradation was observed after more than 1000 h storage in air. Approximately 90% of the pristine PCE (5.75%) was retained after 3000 h light soaking testing (**Figure 3b**),⁶⁶ which was among the best long-term stability performance under illumination reported for QDs-based solar cells. The slight decrease is mainly attributed to the oxidation of PbS QDs. Such stability represents a clear improvement as compared to most of the cases when organic ligands are solely involved.

Organic-inorganic hybrid passivation treatment promises to yield both good passivation and a compact QD layer. The multiple-type-ligand protected QDs are highly promising for producing stable solar cells in addition to leading to high PCE. In one case, MPA molecules were used to form an outer ligand shell and shorten the distance between QDs, while the Cl^- ions fill the interspace between MPA molecules inaccessible owing to the steric effect and reach the deep mid-gap trap states.⁵² Moreover, the surface S sites were passivated by introducing Cd^{2+} ions during the solution state ligand exchange process, which further reduced recombination channels of photogenerated charge carriers.^{51,52} These well passivated PbS QDs led to a certified PCE of ~7% for heterojunction solar cells fabricated under an ambient atmosphere. The PCE degradation was saturated at about 15% decrease after their storage in a N_2 glove box for five days. A similar

strategy was applied to PbSe QDs, which are much less stable than PbS QDs. With cation exchange approach Cd^{2+} ions were introduced in solution to passivate Se^{2-} sites, and Pb^{2+} sites were passivated by both Cl^- and EDT. Air processed heterojunction solar cells based on such PbSe QDs achieved an impressive PCE of over 6%.⁴⁸ After being stored in air for four days, the PCE of the device decreased from $\sim 6.2\%$ to 4% (**Figure 3c**), which may be further improved though. Although the beneficial effect of the hybrid passivation on improving PCE is clearly demonstrated in the above-mentioned reports, its advantage with respect to halide passivation on stability remains to be manifested through further optimization.

In addition to directly contributing to the stability of QD solar cells by passivation, ligands can “indirectly” help with both stability and PCE by enabling the realization of better device structures through their capability of tuning the electronic properties of QDs. Thanks to the high surface-to-volume ratio of QDs, ligands were found to be able to considerably shift the band energy levels of QDs by forming dipoles with QD surface atoms and by presenting their intrinsic dipoles on the QD surface and therefore are capable of manipulating the band alignment of QDs with respect to other semiconductors. For similarly sized PbS QDs, the conduction and valence energy levels can be drastically shifted by up to 0.9 eV via carrying out different ligand treatment.⁶⁸ Taking advantage of this unique feature, PbS QDs of different Fermi levels and band gap energy were introduced to PV devices, allowing addressing the device stability and improving PCE by optimizing the interfacial layer between the major photoactive QD layer and electrode.⁵⁵ As shown in **Figure 4a**, a thin EDT-capped PbS QD layer replaces commonly used MoO_3 and acts as an electron blocking layer or a hole extraction layer in between the major light absorber, the PbS QD film passivated with tetrabutylammonium iodide (TBAI), and the anode. With the favourable band alignment between the QD layers, the use of I^- passivated QD layer and the removal of the MoO_3 interfacial layer, the air processed, un-encapsulated devices achieved an impressively high certified PCE (8.55%) (**Figure 4a**) and outstanding long-term stability, with no performance change being observed for over 150 days of storage in air (**Figure 4b**), among the best long-term stabilities reported so far. Using the similar strategy, i.e., with the thin MPA treated PbSe interfacial layer and halide passivated PbSe QD film as the absorber layer, PbSe QD solar cells also gained impressively good air stability.⁶⁹ Without encapsulation, the device performance remained unchanged for over fifty days in air.

It is noteworthy to point out although the operation of all the aforementioned QD solar cells is based on the p-type QDs, ligand engineering also allows the formation of an air-stable n-type QD layer, which is challenging to achieve in general. Ligands can change the electronic nature of a QD film by acting as dopants.^{57,70} QDs treated with halide ions in an inert atmosphere can show the n-type semiconductor property.⁵⁷ This enables the construction of p-n homojunction solar cells via using oppositely doped QDs on each side of the junction. The effect of halide ligands (I⁻, Br⁻, Cl⁻) treatment on the stability of the n-type QD layer is quite different.¹⁷ As shown in **Figure 4c**, I⁻ treated devices show no obviously performance change after air exposure for ~100 h, while Br⁻ and Cl⁻ treated samples significantly degraded due to QD oxidation. This observation is very different from the halide treated p-type QD layers, where halide ions are generally able to enhance device stability. As seen from **Figure 4d**, the amount of I⁻ ions is much higher than that of Cl⁻ and Br⁻ ions on the QD surface and I⁻ ions can bind much more strongly to the QD surface. Higher surface coverage and strong binding lead to more effective surface passivation and excellent capability of repelling oxidative attack (**Figure 4e**); even trace amounts of oxidation can switch the QDs from the n-type to p-type. The strong binding affinity of I⁻ ions can be explained from the soft/hard base/acid theory.⁷¹ Basically, the soft base iodide binds more strongly than hard base of chloride and bromide to soft acid lead atoms on the QD surface. In addition, the strong binding of I⁻ ions was further confirmed by DFT simulations. The energy demanded to remove iodide ligands is greater than that of other halides.¹⁷

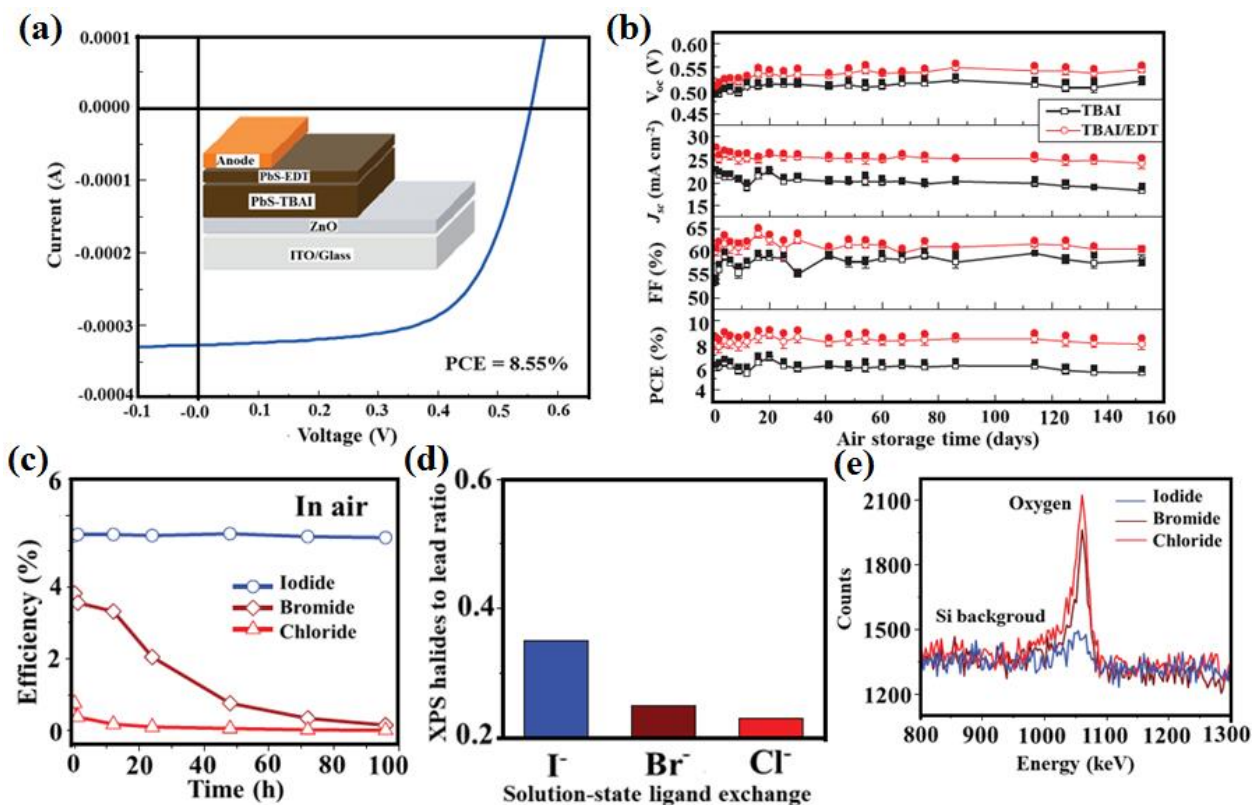


Figure 4. (a) Device performance of a PbS-TBAI/PbS-EDT device certified by an accredited laboratory (Newport) after thirty-seven days of air storage, insert: the device structure. (b) Evolution of PV parameters of un-encapsulated devices PbS-TBAI (black) and PbS-TBAI/PbS-EDT (red) devices with Au anodes in air storage. Open symbols represent the average values and solid symbols represent the values for the best performing device. (a) and (b) reprinted from ref 55. Copyright 2014 Rights Managed by Nature Publishing Group (c) Efficiency of conventional quantum junction devices tested in air and followed over four days (100 h) (d) Atomic halide to lead ratio of the QDs after solution-state ligand exchange. The amount of iodide ligands is much higher than chloride and bromide ones. (e) Rutherford backscattering spectrometry results revealing the oxide content in the film following air exposure for four days. (c), (d) and (e) reprinted with permission from ref 17. Copyright 2016, Rights Managed by Nature Publishing Group.

An alternative potentially effective way to enable air processability and achieve long-term device stability is to form a stable core/shell QD structure. Importantly, the core/shell structure needs to be tailored in such a way that electrons and holes photo-generated inside the core dots can smoothly travel through the shell and become available for the transport among the QD network or the transfer to other semiconductors, which is the key factor in PV applications.^{62,72} Shell thickness needs to be optimized to have a balance between device stability and PCE in order to realize overall high performance solar cells. As shown in **Figure 5a**, the core/shell PbS/CdS QD-

sensitized devices had less photocurrent degradation after 1 h illumination than that of shell-free PbS QD-sensitized devices, since the CdS shell can prevent the PbS core from photocorrosion.⁷³ However, the PCE of the thicker shell sample was lower (0.73% vs 1.18%) than that of the thinner shell sample. Through optimizing the CdS shell thickness (optimal shell thickness: 0.33 nm), the PbS/CdS QD-sensitized device achieved the PCE of 7.19%, among the best performance for liquid-junction PbS QD-sensitized solar cells.⁷⁴ The long-term stability of core/shell QD solar cells needs to be further studied.

Regarding air processability, our group fabricated the bulk heterojunction device based on PbS/CdS core/shell QDs with 0.1 nm thick shell and TiO₂ nanorod arrays in air. While fabricated under otherwise same conditions, the PCE (2.0%) of the PbS/CdS QD devices fabricated in air was much higher than that (1.5%) of the pure PbS QDs ones fabricated under inert atmosphere (**Figure 5b**).⁷⁵ With further device optimization, the PCE of 4.4% was subsequently achieved for air-processed PbS/CdS QD solar cells.⁷⁶ In these studies, only a single type ligand of MPA was used to cap the QDs. As an ultrathin shell may not be thick enough for satisfactory device stability even though core/shell QDs devices are already better than pure QDs devices, ligand engineering is still demanded. With the hybridization passivation strategy, the higher efficiencies of ~5.6% and 6.5% were obtained for the heterojunction devices, based on PbS/CdS and PbSe/PbS QDs, respectively.^{64,77} Although the efficiency of the core/shell QDs solar cells is still lower than that of shell-free NIR QDs devices, considering enhanced stability and air processability, it is worth carrying out more studies on these core/shell QDs based solar cells.

In brief, multiple aspects should be considered to improve both the stability and PCE of NIR QD solar cells. For choosing ligands, they should strongly bind to and fully cover the QD surface and meanwhile are small enough to decrease the distance between QDs to enhance charge carrier transport. Optimized core/shell QDs with favorable air processability and stability are an alternative, promising choice. On the basis of the influence of different surface ligands on the energy level of QDs, combining QDs capped with different types of ligands in the same QD solar cell is another effective way to obtain both the stability and preferable PCE. A comprehensive consideration needs to be taken in designing an approach toward achieving the overall excellent performance of QD solar cells.

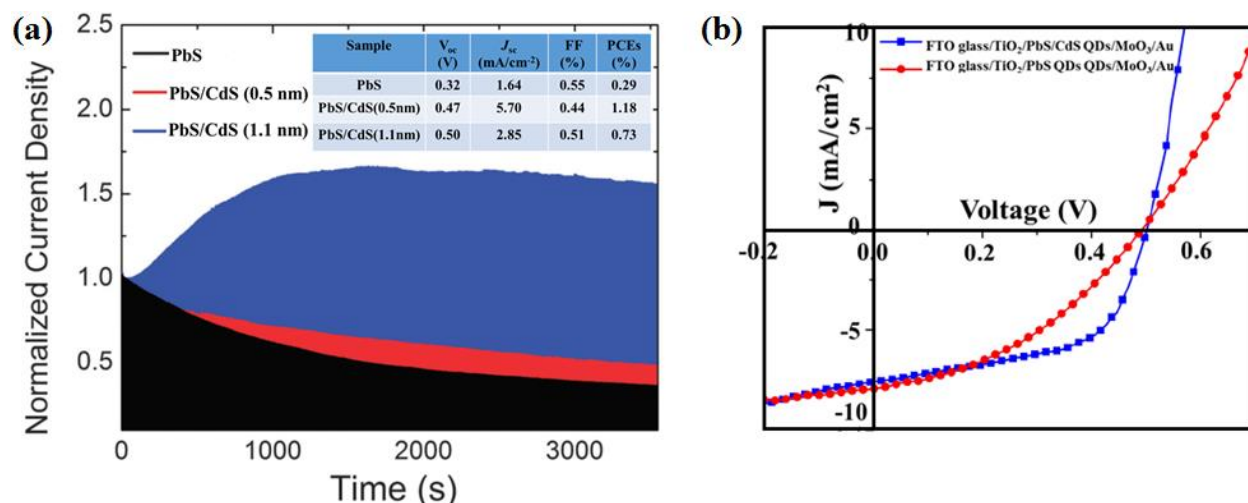


Figure 5. (a) Stability test of QDs-sensitized solar cells fabricated using PbS and PbS/CdS QDs. The normalized photocurrent was measured for 1 h under short circuit conditions under 1 sun AM 1.5 G, chopped light (1s on and 1s off). Insert: Summary of the electrical output of the device. Reprinted from ref 73. Copyright 2014 Royal Society of Chemistry. (b) J-V curves of the devices based on PbS/CdS QDs or PbS QDs. The spin coating and ligand exchange of the PbS/CdS QDs were fabricated in ambient atmosphere; the spin coating and ligand exchange of the PbS QDs were processed in a glovebox. Reprinted from ref 75. Copyright 2014 Elsevier B.V.

Towards Stable NIR QD Ink Solar Cells

For practical applications, NIR QD inks, which can be stored for long-term without any obvious degradation in the structure and dispersion status of QDs is highly desirable. Ideally, the NIR QD inks for large-scale fabrication should have three essential characteristics during the long-term storage. Firstly, QDs should be resistant to chemical oxidation or other forms of chemical degradation, which can negatively affect final device performance. Secondly, they should not show any obvious agglomeration with certain time in solution, allowing them to be deposited into uniform thin films with high batch to batch reproducibility. Similarly importantly, the QDs with the above mentioned stability should be well capped by short ligands, instead of long ligands, and can thus be directly fabricated into functional devices in a one-step film deposition process without the need for any subsequent ligand exchange process. Different types of ligands, such as short organic ligands, inorganic molecular metal-chalcogenide-complex (MCC) ions, halide ligands, metal cation ligands and metal free ligands have been explored for preparing the NIR QD inks.^{21,49,78-80} Among them, mixed ligands capped QDs led to the highest photovoltaic

device performance reported recently, while MCC ligand capped QDs the highest charge carrier mobility.

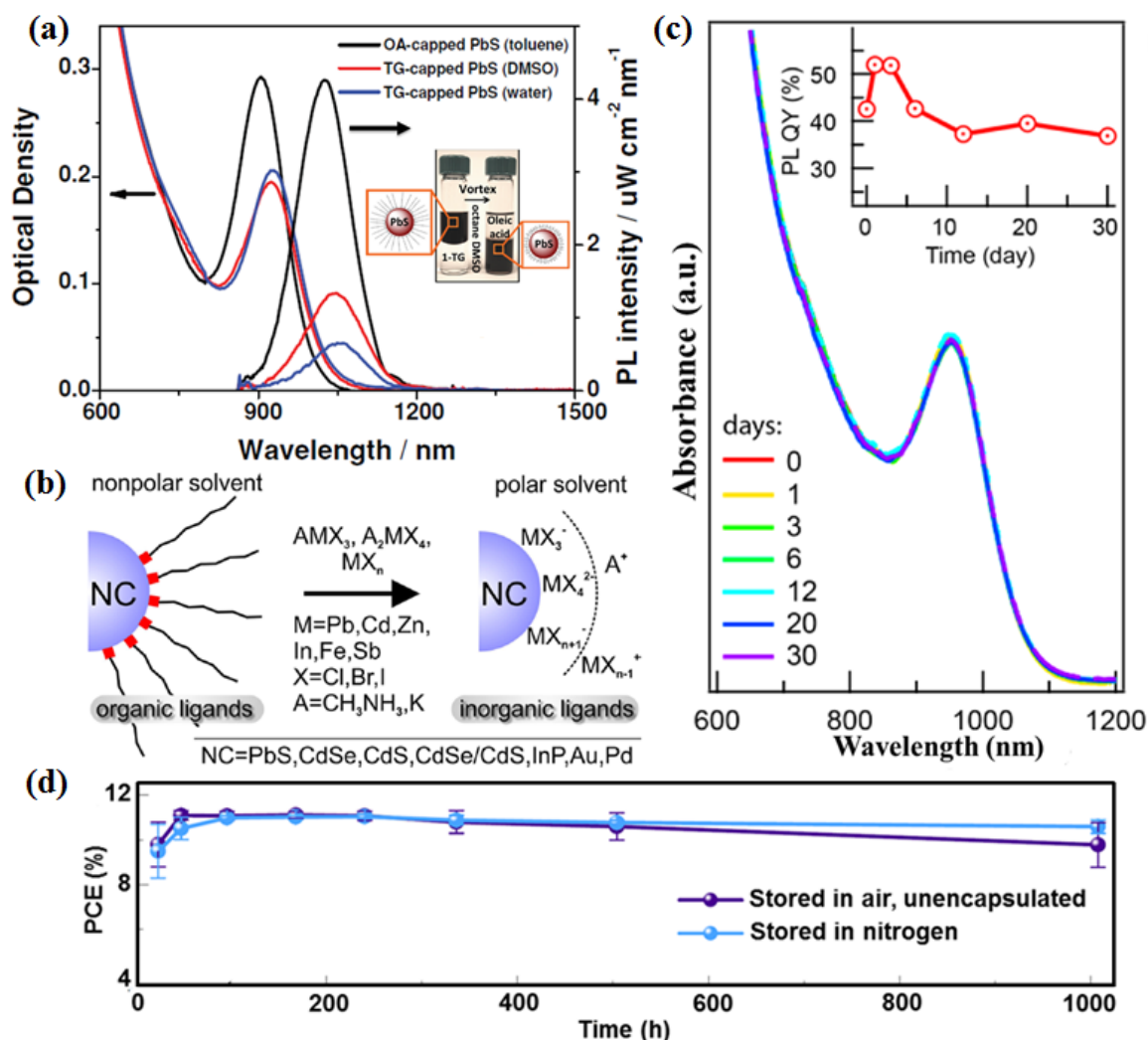


Figure 6 (a) Absorbance and photoluminescence of PbS QDs displaying preserved quantum confinement and quenched photoluminescence after the ligand exchange. Inset is the photograph of the as-synthesized long-ligand-capped PbS QD solution before the solution exchange (left) and the exchanged short-ligand-capped QD solution in a non-polar solvent (right). Reprinted from ref 78. Copyright 2013 Wiley-VCH. (b) Schematics of the ligand-exchange methodology for obtaining halometallate-capped colloidal nanocrystals. Reprinted from ref 81. Copyright 2014 American Chemical Society. (c) Temporal evolution of absorption spectra of hexane solutions of PbSe QDs with the first excitonic peak at 950 nm stored in air. The inset displays the corresponding PLQY as a function of time. Reprinted from ref 48. Copyright 2014 American Chemical Society. (d) Stability test for PbS QD ink fabricated devices stored in air and nitrogen. Reprinted from ref 21. Copyright 2016, Rights Managed by Nature Publishing Group.

Among a few studies on QD ink fabricated solar cells, a major approach to obtain the QD ink is solution-phase ligand exchange. For instance, OA-capped PbS QDs were transferred from octane to dimethyl sulfoxide (DMSO) by efficiently replacing the OA ligand with small hydrophilic mercaptans, such as 1-thioglycerol (TG), thiolactic acid and dimercaptpropionic acid, with TG treatment yielding the best colloidal stability over weeks.⁷⁸ One-step drop casting of the TG-PbS QD ink led to the efficiency of 2.1% for resultant solar cells. The photoluminescence quantum yield (PLQY) of PbS QDs ink decreased after ligand exchange (**Figure 6a**), suggesting that surface passivation should be further improved.

Ligand exchange in solution with lead halide perovskites ($\text{CH}_3\text{NH}_3\text{PbI}_3$), which can form an epitaxial thin shell for improved surface passivation, was also found to be able to yield high quality PbS QD colloidal solutions stable for months without distinct aggregation or precipitation (**Figure 6b**).⁸¹ It offers a new pathway towards making stable QD inks. Single-step-deposition of the ink of PbS QDs capped with $\text{CH}_3\text{NH}_3\text{PbI}_3$ led to a solar cell device with a quite high PCE of 8.95%, much higher than what can be achieved with short organic ligands.⁸² It should be noted that the perovskite-capped PbS QD film was annealed under nitrogen atmosphere, which perhaps suggests that the air stability needs to be further improved by engaging more stable perovskite materials. Compared with organic ligands, perovskites have favorable carrier transport. Therefore, the approach based on the use of perovskites as ligands promises both high stability and PCE.

With strong passivation effect, liquid phase treatment with halide ions is also considered to be an effective approach to form QD inks. Halide termination is mainly done in solution by ligand exchange.^{83,84} In situ chloride and cadmium double passivation through a cation exchange reaction was also applied to instable PbSe QDs.⁴⁸ Since both Pb and Se sites were passivated, this approach led to very stable colloidal PbSe solution. Both the peak position and intensity of absorption spectra and the PLQY of PbSe QDs stored in air remained constant for at least thirty days (**Figure 6c**).⁴⁸ Very recently, a ligand exchange process using the mixed solution of PbX_2 ($\text{X} = \text{Br}$ and I) and ammonium acetate led to a hybrid organic-inorganic QD ink in air, resulting in significantly enhanced, high performance PbS ink based solar cell devices.²¹ The key is that with the aid of ammonium protons, initial OA ligands were completely replaced by $[\text{PbX}_3]^-$ anions and the organic cations were subsequently washed away by solvent, leaving clean $[\text{PbX}_3]^-$

/[PbX]⁺ double-capped PbS QDs with improved surface passivation. In addition to a record high PCE of 11.28%, the excellent long-term stability was obtained with 90% of initial PCE retained after 1000 h storage in air without encapsulation (**Figure 6d**). However, for industrialization, the efficiency and stability of the devices need to be further improved.

In a parallel vein, inorganic and non-halide anions are explored in order to increase carrier mobility of QDs. They indeed opened a highly promising avenue with a vast range of choices to form the air-stable QD ink for device fabrication. For instance, Talapin *et. al.* explored the NIR PbS QDs capped by diverse types of ligands, including metal chalcogenide ligands (such as Sn₂S₆⁴⁻ and AsS₃³⁻), and metal-free inorganic ligands (such as TeS₃²⁻).^{79,80} Similar to organic ligands, these anions bind strongly only with cations (Pb sites) on the QD surface, leaving the chalcogenide sites unpassivated. But unlike most of the organic ligands that offer steric stabilization, these ligands render the QD surface negatively charged. As a consequence, the resultant QDs showed electrostatic repulsion and exhibited good colloidal stability in polar solvents. In particular, metal chalcogenide ligands led to preferable carrier mobility between individual nanocrystals, thanks to their role as molecular solders, producing the electrical coupling in the QD film.^{85,86} However, the solar cell devices based on the NIR QDs capped with these ligands have yet to be extensively studied. Reducing the defect density of the films is an important research direction.

In addition, our group developed NIR PbS/CdS/ZnS QDs with a core/shell/shell structure capped by a short ligand of mercaptopropionic acid, which showed excellent stability in aqueous solution for over 14 months.⁸⁷ The shells show the better effect on keeping the air stability of QDs compared with ligands, meanwhile the suitable surface ligands of the core/shell/shell remain the long stability of QDs inks. Importantly, whether the shells or surface ligands don't affect charge transport between QDs. Although it may be reasonably questioned that two shells can serve as barriers for carrier transport, they actually show high potential for solar cell application once the thickness of two shells can be respectively optimized for balancing charge transport and stability. Such an approach is indeed highly feasible. It was demonstrated that the devices based on the PbS/CdS/ZnS layered structure as light absorber obtained good efficiency of 4.65% after ligands exchange.⁸⁸ It is thus worthwhile to further explore these very stable colloidal core/shell/shell QDs for solar cell application.

In brief, to produce high-quality QD inks for PV device fabrication, the ligands and shells can be combined to serve as protection layers. They should also be optimized to facilitate charge carrier transport. Despite some promising results, overall, reports on NIR QD ink-based solar cells remain lacking. Considering recent, important progress on the PCE of QD solar cells, which makes them closer to commercial applications, much more attention is expected in this research and development direction.

Challenges and Outlook

Over the past 5-10 years, our understanding on the surface chemistry of QDs, such as QD surface geometries, the geometry and intermolecular structure of the ligand layer, core/shell interfaces, surface-ligand bonding and their dynamic interactions, has been tremendously improved. It is largely attributed to the development of new computational techniques and their combination with in-depth experimental explorations. Certain primary QD surfaces have been re-constructed by modeling, which sheds lights on the surface structure details “unmeasurable” by current experimental techniques. Variable experimental tools, such as XPS and nuclear magnetic resonance, have been employed to probe the QD surface. Thanks to these advances, QD surface engineering concept has been used in the field of QD solar cells, mainly in attaining higher PCE. In the same way, QD surface engineering is expected to make a huge impact on the stability issues related to the manufacture and use of QD solar cells, the research of which is falling behind yet highly important for the eventual widespread implementation of QD solar cells. As a matter of fact, the stability represents one of the great challenges for practical use of QD solar cells.

Long-term stability of QD solar cells still needs to be fully and systematically investigated under different conditions, for example, temperature, humidity, and continuous light illumination. QD inks and air processability also require more intense investigations. It is important to gain deep insights on the mechanisms of the QD film and device degradations under different conditions by combining various characterization and analysis tools, which can then guide future work and lead to the design of the most effective surface engineering strategies. We would like to point out that despite the large progress gained on QD surface chemistry, more and deeper QD surface chemistry understanding is still urgently needed by, for example, combining advanced chemical

characterization and a high spatial resolution microscope with theoretical modeling. Then, according to QD surface features, choosing ligands that can provide ideal, complete passivation and strong binding to QDs is a key to gain desired stability. Further optimization of passivation processes with different ligands, including recently emerging perovskites, should also be investigated systematically. On a related note, synthesis of QDs themselves should be further improved to decrease defects because they act as the primary origin of both poor stability and PCE. Some ligands hold high promise to enhance the QD stability during current ligand exchange investigations, which may be adaptable in the QD synthesis process. Additionally, the robust core/shell structure represents another promising alternative to solve the stability problem. In this case, simultaneous optimization of the inorganic shell structure and ligand layer is crucial and deserves more research. Attention should also be made to prepare QD inks in relatively “green” solvents, compatible with large-scale fabrication. It should be noted that, in making an effort to improve stabilities, the important factors related to PCE should be considered. Stability enhancement should not be gained at the significant price of reduced PCE. In view of device structure design of solar cells, optimizations can be conducted by gaining successful experience from perovskite and organic solar cells, in which an additional layer is included in the device as an oxygen/moisture scavenger and/or an interfacial layer to block the side reaction between the active layer and electrodes. Although it is usually preferred to enhance the stability of QDs themselves via surface engineering, such interfacial engineering certainly appears attractive by further enhancing stabilization. Device encapsulation, beyond the scope of the current Perspective, represents another important fabrication step for long-term device stabilization. Although ideally it is desirable to realize highly stable QD solar cells operable under ambient conditions, in reality, device encapsulation is imperative for practical applications. The traditional atomic layer deposition method has been applied to QD solar cells and showed great promise in enhancing performance stability. Recent development of space divided atomic layer deposition further makes this technique potentially scalable. On the other hand, encapsulation methods developed for the RTR fabrication of organic PV devices, such as the lamination method comprising UV curing, pressure-sensitive adhesives, or hotmelt, can be potentially applied to QD solar cells.^{89,90} In brief, in order to achieve the final goal of attaining high-efficiency, cost-effective, and highly stable QD solar cells suitable for practical applications, a

multidisciplinary approach, involving close collaboration of chemists, physicists, theorist, and device engineers, is indispensable.

AUTHOR INFORMATION

Corresponding Author

*E-mail: ma@emt.inrs.ca. Website: <http://www.inrs.ca/dongling-ma/>.

Biographies

Long Tan is currently a Ph.D. candidate under the supervision of Prof. Dongling Ma and Prof. Mohamed Chaker at Institut national de la recherche scientifique-Énergie Matériaux Télécommunications (INRS-EMT). His mainly conducts research on the synthesis of NIR QDs and their applications in photovoltaics technologies.

Pandeng Li is currently a Ph.D. student supervised by Prof. Dongling Ma at INRS and Prof. Baoquan Sun from Soochow University. His research is focused on the application of quantum dots into the organic photovoltaic devices mainly based on low-bandgap polymers.

Baoquan Sun is a full professor of Institute of Functional and Soft Materials (FUNSOM) at Soochow University in Suzhou. He received his PhD in Chemistry at Tsinghua University in Beijing in 2002. He used to be a postdoc. in Prof. Friend's group in Cavendish Laboratory at Cambridge University and in Dr. Klimov's group at Los Alamos National Laboratory. His main research field is dedicated to the physical characterization of conjugated polymer and semiconductor nanostructure, their application in solar cell and light emitting diode.

Mohamed Chaker is a full professor at INRS. Since 2003, he has been holding a Tier I Canada Research Chair in Plasmas applied to micro and nanomanufacturing technologies. His contributions are mainly in the field of plasma-based synthesis and etching of innovative materials at the nanoscale for the fabrication of photonic and energy devices.

Dongling Ma is working as a full professor at INRS. Her main research interest consists in the development of various nanomaterials (e.g., quantum dots, catalytic nanoparticles, plasmonic nanostructures, and different types of nanohybrids) for applications in energy, catalysis and biomedical sectors.

Notes

[[†]] the authors contributed equally to this work.

The authors declare no competing financial interest.

ACKNOWLEDGMENT

Financial support from the Natural Sciences and Engineering Research Council (NSERC) of Canada, in the context of NSERC Discovery and CRD Grants, is greatly appreciated. D. Ma is also grateful for the financial support from Fonds de recherche du Quebec-Nature et technologies (FRQNT) and Quebec Center for Functional Materials (CQMF), Canada.

REFERENCES

- (1) Kamat, P. V. Quantum Dot Solar Cells. Semiconductor Nanocrystals as Light Harvesters. *J. Phys. Chem. C* **2008**, *112*, 18737-18753.
- (2) Kamat, P. V. Quantum Dot Solar Cells. The Next Big Thing in Photovoltaics. *J. Phys. Chem. Lett.* **2013**, *4*, 908-918.
- (3) Kim, M. R.; Ma, D. Quantum-Dot-Based Solar Cells: Recent Advances, Strategies, and Challenges. *J. Phys. Chem. Lett.* **2015**, *6*, 85–99.
- (4) Wang, R.; Shang, Y.; Kanjanaboos, P.; Zhou, W.; Ning, Z.; Sargent, E. H. Colloidal Quantum Dot Ligand Engineering for High Performance Solar Cells. *Energy Environ. Sci.* **2016**, *9*, 1130-1143.
- (5) Gur, I.; Fromer, N. A.; Chen, C.-P.; Kanaras, A. G.; Alivisatos, A. P. Hybrid Solar Cells with Prescribed Nanoscale Morphologies Based on Hyperbranched Semiconductor Nanocrystals. *Nano Lett.* **2007**, *7*, 409-414.
- (6) Wang, D.; Baral, J. K.; Zhao, H.; Gonfa, B. A.; Truong, V.-V.; El Khakani, M. A.; Izquierdo, R.; Ma, D. Controlled Fabrication of PbS Quantum-Dot/Carbon-Nanotube Nanoarchitecture and its Significant Contribution to Near-Infrared Photon-to-Current Conversion. *Adv. Funct. Mater.* **2011**, *21*, 4010-4018.

- (7) Kongkanand, A.; Tvrdy, K.; Takechi, K.; Kuno, M.; Kamat, P. V. Quantum Dot Solar Cells. Tuning Photoresponse through Size and Shape Control of CdSe-TiO₂ Architecture. *J. Am. Chem. Soc.* **2008**, *130*, 4007-4015.
- (8) Robel, I.; Kuno, M.; Kamat, P. V. Size-Dependent Electron Injection from Excited CdSe Quantum Dots into TiO₂ Nanoparticles. *J. Am. Chem. Soc.* **2007**, *129*, 4136-4137.
- (9) Wang, D.; Zhao, H.; Wu, N.; Khakani, M. A. E.; Ma, D. Tuning the Charge-Transfer Property of PbS-Quantum Dot/TiO₂-Nanobelt Nanohybrids via Quantum Confinement. *J. Phys. Chem. Lett.* **2010**, *1*, 1030-1035.
- (10) Tvrdy, K.; Frantsuzov, P. A.; Kamat, P. V. Photoinduced Electron Transfer from Semiconductor Quantum Dots to Metal Oxide Nanoparticles. *PNAS* **2011**, *108*, 29-34.
- (11) Gao, J.; Luther, J. M.; Semonin, O. E.; Ellingson, R. J.; Nozik, A. J.; Beard, M. C. Quantum Dot Size Dependent J-V Characteristics in Heterojunction ZnO/PbS Quantum Dot Solar Cells. *Nano Lett.* **2011**, *11*, 1002-1008.
- (12) Hanna, M. C.; Beard, M. C.; Nozik, A. J. Effect of Solar Concentration on the Thermodynamic Power Conversion Efficiency of Quantum-Dot Solar Cells Exhibiting Multiple Exciton Generation. *J. Phys. Chem. Lett.* **2012**, *3*, 2857-2862.
- (13) Padilha, L. A.; Stewart, J. T.; Sandberg, R. L.; Bae, W. K.; Koh, W.-K.; Pietryga, J. M.; Klimov, V. I. Carrier Multiplication in Semiconductor Nanocrystals: Influence of Size, Shape, and Composition. *Acc. Chem. Res.* **2013**, *46*, 1261-1269.
- (14) Semonin, O. E.; Luther, J. M.; Choi, S.; Chen, H.-Y.; Gao, J.; Nozik, A. J.; Beard, M. C. Peak External Photocurrent Quantum Efficiency Exceeding 100% via MEG in a Quantum Dot Solar Cell. *Science* **2011**, *334*, 1530-1533.
- (15) Hines, D. A.; Kamat, P. V. Quantum Dot Surface Chemistry: Ligand Effects and Electron Transfer Reactions. *J. Phys. Chem. C* **2013**, *117*, 14418-14426.

- (16) Tang, J.; Kemp, K. W.; Hoogland, S.; Jeong, K. S.; Liu, H.; Levina, L.; Furukawa, M.; Wang, X.; Debnath, R.; Cha, D.; et al. Colloidal-Quantum-Dot Photovoltaics Using Atomic-Ligand Passivation. *Nat. Mater.* **2011**, *10*, 765-771.
- (17) Ning, Z.; Voznyy, O.; Pan, J.; Hoogland, S.; Adinolfi, V.; Xu, J.; Li, M.; Kirmani, A. R.; Sun, J. P.; Minor, J.; et al. Air-Stable n-Type Colloidal Quantum Dot Solids. *Nat. Mater.* **2014**, *13*, 822-828.
- (18) McDonald, S. A.; Konstantatos, G.; Zhang, S.; Cyr, P. W.; Klem, E. J. D.; Levina, L.; Sargent, E. H. Solution-processed PbS Quantum Dot Infrared Photodetectors and Photovoltaics. *Nat. Mater.* **2005**, *4*, 138-142.
- (19) Maria, A.; Cyr, P. W.; Klem, E. J. D.; Levina, L.; Sargent, E. H. Solution-processed Infrared Photovoltaic Devices with >10% Monochromatic Internal Quantum Efficiency. *Appl. Phys. Lett.* **2005**, *87*, 213112.
- (20) Lan, X.; Voznyy, O.; Kiani, A.; Arquer, F. P. G. d.; Abbas, A. S.; Kim, G.-H.; Liu, M.; Yang, Z.; Walters, G.; Xu, J.; et al. Passivation Using Molecular Halides Increases Quantum Dot Solar Cell Performance. *Adv. Mater.* **2016**, *28*, 299-304.
- (21) Liu, M.; Voznyy, O.; Sabatini, R.; Garcia de Arquer, F. P.; Munir, R.; Balawi, A. H.; Lan, X.; Fan, F.; Walters, G.; Kirmani, A. R.; et al. Hybrid Organic-Inorganic Inks Flatten the Energy Landscape in Colloidal Quantum Dot Solids. *Nat. Mater.* **2016**, *16*, 258-263.
- (22) Hines, D. A.; Becker, M. A.; Kamat, P. V. Photoinduced Surface Oxidation and Its Effect on the Exciton Dynamics of CdSe Quantum Dots. *J. Phys. Chem. C* **2012**, *116*, 13452-13457.
- (23) Hines, D. A.; Forrest, R. P.; Corcelli, S. A.; Kamat, P. V. Predicting the Rate Constant of Electron Tunneling Reactions at the CdSe-TiO₂ Interface. *J. Phys. Chem. B* **2015**, *119*, 7439-7446.

- (24) Kim, S.; Noh, J.; Choi, H.; Ha, H.; Song, J. H.; Shim, H. C.; Jang, J.; Beard, M. C.; Jeong, S. One-Step Deposition of Photovoltaic Layers Using Iodide Terminated PbS Quantum Dots. *J. Phys. Chem. Lett.* **2014**, *5*, 4002-4007.
- (25) Hong, J.; Hou, B.; Lim, J.; Pak, S.; Kim, B. S.; Cho, Y.; Lee, J.; Lee, Y. W.; Giraud, P.; Lee, S.; et al. Enhanced Charge Carrier Transport Properties in Colloidal Quantum Dot Solar cells via Organic and Inorganic Hybrid Surface Passivation. *J. Mater. Chem. A* **2016**, *4*, 18769-18775.
- (26) Anderson, N. C.; Hendricks, M. P.; Choi, J. J.; Owen, J. S. Ligand Exchange and The Stoichiometry of Metal Chalcogenide Nanocrystals: Spectroscopic Observation of Facile Metal-Carboxylate Displacement and Binding. *J. Am. Chem. Soc.* **2013**, *135*, 18536-18548.
- (27) Choi, H.; Ko, J. H.; Kim, Y. H.; Jeong, S. Steric-Hindrance-Driven Shape Transition in PbS Quantum Dots: Understanding Size-Dependent Stability. *J. Am. Chem. Soc.* **2013**, *135*, 5278-5281.
- (28) Boles, M. A.; Ling, D.; Hyeon, T.; Talapin, D. V. The Surface Science of Nanocrystals. *Nat. Mater.* **2016**, *15*, 141-153.
- (29) Hwang, G. W.; Kim, D.; Cordero, J. M.; Wilson, M. W.; Chuang, C. M.; Grossman, J. C.; Bawendi, M. G. Identifying and Eliminating Emissive Sub-bandgap States in Thin Films of PbS Nanocrystals. *Adv. Mater.* **2015**, *27*, 4481-4486.
- (30) Woo, J. Y.; Ko, J. H.; Song, J. H.; Kim, K.; Choi, H.; Kim, Y. H.; Lee, D. C.; Jeong, S. Ultrastable PbSe Nanocrystal Quantum Dots via In situ Formation of Atomically Thin Halide Adlayers on PbSe(100). *J. Am. Chem. Soc.* **2014**, *136*, 8883-8886.
- (31) Zherebetsky, D.; Scheele, M.; Zhang, Y.; Bronstein, N.; Thompson, C.; Britt, D.; Salmeron, M.; Alivisatos, P.; Lin, W. W. Hydroxylation of the Surface of PbS Nanocrystals Passivated with Oleic Acid. *Science* **2014**, *344*, 1380-1384.

- (32) Ma, J.-X.; Jia, Y.; Song, Y.-L.; Liang, E.-J.; Wu, L.-K.; Wang, F.; Wang, X.-C.; Hu, X. The Geometric and Electronic Properties of the PbS, PbSe and PbTe (001) Surfaces. *Surf. Sci.* **2004**, *551*, 91-98.
- (33) Koleilat, G. I.; Levina, L.; Shukla, H.; Myrskog, S. H.; Sean Hinds; Pattantyus-Abraham, A. G.; Sargent, E. H. Efficient, Stable Infrared Photovoltaics Based on Solution-Cast Colloidal Quantum Dots. *ACS Nano* **2008**, *2*, 833-840.
- (34) Moreels, I.; Justo, Y.; Geyter, B. D.; Haustraete, K.; Martins, J. C.; Hens, Z. Size-Tunable, Bright, and Stable PbS Quantum Dots: A Surface Chemistry Study. *ACS Nano* **2011**, *5*, 2004–2012.
- (35) Webber, D. H.; Brutchey, R. L. Ligand Exchange on Colloidal CdSe Nanocrystals Using Thermally Labile Tert-Butylthiol for Improved Photocurrent in Nanocrystal Films. *J. Am. Chem. Soc.* **2012**, *134*, 1085-1092.
- (36) Munro, A. M.; Plante, I. J.-L.; Ng, M. S.; Ginger, D. S. Quantitative Study of the Effects of Surface Ligand Concentration on CdSe Nanocrystal Photoluminescence. *J. Phys. Chem. C* **2007**, *111*, 6220-6227.
- (37) Morris-Cohen, A. J.; Frederick, M. T.; Lilly, G. D.; McArthur, E. A.; A.Weiss, E. Organic Surfactant-Controlled Composition of the Surfaces of CdSe Quantum Dots. *J. Phys. Chem. Lett.* **2010**, *1*, 1078-1081.
- (38) Mastronardi, M. L.; Hennrich, F.; Henderson, E. J.; Maier-Flaig, F.; Blum, C.; Reichenbach, J.; Lemmer, U.; Kubel, C.; Wang, D.; Kappes, M. M.; et al. Preparation of Monodisperse Silicon Nanocrystals Using Density Gradient Ultracentrifugation. *J. Am. Chem. Soc.* **2011**, *133*, 11928-11931.
- (39) Hill, H. D.; Millstone, J. E.; Banholzer, M. J.; Mirkin, C. A. The Role Radius of Curvature Plays in Thiolated Oligonucleotide Loading on Gold Nanoparticles. *ACS Nano* **2009**, *3*, 418–424

- (40) Wang, D.; Nap, R. J.; Lagzi, I.; Kowalczyk, B.; Han, S.; Grzybowski, B. A.; Szeleifer, I. How and Why Nanoparticle's Curvature Regulates the Apparent pKa of The Coating Ligands. *J. Am. Chem. Soc.* **2011**, *133*, 2192-2197.
- (41) Owen, J. The Coordination Chemistry of Nanocrystal Surfaces. *Science* **2015**, *347*, 615-616.
- (42) Bozyigit, D.; Volk, S.; Yarema, O.; Wood, V. Quantification of Deep Traps in Nanocrystal Solids, Their Electronic Properties, and Their Influence on Device Behavior. *Nano Lett.* **2013**, *13*, 5284-5288.
- (43) Tang, J.; Brzozowski, L.; Barkhouse, D. A. R.; Wang, X.; Debnath, R.; Wolowiec, R.; Palmiano, E.; Levina, L.; Pattantyus-Abraham, A. G.; Jamakosmanovic, D.; et al. Quantum Dot Photovoltaics in the Extreme Quantum Confinement Regime: The Surface-Chemical Origins of Exceptional Air- and Light-Stability. *ACS Nano* **2010**, *4*, 869-878.
- (44) Moreels, I.; Lambert, K.; Muynck, D. D.; Vanhaecke, F.; Poelman, D.; Martins, J. C.; Allan, G.; Hens, Z. Composition and Size-Dependent Extinction Coefficient of Colloidal PbSe Quantum Dots. *Chem. Mater.* **2007**, *19*, 6101–6106.
- (45) Bae, W. K.; Joo, J.; Padilha, L. A.; Won, J.; Lee, D. C.; Lin, Q.; Koh, W.-k.; Luo, H.; Klimov, V. I.; Pietryga, J. M. Highly Effective Surface Passivation of PbSe Quantum Dots through Reaction with Molecular Chlorine. *J. Am. Chem. Soc.* **2012**, *134*, 20160-20168.
- (46) Woo, J. Y.; Lee, S.; Lee, S.; Kim, W. D.; Lee, K.; Kim, K.; An, H. J.; Lee, D. C.; Jeong, S. Air-Stable PbSe Nanocrystals Passivated by Phosphonic Acids. *J. Am. Chem. Soc.* **2016**, *138*, 876-883.
- (47) Sykora, M.; Kuposov, A. Y.; McGuire, J. A.; Schulze, R. K.; Tretiak, O.; Pietryga, J. M.; Klimov, V. I. Effect of Air Exposure on Surface Properties, Electronic Structure, and Carrier Relaxation in PbSe Nanocrystals. *ACS Nano* **2010**, *4*, 2021-2034.

- (48) Zhang, J.; Gao, J.; Church, C. P.; Miller, E. M.; Luther, J. M.; Klimov, V. I.; Beard, M. C. PbSe Quantum Dot Solar Cells with More than 6% Efficiency Fabricated in Ambient Atmosphere. *Nano Lett.* **2014**, *14*, 6010-6015.
- (49) Zhang, J.; Gao, J.; Miller, E. M.; Luther, J. M.; Beard, M. C. Diffusion-controlled Synthesis of PbS and PbSe Quantum Dots with In situ Halide Passivation for Quantum Dot Solar Cells. *ACS Nano* **2014**, *8*, 614–622.
- (50) Jones, M.; Nedeljkovic, J.; Ellingson, R. J.; Nozik, A. J.; Rumbles, G. Photoenhancement of Luminescence in Colloidal CdSe Quantum Dot Solutions. *J. Phys. Chem. B* **2003**, *107*, 11346-11352.
- (51) Hines, D. A.; Kamat, P. V. Recent Advances in Quantum Dot Surface Chemistry. *ACS Appl. Mater. Interfaces* **2014**, *6*, 3041–3057.
- (52) Ip, A. H.; Thon, S. M.; Hoogland, S.; Voznyy, O.; Zhitomirsky, D.; Debnath, R.; Levina, L.; Rollny, L. R.; Carey, G. H.; Fischer, A.; et al. Hybrid Passivated Colloidal Quantum Dot Solids. *Nat. Nanotechnol.* **2012**, *7*, 577–582.
- (53) Bozyigit, D.; Lin, W. M.; Yazdani, N.; Yarema, O.; Wood, V. A Quantitative Model for Charge Carrier Transport, Trapping and Recombination in Nanocrystal-based Solar Cells. *Nat. Commun.* **2015**, *6*, 6180.
- (54) Zhang, Y.; Zhrebetsky, D.; Bronstein, N. D.; Barja, S.; Lichtenstein, L.; Alivisatos, A. P.; Wang, L.-W.; Salmeron, M. Molecular Oxygen Induced In-Gap States in PbS Quantum Dots. *ACS Nano* **2015**, *9*, 10445-10452.
- (55) Chuang, C. H. M.; Brown, P. R.; Bulovic, V.; Bawendi, M. G. Improved Performance and Stability in Quantum Dot Solar Cells through Band Alignment Engineering. *Nat. Mater.* **2014**, *13*, 796-801.
- (56) Liu, Y.; Gibbs, M.; Puthussery, J.; Gaik, S.; Ihly, R.; Hillhouse, H. W.; Law, M. Dependence of Carrier Mobility on Nanocrystal Size and Ligand Length in PbSe Nanocrystal Solids. *Nano Lett.* **2010**, *10*, 1960-1969.

- (57) Voznyy, O.; Zhitomirsky, D.; Stadler, P.; Ning, Z.; Hoogland, S.; Sargent, E. H. A Charge-Orbital Balance Picture of Doping in Colloidal Quantum Dot Solids. *ACS Nano* **2012**, *6*, 8448-8455.
- (58) Zhao, H.; Liang, H.; Gonfa, B. A.; Chaker, M.; Ozaki, T.; Tijssen, P.; Vidala, F.; Ma, D. Investigating Photoinduced Charge Transfer in Double- and Single-Emission PbS@CdS Core@Shell Quantum Dots. *Nanoscale* **2014**, *6*, 215-225.
- (59) Lifshitz, E.; Brumer, M.; Kigel, A.; Sashchiuk, A.; Bashouti, M.; Sirota, M.; Galun, E.; Burshtein, Z.; Quang, A. Q. L.; Ledoux-Rak, I.; et al. Air-Stable PbSe/PbS and PbSe/PbSe_xS_{1-x} Core-Shell Nanocrystal Quantum Dots and Their Applications. *J. Phys. Chem. B* **2006**, *110*, 25356-25365.
- (60) Zhao, H.; Chaker, M.; Wu, N.; Ma, D. Towards Controlled Synthesis and Better Understanding of Highly Luminescent PbS/CdS Core/Shell Quantum Dots. *J. Mater. Chem.* **2011**, *21*, 8898-8904.
- (61) Yanover, D.; Vaxenburg, R.; Tilchin, J.; Rubin-Brusilovski, A.; Zaiats, G.; Capek, R. K.; Sashchiuk, A.; Lifshitz, E. Significance of Small-Sized PbSe/PbS Core/Shell Colloidal Quantum Dots for Optoelectronic Applications. *J. Phys. Chem. C* **2014**, *118*, 17001-17009.
- (62) Geyter, B. D.; Justo, Y.; Moreels, I.; Lambert, K.; Smet, P. F.; Thourhout, D. V.; Houtepen, A. J.; Grodzinska, D.; Donega, C. d. M.; Meijerink, A.; et al. The Different Nature of Band Edge Absorption and Emission in Colloidal PbSe/CdSe Core/Shell Quantum Dots. *ACS Nano* **2011**, *5*, 58-66.
- (63) Etgar, L.; Yanover, D.; Čapek, R. K.; Vaxenburg, R.; Xue, Z.; Liu, B.; Nazeeruddin, M. K.; Lifshitz, E.; Grätzel, M. Core/Shell PbSe/PbS QDs TiO₂ Heterojunction Solar Cell. *Adv. Funct. Mater.* **2013**, *23*, 2736-2741.
- (64) Neo, D. C. J.; Cheng, C.; Stranks, S. D.; Fairclough, S. M.; Kim, J. S.; Kirkland, A. I.; Smith, J. M.; Snaith, H. J.; Assender, H. E.; Watt, A. A. R. Influence of Shell Thickness

- and Surface Passivation on PbS/CdS Core/Shell Colloidal Quantum Dot Solar Cells. *Chem. Mater.* **2014**, *26*, 4004-4013.
- (65) Cirloganu, C. M.; Padilha, L. A.; Lin, Q.; Makarov, N. S.; Velizhanin, K. A.; Luo, H.; Robel, I.; Pietryga, J. M.; Klimov, V. I. Enhanced Carrier Multiplication in Engineered Quasi-Type-II Quantum Dots. *Nat. Commun.* **2014**, *5*, 4148.
- (66) Wang, H.; Kubo, T.; Nakazaki, J.; Segawa, H. PbS Colloidal Quantum Dot/ZnO-Based Bulk-Heterojunction Solar Cells With High Stability under Continuous Light Soaking. *Phys. Status Solidi RRL* **2014**, *8*, 961-965.
- (67) Wang, H. B.; Kubo, T.; Nakazaki, J.; Kinoshita, T.; Segawa, H. PbS-Quantum-Dot-Based Heterojunction Solar Cells Utilizing ZnO Nanowires for High External Quantum Efficiency in the Near-Infrared Region. *J. Phys. Chem. Lett.* **2013**, *4*, 2455-2460.
- (68) Brown, P. R.; Kim, D.; Lunt, R. R.; Zhao, N.; Bawendi, M. G.; Grossman, J. C.; Bulović, V. Energy Level Modification in Lead Sulfide Quantum Dot Thin Films through Ligand Exchange. *ACS Nano* **2014**, *8*, 5863-5872.
- (69) Kim, S.; Marshal, A. R.; Kroupa, D. M.; Miller, E. M.; Luther, J. M.; Jeong, S.; Beard, M. C. Air-Stable and Efficient PbSe Quantum-Dot Solar Cells Based upon ZnSe to PbSe Cation-Exchanged Quantum Dots. *ACS Nano* **2015**, *9*, 8157-8164.
- (70) Engel, J. H.; Alivisatos, A. P. Postsynthetic Doping Control of Nanocrystal Thin Films: Balancing Space Charge to Improve Photovoltaic Efficiency. *Chem. Mater.* **2014**, *26*, 153-162.
- (71) Pearson, R. G. Hard and Soft Acids and Bases. *J. Am. Chem. Soc.* **1963**, *85*, 3533-3539.
- (72) Casavola, M.; van Huis, M. A.; Bals, S.; Lambert, K.; Hens, Z.; Vanmaekelbergh, D. Anisotropic Cation Exchange in PbSe/CdSe Core/Shell Nanocrystals of Different Geometry. *Chem. Mater.* **2012**, *24*, 294-302.
- (73) Lai, L. H.; Protesescu, L.; Kovalenko, M. V.; Loi, M. A. Sensitized Solar Cells with Colloidal PbS-CdS Core-Shell Quantum Dots. *Phys.Chem.Chem.Phys.* **2014**, *16*, 736-742.

- (74) Jiao, S.; Wang, J.; Shen, Q.; Li, Y.; Zhong, X. Surface Engineering of PbS Quantum Dot Sensitized Solar Cells with a Conversion Efficiency Exceeding 7%. *J. Mater. Chem. A* **2016**, *4*, 7214-7221.
- (75) Atomsa Gonfa, B.; Zhao, H.; Li, J.; Qiu, J.; Saidani, M.; Zhang, S.; Izquierdo, R.; Wu, N.; El Khakani, M. A.; Ma, D. Air-Processed Depleted Bulk Heterojunction Solar Cells Based on PbS/CdS Core-Shell Quantum Dots and TiO₂ Nanorod Arrays. *Sol. Energ. Mat. Sol. Cells* **2014**, *124*, 67-74.
- (76) Gonfa, B. A.; Kim, M. R.; Deegan, N.; Tavares, A. C.; Izquierdo, R.; Wu, N.; El Khakani, M. A.; Ma, D. Towards High Efficiency Air-Processed Near-Infrared Responsive Photovoltaics: Bulk Heterojunction Solar Cells Based on PbS/CdS Core-Shell Quantum Dots and TiO₂ Nanorod Arrays. *Nanoscale* **2015**, *7*, 10039-10049.
- (77) Choi, H.; Song, J. H.; Jang, J.; Mai, X. D.; Kim, S.; Jeong, S. High Performance of PbSe/PbS Core/Shell Quantum Dot Heterojunction Solar Cells: Short Circuit Current Enhancement without the Loss of Open Circuit Voltage by Shell Thickness Control. *Nanoscale* **2015**, *7*, 17473-17481.
- (78) Fischer, A.; Rollny, L.; Pan, J.; Carey, G. H.; Thon, S. M.; Hoogland, S.; Voznyy, O.; Zhitomirsky, D.; Kim, J. Y.; Bakr, O. M.; et al. Directly Deposited Quantum Dot Solids Using a Colloidally Stable Nanoparticle Ink. *Adv. Mater.* **2013**, *25*, 5742-5749.
- (79) Kovalenko, M. V.; Bodnarchuk, M. I.; Zaumseil, J.; Lee, J.-S.; Talapin, D. V. Expanding the Chemical Versatility of Colloidal Nanocrystals Capped with Molecular Metal Chalcogenide Ligands. *J. Am. Chem. Soc.* **2010**, *132*, 10085-10092.
- (80) Nag, A.; Kovalenko, M. V.; Lee, J. S.; Liu, W.; Spokoyny, B.; Talapin, D. V. Metal-Free Inorganic Ligands for Colloidal Nanocrystals: S²⁻, HS⁻, Se²⁻, HSe⁻, Te²⁻, HTe⁻, TeS₃²⁻, OH⁻, and NH₂²⁻ as Surface Ligands. *J. Am. Chem. Soc.* **2011**, *133*, 10612-10620.
- (81) Dirin, D. N.; Dreyfuss, S.; Bodnarchuk, M. I.; Nedelcu, G.; Papagiorgis, P.; Itskos, G.; Kovalenko, M. V. Lead Halide Perovskites and Other Metal Halide Complexes As

- Inorganic Capping Ligands for Colloidal Nanocrystals. *J. Am. Chem. Soc.* **2014**, *136*, 6550-6553.
- (82) Yang, Z.; Janmohamed, A.; Lan, X.; Garcia de Arquer, F. P.; Voznyy, O.; Yassitepe, E.; Kim, G. H.; Ning, Z.; Gong, X.; Comin, R.; et al. Colloidal Quantum Dot Photovoltaics Enhanced by Perovskite Shelling. *Nano Lett.* **2015**, *15*, 7539-7543.
- (83) Owen, J. S.; Park, J.; Trudeau, P. E.; Alivisatos, A. P. Reaction Chemistry and Ligand Exchange at Cadmium-Selenide Nanocrystal Surfaces. *J. Am. Chem. Soc.* **2008**, *130*, 12279-12281.
- (84) Anderson, N. C.; Owen, J. S. Soluble, Chloride-Terminated CdSe Nanocrystals: Ligand Exchange Monitored by ^1H and ^{31}P NMR Spectroscopy. *Chem. Mater.* **2013**, *25*, 69-76.
- (85) Lee, J. S.; Kovalenko, M. V.; Huang, J.; Chung, D. S.; Talapin, D. V. Band-like Transport, High Electron Mobility and High Photoconductivity in All-inorganic Nanocrystal Arrays. *Nat. Nanotechnol.* **2011**, *6*, 348-352.
- (86) Dolzhenkov, D. S.; Zhang, H.; Jang, J.; Son, J. S.; Panthani, M. G.; Shibata, T.; Chattopadhyay, S.; Talapin, D. V. Composition-Matched Molecular “Soldiers” for Semiconductors. *Science* **2015**, *347*, 425-428.
- (87) Ren, F.; del Rosal, B.; An, S. Y.; Yang, F.; Carrasco, E.; Benayas, A.; Oh, J. K.; Jaque, D.; de la Fuente, Á. J.; Vetrone, F.; et al. Development and Investigation of Ultrastable PbS/CdS/ZnS Quantum Dots for Near-Infrared Tumor Imaging. *Part. Part. Syst. Charact.* **2017**, *34*, 1600242.
- (88) de la Fuente, M. S.; Sanchez, R. S.; Gonzalez-Pedro, V.; Boix, P. P.; Mhaisalkar, S. G.; Rincon, M. E.; Bisquert, J.; Mora-Sero, I. Effect of Organic and Inorganic Passivation in Quantum-Dot-Sensitized Solar Cells. *J. Phys. Chem. Lett.* **2013**, *4*, 1519-1525.
- (89) Hösel, M.; Søndergaard, R. R.; Jørgensen, M.; Krebs, F. C., Comparison of UV-Curing, Hotmelt, and Pressure Sensitive Adhesive as Roll-to-Roll Encapsulation Methods for Polymer Solar Cells. *Adv. Eng. Mater.* **2013**, *15*, 1068-1075.
- (90) Cheng, P.; Zhan, X., Stability of organic solar cells: challenges and strategies. *Chem. Soc. Rev.* **2016**, *45*, 2544-2582.

2.4 Morphology control of the active layer of PSCs

As discussed in section 1.3.4, the Frenkel excitons generated in conjugated polymers have a high binding energy, and the carrier mobility between polymer molecules is low. It is necessary to avoid recombination of excitons and charge carriers before they reach the D/A interface and electrode, respectively. Therefore, the BHJ morphology is preferred for PSCs rather than the planar heterojunction one, to provide a short distance for carrier and exciton transport without sacrificing the light absorption. Such a BHJ morphology is a bi-continuous interpenetration network composed by D/A materials, which provides continuous charge transport channels towards the electrodes in the bulk film. On the basis of diffusion length of excitons (~10 nm), the required domain size for D/A material should be within 20 nm to achieve efficient separation of photo-generated excitons. It worth mentioning that there is a special type of morphology of the D/A film called vertical phase segregation (VPS).[76-79] In this morphology, the components of the D/A materials are inhomogenously distributed along the perpendicular direction to the electrodes (Figure 2.2). Active film with such morphology is demonstrated to be suitable for exciton separation, charge transport, and electron/hole collection at the fullerene derivative/polymer enriched side, respectively, which can effectively suppress the recombination loss.

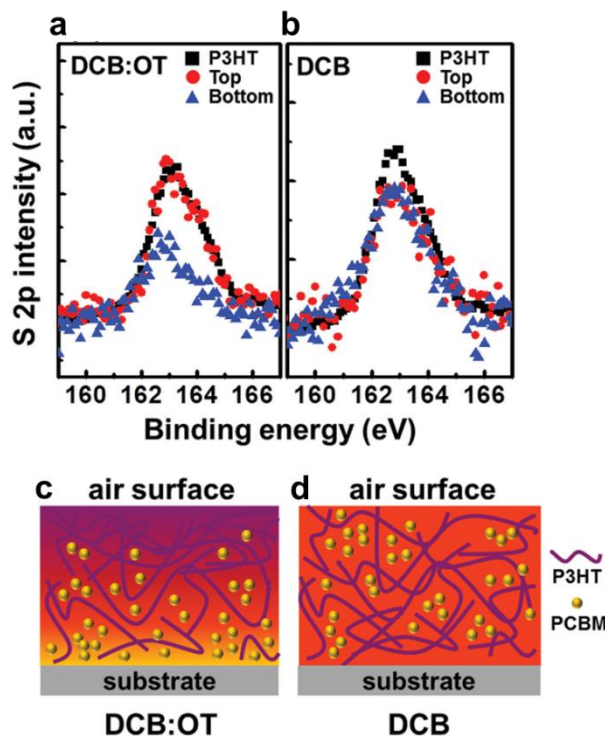


Figure 2.2 The normalized S 2p X-ray photoelectron spectroscopy (XPS) spectra of the air surface and the buried interface in the photoactive layers prepared in a) dichlorobenzene (DCB):1,8-octanedithiol (OT) and b) DCB. All spectra were normalized to the C 1s intensity. c) Schematic morphologies of the P3HT:PCBM films prepared in DCB and DCB:OT, as reconstructed from the results of the secondary ion mass spectroscopy (SIMS), transmission electron microtomography (TEMT), and XPS investigations. The purple lines are P3HT nanocrystals and the yellow circles are pure PCBM phases.[77]

Over all, the key factors to obtain a preferred morphology of D/A are solvent selection,[80] solvent/thermal annealing,[81-82] the use of additives[83] and interface effect[84]. The atomic force microscopy (AFM), TEM, scanning electron microscope (SEM), grazing incidence X-ray scattering (GIXS), optical microscopy and XPS measurements have been applied to investigate the morphology of the active layer.

At present stage, the commonly used solvents for fabrication of PSCs include the halogenated solvents such as 1,2-dichlorobenzene, chlorobenzene, chloroform, and non-halogenated solvents such as toluene and o-xylene. In most of the cases, the halogenated solvents result in better performance than non-halogenated ones, due to the induced preferable morphology of the active layer. It can be correlated to the difference of solubility of materials and the vapor pressure of the

solvent. Generally, solvent having good solubility for the fullerene derivatives such as PCBM and relative high vapor pressure can benefit the formation of a preferred morphology, leading to better PCE. The intrinsic mechanism is that these properties of solvents can affect the mobility of the components in the film. For the solvent with high vapor pressure, it enables a slowly drying process of the wet film during spin-coating and the subsequently keeping time (in a sealed space), which is well-known as solvent annealing process.[85] This is a crucial process to form preferred bi-continuous interpenetration morphology, in that, the interpenetrating polymer and fullerene derivative domains are formed by their self-organization and self-aggregation. Figure 2.3 (a-f) shows the characterization results from different-time processed P3HT:PCBM film.[85] The authors demonstrated that the 30 s film has a significant rougher surface (root-mean-square roughness (RMS): 3.0 nm) than that of the 80 s one (RMS: 0.8 nm). Also, the 80 s film shows a longer disordered zone as compared to the 30 s film, leading to higher energy barrier for inter-fibrillar hopping and therefore low carrier mobility. It can be the reason of weaker absorption of the film and worse performance of the corresponding device. In addition, post-treatment of the D/A film by solvent vapors has also been reported to optimize the morphology of the film. These solvents include chloroform, chlorobenzene, tetrahydrofuran, carbon disulfide and methanol *etc.*[82, 86-88] The solubility and viscosity of the solvent are important.

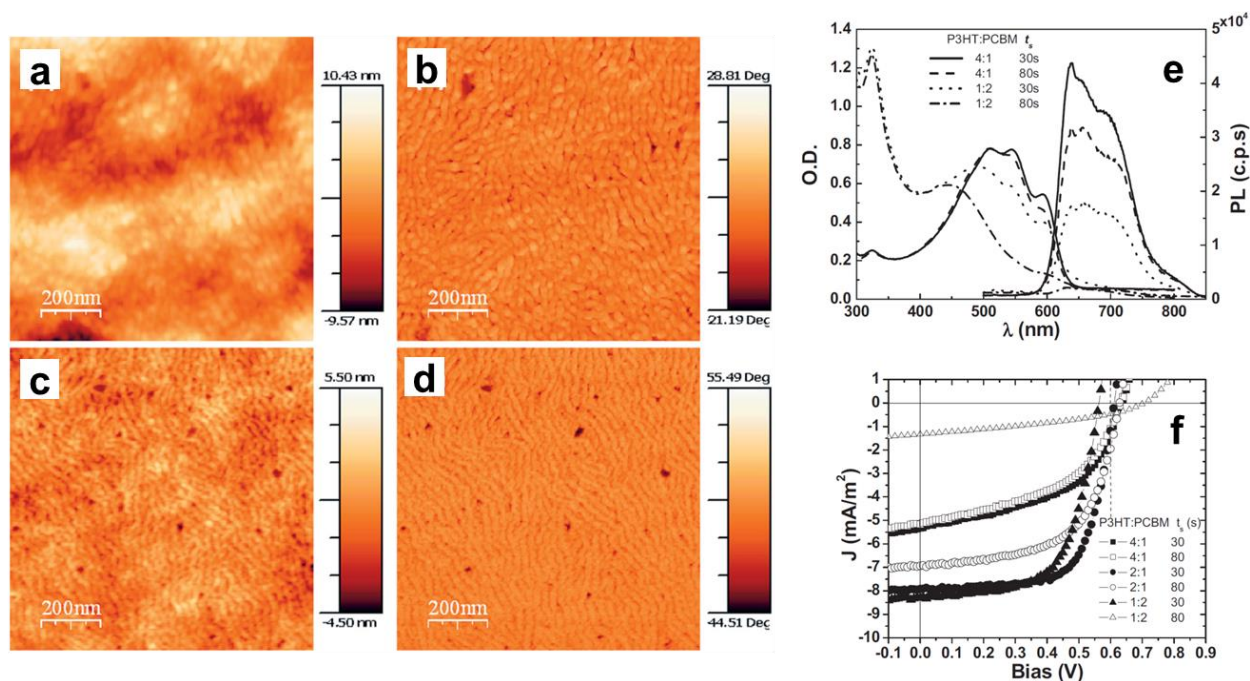


Figure 2.3 AFM topography (left) and phase (right) images for RR-P3HT:PCBM films fabricated using different processing conditions. The spin-coating times are (a,b) 30 s and (c,d) 80 s. (e) Effect of solvent annealing on the absorption and PL spectra of RR-P3HT:PCBM films with 4:1 and 1:2 weight ratios of the components. (f) $J-V$ characteristics of RR-P3HT:PCBM (4:1 squares, 2:1 circles, and 1:2 triangles) solar cells with (solid symbols, 30 s) and without (hollow symbols, 80 s) solvent annealing. The differences in device performance become more pronounced for higher PCBM loading fractions.[85]

In addition, the thermal annealing treatment has been frequently used to enhance the performance of PSCs.[81, 89] Intrinsically, the molecular mobility is enhanced during the thermal annealing, which accelerates the phase separation of polymer and fullerene derivatives. As a result, the absorption of relatively long wavelength (~ 600 nm) photons is enhanced, owing to the improved crystallinity of polymer materials. At the same time, the aggregation of PCBM molecules occurs. Depending on the material composition, heating temperature, lasting time and the geometrical confinement (*e.g.* with and without electrode), the size and shape of the PCBM domain can be tuned.[76, 81, 90-91] For instance, the size of PCBM domains increased from 10 to 100 nm by annealing the film at 100 °C for 5 min.[92] By further prolonging the annealing time (>30 min) and increasing temperature (>130 °C), the size of PCBM domains can be increased up to tens of micrometres.[81, 91] Moreover, both the disc-like and needle-like shapes of PCBM domain have been obtained by varying the heating treatments and blend compositions (Figure 2.4).[93] It worth mentioning that the thermal annealing treatment also changes the contact area between the D/A film and the electrode, which can also affect the performance of the device. However, it is still under debate that the D/A film with a high or low RMS surface can benefit the performance of devices.[94-95] Perhaps it should be analyzed by combining with the effect from the interpenetration morphology of the film, since both of them can affect the performance of devices.

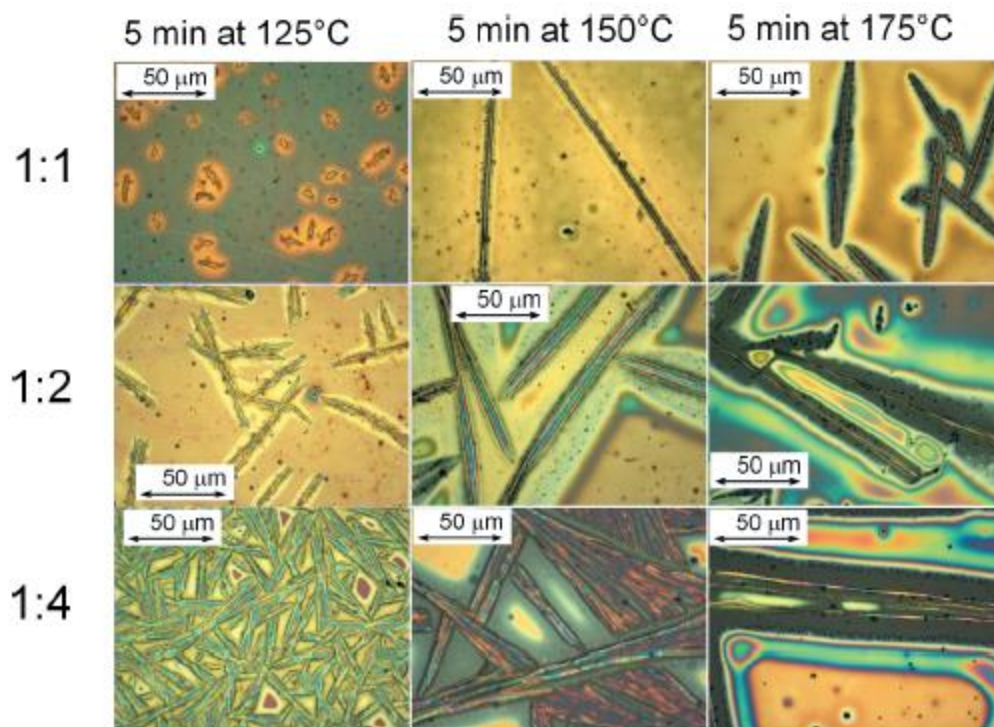


Figure 2.4 Optical microscopy images of P3HT:PCBM matrix. Blend ratio was varied from 1:1 to 1:4. Annealing time was kept constant at 5 min at temperatures of 125, 150, and 175 °C.[93]

As compared to the solvent (vapor) and thermal annealing, which is time- and energy-consuming, respectively, volatile additives have been proposed to conveniently optimize the morphology of D/A film by their synergistic effect with the main solvents. To choose an appropriate additive, the solubility and boiling point need to be taken into consideration.[83, 96] Generally, an additive with good solubility for the fullerene derivatives and a high boiling point are preferred for optimizing the morphology of PSCs (Figure 2.5(a)).[97] Intrinsically, it can induce strong inter-chain interaction, increase the degree of local structure order, and control the aggregation of the mobile fullerene derivatives. As seen in Figure 2.5(b,c), compared to the 1,9-nananedithiol (NDT) sample, the PCBM domain (dark area) size of 1,6-hexanedithiol (HDT) sample is smaller, and the phase segregation (contrast differences) is more distinct. This strategy is now employed to achieve high PCE for both conventional polymer and low band-gap polymer system without the usage of the thermal annealing treatment.[78, 96, 98]

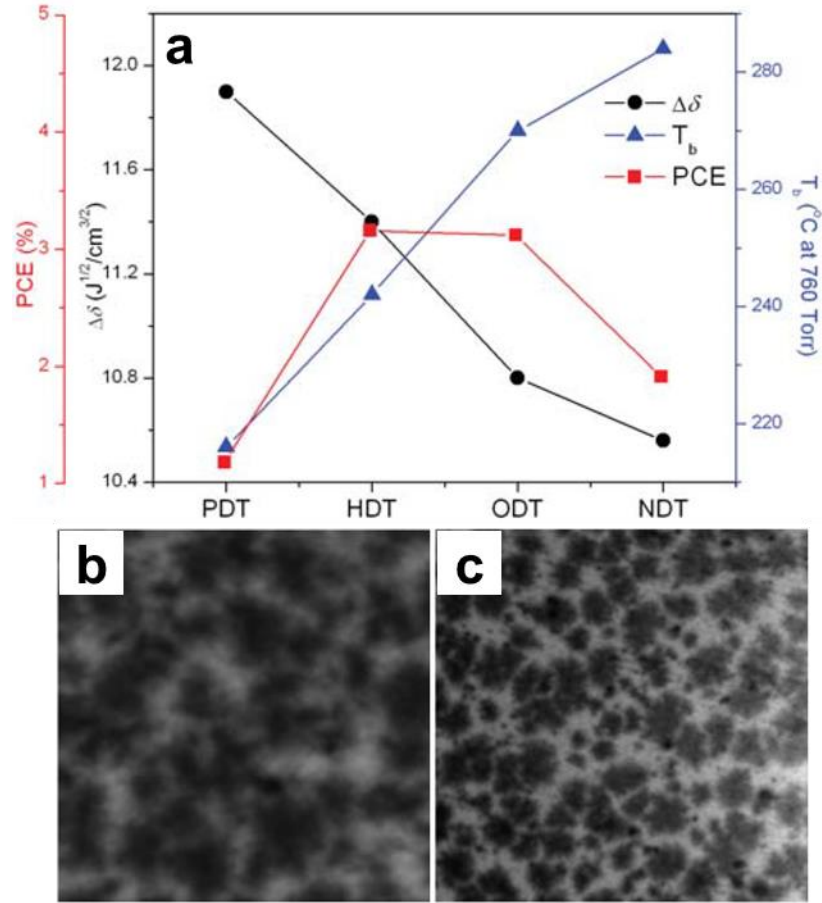


Figure 2.5 (a) Relationship between boiling point, difference in solubility parameter and device PCE of the different additive systems. 15×15 mm scanning transmission X-ray microscopy (STXM) images taken at 285 eV for P3HT:PC₆₁BM blends processed with: (a) NDT and (b) HDT.[96]

CHAPTER 3 EXPERIMENTAL

This chapter introduces the details of QDs synthesis and surface treatments, such as PbS QDs prepared by TMS and TBP involved method, CdS shell coating by different techniques and the way of performing surface ligand exchange. Various characterizations on nanostructure materials, film samples and devices are also included. Devices testing conditions are presented in the end.

3.1 Chemicals and Materials

Lead chloride (98%), oleylamine (technical grade, 70%), sulfur (100%), tributylphosphine (97%), cadmium oxide (99%), oleic acid, lauryl methacrylate, ethylene glycol dimethacrylate, diphenyl(2,4,6-trimethylbenzoyl)phosphine oxide, cardiogreen (IR 125), 1,2-dichloroethane, octadecene, n-butylamine (95%), zinc acetate dihydrate ($\text{Zn}(\text{CH}_3\text{COO})_2 \cdot 2\text{H}_2\text{O}$, 99.9%), ethanolamine ($\text{NH}_2\text{CH}_2\text{CH}_2\text{OH}$, 99.5%) and 2-methoxyethanol ($\text{CH}_3\text{OCH}_2\text{CH}_2\text{OH}$, 99.8%) were obtained from Sigma-Aldrich Inc. 4-(7-(2-phenyl-4H-1-benzothiopyran-4-ylidene)-4-chloro-3,5-trimethylene-1,3,5-heptatrienyl)-2-phenyl-1-benzothiopyrylium perchlorate (IR 26, 97%), dimethyl sulfoxide, toluene, and ethanol were purchased from Fisher Scientific Company. Regio-regular P3HT (RR93-95) and PCBM (>99.5%) were purchased from solaris chem incorporation. All of the materials were used without further purification.

3.2 PbS QD Synthesis

3.2.1 One-step injection of TBP route

In this route, typically 2 g of PbCl_2 and 15 mL of OLA were first heated at 160°C for 30 min under N_2 flow. Then the solution was pumped for at least 30 min to eliminate remaining water and possible impurities from reagents. Meanwhile, 20 mg of S was dissolved in 5 mL of OLA and different volume of TBP was then added for synthesizing the QDs of different sizes. The S-OLA/TBP solution was subsequently injected into the Pb precursor solution after it is cooled down to 70°C . Finally, the reaction was quickly quenched with cold toluene after 5 s, and the obtained PbS QDs were purified several times by repeated centrifugation-dispersion processes and eventually stabilized by the addition of oleic acid ligands.

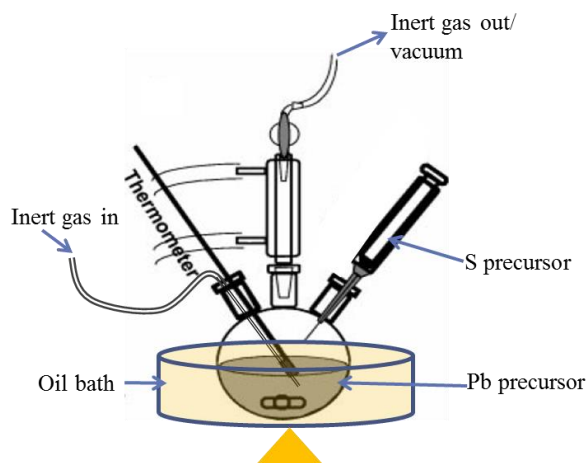


Figure 3.1 Scheme illustration of QD synthesis.[99]

3.2.2 Two-step injection of TBP route

For the two-step injection, TBP of varying volume was directly introduced into the Pb precursor solution before the addition of the S-OLA solution. All other experimental conditions, including precursor preparation, reaction, purification and re-dispersion, were the same as that described in section 3.2.1.

3.2.3 TMS route

PbS QDs were synthesized following the procedure previously reported by our group [100]. Typically, 760 mg of $\text{Pb}(\text{OAc})_2 \cdot 3\text{H}_2\text{O}$ ($\geq 99.99\%$), 2.4 mL of oleic acid ($\geq 99\%$) and 15 mL ODE were added to a three neck round bottom flask and heated to 150°C for 1 h while being stirred and purged with N_2 flow. This lead precursor solution was cooled under vacuum to 130°C and N_2 flow was resumed. Two mL of mixture of TMS and TOP (technical grade, 90%) in volume ratio of 1:10 were injected into the flask, and the temperature was cooled down to 100°C very quickly. The QD growth reaction was quenched with cold water after 5 minutes. The obtained PbS QDs were dissolved in toluene and kept at 4°C for 2 days before purification with repeated centrifugation/re-dispersion processes. The concentration of the PbS QDs can be determined by measuring their absorption spectrum, and the calculation details can be found in Supporting Information.

3.3 PbS/CdS QD Synthesis

3.3.1 PbS/CdS QD synthesis by microwave-assisted method

PbS/CdS core/shell QDs were synthesized by cation exchange method, following our previously reported procedures.[101] Briefly, as-prepared ultras-small PbS was dissolved in 20 mL toluene after purification. Appropriate amounts of Cd-OA solution (CdO dissolved in OA) was added to the PbS solution. After 3-min stirring and 6-min bubbling by N₂, the solution was reacted in a microwave oven for 8 s at 100 °C to get the PbS/CdS with 0.1 nm CdS shell. Finally, the solution was purified by ethanol for the next step.

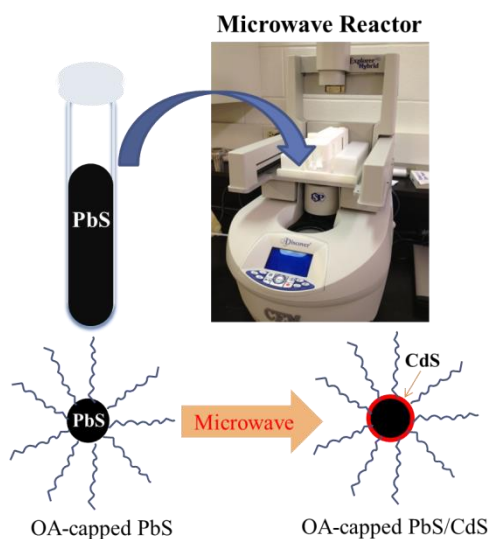


Figure 3.2 Scheme illustration of CdS-shell coating

3.3.2 PbS/CdS QD synthesis by oil-bath method

PbS QD suspension in toluene (1 mL, Absorbance = 3 at the first exciton peak) was first diluted to 10 mL. After N₂ bubbling for 30 min, the PbS QD suspension was heated to 100 °C, followed by the immediate injection of 1 mL of Cd-OA solution. The reaction was then allowed to proceed for different time in order to get different shell thickness. Specifically, for growing the CdS shell of 0.5 nm in thickness for the LSC device fabrication, the reaction was stopped after 5 h. Finally, the PbS/CdS QDs were purified and re-dispersed in toluene for LSC device fabrication.

3.3.3 Metal halide treatment

Halide treatment was carried out in solution following the ligand exchange procedure previously reported.[102] First, a stock CdCl_2 solution was prepared by mixing 600 mg of CdCl_2 (99.999% trace metals basis), 66 mg of tetradecylphosphonic acid (97%) and 10 mL of OLA (technical grade, 70%) in a flask and heating the mixture at 100 °C under vacuum for 1 h. Subsequently, 10 mL of PbS/CdS QDs solution (25 mg/mL in toluene) was heated to 60 °C under N_2 flow, and 0.75 mL of CdCl_2 stock solution was injected and kept at 60 °C for 30 min under magnetic stirring. The obtained halide-PbS/CdS QDs were purified by ethanol and acetone washing successively and further dispersed in dichlorobenzene for characterization and solar cell fabrication.

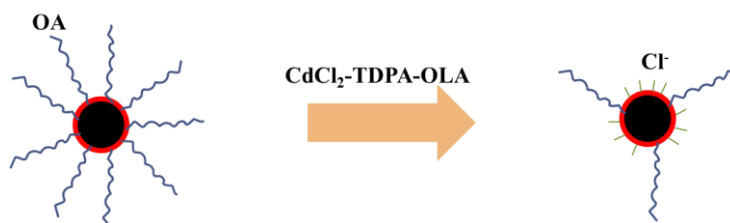


Figure 3.3 Scheme illustration of ligand-exchange.

3.4 Device Fabrication

3.4.1 Fabrication of LSC devices

Similar to the procedures described in references,[56-57] the LSCs were fabricated by embedding the TBP-route synthesized QDs into a polymer matrix. Briefly, the QDs were precipitated by adding ethanol. The monomer precursor of lauryl methacrylate and cross-linker of ethylene glycol dimethacrylate were mixed at a mass loading of approximately 20%, and then added into the QDs. Diphenyl(2,4,6-trimethylbenzoyl)phosphine oxide was added to the resulting solution as a UV initiator. A clear solution was obtained by ultrasound treatment. Finally, the mixture was illuminated by a UV lamp for 2 h in a mold consisting of two glass slides separated by a flexible rubber spacer with thickness around 2 mm.

3.4.2 Fabrication of solar cell devices

The details of PSC fabrication processes are shown in **Figure 2.4**. ITO glass substrates (2.5 cm×2.5 cm) were sequentially washed in water, acetone and isopropanol for 20 min each. An

optical lithography technique was then used to pattern the substrates. The patterned ITO glass substrates were cleaned again in acetone and isopropanol for 10 min each, followed by oxygen plasma treatment for 2 min. The ZnO precursor solution was then spin-coated onto the patterned ITO glasses and annealed at 200 °C for 30 minutes in air to get the ZnO film (an electron transport and hole blocking layer). P3HT (RR93-95, solaris):PCBM (>99.5%, solaris) (1:0.8 by weight) solution (with and without the solvent additive or QDs) in 1,2-dichlorobenzene was spin-coated onto the ZnO layer to form the photoactive film and kept in a petri dish for 30 min for aging before the thermal annealing step at 140 °C for 10 min. Finally, the fabrication of the solar cell device was completed by depositing a 20 nm thick layer of MoO₃ on the photoactive film followed by an 80 nm thick layer of Ag through a shadow mask, which makes the photoactive area of about 6 mm².

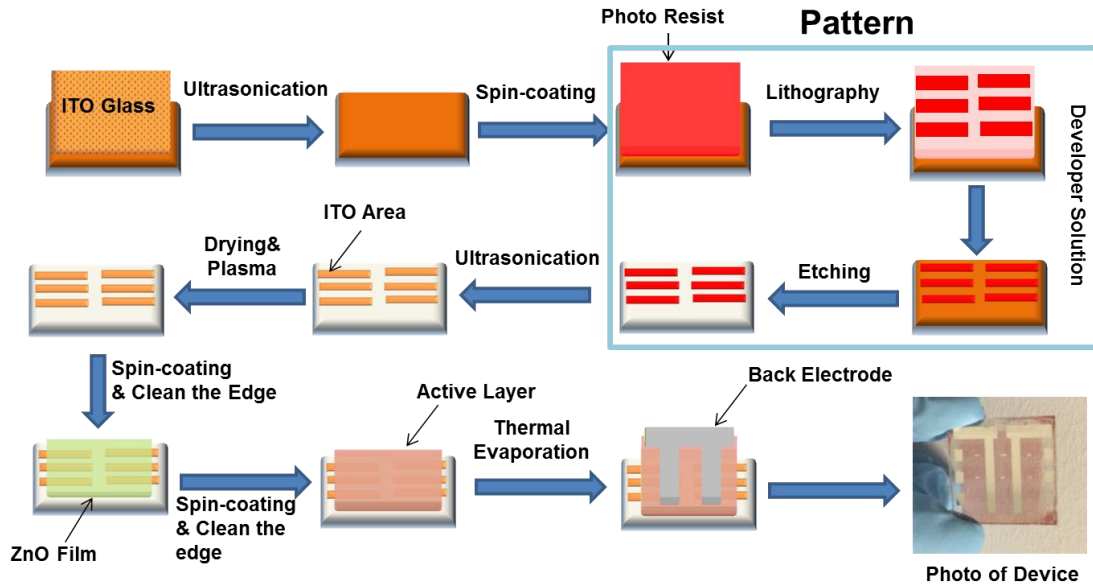


Figure 3.4 ITO substrate pattern and process of PSC devices fabrication.

3.5 QD concentration calculation

Firstly, we determined the molar concentration of synthesized PbS QDs in toluene using the Beer-Lambert's law: $A = \epsilon CL$, where A is the absorbance at the position of the first exciton absorption peak for a given sample, ϵ is the extinction coefficient per mole of PbS QDs, C is the molar concentration of QDs, and L is the light path length depending on the cuvette. ϵ was determined using $\epsilon = 19600 r^{2.32}$, [103] where r is the radius of QDs. R can be calculated by the

following formula: $E = 0.41 + 1/(0.0252d^2 + 0.283d)$, where E and d are the band gap and diameter of obtained QDs, respectively.[104] Then, the calculated C was converted to mass concentration.² Finally, the product yield per batch can be obtained by using the mass concentration multiplying the total volume of QDs solution. We assumed that the concentration of PbS/CdS QDs with a thin shell (0.1 nm) is equal to that of the plain PbS QDs.

3.6 Characterizations

Absorption spectra of the solution and solid-state samples were acquired with a Cary 5000 UV-Vis-NIR spectrophotometer (Varian) with a scan speed of 600 nm/min. Fluorescence spectra were taken with a Fluorolog®-3 system (Horiba Jobin Yvon). PL QY of QDs with emission peaks in the range of 800-1000 nm was measured using IR 125 dye (dissolved in dimethyl sulfoxide) as a reference, while the PL QY of the samples with emission peaks between 1100-1200 nm were measured using IR 26 dye (dissolved in 1,2-dichloroethane) as a reference. The size and morphology of PbS QDs were characterized by TEM (JEOL 2100F). Assuming the QDs have spherical morphology, the size histograms of corresponding samples were obtained following the equation: $S = \pi(d/2)^2$, where S is the areas of a single QD estimated by the imageJ software, and d is the diameter. Over 200 QDs were counted for each sample. The standard deviation was obtained by fitting the histograms using the Gaussian function. Nuclear magnetic resonance (NMR, Bruker, Advance III HD, 600 MHz) was applied to examine the surface ligand of QDs and assess the change of TBP following the reaction using toluene-D8 (deuterated chemical) as a solvent. It was also employed to examine the butylamine in the film by dissolving the film in deuterium chloroform. Pb/S ratio was detected by inductively coupled plasma / atomic emission spectrometry (ICP-AES, Agilent Technologie, 5100). The powder X-ray diffraction (XRD) study was carried out with a Bruker D8 advanced diffractometer using a Cu K_α radiation source. The optical efficiency of the LSCs was measured by using an ABET2000 solar simulator at AM 1.5G (100 mW cm^{-2}) calibrated using a reference silicon diode.

X-Ray photoelectron spectrometry was performed using a VG Escalab 220i-XL equipped with an Al K_α source. The XPS data were analyzed with the Casa software. Atomic force microscopy (Bruker Corporation) with a silicon tip on a nitride lever was employed to investigate the film morphology. Topography images of the photoactive layers were obtained in the ScanAsyst mode.

The different domains composed of inorganic QDs and organic materials were detected in the contact mode by measuring the lateral bending of the cantilever. XRD (Panalytical X-Pert PRO MRD, Bruker Corporation) characterization was performed on the film samples. The profilometer (Bruker, Dektak XT) was applied to measure the thickness of the active layer. The films were covered by a MoO₃/Ag layer during long-term aging to simulate the actual device conditions. Fourier transform infrared spectroscopy (FTIR, Digilab FTS7000) in the transmittance mode was employed to detect the change of chemical bonds of the organic material in the film. The solar cells were characterized by current-voltage (J-V) measurements under illumination by an AM 1.5 solar simulator. External quantum efficiency (EQE) measurements were also conducted using an IQE200B system (Newport Corporation).

CHAPTER 4 RESULTS

This chapter is divided into three parts, each corresponding to one article. The first part introduces a facile and “greener” route to synthesize small-size PbS QDs, and their application in LSC devices. The second part is about the first demonstration of enhanced stability of PSCs by incorporation of QDs into the active film. The last part is focused on PCE enhancement of PSCs via morphology manipulation of the active film.

4.1 Ultrasmall PbS Quantum Dots: A Facile and Greener Synthetic Route and Their High Performance in Luminescent Solar Concentrators

Long Tan, Yufeng Zhou, Fuqiang Ren, Daniele Benetti, Fan Yang, Haiguang Zhao, Federico Rosei, Mohamed Chaker and Dongling Ma

J. Mater. Chem. A, **2017**, *5*, 10250-10260.

Due to the better surface passivation, the small QDs normally have higher PL QY and better stability than the large ones. Additionally, their absorption and PL spectrum are well separated with less overlap area than that of the large ones. Taking all of these aspects into consideration, the very small-size QDs are suitable for the LSC device application by acting as the fluorophore.

In this section, synthesis of very small PbS QDs is performed via a facile and “greener” route using PbCl₂ and elemental S as the precursors with the aid of tributylphosphine. The optical properties, surface chemistry, synthesis mechanism and scale-up synthesis of the QDs are systematically investigated. By applying QDs synthesized by this route in LSC devices, a record-high optical efficiency of ~1.2% at a geometric (G) factor of ~50 (10 cm in length) has been obtained.

I did most of the experimental work and wrote the draft of this manuscript. I also got the help from Yufeng Zhou, Daniele Benetti and Haiguang Zhao, who fabricated and characterized the LSC devices. In addition, Fuqiang Ren helped me to do the Pb/S ratio measurements and to take the photoluminescence image of the LSC device.

Ultrasmall PbS quantum dots: a facile and greener synthetic route and their high performance in luminescent solar concentrators

Long Tan, Yufeng Zhou, Fuqiang Ren, Daniele Benetti, Fan Yang, Haiguang Zhao, Federico Rosei, Mohamed Chaker and Dongling Ma*

Abstract: Synthesis of quantum dots (QDs) with widely size-tunable optical absorption and high photoluminescence quantum yield (PL QY) via a facile route is highly desired. By introducing tributylphosphine (TBP) into a relatively green synthesis method based on the use of S, PbCl₂ and oleylamine (OLA), we conveniently synthesized ultrasmall PbS QDs with the first excitonic absorption peak wavelength as short as 705 nm, without using a glove box, which cannot be achieved by previously reported approaches, without involving smelly S precursors (such as bis(trimethylsilyl) sulfide). Such synthesized PbS QDs show narrow size distributions without any aggregation and demonstrate high PL QY in the range of 60-90%, depending on the QD size. Based on nuclear magnetic resonance spectroscopy and X-ray diffraction investigations, TBP was found to act as the passivation ligand on the surface of QDs while simultaneously assisting the transformation of PbCl₂-OLA into more reactive Pb(OH)Cl that can directly participate the nucleation process, yielding ultrasmall PbS QDs. This new finding renders Pb(OH)Cl a very promising, new lead precursor for convenient synthesis of PbS and other lead-based QDs. We also demonstrate that the process can be readily scaled up. After synthesizing a thin CdS shell (~0.1 nm), ultrasmall core/shell QDs with a large Stokes shift (0.36 eV) and good stability were employed for fabricating near infrared (NIR) luminescent solar concentrators, which led to a record-high optical efficiency of ~1.2% at a geometric factor of ~50 (10 cm in length). The TBP route developed herein is very promising for synthesizing high quality ultrasmall QDs that have high potential in NIR-related applications.

Introduction

PbS quantum dots (QDs) have attracted increasing attention due to their size tunable optical properties in the near infrared (NIR) range arising from the quantum confinement effect. They are widely applied in optoelectronics, biological imaging and sensors.¹⁻⁷ Their performance in various applications are largely determined by their size, monodispersity and photoluminescence quantum yield (PL QY), which highly depend on QD synthesis.

Various methods have been explored for synthesizing PbS QDs. Among diverse synthetic routes, the wet chemical method is well-known as an efficient low-cost path to obtain high quality PbS QDs. One of the most popular methods uses lead oxide and bis(trimethylsilyl) sulfide (TMS) as precursors and the size of PbS QDs can be tuned in the range of 2.6–7.2 nm, corresponding to first-excitonic absorption peaks of 825–1750 nm.⁸ However, TMS involved in the QD synthesis (denoted as the TMS route herein) shows very high reactivity and is malodorous. A glove box is always required for the manipulation of TMS for this type of synthesis, which is inconvenient, especially for industrially relevant reaction scales. Alternatively, a greener synthesis has been explored by employing elemental sulfur (S) as a replacement of TMS, as first demonstrated by Cademartiri *et al.* and is now widely used.⁹ In this scenario (defined as the PbCl₂-S route herein), PbS QDs are formed by injecting S-oleylamine (OLA) solution into the pre-heated PbCl₂-OLA solution. Although it is greener and more convenient as well as can be conducted at a larger scale, this method yields PbS QDs in a limited range of 4.2–6.4 nm as compared to the TMS route, corresponding to the first-excitonic absorption peaks of 1200 nm–1600 nm.⁹ Very recently, Owen's group developed a new method to synthesize PbS QDs with relatively small sizes (with the first-excitonic absorption peak tuned down to 850 nm), narrow size distribution and good batch to batch consistency at industrially relevant reaction scales by using thioureas as S precursor.¹⁰ However, additional procedures are needed to synthesize new precursors and a glove box cannot be completely avoided in the synthesis. Among these methods, the PbCl₂-S route has the advantages of using “greener” and stable S source, involving convenient synthetic procedures and being cost-effective. It is worth more intense attention.

To expand the tunable range of the first-excitonic absorption peaks of PbS QDs synthesized via the facile PbCl₂-S route without the use of a glove box and TMS, Hen's group introduced trio-n-octylphosphine (TOP) into the S precursor solution during the synthesis, by which PbS QDs with first-excitonic absorption peaks in the range of 925–2100 nm were obtained.¹¹ The authors described that the major role of TOP was to form strong bond with sulfur, which led to a prolonged ripening process. Since the size-tunable optical characteristics of QDs remain one of the major driving forces for their development and practical applications, it is highly desirable to further blue-shift the first-excitonic absorption peak of PbS QDs by decreasing their sizes. Specifically, very small QDs normally have higher PL QY and optical constant, and better

stability than large ones,^{12,13} which makes them promising in various applications, such as multijunction solar cells, light emitting diodes in “the first working window” and luminescence solar concentrators (LSCs). Additionally, the scale up of reactions, which is also of high importance, was not mentioned in this TOP-involved PbCl₂-S synthesis. Last but not least, the exploration of small QDs synthesized by the PbCl₂-S route in electronic and optoelectronic devices, such as LSCs, is quite limited to the best of our knowledge.

LSCs are composed of fluorophores embedded in a polymer matrix which acts as a wave guide. They are able to convert photons over a wide range of the solar spectrum into concentrated light in a specific range suitable for exciting integrated solar cells. Considered as a potentially effective approach to both decrease the cost of power and improve solar cell efficiencies, LSCs are now being widely studied.^{14,15} Recent advances in the synthesis of inorganic QDs with high PL QY, size-tunable optical properties, and good chemical-/photo-stability make them excellent candidates for LSC technologies. To the best of our knowledge, although UV-visible (Vis) QDs are widely investigated in LSCs,^{16,17} only several papers on NIR QDs can be found in this field.¹⁸⁻²¹

Here, we introduce tributylphosphine (TBP) into the PbCl₂-S route, which leads to the important decrease in the size of PbS QDs below 2.5 nm (referred to as the TBP route herein). As a result, the first-excitonic absorption peak of PbS QDs synthesized by the PbCl₂-S method is now further extended down to 705 nm and can be tuned to cover previously not-achieved wavelength range of 705–900 nm by this method, promising for various applications. We further demonstrate that such synthesized PbS QDs show very high PL QY (60-90%), comparable to those synthesized by the TMS route and the synthesis can be easily scaled up. In addition, we discovered a surprising interaction between TBP and PbCl₂-OLA. To improve the stability of as-synthesized QDs, a thin CdS layer was further coated on PbS QDs via cation exchange. The as-prepared PbS/CdS core/shell QDs exhibit the PL QY of ~70% and Stokes shift of 0.36 eV. The LSCs using PbS/CdS core/shell QDs yield an impressive optical efficiency of 1.2% at geometric factor (G factor) ~50 (10 cm in length), among the highest values reported for QDs LSCs with similar G factor. Therefore, our work contributes to the development of both QDs and LSCs technologies in the NIR range.

Experimental

Chemicals and materials

Lead chloride (98%), oleylamine (OLA) (technical grade, 70%), sulfur (100%), tributylphosphine (97%), cadmium oxide (99%), oleic acid, lauryl methacrylate, ethylene glycol dimethacrylate, diphenyl(2,4,6-trimethylbenzoyl)phosphine oxide, cardiogreen (IR 125), 1,2-dichloroethane and octadecene (ODE) were obtained from Sigma-Aldrich Inc. 4-(7-(2-phenyl-4H-1-benzothiopyran-4-ylidene)-4-chloro-3,5-trimethylene-1,3,5-heptatrienyl)-2-phenyl-1-benzothiopyrylium perchlorate (IR 26, 97%), dimethyl sulfoxide, toluene, and ethanol were purchased from Fisher Scientific Company. All chemicals were used without any purification.

PbS QD synthesis by TBP route

In this route, typically 2 g of PbCl_2 and 15 mL of OLA were first heated at 160°C for 30 min under N_2 flow. Then the solution was pumped for at least 30 min to eliminate remaining water and possible impurities from reagents. Meanwhile, 20 mg of S was dissolved in 5 mL of OLA and different volume of TBP was then added for synthesizing the QDs of different sizes. The S-OLA/TBP solution was subsequently injected into the Pb precursor solution after it was cooled down to 70°C . Finally, the reaction was quickly quenched with cold toluene after 5 s, and the obtained PbS QDs were purified several times by repeated centrifugation-dispersion processes and eventually stabilized by the addition of oleic acid ligands.

For the two-step injection, TBP of varying volume was directly introduced into the Pb precursor solution before the addition of the S-OLA solution. All other experimental conditions, including precursor preparation, reaction, purification and re-dispersion, were the same as that described above.

PbS/CdS QD synthesis via cation exchange

PbS/CdS core/shell QDs were synthesized by cation exchange method, following our previously reported procedures.²² Briefly, as-prepared ultrasmall PbS was dissolved in 20 mL toluene after purification. Appropriate amounts of Cd-OA solution (CdO dissolved in OA) was added to the PbS solution. After 3-min stirring and 6-min bubbling by N_2 , the solution was reacted in a

microwave oven for 8 s at 100 °C to get the PbS/CdS with 0.1 nm CdS shell. Finally, the solution was purified by ethanol for the next step.

LSC fabrication

Similar to the procedures described in references,^{20,23} the LSCs were fabricated by embedding the TBP-route synthesized QDs into a polymer matrix. Briefly, the QDs were precipitated by adding ethanol. The monomer precursor of lauryl methacrylate and cross-linker of ethylene glycol dimethacrylate were mixed at a mass loading of approximately 20%, and then added into the QDs. Diphenyl(2,4,6-trimethylbenzoyl)phosphine oxide was added to the resulting solution as a UV initiator. A clear solution was obtained by ultrasound treatment. Finally, the mixture was illuminated by a UV lamp for 2 h in a mold consisting of two glass slides separated by a flexible rubber spacer with thickness around 2 mm.

Characterization

Absorption spectra of the QDs were acquired with a Cary 5000 UV-Vis-NIR spectrophotometer (Varian) with a scan speed of 600 nm/min. Fluorescence spectra were taken with a Fluorolog®-3 system (Horiba Jobin Yvon). PL QY of QDs with emission peaks in the range of 800-1000 nm was measured using IR 125 dye (dissolved in dimethyl sulfoxide) as a reference, while the PL QY of the samples with emission peaks between 1100-1200 nm were measured using IR 26 dye (dissolved in 1,2-dichloroethane) as a reference. The size and morphology of PbS QDs were characterized by TEM (JEOL 2100F). Assuming the QDs have spherical morphology, the size histograms of corresponding samples were obtained following the equation: $S = \pi(d/2)^2$, where S is the areas of a single QD estimated by the imageJ software, and d is the diameter. Over 200 QDs were counted for each sample. The standard deviation was obtained by fitting the histograms using the Gaussian function. Nuclear magnetic resonance (NMR, Bruker, Avance III HD, 600 MHz) was applied to examine the surface ligand of QDs and assess the change of TBP following the reaction using toluene-D8 as a solvent. Pb/S ratio was detected by inductively coupled plasma / atomic emission spectrometry (ICP-AES, Agilent Technologie, 5100). The powder X-ray diffraction (XRD) study was carried out with a Bruker D8 advanced diffractometer using a Cu K_{α} radiation source. The optical efficiency of the LSCs was measured

by using an ABET2000 solar simulator at AM 1.5G (100 mW cm^{-2}) calibrated using a reference silicon diode.

Results and discussion

One-step TBP route synthesis of PbS QDs

Based on the widely used facile and “greener” $\text{PbCl}_2\text{-S}$ route, we further developed the TBP-route to synthesize ultrasmall PbS QDs herein. All of the synthesis procedures were conveniently conducted out of the glove box. To study the effect of TBP, the synthesis was performed under identical conditions, with the only difference being the amount of TBP introduced. Briefly, TBP was first mixed with S-OLA and then this mixture was injected into $\text{PbCl}_2\text{-OLA}$ solution. It was found that the optical absorption of such synthesized PbS QDs can be well controlled by varying the amount of TBP added into the S precursor solution as demonstrated in Figure 1(a). For the purpose of straightforwardly comparing the shape, width and position of the first-excitonic absorption peaks of the QDs synthesized with different contents of TBP, all the spectra were normalized by their respective peak intensity. The exact amount of TBP used for QD synthesis and corresponding first-excitonic absorption peak positions are listed in Table S1. For the TBP-free $\text{PbCl}_2\text{-S}$ reaction, the shortest absorption peak wavelength of synthesized PbS QDs is limited to $\sim 1056 \text{ nm}$, whereas the introduction of TBP largely extends the first-excitonic absorption peak range of obtained QDs to shorter wavelengths. Specifically, by increasing the volume of TBP from 10 to 40 μL , the first-excitonic absorption peak of QDs is blue-shifted from 1028 to 705 nm, corresponding to the QD diameter changing from ~ 3.4 to 2.2 nm (calculated from the first excitonic peak of QDs, following the previously reported method), in line with TEM observations.²⁴ Nonetheless, with the further increase of TBP amount to 60 μL , no PbS QDs could be collected, due to the formation of the stable bond between TBP and sulfur, as partially evidenced from the color of S precursor solution. Initially appearing red/yellow without TBP or with less TBP, the color of sulfur solution becomes almost colorless with the addition of 60 μL TBP, suggesting the interaction between TBP and S. Consistently, mixing of Pb and S precursor solutions during the synthesis leads to no obvious color change, indicative of the lack of PbS formation, in clear contrast to other cases where grey color was immediately observed due to the instantaneous nucleation reaction.

The PL spectra of obtained PbS QDs are shown in Figure 1(b), and the corresponding values of PL peak position and full width at half maximum (FWHM) of PL are summarized in Table S1. Based on FWHM data, all the samples synthesized by the TBP-route show narrow size distributions. PL QY was measured according to the method described in the literature²⁵ with 2-[7-[1,3-dihydro-1,1-dimethyl-3-(4-sulfobutyl)-2H-benz[e]indol-2-ylidene]-1,3,5-heptatrienyl]-1,1-dimethyl-3-(4-sulfobutyl)-1H-benz[e]indolium hydroxide (IR 125, for 2.2, 2.8 and 3.1 nm samples) or 4-(7-(2-phenyl-4H-1-benzothiopyran-4-ylidene)-4-chloro-3,5-trimethylene-1,3,5-heptatrienyl)-2-phenyl-1-benzothiopyrylium perchlorate (IR 26, for 3.4 nm and TBP-free samples) as the standard samples. As seen in Figure 1(c), all of the QDs show high PL QY in the range of 60–90 %, comparable to the TMS-route synthesized QDs of similar emission wavelengths.¹³ In particular, for the TBP-samples, the PL QY increases from ~67% (average value) for 3.4 nm QDs to ~83% (average value) for 2.2 nm QDs, very likely due to the better passivation for smaller sized QDs.¹² To gain deeper insights into exciton kinetics, transient PL spectroscopy was used to measure the PL decay of the PbS QDs dispersed in toluene. Figure 1(d) shows the typical decay curves for QDs with different diameters achieved by either the TBP-free PbCl₂-S route or the TBP-route. All the curves can be fit sufficiently well by a bi-exponential decay function, and the average lifetime (τ) was calculated from two resolved lifetime components. All lifetimes are in line with those reported for PbS QDs in the literature,²⁶ except for the 2.2 nm QDs, which show unusually long lifetime over 3 μ s. Radiative recombination rates (K_{rad}) and non-radiative recombination rates (K_{nr}) were then calculated using the following equations²⁷: $\text{PL QY} = K_{\text{rad}}/(K_{\text{rad}}+K_{\text{nr}})$ and $\tau = 1/(K_{\text{rad}}+K_{\text{nr}})$. The values of K_{rad} and K_{nr} of all the samples are included in the inset of Figure 1(c). The K_{rad} for all samples are more or less similar, while the trend of the large increase of K_{nr} with QD size is well in line with the opposite trend in the PL QY of these QDs; the presence of more surface defects must be mainly responsible for the decrease of the PL QY in larger QDs.

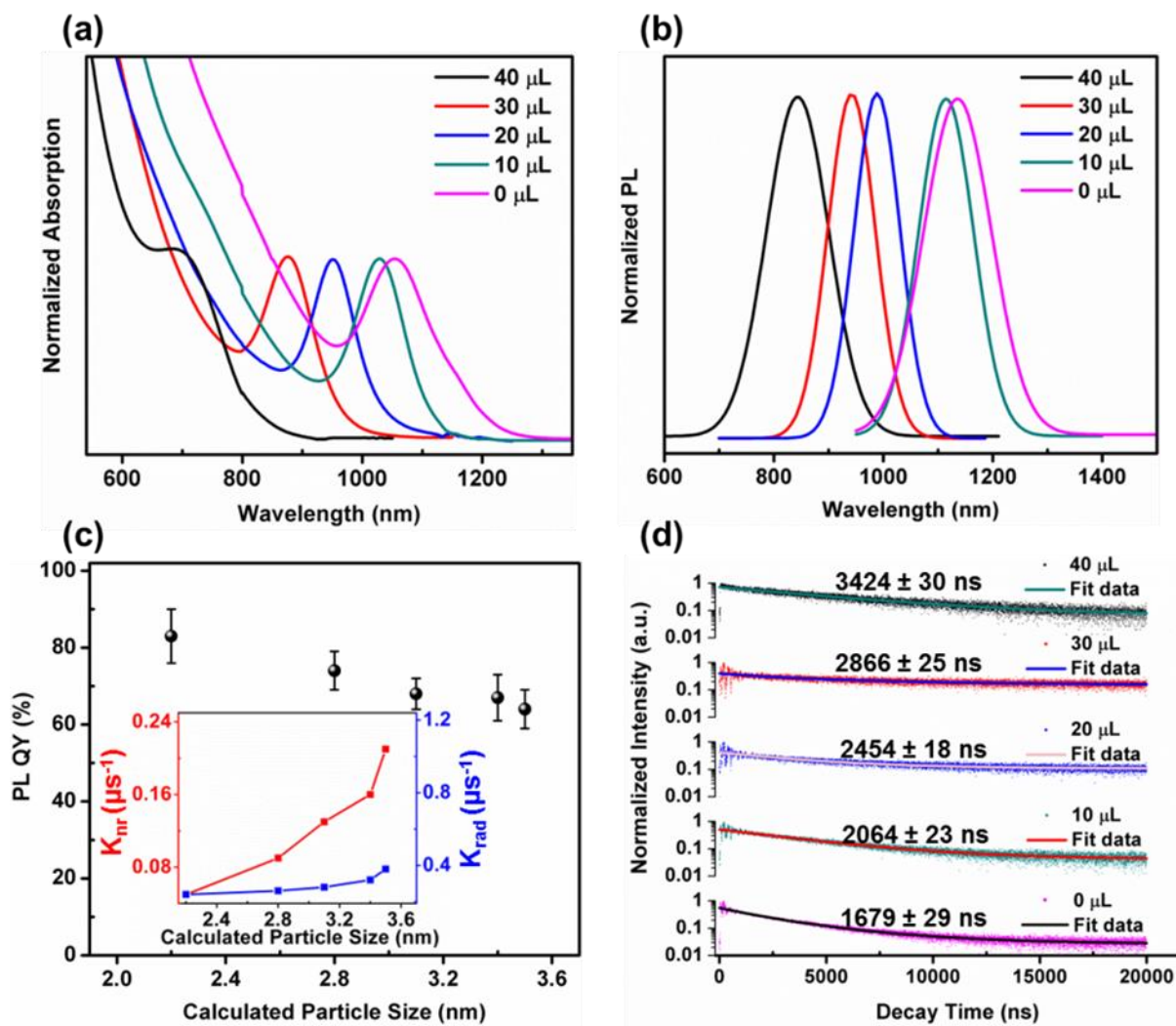


Figure 1. Absorption spectra (a), PL spectra (b), PL QY (c), and PL decay (d) of QDs synthesized without TBP and by the TBP route. Inset in figure (c) shows K_{rad} and K_{nr} values calculated from measured lifetime and PL QY data. The lines are shown as guide the eye.

Figure 2 shows transmission electron microscopy (TEM) images of obtained PbS QDs. It shows that the morphology of QDs is significantly affected, from irregular to quasi-spherical, with the introduction of TBP into the reaction. It can be explained from the ligand passivation point of view as the morphology is known to be largely associated with ligand passivation. TBP herein acts as ligand, as confirmed by NMR results to be presented in the later text. Moreover, statistical histograms were obtained to further analyze the effect of TBP on QD diameter and size distribution. When the volume of TBP is zero, PbS QDs with an average diameter of 4.1 nm are obtained. With the presence of TBP in the reaction, the average diameter of PbS QDs gradually

decreases with increasing volume of TBP, in agreement with the blue shift of the first-excitonic absorption peaks mentioned above. A representative high resolution (HR) TEM image of the 3.1 nm sample (inset in Figure 2(c)) shows lattice fringes, corresponding to the (200) facet of PbS QDs and in line with their crystalline structure (Figure S1). Additionally, in most of the cases the size distribution is improved with the presence of TBP. In particular, the size distributions for 2.9, 3.1 and 3.6 nm QDs are significantly narrower than that of 4.1 nm QDs synthesized without TBP. From many TEM images, we also noticed that QD aggregation is effectively hindered with the presence of TBP, even for the QDs with the average diameter as small as 2.3 nm. The narrow size distribution and lack of aggregation along with high PL QY of the QDs strongly suggest that high quality of QDs have been synthesized by the TBP route. TBP must play a significant role in determining important structural parameters, including the morphology, average diameter, size distribution and dispersity of QDs. Alkylphosphine compounds, acting as solvent and/or ligand, have been widely applied to synthesize II–VI and IV–VI QDs.^{11,28,29} It was reported that they can affect the nucleation reaction or crystal growth process and thereby affecting the QDs synthesis in a complicated way. Herein, we focus on a specific alkylphosphine, TBP, which was not previously explored in PbS QD synthesis, and found that it is able to considerably decrease the size of PbS QDs. Its effect on the synthesis of PbS QDs will be discussed in detail in the next section.

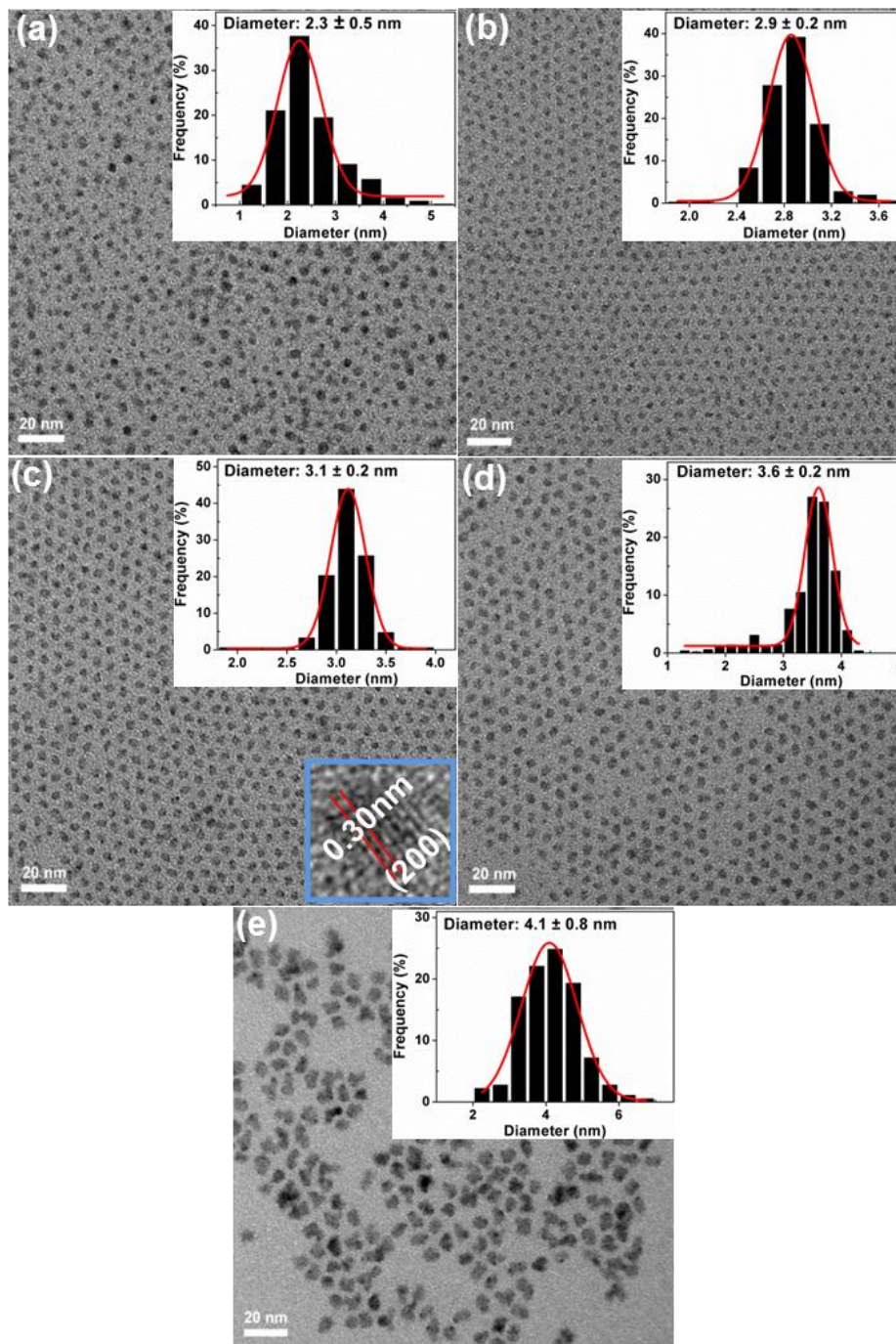


Figure 2. TEM images of the PbS QDs synthesized by using different volumes of TBP: (a) 40 μl , (b) 30 μl , (c) 20 μl , (d) 10 μl and (e) 0 μl . Insets: size histograms (a-e) and HRTEM image (c).

Inductively coupled plasma atomic emission spectrometry (ICP-AES) and ^{31}P NMR spectroscopy were used to probe the surface chemistry of the TBP-route synthesized QDs, which can significantly influence their properties. Figure 3(a) shows the results obtained in the current

study and the data from the TMS route in the literature¹² for comparison. We found that the Pb/S ratio of the TBP route synthesized QDs is much lower than that reported in the literature, although the trend of the Pb/S ratios with size is similar. In all these cases of ultras-small QDs, Pb-rich surfaces were identified. In the literature¹², the size, capping ligand and coverage of QDs and their external facets are highly correlated, and in general small-size QDs were confirmed to have more Pb-rich (111) external facets than larger ones. Our results suggest that TBP can alter the surface arrangement of Pb and S atoms, with respect to that reported in reference¹².

To better understand the surface chemistry, ³¹P NMR was conducted on purified 3.1 nm PbS QDs (Figure 3(b)). New phosphorous resonance at -13.7 ppm was detected, indicating the presence of TBP ligands on the surface of QDs. The dramatic downfield chemical shift from around -31 ppm for pristine TBP to -13.7 ppm for TBP-QDs is ascribed to the strong interaction between TBP and S atoms on the surface of QDs.³⁰ The presence of the TBP ligand on the surface could contribute to the high PL QY of the TBP route synthesized QDs by providing extra passivation to the S-site compared to the QDs from the normal, TBP-free PbCl₂-S route and TMS route. Controversial results regarding the role of alkylphosphines as passivating ligands have been reported in the literature.^{11,31} For instance, highly photoluminescent PbS QDs with a narrow size distribution can be obtained by using TOP as an additional ligand in the TMS route.³¹ The authors attributed the improvement to the enhanced surface passivation because both Pb and S surface atoms are passivated in this case, by oleic acid and TOP, respectively. However, different result was reported by Moreels *et al.*¹¹ In that case, TOP could not be found on the PbS QD surface. In our case, we believe that TBP (with short organic chains) has less steric effect than the analogous TOP, which facilitates its interaction with the S-sites. In addition to leading to the high PL QY, such passivation effect may induce an additional barrier for the QD growth during the synthesis. Along with the known strong binding effect between phosphines and S, the growth rate of PbS QDs decreases, leading to the observed smaller sizes.

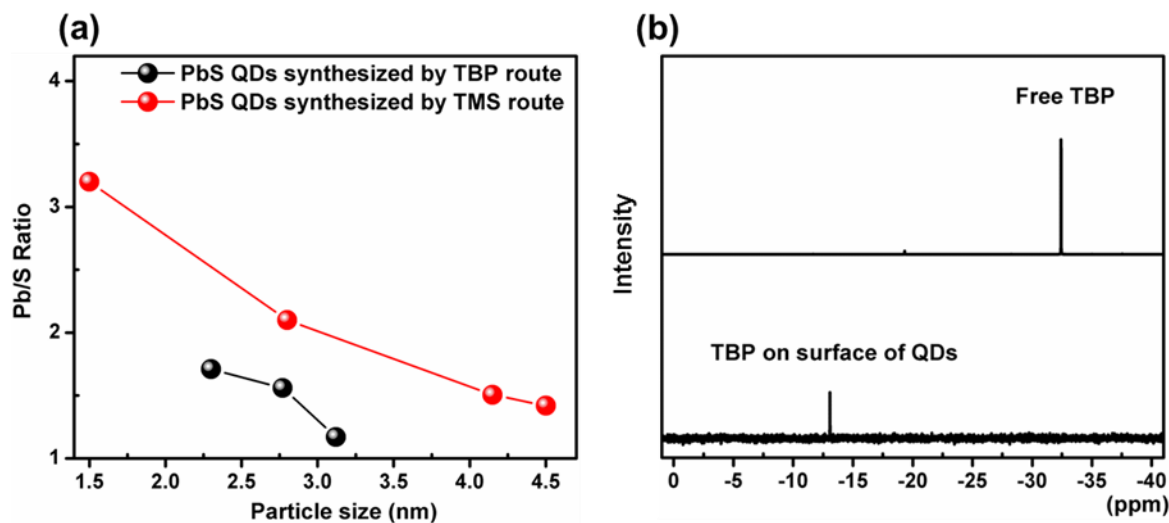


Figure 3. (a) Pb/S ratios of PbS QDs of different sizes synthesized by the TBP route; for the purpose of comparison, data on TMS-route synthesized QDs from the literature¹² are included. (b) ³¹P NMR spectra of pristine TBP and PbS QDs synthesized by the TBP route.

Overall, with increasing TBP content in the S precursor solution, the first-excitonic absorption peak of synthesized PbS QDs is gradually blue-shifted from 1056 nm to 705 nm, owing to decreased QD size. TBP as the surface capping ligands could have contributed to the improved optical properties, size-distribution and affected the surface composition of TBP route synthesized QDs. In brief, the smallest QDs show the highest PL QY and longest life-time, while QDs with the average diameter in the range of 2.9-3.6 nm have the narrowest size-distribution.

Two-step TBP route synthesis of ultrasmall PbS QDs

Motivated by the “TBP-effect”, which was able to extend the first-excitonic absorption peak of PbS QDs down to 705 nm in the one-step TBP route, we further examined the effect of TBP on PbS QD formation when it was separately injected into the PbCl₂-OLA solution followed by the S-OLA injection. When large amounts of TBP (TBP:PbCl₂ = 1:1 by molar) were injected, very well-defined absorption and PL spectra of the PbS QDs with peak position located at ~780 and ~890 nm were obtained (Figure 4(a)). This two-step TBP route can also result in largely extended excitonic absorption peak as compared to PbS QDs synthesized by the normal PbCl₂-S route. The FWHM of the PL peak (160 meV) formed by this method is even narrower than what can be achieved by the TMS route for the QDs (170 meV) of similar size.³² The calculated PL

QY of ultrasmall QDs synthesized by this two-step route is around 80%. Repeated experiments show that this two-step TBP route is highly reproducible and easily controllable. These results highlight the importance of this new, safer approach for the synthesis of ultrasmall QDs in a convenient way. As seen in the TEM image displayed in Figure 4(b), PbS QDs with diameter around 2.5 nm have excellent dispersity without any aggregation, in good agreement with the PL result. Nevertheless, when less TBP (20 μ L) was used in the two-step TBP route, bimodal absorption peaks were observed at around 973 and 1065 nm, respectively (Figure S2). Obviously, the presence of large amounts of TBP ligands played an important role in obtaining ultrasmall PbS QDs with a single and narrow peak. To better understand the interaction between PbCl₂-OLA and TBP, we performed additional investigations by focusing on lead precursors and TBP. Specifically two samples were prepared and compared. In the first case, PbCl₂-OLA was first prepared by heating the mixture of PbCl₂ and OLA following the same procedure used in the one-step TBP-route. The solution was then centrifuged and the obtained precipitates were washed and then dried. In the other case, large amounts of TBP were injected into the PbCl₂-OLA solution at 70 °C followed by the same precipitation and drying operations. XRD was performed on these two samples and results are shown in Figure 4(c), where the spectrum of commercial PbCl₂, as a reference, is also included. The diffraction pattern of PbCl₂ (JCPDS card NO. 26-1150) is totally changed after reacting with OLA. Surprisingly, when TBP was involved in the reaction, the Pb compound with the crystal structure of laurionite (JCPDS card NO. 74-2022) could be identified, suggesting the formation of Pb(OH)Cl.³³

³¹P NMR spectroscopy was further employed to monitor the possible change in TBP following the reaction. Figure 4(d) shows the NMR spectra of pristine TBP and that after Pb(OH)Cl formation, where no chemical shift was observed. As P is the only element in TBP that may react in this process, this finding suggests that highly likely, there is no change in the molecular structure of TBP in solution. It was reported that TBP can be considered as a catalyst in acylation reaction,³⁴ and different types of alkylphosphines cause considerable changes in the product yield of PbSe QDs by different effects.²⁹ Nevertheless, this is the first time that TBP was found to assist the transformation of the PbCl₂-OLA complex to Pb(OH)Cl. Since the reaction was conducted under N₂, the oxygen atom in Pb(OH)Cl may mainly come from the large excess of the commercial OLA reagent (Technical grade: 70%). Although the detailed mechanism for

transforming the $\text{PbCl}_2\text{-OLA}$ complex to Pb(OH)Cl in this reaction still requires further investigations, it is already clear that the presence of TBP directly induces such a transformation, which highly likely changes the Pb-S reaction rate and leads to small QD sizes.

Pb(OH)Cl has recently been reported as a lead source to synthesize zero-dimension (0D) and 1D PbSe nanomaterials at relative low temperature, although the optical properties of such synthesized nanomaterials were not mentioned.³³ Herein, to confirm that Pb(OH)Cl serves as the actual precursor for the formation of ultrasmall, high quality QDs shown in Figure 4(a) and (b), precipitated Pb(OH)Cl was also employed for the QD synthesis. To do it, Pb(OH)Cl was first re-dispersed in toluene and heated to 70 °C, then an appropriate amount of S:OLA solution was injected. The reaction was quenched by cold-water bath, and the absorption and PL spectra of the as-synthesized PbS QDs are shown in Figure 4(e). The first-excitonic absorption peak position of the sample is around 785 nm, which is impressively consistent with that of two-step TBP route synthesized QDs. The corresponding PL peak is also around 890 nm. The high consistency of both absorption and PL peak wavelengths of QDs synthesized by the two-step TBP route and precipitated Pb(OH)Cl strongly suggests that Pb(OH)Cl is formed first during the two-step route and acts as Pb precursor for the synthesis of ultrasmall QDs. The PL FWHM (210 meV), however, is much broader for the QDs synthesized from precipitated Pb(OH)Cl . This can be ascribed to the involved washing process after the Pb(OH)Cl synthesis, which removed many OLA and TBP molecules in solution that can act as the ligands and control size uniformity during the QD synthesis process. Having that said, TEM image (Figure 4(f)) of such obtained PbS QDs still shows relatively good dispersity without any obvious QD aggregation, indicating that Pb(OH)Cl is a very promising precursor for ultra-small PbS QDs synthesis.

The above investigations indicate that TBP can facilitate the formation of Pb(OH)Cl and lead to the formation of ultrasmall QDs in the two-step TBP route, although alkylphosphines were thought to only interact with S. The case was different from the one-step TBP route, where TBP-S and OLA-S were homogeneously mixed before their injection into the Pb precursor solution. As the nucleation is instantaneous, no Pb(OH)Cl formation is expected. In this case, the TBP mainly plays a role in retarding QD growth by strongly interacting with S and passivating surface S-sites (More information can be found in Mechanism Investigations in SI and Figure S2). As a result, ultrasmall QDs with single absorption and PL peaks could be obtained in the

one-step TBP route. So the actual roles of TBP in QD synthesis can be different depending on the way it is introduced. Based on these studies, the TBP route can be actually done in one-step or two-step injections for synthesizing ultrasmall QDs.

Moreover, the scale-up synthesis of PbS QDs by both one-step and two-step TBP routes has been performed (Supporting Information). The results show that both ultrasmall and slightly larger QDs in high quality can be synthesized at larger scale by the new TBP route, which strongly suggests that the TBP route, as a greener approach as compared to the TMS route, is a promising, facile way to produce large amounts of small sized PbS QDs.

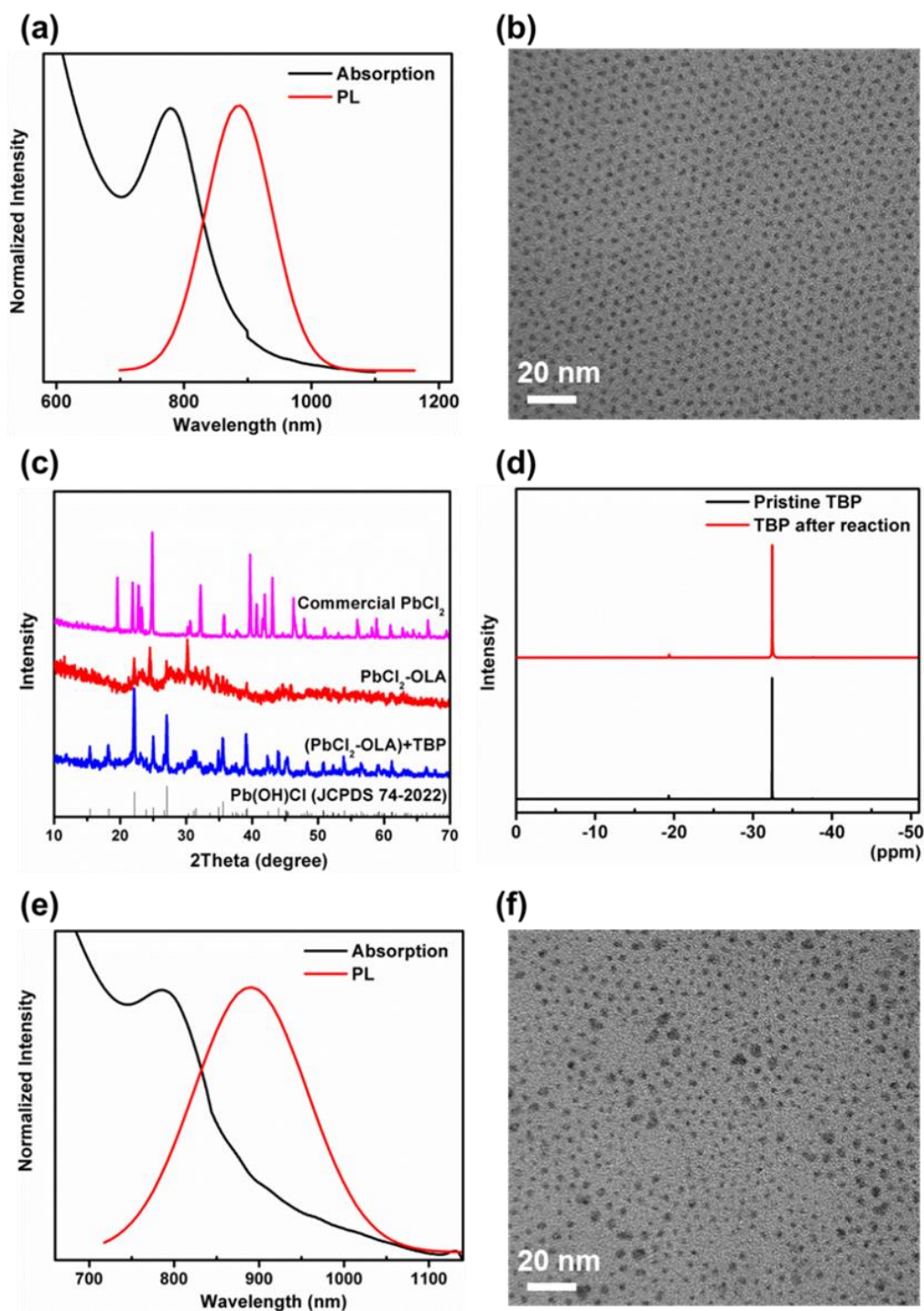


Figure 4. (a) Absorption and PL spectra of PbS QDs obtained by two-step injections of large amounts of TBP and then S-OLA. (b) TEM image of PbS QDs obtained by two-step injections. (c) XRD spectra of lead precursors and commercial PbCl₂. (d) ³¹P NMR spectra taken from pristine TBP solution and that after reaction. (e) Absorption and PL spectra and (f) TEM image of PbS QDs synthesized by Pb(OH)Cl and S-OLA.

LSC application

Significant overlapped absorption and PL spectra of QDs could induce serious reabsorption and thus lower the efficiency of LSCs, especially for large-area devices. In general, the performance can be improved by enhancing the PL QY of QDs and better separating their absorption and emission spectra.^{16,17} It has been reported that heterostructured UV-Visible QDs, such as CdSe/CdS, can help to separate absorption and PL spectra and reduce re-absorption loss.^{16,17} In previous work, NIR PbS/CdS QDs have been confirmed to have a quasi-type II band alignment, in that, electron leakage takes place from the PbS core to CdS shell, causing the red-shift of PL spectrum and longer life-time of electrons with respect to bare PbS QDs.³⁵ This PbS/CdS core/shell structure was confirmed to efficiently reduce the reabsorption of LSC.²⁰

Herein, the two-step TBP route synthesized ultrasmall PbS QDs with the Stokes shift of ~0.25 eV were first coated by a thin CdS shell (~0.1 nm) via cation exchange method to increase the Stokes shift value to as large as ~0.36 eV as well as to make the QDs more stable.²⁰ These core/shell QDs exhibit a fairly high PL QY of 70%. They were then employed as a luminescent material in LSCs, which can absorb the light and re-emit photons in between 700 and 1100 nm, coupling very well with the optical excitation wavelength range of Si solar cells (absorbing up to ~1100 nm). As seen in Figure 5(a), after transferring the core/shell QDs from solution into the polymer matrix followed by UV-initiated polymerization, the PL peak position and FWHM were not changed, indicating the excellent stability of synthesized PbS/CdS QDs as expected. The optical efficiency (η_{opt}) was measured with a definition of $\eta_{opt} = \frac{I_{LSC}}{I_{sc} \times G}$, where I_{LSC} and I_{sc} are the short circuit photocurrent from the Si diode coupled with a LSC and the short circuit photocurrent from the Si diode under direct illumination (AM 1.5G).

As seen in Figure 5(b), the optical efficiency decrease with increasing length of the LSC devices mainly due to the reabsorption phenomena caused by the small overlap of the absorption and emission spectra of the QDs, where the G factor is defined as the top surface area divided by the area of side facing the solar cell (the other three sides were covered by mirrors while measuring the efficiency). The optical efficiency with the QD concentration of 24 μM is around 4% at G factor of 10, which is much higher than the previous record optical efficiency (~1.4%)¹⁹ of the core/shell PbSe/PbS QDs based LSCs at a much higher QD concentration of 193 μM (G factor:

11) with a flat structure. Even at large G factor ($G=50$, 10 cm in length) the η_{opt} is still around 1.2%, among the best efficiencies of the LSCs based on the CdSe/CdS QDs (1%)¹⁷, CdSe/Cd_xPbS_{1-x} QDs (1.15%)³⁶, PbS/CdS QDs (1.1%)²⁰ with similar G factors. It can be attributed to the high PL QY, large Stokes shift and good stability of TBP-route synthesized QDs; their integration into the polymer matrix does not lead to any dramatic degradation of their PL QY. Compared with previously reported giant core/shell QDs with a thick shell, a comparable Stokes shift was obtained for ultrasmall QDs with only a 0.1 nm thin shell. It is a significant way to overcome the trade-off between shell thickness and PL QY. In many cases, PL QY is inversely proportional to shell thickness, like the cases of CdSe/CdS²³ and PbS/CdS²⁰. Moreover, higher temperature (over 200 °C) or longer reaction time (several hours or longer) for preparing the giant core/shell QDs can be avoided. For instance, we conveniently obtained PbS/CdS QDs (shell thickness: 0.1 nm) in 8 s at 100 °C. Overall, ultrasmall QDs synthesized by the TBP route are promising for LSC application in the NIR range by taking PL QY, separation of absorption/emission spectra and photo-stability of these QDs into consideration.

To further evaluate the performance of the LSC device based on PbS/CdS QDs, quantum efficiency (η_{quan}) defined as $\eta_{quan} = \frac{I_{LSC}}{I_{sc}^{Abs} \times G}$ was calculated (Figure 5(b)), where I_{sc}^{Abs} is the short circuit photocurrent from the Si diode under the illumination of light absorbed by QDs. Similar to the trend of η_{opt} , the η_{quan} of the device decreases from 9.6% to 2.9% with increasing G-factor of LSCs from 10 to 50. The quantum efficiency gives an idea of the amount of photons that reach the edge of the LSC and so it is a useful indication of the feasibility to realize large-scale LSC. Also in this case, even at large G factor ($G=50$), the internal quantum efficiency is still around 2.9%, one of the best values for NIR LSCs based on lead chalcogenides and also comparable to the values of the best LSCs involving other types of QDs such as CdSe/CdS¹⁷. In addition, it can be further improved by increasing the shell thickness, resulting in more separated absorption and emission spectra, and thus less reabsorption in the LSC device. These results indicate that these ultrasmall QDs are quite promising for large-area LSC device application. LSC devices composed of relatively large PbS QDs and PbS/CdS QDs with a thick shell (0.5 nm) were also fabricated. Their device performance is shown in the supporting information.

Figure 5(c) shows that the as-prepared LSC device has quite good transparency, attributed to homogeneously dispersed PbS QDs in a polymer matrix. Moreover, a NIR camera with a 780 nm long-pass filter was used to capture the photograph of an illuminating LSC excited by a 636 nm laser light source (Figure 5(d) and (e)). A large portion of the generated photons was successfully guided to the edge of the LSC device with brightness comparable to the excited area under direct illumination, indicating the good quality of the prepared LSC device.

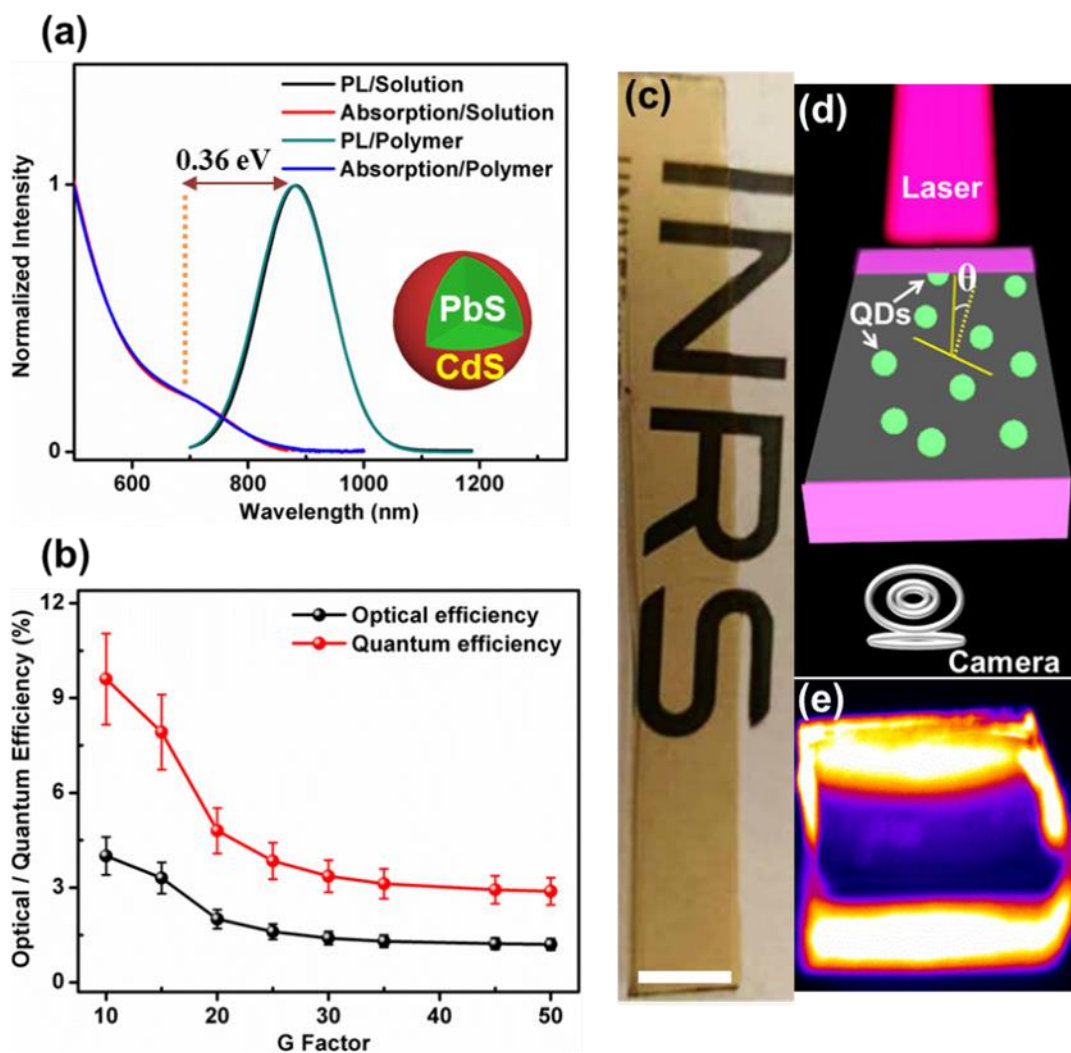


Figure 5. (a) Absorption and PL spectra of PbS/CdS in solution and a polymer matrix. (b) Optical/quantum efficiency of PbS/CdS QDs embedded LSCs with different G factors. (c) Photograph of a LSC device (scale bar: 1 cm). (d) Scheme of the experimental setup for exciting and taking the photograph of an illuminating

LSC device (Region of θ angle is the escape cone of emitted light). (e) Photograph of an illuminating LSC, captured by a NIR camera with a 780 nm long-pass filter.

Conclusions

In summary, the TBP route has been developed, for the first time, as an effective and less toxic way to synthesize high quality, ultrasmall PbS QDs, without involving the use of smelly S precursors (such as TMS) and a glove box. Via this method, PbS QDs with diameter below 2.5 nm can be synthesized, showing the optical absorption peak wavelength as short as 705 nm, which have been challenging to achieve with previously reported TMS-free methods. In addition to yielding quite high PL QY up to 90%, this synthesis route can be readily scaled up. By performing detailed investigation on experimental parameters and conducting structural, surface chemistry and optical characterization, the actual role of TBP in QD synthesis was found to be different depending on the way it was introduced into the synthesis. Surprisingly, it can promote the transformation of $\text{PbCl}_2\text{-OLA}$ to Pb(OH)Cl , leading to the synthesis of ultrasmall PbS QDs. Moreover, it was confirmed that TBP is capable of slowing down the crystal growth process and passivating the surface S-sites. The high quality of such synthesized PbS QDs (and subsequently synthesized PbS/CdS QDs) was further demonstrated by the impressively high efficiency achieved by QD-based LSC devices, revealing the success of the developed TBP route and the high potential of these QDs in NIR optoelectronics.

Acknowledgements

Financial support from the Natural Sciences and Engineering Research Council (NSREC) of Canada, in the context of a NSREC Discovery Grant, a NSERC Strategic Grant (industry partners: Canadian Solar Inc. and OLA Display Corp.) and an Engage Grant (industry partner: 1-Material Inc.) is greatly appreciated. D. Ma is also grateful for the financial support from Fonds de recherche du Québec-Nature et technologies (FRQNT) and Quebec Center for Functional Materials (CQMF), Canada.

References

1. S. A. McDonald, G. Konstantatos, S. Zhang, P. W. Cyr, E. J. D. Klem, L. Levina, E. H. Sargent, *Nat. Mater.*, 2005, **4**, 138.

2. C. H. M. Chuang, P. R. Brown, V. Bulović, M. G. Bawendi, *Nat. Mater.*, 2014, **13**, 796.
3. X. Lan, O. Vozny, A. Kiani, F. P. Arquer, A. S. Abbas, G. H. Kim, M. Liu, Z. Yang, G. Walters, J. Xu, M. Yuan, Z. Ning, F. Fan, P. Kanjanaboos, I. Kramer, D. Zhitomirsky, P. Lee, A. Perelgut, S. Hoogland, E. H. Sargent, *Adv. Mater.*, 2016, **28**, 299.
4. R. Hu, W. C. Law, G. Lin, L. Ye, J. Liu, J. Liu, J. L. Reynolds, K. T. Yong, *Theranostics*, 2012, **2**, 723.
5. Z. Sun, Z. Liu, J. Li, G. Tai, S. P. Lau, F. Yan, *Adv. Mater.*, 2012, **24**, 5878.
6. L. Sun, Q. Wang, *ACS Appl. Mater. Interfaces*, 2014, **6**, 14239.
7. L. Sun, Z. Y. Koh, Q. Wang, *Adv. Mater.*, 2013, **25**, 4598.
8. M. A. Hines, G. D. Scholes, *Adv. Mater.*, 2003, **15**, 1844.
9. L. Cademartiri, J. Bertolotti, R. Sapienza, D. S. Wiersma, G. Freymann, G. A. Ozin, *Phys. Chem. B*, 2006, **110**, 671.
10. M. P. Hendricks, M. P. Campos, G. T. Cleveland, I. J. L. Plante, J. S. Owen, *Science*, 2015, **348**, 1226.
11. I. Moreels, Y. Justo, B. D. Geyter, K. Haustreaete, J. C. Martins, Z. Hens, *ACS Nano*, 2011, **5**, 2004.
12. H. Choi, J. H. Ko, Y. H. Kim, S. Jeong, *J. Am. Chem. Soc.*, 2013, **135**, 5278.
13. O. E. Semonin, J. C. Johnson, J. M. Luther, A. G. Midgett, A. J. Nozik, M. C. Beard, *J. Phys. Chem. Lett.*, 2010, **1**, 2445.
14. M. J. Debije, P. P. C. Verbunt, *Adv. Energy Mater.*, 2012, **2**, 12.
15. W. E. Benjamin, D. R. Veit, M. J. Perkins, E. Bain, K. Scharnhorst, S. McDowall, D. L. Patrick, J. D. Gilbertson, *Chem. Mater.*, 2014, **26**, 1291.
16. C. S. Erickson, L. R. Bradshaw, S. McDowall, J. D. Gilbertson, D. R. Gamelin, D. L. Patrick, *ACS Nano*, 2014, **8**, 3461.

17. F. Meinardi, A. Colombo, K. A. Velizhanin, R. Simonutti, M. Lorenzon, L. Beverina, R. Viswanatha, V. I. Klimov, S. Brovelli, *Nat. Photonics*, 2014, **8**, 392.
18. R. H. Inman, G. V. Shcherbatyuk, D. Medvedko, A. Gopinathan, S. Ghosh, *Opt. Express*, 2011, **19**, 24308.
19. U. Aeberhard, R. Vaxenburg, E. Lifshitz, S. Tomić, *Phys. Chem. Chem. Phys.*, 2012, **14**, 16223.
20. Y. Zhou, D. Benetti, Z. Fan, H. Zhao, D. Ma, A. O. Govorov, A. Vomiero, F. Rosei, *Adv. Energy Mater.*, 2016, **6**, 1501913.
21. F. Meinard, H. McDaniel, F. Carulli, A. Colombo, K. A. Velizhanin, N. S. Makarov, R. Simonutti, V. I. Klimov, S. Brovelli, *Nat. Nanotechnol.*, 2015, **10**, 878.
22. F. Ren, H. Zhao, F. Vetrone, D. Ma, *Nanoscale*, 2013, **5**, 7800.
23. I. Coropceanu, M. G. Bawendi, *Nano Lett.*, 2014, **14**, 4097.
24. I. Moreels, K. Lambert, D. Smeets, D. D. Muynck, T. Nollet, J. C. Martins, F. Vanhaecke, A. Vantomme, C. Delerue, G. Allan, Z. Hens, *ACS Nano*, 2009, **3**, 3023.
25. C. WÜRth, M. Grabolle, J. Pauli, M. Spieles, U. R. Genger, *Nat. Protoc.*, 2013, **8**, 1535.
26. E. V. Ushakova, A. P. Litvin, P. S. Parfenov, A. V. Fedorov, M. Artemyev, A. V. Prudnikau, I. D. Rukhlenko, A. V. Baranov, *ACS Nano*, 2012, **6**, 8913.
27. F. Ren, S. A. Lindley, H. Zhao, L. Tan, B. A. Gonfa, Y. C. Pu, F. Yang, X. Liu, F. Vidal, J. Z. Zhang, F. Vetrone, D. Ma, *Phys. Chem. Chem. Phys.*, 2016, **18**, 31828.
28. C. M. Evans, M. E. Evans, T. D. Krauss, *J. Am. Chem. Soc.*, 2010, **132**, 10973.
29. J. S. Steckel, B. K. H. Yen, D. C. Oertel, M. G. Bawendi, *J. Am. Chem. Soc.*, 2006, **128**, 13032.
30. N. C. Anderson, J. S. Owen, *Chem. Mater.*, 2013, **25**, 69.

31. K. A. Abel, J. Shan, J. C. Boyer, F. Harris, F. C. J. M. van Veggel, *Chem. Mater.*, 2008, **20**, 3794.
32. J. J. Peterson, T. D. Krauss, *Nano Lett.*, 2006, **6**, 510.
33. H. Shen, J. Li, H. Shang, J. Niu, W. Xu, H. Wang, F. Guo, L. S. Li, *ACS Appl. Mater. Interfaces* **2013**, *5*, 10331.
34. E. Vedejs, S. T. Diver, *J. Am. Chem. Soc.*, 1993, **115**, 3358.
35. H. Zhao, H. Liang, F. Vidal, F. Rosei, A. Vomiero, D. Ma, *J. Phys. Chem. C*, 2014, **118**, 20585.
36. H. Zhao, D. Benetti, L. Jin, Y. Zhou, F. Rosei, A. Vomiero, *Small*, 2016, **12**, 5354.

SUPPORTING INFORMATION

Ultrasmall PbS quantum dots: a facile and greener synthetic route and their high performance in luminescent solar concentrators

*Long Tan, Yufeng Zhou, Fuqiang Ren, Daniele Benetti, Fan Yang, Haiguang Zhao, Federico
Rosei, Mohamed Chaker and Dongling Ma**

Centre Énergie, Matériaux et Télécommunications, Institut National de la Recherche Scientifique
(INRS), 1650 Boul. Lionel-Boulet, Varennes, Québec J3X 1S2, Canada

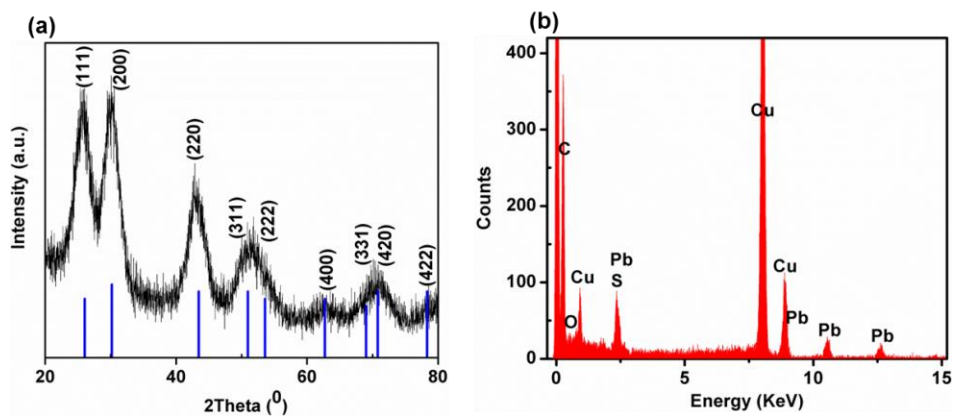
Email: ma@emt.inrs.ca

Table S1 Absorption and PL characteristics and calculated size of PbS QDs synthesized with different volumes of TBP.

Contents of TBP (μL)	0	10	20	30	40	60
Absorption Peak (nm)	1056	1028	951	876	705	N/A
Calculated QD Size (nm)	3.5	3.4	3.1	2.8	2.2	N/A
PL Peak (nm)	1136	1115	989	942	844	N/A
PL FWHM (meV)	119	100	107	122	197	N/A

N/A means that no QDs were collected.

Figure S1. X-ray diffraction (XRD) spectrum (a) and energy-dispersive X-ray spectroscopy (EDS) of PbS quantum dots (QDs) with an average diameter around 3.1 nm. The XRD pattern is in accordance with the PbS standard JCPDS card no. 02-0699. EDS results confirm the QDs are composed of Pb and S.

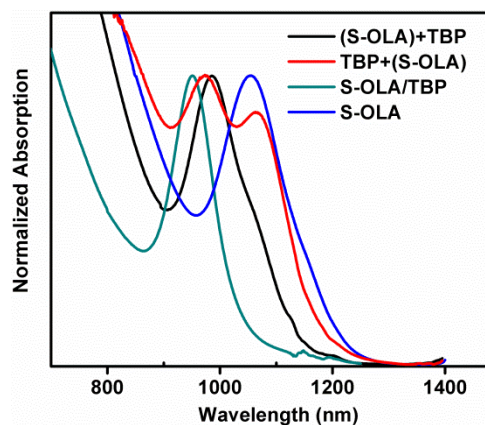


Mechanism investigations. Understanding the effect of different molecular species on the formation of nanocrystals is crucial to control the diameter, dispersity, yields and properties of QDs and ultimately their utility in functional devices.¹ In this respect, it is important to know the role of TBP in synthesizing ultrasmall PbS QDs. For the normal PbCl₂-S synthesis, without the presence of any alkylphosphines, the mechanism investigations have been focused on the reactions between sulfur and amine.¹ It was reported that sulfur exists as S₈ rings at its standard state, which can firstly react with alkylamine to form the sulfur precursor alkylammonium polysulfides at relatively low temperature. Upon heating to a higher temperature, such as 130 °C, the polysulfide ions react with excess amine to generate H₂S, which then react with lead precursors to form PbS QDs. For the TOP involved PbCl₂-S synthesis, it was reported that the presence of TOP can affect the “crystal growth” in a complicated way (for example, by forming S-TOP complex), but without really participating in the nucleation process.²

Herein, the effect of TBP on the nucleation and crystal growth of PbS QDs was investigated by varying the way TBP was introduced into the reaction solution (please note: in the one-step route mentioned in the manuscript, TBP was first mixed with the S-OLA solution and then one step injection of S-OLA/TBP was done). In one case, 20 µl of TBP was separately injected into the reaction solution immediately after the S-OLA solution being added to the pre-heated Pb precursor solution (denoted as (S-OLA)+TBP). The absorption spectrum of the obtained QDs with an absorption peak position around 985 nm is shown in Figure S2, which is clearly blue shifted as compared to the case of the TBP-free reaction. Assuming the nucleation process is instantaneous upon the S-OLA injection, this observation suggests that TBP affects QD growth by decreasing the chemical reactivity of the S precursor, highly likely due to the already known strong binding effect between phosphines and S although the TBP effect on the Pb precursor reactivity cannot be absolutely excluded either. In addition, the passivation of the surface S sites by TBP, as confirmed by ³¹P NMR (Figure 3b), increases the barrier for the QDs growth. Both effects can decrease the growth rate of PbS QDs, leading to a smaller size and thereby an absorption peak at a shorter wavelength. Similar “retarding” effect on the crystal growth was also observed in our group by using TOP as an additive, although in that case we did not identify the presence of TOP on the QD surface.³ Surprisingly when we switched the order of injections of S-OLA and TBP, bimodal absorption peaks were clearly observed, with one located at 973 nm

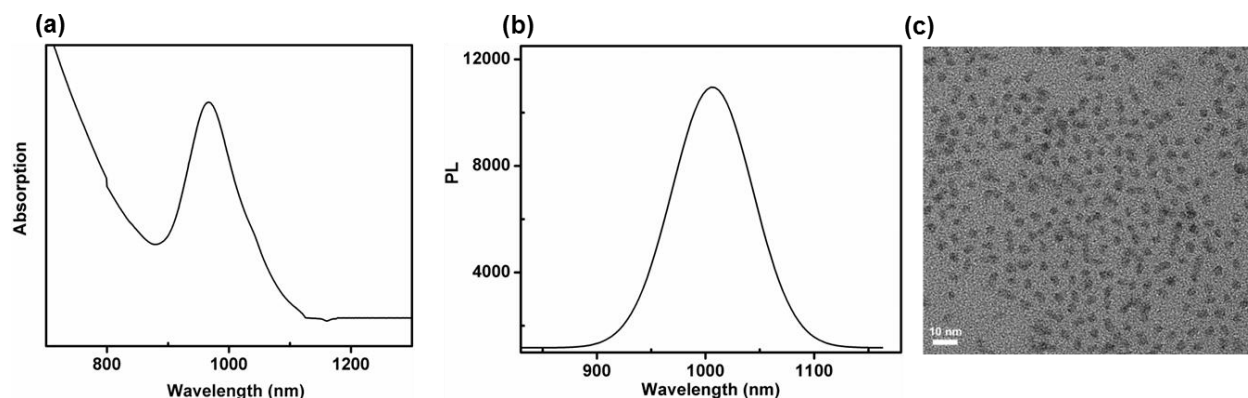
close to that of QDs obtained by the one-step TBP route, and the other at 1065 nm close to that of the TBP-free sample. We speculate that TBP possibly has imposed certain effect on the lead precursor as well, which affects the nuclei formation, although usually we tend to think that alkylphosphines only interact with S. The effect of TBP (at larger amount) on the Pb precursor was investigated in depth in the manuscript, which was found to facilitate the formation of Pb(OH)Cl.

Figure S2. Two-step injection: absorption spectra of PbS QDs synthesized by injecting (S-OLA) and then 20 μL TBP (Black: (S-OLA)+TBP) and by injecting 20 μL TBP and then (S-OLA) (Red: TBP+(S-OLA)) into the Pb precursor solution; One-step injection: absorption spectra of PbS QDs synthesized by injecting the mixture of S-OLA and TBP (TBP: 20 μL , dark green: S-OLA/TBP), and by injecting S-OLA only (no TBP, Blue: S-OLA) into the lead precursor solution.



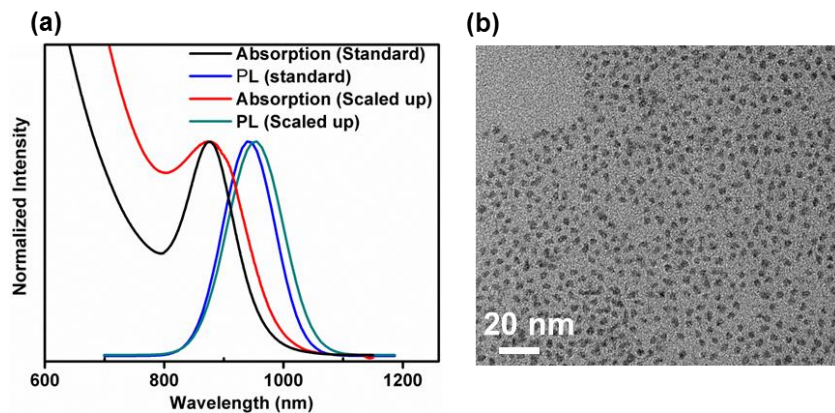
Synthesis scale-up of ~3.1 nm PbS QDs. The quantities of major chemicals were enlarged by 6-folds (PbCl_2 :12g S:120 mg TBP: 120 μl), whereas the volume of OLA for dissolving PbCl_2 and S was slightly increased (50 ml) and unchanged (5 ml), respectively. The absorption spectroscopy, photoluminescence (PL) spectroscopy and TEM were employed to determine the quality of the synthesized QDs. The absorption spectral with well-shaped narrow peak around 967 nm has been obtained for the as-prepared PbS QDS as shown in Figure S3(a), and its corresponding PL spectrum with strong intensity and low value of full width at half maximum (FWHM) (98.6 meV) is shown in the Figure S3(b). Figure S3(c) further proves that the as-prepared QDs have uniform size distribution, which accords well with the PL and absorption results. We conclude that the high quality PbS QDs have been successfully obtained by the up-scaling reaction. Each batch yields around 470 mg of QDs. There is still large room for further quantity increase.

Figure S3. Characterizations of PbS QDs (~3.1 nm in diameter) synthesized by one-step TBP-route in the scaled-up reaction: absorption spectrum (a), PL spectrum (b), and transmission electron microscopy (TEM) image (c).



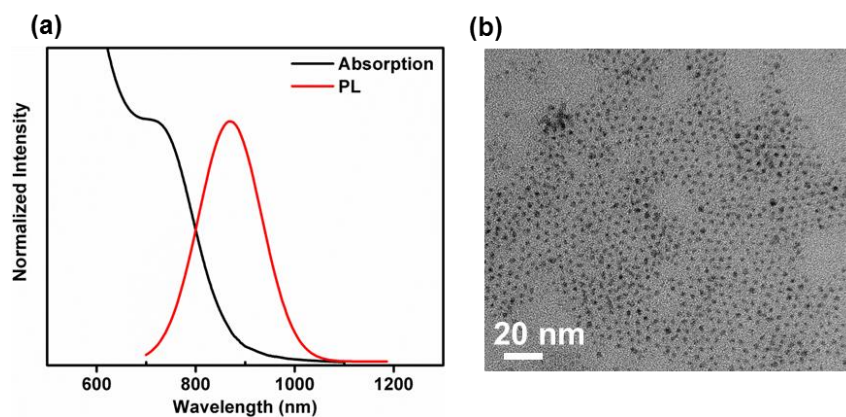
Synthesis scale-up of ~2.8 nm PbS QDs. In this synthesis, the quantities of major chemicals were enlarged by 5-folds (PbCl_2 : 10 g; S: 100 mg), whereas the volume of OLA for dissolving PbCl_2 and S was slightly increased (50 ml) and unchanged (5 ml), respectively. The volume of TBP was increased by 10 folds. Absorption spectroscopy, PL spectroscopy and TEM were employed to assess the quality of the QDs synthesized at the larger reaction scale. Both absorption and PL peaks remain at similar wavelengths after reaction scale-up (Figure S4(a)). Although the absorption peak is broadened, the FWHM of the PL peak remains almost unchanged. The integrated PL intensity of the up-scaled sample is around 89% of that of the standard sample, before scaling up, measured at the same QD concentration. Fig. S4(b) confirms that the as-prepared QDs have uniform morphology and size distribution with the average diameter around 2.8 nm, consistent with the results got from the PL and absorption spectra. Clearly high quality PbS QDs can be obtained by the up-scaled reaction, which yields QDs around 150 mg.

Figure S4 Characterizations of PbS QDs synthesized by the TBP-route in scale-up reactions: (a) absorption and PL spectra and (b) TEM image of QDs (~ 150 mg per batch) synthesized by scaling up the synthesis for 3.1 nm QDs (one-step injection). Absorption and PL spectra of PbS QDs with similar diameter synthesized in a standard scale are also included for comparison.



Synthesis scale-up of PbS QDs with diameter ~2.3 nm. Synthesis of PbS QDs with first-excitonic absorption peaks shorter than 800 nm was also successfully scaled up by separately injecting large amounts of TBP firstly, and then S-OLA (TBP:PbCl₂:S = 1:1:0.42 in molar), instead of using the one-step TBP-route. As an example, PbS QDs with an absorption peak at ~730 nm and a PL peak at 870 nm can be synthesized from one batch at the quantity of ~200 mg (Figure S5).

Figure S5 Absorption/PL spectra (a) and TEM image (b) of ultra-small PbS QDs synthesized by the two-step injection.



Synthesis of PbS/CdS QDs with the shell thickness around 0.5 nm. PbS QD suspension in toluene (1 mL, Absorbance = 3 at the first exciton peak) was first diluted to 10 mL. After N₂ bubbling for 30 min, the PbS QD suspension was heated to 100 °C, followed by the immediate injection of 1 ml of Cd-oleate solution. The reaction was then allowed to proceed for different time in order to get different shell thickness. Specifically, for growing the CdS shell of 0.5 nm in thickness for the LSC device fabrication, the reaction was stopped after 5 h. Finally, the PbS/CdS QDs were purified and re-dispersed in toluene for LSC device fabrication. TEM image and energy-dispersive spectroscopy (EDS) of obtained PbS/CdS are shown in Figure S6.

Figure S6. TEM image (a) and EDS spectrum (b) of PbS/CdS QDs synthesized via cation exchange for luminescence solar concentrator (LSC) application.

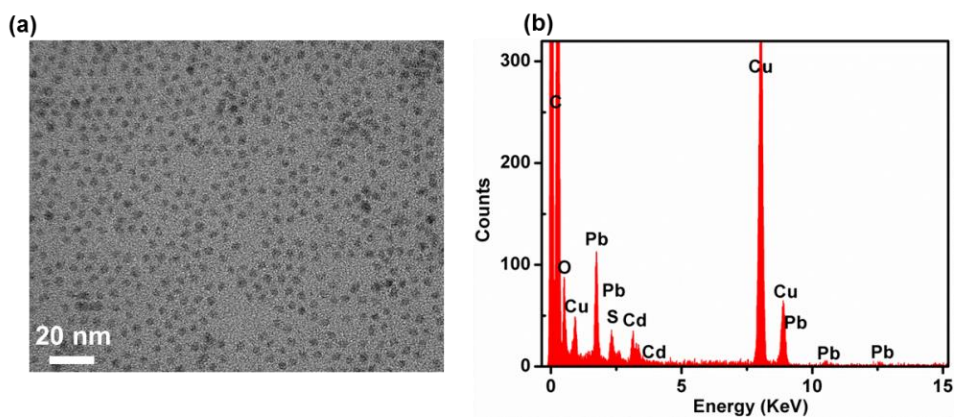


Figure S7. (a) Absorption and PL spectra of PbS QDs (first excitonic peak: ~900 nm; PL: ~960 nm) in solution and a polymer matrix. (b) Optical/quantum efficiency of PbS QDs embedded LSCs with different G factors. (c) Absorption and PL spectra of PbS/CdS QDs (Shell thickness: ~0.5 nm) in solution and a polymer matrix. (d) Quantum efficiency of PbS/CdS QDs embedded LSC devices with different G factors.

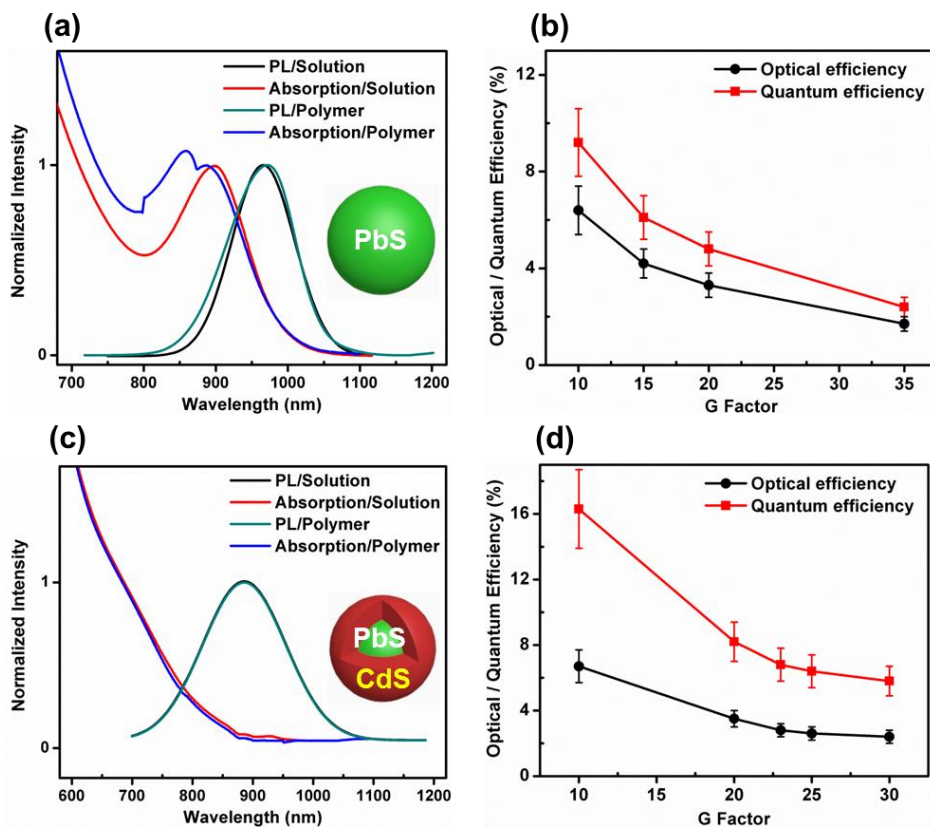


Table S2 Detailed information for fabricated LSC devices using relatively larger PbS (first excitonic peak: ~900 nm; PL peak: ~960 nm) and thicker-shell (0.5 nm) PbS/CdS QDs as luminescent materials, respectively.

Samples	Concentration of QDs (μM)	Length (cm)	G factor	Optical efficiency (%)	Quantum efficiency (%)
PbS-1	14	2	10	6.4	9.2
PbS-2	14	3	15	4.2	6.1
PbS-3	14	4	20	3.3	4.8
PbS-4	14	7	35	1.7	2.4
PbS/CdS-1	24	2	10	6.72	16.3
PbS/CdS-2	24	4.6	23	2.81	6.8
PbS/CdS-3	24	5	25	2.63	6.4
PbS/CdS-4	24	5.8	29	2.38	5.8

Error of quantum/optical efficiency: $\pm 10\%$.

Determination of PbS QD quantity in the scaled-up reaction

Firstly, we determined the molar concentration of synthesized PbS QDs in toluene using the Beer-Lambert's law: $A = \varepsilon CL$, where A is the absorbance at the position of the first exciton absorption peak for a given sample, ε is the extinction coefficient per mole of PbS QDs, C is the molar concentration of QDs, and L is the light path length depending on the cuvette. ε was determined using $\varepsilon = 19600 r^{2.32,4}$, where r is the radius of QDs. R can be calculated by the following formula: $E = 0.41 + 1/(0.0252d^2 + 0.283d)$, where E and d are the bandgap and diameter of obtained QDs, respectively.⁵ Then, the calculated C was converted to mass concentration.² Finally, the product yield per batch can be obtained by using the mass concentration multiplying the total volume of QDs solution.

References

- 1) J. W. Thomson, K. Nagashima, P. M. Macdonald, G. A. Ozin, *J. Am. Chem. Soc.*, 2011, **133**, 5036.
- 2) I. Moreels, Y. Justo, B. D. Geyter, K. Haestraete, J. C. Martins, Z. Hens, *ACS Nano*, 2011, **5**, 2004.
- 3) H. Zhao, M. Chaker, D. Ma, *J. Phys. Chem. C*, 2009, **11**, 6497.
- 4) L. Cademartiri, E. Montanari, G. Calestani, A. Migliori, A. Guagliardi, G. A. Ozin, *J. Am. Chem. Soc.*, 2006, **128**, 10337.
- 5) I. Moreels, K. Lambert, D. Smeets, D. D. Muynck, T. Nollet, J. C. Martins, F. Vanhaecke, A. Vantomme, C. Delerue, G. Allan, Z. Hens, *ACS Nano*, 2009, **3**, 3023.

4.2 Enhanced Long-term and Thermal Stability of Polymer Solar Cells in Air at High Humidity with the Formation of Unusual Quantum Dot Networks

Long Tan, Fan Yang, Mee Rahn Kim, Pandeng Li, Deepak Thrithamarassery Gangadharan, Joëlle Margot, Ricardo Izquierdo, Mohamed Chaker, and Dongling Ma

ACS Appl. Mater. Interfaces **2017**, *9*, 26257–26267.

Concerning the practical application, the stability of the solar cell devices is also very important in addition to their PCE. To the best of our knowledge, investigations on the stability of PSCs are quite limited, and it is challenging to improve their stability performance, especially for the devices operating under abnormal or un-expected conditions.

In this section, both of the long-term and thermal stability of PSCs based on P3HT:PCBM have been largely improved by incorporating inorganic QDs, which are able to stabilize the active film and impede the oxidization of P3HT material by forming unusual QD-networks. The effects of surface ligands on the morphology of the active film, then performance of the devices, were discussed based on characterization results of the active film and device.

I did most of the experimental work and wrote the draft of this manuscript. I also got the help from Fan Yang, who did the FTIR measurement.

Enhanced Long-term and Thermal Stability of Polymer Solar Cells in Air at High Humidity with the Formation of Unusual Quantum Dot Networks

*Long Tan,^a Fan Yang,^a Mee Rahn Kim,^a Pandeng Li,^a Deepak Thrithamarassery Gangadharan,^{a,b}
Jo ðle Margot,^c Ricardo Izquierdo,^b Mohamed Chaker,^a Dongling Ma^{a,*}*

^a Énergie, Matériaux et Télécommunications, Institut National de la Recherche Scientifique (INRS), 1650 Boul. Lionel-Boulet, Varennes, Quebec J3X 1S2, Canada

^b Département d'informatique, University du Québec à Montréal (UQAM), Case postale 8888, succursale Centre-ville, Montreal, Quebec, H3C 3P8, Canada

^c Département de physique, Université de Montréal, 2900 Edouard Montpetit Blvd, Montreal, Quebec, H3T 1J4, Canada

KEYWORDS: Photovoltaic; Organic solar cells; Quantum dots; Near infrared; Stability; Chemical degradation, Morphology stabilization

ABSTRACT: Due to the practical applications of polymer solar cells (PSCs), their stability recently has received increasing attention. Herein, a new strategy was developed to largely enhance the long-term and thermal stability of PSCs in air with a relatively high humidity of 50-60% without any encapsulation. In this strategy, semiconductor PbS/CdS core/shell quantum dots (QDs) were incorporated into the photoactive blend of poly(3-hexylthiophene) (P3HT) and phenyl-C₆₁-butyric acid methyl ester (PCBM). By replacing the initial ligands of oleic acid with halide ligands on the surface of PbS/CdS QDs via solution-phase ligand exchange, we were able to form unusual, continuous QD networks in the film of P3HT:PCBM, which effectively stabilized the photoactive layer. Air-processed PSCs based on the stabilized P3HT:PCBM film showed excellent long-term stability under high humidity, while providing over 3% of power conversion efficiency (PCE) simultaneously. Around 91% of pristine PCE was retained after 30 days storage in high humidity air without encapsulation. This constitutes a remarkable improvement as compared to ~53% retained PCE for the QDs free devices, which can be ascribed to the efficient suppression of both PCBM aggregation and oxidation of the thiophene ring in P3HT thanks to the formation of robust QD networks. Furthermore, the presence of QD networks was able to enhance the stability of the P3HT:PCBM film against thermal stress/oxidation under high humidity environment (50-60%) as well. The device kept 60% of pristine PCE after thermal treatment for 12 h at 85 °C in air, which is more than twice higher than that for the QD-free device. To the best of our knowledge, the work represents the first unambiguous demonstration of the formation of QD networks in the photoactive layer and of their important contribution to the stability of PSCs. This strategy is highly promising for other fullerene-based PSCs, and opens a new avenue toward achieving PSCs with high PCE and excellent stability.

1. Introduction

Solar cells based on inorganic semiconductor nanocrystals^{1,2}, organic materials³⁻⁵ and perovskite materials^{6,7} are considered as promising candidates for next-generation solar cells with both high efficiency and low cost as well as excellent stability. Among these solar cells, polymer solar cells (PSCs) made of earth-abundant, light weight, flexible, low-cost materials,³ have attracted tremendous attention. Thanks to decades of efforts from many research groups, the reported power conversion efficiency (PCE) for single-junction PSCs now exceeds 10%,⁴ which is

considered as the minimum efficiency requirement for their commercialization. Nonetheless, the stability of PSCs, another critical challenge to address in view of commercialization, remains rather limited. One of the major reasons for PCE degradation of PSCs is “chemical degradation”⁸: Oxygen and/or water react with polymer materials and/or metal electrodes (such as Al) which can further be accelerated under illumination via the process known as photochemical degradation. Specifically for polymers, such processes alter their band gap, and their optical, electronic and electrical properties, all directly influencing the solar cell performance. In addition, the morphology of the active layer plays a significant role in determining the PCE of PSCs based on polymer and fullerene materials.⁹⁻¹² In many cases, the optimum morphology giving rise to the high PCE achieved by solvent/additive engineering or film annealing treatment is metastable. The gradual relaxation of this optimum morphology with time toward the thermodynamic equilibrium state can lead to PCE loss. For instance, phenyl-C₆₁-butyric acid methyl ester (PCBM) as a small molecule with weak intermolecular interactions is highly likely to diffuse in the entire blend film with time and to eventually form macro-scale PCBM aggregates/crystallites.¹³ These aggregates can cause poor charge separation and transport, and electrode delamination.¹³⁻¹⁷ All of these degradation issues become even worse when PSCs have to be operated under abnormal conditions, such as high humidity or elevated temperature.¹⁸ It is important to realize that although the chemical (photochemical) degradation of PSCs can be delayed by proper encapsulation, the morphology stabilization is hard to achieve.

In view of reducing the chemical degradation for improving the stability of PSCs, recent advances are mainly focused on three aspects. First, a blocking layer (also named buffer layer), made of materials like TiO_x and ZnO, between the photoactive material and the metal electrode was employed to scavenge oxygen and impede the permeation of oxygen and moisture into polymer through the metal electrode.¹⁹⁻²¹ Another effective approach to improve the stability of PSCs is to design and build so-called inverted solar cells, in which a low-work-function metal is replaced by a less air-sensitive, higher-work-function metal as hole-collecting back electrode, whereas the commonly used, highly acidic poly(3,4-ethylenedioxythiophene):polystyrene sulfonate is replaced by metal oxide as electron selective electrode.^{22,23} In this case, the nature of charge collection is reversed. The design and synthesis of new polymers with a highest occupied molecular orbital (HOMO) energy level deeper than that of conventional polymers is also able to improve the inherent stability of polymer materials.²⁴ To control the morphology of the active

layer, several approaches were attempted. These include (i) cross-linking fullerene derivatives or polymer networks, (ii) chemical coupling of fullerene and polymer, and (iii) increasing the glass transition temperature (T_g) by using higher molecular weight polymers, which can slow down the migration of small organic molecules like PCBM.¹³⁻¹⁷ Alternatively, enhanced morphology stability was also obtained by adjusting the electron extraction layer. This was found to significantly affect the nucleation of PCBM aggregates at the interface between the active layer and the electron transport material.¹³ In addition, in a promising study SiO₂ nanoparticles were used as inorganic additives to manipulate the morphology of organic thin films and improve the transistor performance,²⁵ which may be applied to PSCs as well.

Quantum dots (QDs) have attracted tremendous attention in the photovoltaic (PV) field, owing to their unique, size-tunable optical properties and band gap, high potential for efficient multiple exciton generation and hot carrier extraction, and low-cost solution processability.^{1,26,27} In addition to being considered as the major light absorber in QD-sensitized solar cells, QD-based Schottky solar cells and QD-metal oxide heterojunction solar cells, an active layer composed of organic polymer and inorganic QDs was proposed to offer opportunities for fabricating PV devices (known as inorganic-organic hybrid solar cells) with advantages from both organic materials and QDs.^{28,29} In particular, near infrared (NIR) QDs featuring broad absorption from the ultraviolet and visible spectral ranges to NIR are highly attractive to expand the photoresponse of PSCs.³⁰⁻³² Further considering these less-than-10 nm QDs may act as nanoparticle additives to stabilize the morphology, we developed a new strategy to improve the performance of PSCs based on poly-3-hexylthiophene (P3HT):PCBM using NIR PbS/CdS QDs capped by short halide ligands as structural stabilizer. Different from the traditional hybrid solar cell, the content of incorporated QDs was around 10 wt %, much less than over 50 wt % commonly reported in previous work.^{33,34} Therefore, P3HT acted as the major light absorbing material in our case, whereas QDs were expected to mainly play a role for improving the stability of the solar cell device and increase the NIR photoresponse of device. By manipulating the surface ligand of QDs, a unique, continuous network mainly composed of QDs was formed for the first time, leading to excellent long-term air stability under high humidity, achieving a PCE comparable to that reported for P3HT:PCBM based devices.³⁵ Furthermore, the QD networks were found to stabilize the P3HT:PCBM film under thermal stress at high humidity. This solves a highly challenging issue as the P3HT:PCBM blend has a low T_g (~40 °C with a

PCBM content of 40%).³⁶ It is worth highlighting that all of the stability performance investigations were conducted in air with high humidity of 50-60%, which is typical in actual applications of PSCs, even though such conditions are rarely reported in the literature. Therefore, our work opens new opportunities toward the achievement of highly stable PSCs and toward their commercialization.

2. Experimental

2.1 Synthesis of PbS QDs

PbS QDs were synthesized following the procedure previously reported by our group.³⁷ Typically, 760 mg of $\text{Pb}(\text{OAc})_2 \cdot 3\text{H}_2\text{O}$ ($\geq 99.99\%$), 2.4 mL of oleic acid (OA, $\geq 99\%$) and 15 mL of 1-octadecene (ODE, 90%) were added to a three neck round bottom flask and heated to 150 °C for 1 h while being stirred and purged with N_2 flow. This lead precursor solution was cooled under vacuum to 130 °C and N_2 flow was resumed. Two millilitres of mixture of bis(trimethylsilyl) sulfide (synthesis grade) and trioctylphosphine (technical grade, 90%) in a volume ratio of 1:10 were injected into the flask, and the temperature was decreased to 100 °C very quickly. The QD growth reaction was quenched with cold water after 5 minutes. The obtained PbS QDs were dissolved in toluene and kept at 4 °C for 2 days before purification with repeated centrifugation/re-dispersion processes. The concentration of the PbS QDs can be determined by measuring their absorption spectrum, and the calculation details can be found in Supporting Information.

2.2 Synthesis of PbS/CdS QDs

A high concentration of Cd-OA was prepared by mixing CdO ($\geq 99.99\%$ trace metals basis), ODE and OA, and by heating the mixture to 250 °C. After CdO was dissolved (solution changed to transparent), the mixture solution was cooled to about 160 °C, and pumped for 30 min. Then, the as-prepared PbS QDs were dissolved in 20 mL toluene after purification. Appropriate amounts of Cd-OA solution were added into the PbS QD dispersion. After 3-min stirring and 6-min bubbling by N_2 , the solution was placed in a microwave reactor for 8 s at 100 °C to get PbS/CdS core/shell QDs with 0.1 nm CdS shell. Finally, the QDs were purified by ethanol and then by acetone washing.

2.3 Metal halide treatment to the PbS/CdS QDs

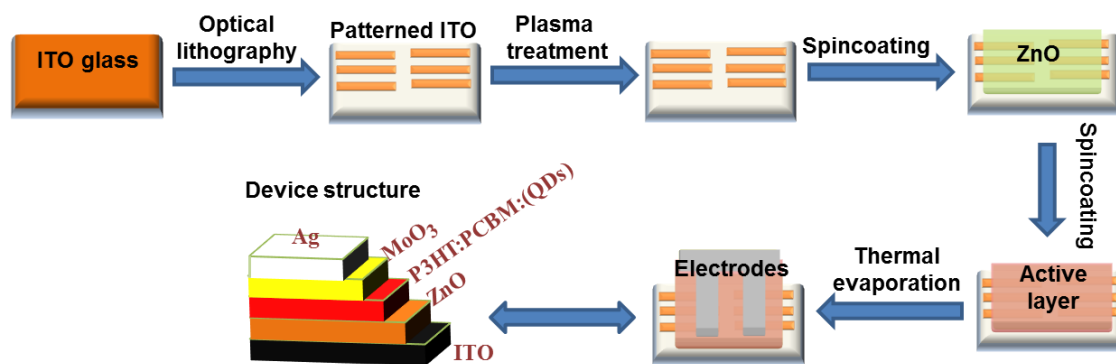
Halide treatment was carried out in solution following the ligand exchange procedure previously reported.^{26,38} First, a stock CdCl₂ solution was prepared by mixing 600 mg of CdCl₂ (99.999% trace metals basis), 66 mg of tetradecylphosphonic acid (97%) and 10 ml of oleylamine (technical grade, 70%) in a flask and heating the mixture at 100 °C under vacuum for 1 h. Subsequently, 10 mL PbS/CdS QDs solution (25 mg/mL in toluene) was heated to 60 °C under N₂ flow, and 0.75 mL of CdCl₂ stock solution was injected and kept at 60 °C for 30 min under magnetic stirring. The obtained halide-PbS/CdS QDs were purified by ethanol and acetone washing successively and further dispersed in dichlorobenzene for characterization and solar cell fabrication.

2.4 Preparation of ZnO precursor solution

ZnO precursor was prepared by dissolving zinc acetate dihydrate (Zn(CH₃COO)₂ · 2H₂O, 99.9%) and ethanolamine (NH₂CH₂CH₂OH, 99.5%) in 2-methoxyethanol (CH₃OCH₂CH₂OH, 99.8%) under vigorous stirring for 12 h for the hydrolysis reaction in air.

2.5 Fabrication of solar cell devices

Indium tin oxide (ITO) glass substrates (2.5 cm × 2.5 cm) were sequentially washed in water, acetone and isopropanol for 20 min each. An optical lithography technique was then used to pattern the substrates (Scheme 1). The patterned ITO glass substrates were cleaned again in acetone and isopropanol for 10 min each, followed by oxygen plasma treatment for 2 min. The ZnO precursor solution was then spin-coated onto the patterned ITO glasses and annealed at 200 °C for 30 min in air to get the ZnO film (an electron transport and hole blocking layer). P3HT (RR93-95, solaris):PCBM (>99.5%, solaris):QDs (1:0.8:0.2 by weight) solution in 1,2-dichlorobenzene was spin-coated onto the ZnO layer to form the photoactive film and kept in a petri dish for 30 min for aging before the thermal annealing step at 140 °C for 10 min. Finally, the fabrication of the solar cell device was completed by depositing a 20 nm thick layer of MoO₃ on the photoactive film followed by an 80 nm thick layer of Ag through a shadow mask, which makes the photoactive area of about 6 mm².



Scheme 1. Illustration of PSC device fabrication process.

2.6 Characterization

Absorption spectra of the QDs were acquired with a Cary 5000 UV-Vis-NIR spectrophotometer (Varian) scanning the sample at a speed of 600 nm/min. Synthesized PbS and PbS/CdS QDs were also characterized by transmission electron microscopy (TEM, JEOL 2100F). The Fluorolog®-3 system (Horiba Jobin Yvon) was employed to measure the relative photoluminescence quantum yield (QY) of QDs using IR 125 dye as a reference. X-Ray photoelectron spectrometry (XPS) was performed using a VG Escalab 220i-XL equipped with an Al K_α source. The XPS data were analyzed with the Casa software. Atomic force microscopy (AFM) (Bruker Corporation) with a silicon tip on a nitride lever was employed to investigate the film morphology. Topography images of the photoactive layers were obtained in the ScanAsyst mode. The different domains composed of inorganic QDs and organic materials were detected in the contact mode by measuring the lateral bending of the cantilever. X-ray diffraction (XRD, Panalytical X-Pert PRO MRD, Bruker Corporation) characterization was performed on the film samples. The films were covered by a MoO₃/Ag layer during long-term aging to simulate the actual device conditions. Fourier transform infrared spectrometer (FTIR, Digilab FTS7000) in the transmittance mode was employed to detect the change of chemical bonds of the organic material in the film. The solar cells were characterized by current-voltage (J-V) measurements under illumination by an AM 1.5 solar simulator. External quantum efficiency (EQE) measurements were also conducted using an IQE200B system (Newport Corporation).

3. Results and discussion

The surface of the PbS QDs was modified before using them for PV applications. As seen in Figure 1(a), as-prepared OA-capped PbS QDs (denoted as OA-PbS) have their first-excitonic absorption peak position around 996 nm. After cation-exchange reaction, Pb^{2+} ions are partially replaced by Cd^{2+} ions, yielding a thin shell of CdS on the QDs, without changing their overall diameter.^{39,40} Such a thin shell formation results in the blue shift of the absorption spectrum of QDs. In our case, the absorption peak is blue-shifted to 954 nm, which corresponds to the formation of a shell thickness of 0.1 nm.⁴¹ The purpose of forming such a thin CdS shell was to significantly improve the air-stability of PbS QDs as well as their thermal- and photo-stability, without blocking charge carrier transport, all of which are highly relevant to solar cell applications.^{37,42,43} Both PbS QDs (diameter: ~3.3 nm) and PbS/CdS core/shell QDs (denoted as OA-PbS/CdS) are mono-dispersed without any aggregation, with high QY of 72 and 68%, a feature indicating the high quality of the obtained QDs (Figure 1 (b)). Metal halide treatment was further employed to largely replace OA on the QD surface with much smaller halide. The produced halide passivated PbS/CdS QDs (denoted as halide-PbS/CdS) cause the red shift of the first excitonic absorption peak, in agreement with already reported results.³⁸ XPS was employed to examine the surface chemistry of the PbS/CdS QDs before and after metal halide treatment. As seen in Figure 1(c), lines associated with Pb, S, C, Cd and O are detected for both OA-PbS/CdS and ligand-exchanged PbS/CdS QDs, whereas the Cl 2p peak is only observed for halide-PbS/CdS (the Si peak originates from the substrate holder). Additionally, the atomic ratios of C/O/Pb of OA^- and halide-PbS/CdS are estimated to be 55:10:1 and 17:3:1, respectively, thereby confirming that large numbers of OA^- ligands are replaced by Cl^- ligands. Figure 1(d) displays the high resolution Cl 2p spectrum of halide-PbS/CdS. The Cl 2p_{3/2} binding energies are located around 197.7 eV, which is in line with that of Cl^- found in chelate compounds.⁴⁴ This could be attributed to the formation of electrostatic bonds between metal cations and Cl^- ions on the QD surface. The halide ligands are able to form a dense ligand shell and to reach the midgap trap states, which cannot be achieved by long-chain ligands, like OA^- , owing to the “steric effect”.⁴⁵ Therefore, this surface treatment can effectively reduce the density of trap states, which leads to the recombination of photo-generated carriers. Additionally, the surface S atoms with unsaturated dangling bonds can also be passivated by Cd^{2+} via this treatment. Therefore, the halide-PbS/CdS obtained by surface engineering is suitable for solar cell application.

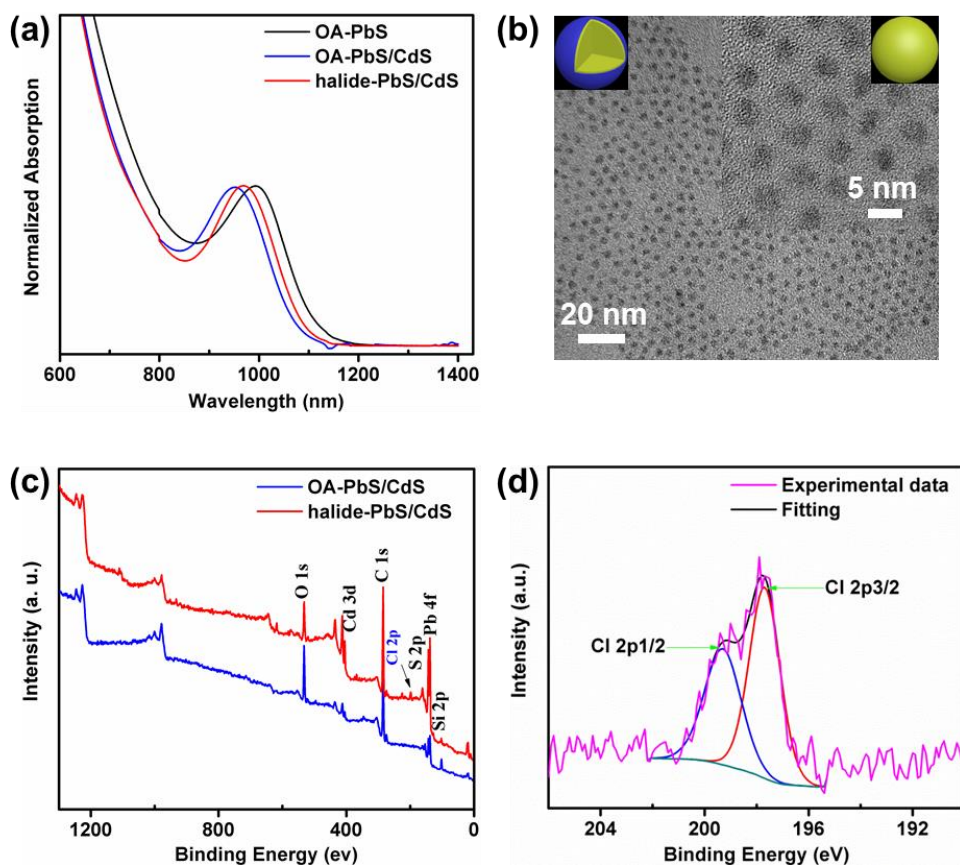


Figure 1. (a) Absorption spectra of OA-PbS, OA-PbS/CdS and halide-PbS/CdS; (b) TEM images of as prepared OA-PbS/CdS and OA-PbS (inset); (c) XPS survey spectra of OA- and halide-PbS/CdS; (d) High resolution XPS Cl2p spectrum of halide-PbS/CdS.

The morphology of the photoactive layer is crucial for the performance of polymer:fullerene based PSCs. To prevent the undesired effect of solvent on film morphology with and without the presence of QDs, the as-prepared halide-PbS/CdS QDs were first dispersed in the same dichlorobenzene solvent as used for preparing the QD-free film of P3HT:PCBM, prior to their mixing with P3HT:PCBM blend solution. The morphology of fabricated P3HT:PCBM:halide-PbS/CdS film was analyzed by AFM and compared to that of the QD-free P3HT:PCBM film. Figure 2(a) shows the topography image of P3HT:PCBM film, which displays a typical morphology relatively uniform with root-mean-square (RMS) roughness of about 9.2 nm. As for the P3HT:PCBM:halide-PbS/CdS film, an unusual, continuous network appears in the whole film (RMS: 9.5 nm, Figure 2(b)). Lateral force images were acquired in the contact mode scanning. In this mode, the surface features corresponding to different friction characteristics can be revealed. These characteristics are determined from the voltage response corresponding to the

lateral force applied on the cantilever. As seen in Figure 2(c), the voltage response is very similar over the whole surface of the P3HT:PCBM film, indicating that the exerted lateral forces are homogeneous. This result is in good agreement with the morphology of the corresponding topography image (Figure 2(a)). For the P3HT:PCBM:halide-PbS/CdS film, much higher response voltage was observed in the regions corresponding to the observed network (Figure 2(d)) as can be seen by comparison with the topography image (Figure 2(b)). Such a dramatic difference can be attributed to the formation of inorganic QD-rich domains (denoted as QD networks herein), which can provide stronger lateral forces on the AFM cantilever than the organic-material-rich domain.

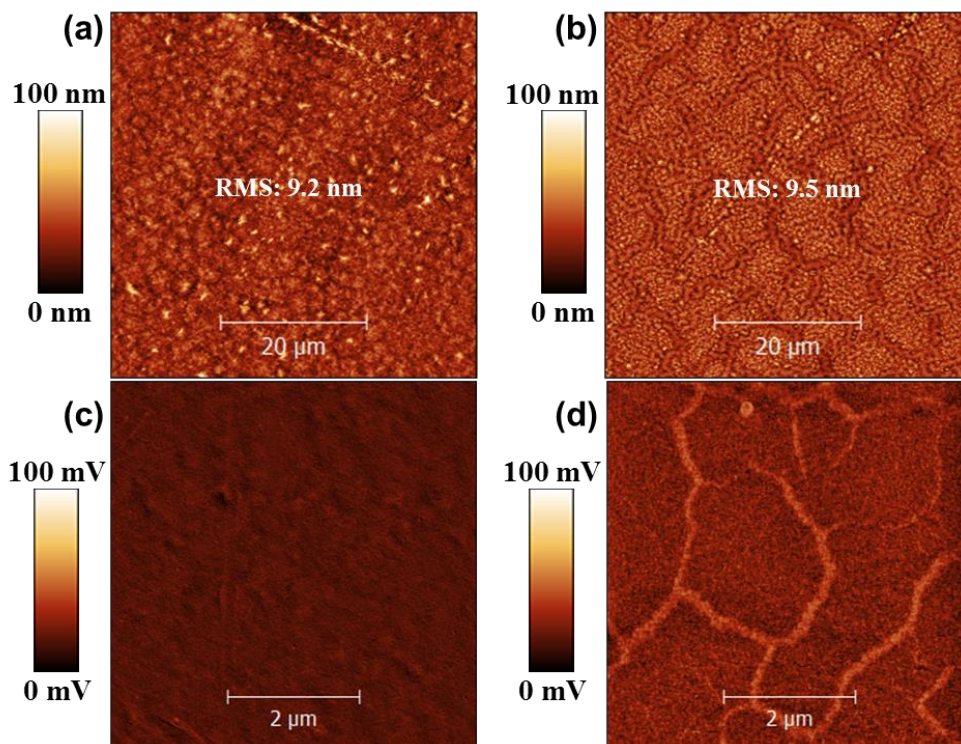


Figure 2. AFM topography images of P3HT:PCBM (a) and P3HT:PCBM:halide-PbS/CdS (b) films by ScanAsyst mode scanning; Lateral force images of P3HT:PCBM (c) and P3HT:PCBM:halide-PbS/CdS (d) films by contact mode scanning.

Because quite different film morphologies have been identified with and without halide-PbS/CdS, it is very interesting to examine their PV performance that is known to be strongly correlated to the morphology. We thus fabricated solar cell devices based on these two films. The device band diagram is shown in Figure 3(a). The J-V measurements were performed under

AM 1.5 illumination. As seen in Figure 3(b), by incorporating halide-PbS/CdS into the active layer, the short-circuit current (J_{sc}) of the device is slightly enhanced, whereas the open circuit voltage (V_{oc}) and fill factor (FF) are decreased compared to those of QD-free device. These results can be understood by considering the roles of QDs in the active layer. Indeed, the halide-PbS/CdS QDs regarded as a broad-band light absorbing material are able to generate excitons. These excitons can possibly dissociate to produce charge carriers due to the band alignment of the three components (Figure 3(a)). Electrons can then be transported by PCBM to ZnO, and holes by P3HT and/or QD networks to MoO₃/Ag. Therefore, the presence of halide-PbS/CdS could contribute to increase J_{sc} , while slightly lowering V_{oc} due to their narrower band gap than P3HT. Figure 3(c) shows the EQE spectra for both halide-PbS/CdS and QD-free samples. We can see that the efficiency in the 340-500 nm range is slightly increased compared to those of the QD-free sample, which can be attributed to the enhancement of light absorption in the active layer due to the presence of QDs. The total J_{sc} calculated from these spectra is about 8.3 and 8.5 mA cm⁻² for the QD-free and halide-PbS/CdS samples, respectively. These values are in good agreement with the results obtained from J-V measurements. Furthermore, as shown in the inset in Figure 3(c), the photoresponse of the halide-PbS/CdS device was extended to the NIR range. Overall, the halide-PbS/CdS device yields a PCE of about $3.17 \pm 0.15\%$, (average), which is comparable to that of the QD-free device (average PCE: $3.37 \pm 0.24\%$) as well as to the commonly reported values for P3HT:PCBM (average PCE: $\sim 3.0\%$).^{35,46}

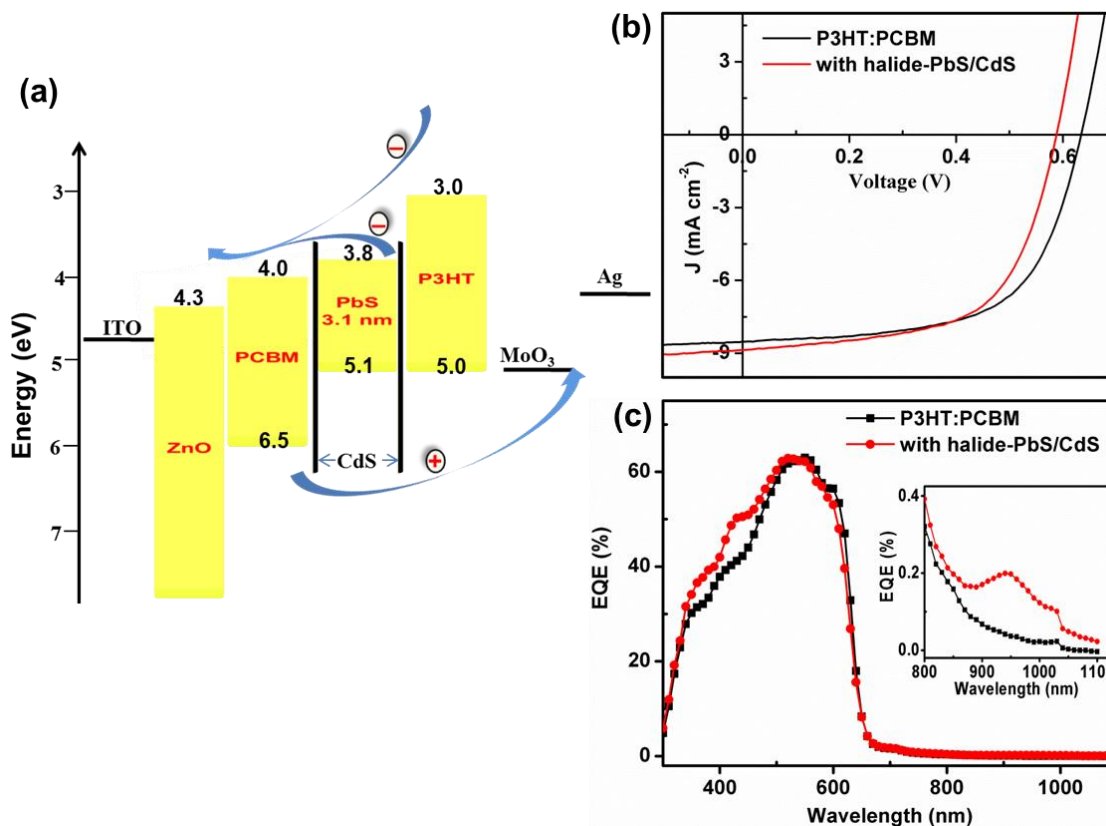


Figure 3. (a) Band diagram of the device with the inverted structure of ITO/ZnO/P3HT:PCBM:QDs/MoO₃/Ag; representative J-V curves (b) and EQE spectra (c) of the QD-free and halide-PbS/CdS QDs incorporated devices.

The long-term stability of the fabricated devices with and without halide-PbS/CdS was examined by maintaining them in an environment with air at a relatively high humidity of 50-60% and in the dark. For the QD-free device, the efficiency gradually decreases from 3.37% to 1.8%, that is, by nearly 50% after 1 month storage (Figure 4(a)). This performance is better than that for the conventional device,²² which emphasizes the advantage of the inverted structure. Moreover, the PCE degradation is further slowed down for the halide-PbS/CdS incorporated device. In this case, after one month storage, 90.7% (PCE: 2.87%) of the pristine efficiency (PCE: 3.17%) is maintained (Figure 4(b)), which is comparable to the previously published best results (~89% remaining after 32 days in ambient air with unknown humidity, whereas the current work was under high humidity of 50-60%) in similar conditions.²² The long-term stability of our devices (un-encapsulated) is even better than that of the encapsulated P3HT:PCBM devices (85% of PCE was retained after 30 days)¹¹. It is also better than the recently reported work for P3HT:PCBM

devices (90% of pristine PCE was retained in ~23 days and 80% in ~34 days)⁴⁷. The analysis of the PV parameters J_{sc} , V_{oc} and FF of the QD-free device reveals that each tends to decrease with time, resulting in the decrease of PCE as well. However, the reduction of the FF (by 27%), which is greatly affected by charge carrier recombination and transport, is more severe than that of J_{sc} (by 15.8%) and V_{oc} (by 13.1%). This finding implies that the degradation of the photoactive layer is related to the appearance of charge carrier recombination sites. In contrast, quite different results were obtained for the device containing the halide QDs. First, J_{sc} is relatively stable over the whole storage duration. Second, V_{oc} even increases unexpectedly, which could be ascribed to the oxidization of QDs and thereby to the increase of their band gap. Similar results were obtained by exposing the device based on a compact PbS QDs layer to air, although the mechanism yielding the V_{oc} increase is still unclear.^{2,27} On the other hand, the oxidization of QDs could produce $PbSO_4$ on the QD surface, which introduces a mid-gap state that serves as a recombination center for photo-generated charge carriers, leading to the slight decrease of the FF. These results clearly show that the stability of PSCs is dramatically improved in the presence of QDs. The series (R_s) and shunt resistances (R_{sh}) were extracted from the J-V curves to further analyze the cause of long-term stability enhancement. For the QD-free device, R_s increases from 9.5 to 17.5 $\Omega\text{ cm}^2$, while R_{sh} decreases from 1145 to 289.4 $\Omega\text{ cm}^2$. However, these changes of R_s (from 10 to 12.5 $\Omega\text{ cm}^2$) and of R_{sh} (from 857.7 to 833.3 $\Omega\text{ cm}^2$) are considerably reduced for the QD device. These results explain the larger increase of charge recombination centers for the QD-free device as compared to the QD device, which leads to faster degradation.

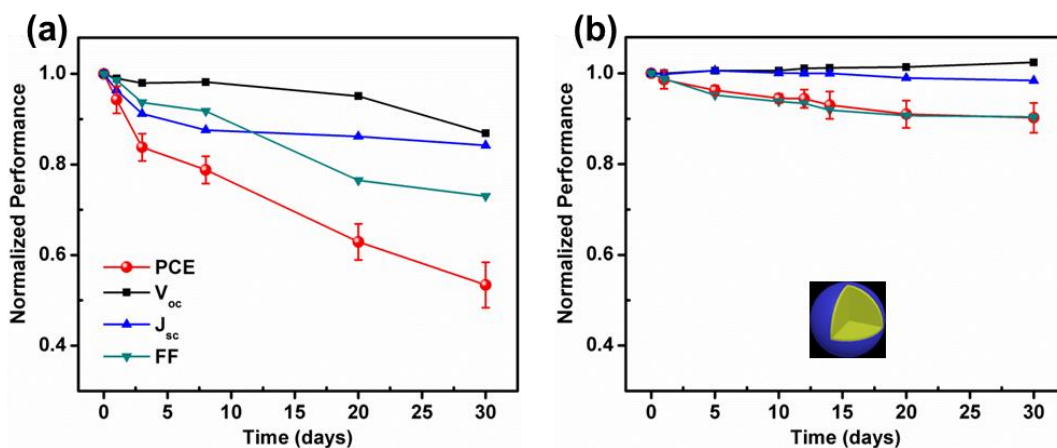


Figure 4. Long-term stability performance of unencapsulated devices in air under high humidity of 50-60% based on the film of P3HT:PCBM (a) and P3HT:PCBM:halide-PbS/CdS (b).

To elucidate the underlying mechanism yielding the strongly enhanced long-term stability of cells in the presence of QDs, XRD was employed to get deeper insights into the morphology change of the film after 30 days storage as compared to the pristine film. For both P3HT:PCBM and P3HT:PCBM:halide-PbS/CdS (Figure 5(a,b)), the pristine films shows a sharp diffraction peak around 5.3° which is attributed to the (100) plane of crystallized P3HT.⁴⁸ This indicates a high degree of film crystallinity. Based on the full width at half maximum of the peak, we calculated the mean size of the P3HT crystallites for both samples, which are about 15 nm (QD-free) and 13 nm (with halide-PbS/CdS), respectively.⁴⁹ After 30 days storage, the intensity of the (100) peak for the P3HT:PCBM film has decreased by 19%. On the other hand, an additional well-shaped peak, although not intense, appears around 12.3° together with a bump centered at 18° , which reflects the formation of PCBM crystallites clusters. These results indicate that the degree of crystallinity of P3HT has decreased and that PCBM has aggregated when exposed to highly humid air. The lower level of structural ordering of P3HT causes lower carrier mobility in the P3HT domain and phase segregation leads to a reduced donor/acceptor interface, which requires excitons to diffuse over longer distances before their dissociation at the interface. As a consequence, recombination events can grow, consistently with the large drop of FF. This finding differs from that of the device kept in inert atmosphere, where the active layer is claimed to be relatively stable.⁵⁰ In our case, the oxidization risk of P3HT is drastically increased when stored in highly moisturized air, which leads to the reduction of the P3HT crystallinity.^{46,51} The latter decrease could facilitate the diffusion of PCBM and therefore the re-arrangement of the microstructure of P3HT:PCBM, resulting in a further deterioration of the device performance. Interestingly, the diffraction pattern of the P3HT:PCBM:halide-QDs film remains almost unchanged after 30 days storage. This observation supports the successfully stabilized structure of the active film, in good agreement with the excellent long-term stability obtained for the device based on halide-PbS/CdS.

FTIR was employed for getting in-depth insights into the possible change of chemical structure of the P3HT:PCBM film with and without halide-PbS/CdS in the presence of air. To this purpose, the film of the photoactive layer was scratched from the substrate and mixed with KBr powder to prepare a thin plate sample for FTIR measurements. This procedure was completed in air over a short time (~15 min), and was reproduced for all samples. Figures 5(c,d) (black lines) shows the FTIR spectra of pristine P3HT:PCBM and P3HT:PCBM:halide-PbS/CdS,

respectively. The characteristic absorption bands for P3HT and PCBM such as those located at 1737 cm^{-1} (C=O stretching vibration of PCBM), and 1269 cm^{-1} (C-C vibration) and between 1565 and 1470 cm^{-1} (C=C vibration in the aromatic ring) are clearly observed for the P3HT:PCBM sample.^{46,52,53} It is noteworthy that a sharp and relatively strong band at 1386 cm^{-1} ascribed to the S=O stretching vibration is also detected.⁴⁶ The presence of this peak features the oxidation reaction between the thiophene ring and $\text{O}_2/\text{H}_2\text{O}$ that occurred during the device fabrication and/or the sample preparation. This reaction is confirmed from both experimental results and theoretical calculations, although the detailed oxidation mechanism is still under debate.^{54,55} For the P3HT:PCBM:halide-PbS/CdS sample, the above mentioned P3HT and PCBM characteristic bands were also observed, even though some of them are shifted (Figure 5(c,d)), likely due to the presence of QDs affecting the electric dipoles and vibration of the chemical bonds. A similar effect was found by incorporating aluminum particles into P3HT:PCBM film.⁴⁶ Interestingly, the band of S=O stretching vibration was absent in the FTIR spectrum of the P3HT:PCBM:halide-PbS/CdS sample. This strongly suggests that the chemical degradation of P3HT is significantly reduced by incorporating halide-PbS/CdS. A rather weak peak at 1377 cm^{-1} is observed, which characterizes terminal $-\text{CH}_3$ groups of hexyl side chains connected to the thiophene ring.⁵⁶ Its appearance can be attributed to the π - π stacking of P3HT chain slightly affected with the addition of QDs. As for the aged P3HT:PCBM sample (red lines), the S=O stretching band was observed as expected. Because the 1548 cm^{-1} band is considered as characterizing the C=C stretch of thiophene ring and because its intensity decreases with the chemical degradation of P3HT,⁴⁶ we have evaluated the level of chemical degradation by comparing the intensity ratio of 1386 to 1548 cm^{-1} between pristine and aged samples. The intensity ratio was found to considerably increase from ~ 2.1 to ~ 3.8 with aging, strongly confirming the significant chemical degradation taking place during storage of the P3HT:PCBM sample. In contrast, the aged P3HT:PCBM:halide-PbS/CdS film does not show any obvious change of its spectrum, in agreement with the high stability of its PV performance. No oxidation signs of PCBM are discernable from the obtained FTIR spectra.

We speculate that the positive contribution of QDs to the stability could mainly originate from the following features: 1) the QDs themselves acting as $\text{O}_2/\text{H}_2\text{O}$ scavengers, 2) the QD network serving as an effective diffusion barrier to $\text{O}_2/\text{H}_2\text{O}$ and remarkably retarding their diffusion into the organic materials; and 3) the QD network limiting the PCBM diffusion toward aggregation.

The important role of the QD network was further confirmed by using OA-PbS/CdS in solar cells. By means of different surface ligands of QDs, the morphology of the active film was manipulated, which allowed us to evaluate the contribution of the QD network to PV performance. As seen in Figure 5(e), the active film based on P3HT:PCBM:OA-PbS/CdS presents a morphology quite different from that of the film with halide-PbS/CdS. Specifically, the OA-PbS/CdS QDs are homogeneously distributed in the organic P3HT:PCBM matrix without the formation of QDs networks, leading to a quite smooth active surface with a low RMS of 2.2 nm. The corresponding lateral force image (the inset of Figure 5(e)) with constant value of voltage response further confirmed the absence of QD networks in the film. It is ascribed to the different chemical nature of the surface ligands.⁵⁷ Because of their long hydrocarbon chain of OA ligands, OA-capped QDs show much better compatibility with P3HT:PCBM, while halide ligands result in lower compatibility, leading to the formation of well separated QD domains (refer to Figure S1 for the process of the QD network formation). The “beneficial effect” of the QDs on the long-term stability strongly diminishes in this case. After 30 days of storage under the same high humidity conditions, the average PCE of the P3HT:PCBM:OA-PbS/CdS device decreased from 2.82% to 1.73% by 38.7% (Figure 5(f)), although “oxygen scavenging effect” was likely causing a slight increase of V_{oc} . These results strongly suggest the importance of the surface treatment of QDs and of the formation of QD networks in impeding the degradation of the active film. The scavenging effect of the QDs themselves is definitely not a dominant factor. The ligands on the QD must have played a significant role in the network formation and stability enhancement, resulting from different QD-P3HT:PCBM and P3HT:PCBM:QDs-MoO₃/Ag interfaces.

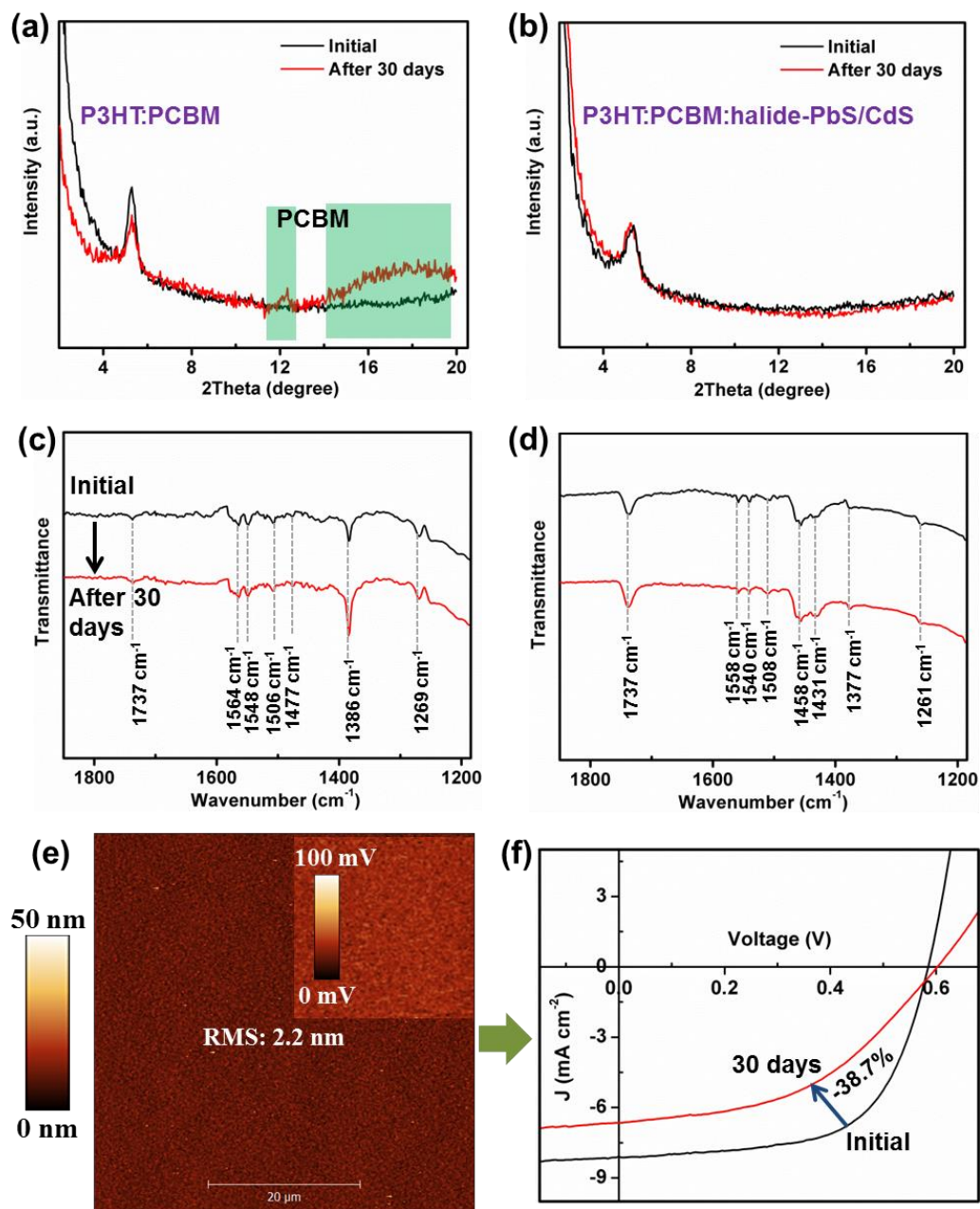


Figure 5. XRD spectra of P3HT:PCBM (a) and P3HT:PCBM:Halide-QDs (b) films before and after being kept 30 days in air at humidity of 50-60%. FTIR spectra of samples prepared by scratching the P3HT:PCBM (c) and P3HT:PCBM:Halide-QDs (d) film. AFM topography images of P3HT:PCBM:OA-PbS/CdS film (e) and the corresponding lateral force image (inset). Typical J-V curve of devices, based on P3HT:PCBM:OA-PbS/CdS film, before and after 30 days storage (f).

For ensuring the thermal stability of PSCs, a stabilized photoactive layer is certainly important but challenging to achieve, especially for the P3HT:PCBM blend with low T_g .³⁶ Herein, we

examine the morphology change of the P3HT:PCBM:halide-PbS/CdS and P3HT:PCBM films after thermal annealing at 85 °C (temperature applied as a PV industry standard¹³) for 30 min under high humidity of 50-60%. As seen in Figure 6(a,b) for the P3HT:PCBM film before and after thermal treatment, although the RMS for the entire film is relatively stable, deep and wide cracks appear under thermal stress. The geometric details of these cracks were extracted from the AFM image, and are displayed in Figure 6(e). Such cracks are expected to induce the contact problem between the P3HT:PCBM film and the MoO₃/Ag electrode, and destroy the carriers transport channels in the photoactive film, both leading to some PCE loss. As for the film with QD networks, there is no obvious change after thermal treatment (Figure 6(c,d)), suggesting that damages from the thermal stress are significantly reduced. In other words, the presence of robust QD networks helps to freeze (immobilize) the organic film morphology under thermal stress.

The FTIR spectra of both P3HT:PCBM and P3HT:PCBM:halide-PbS/CdS samples before and after thermal annealing are exhibited with the aim of investigating the “thermal effect” on the change of chemical state (Figure 6(f)). We notice that the intensity ratio of the 1386 to 1548 cm⁻¹ peaks is obviously increased for the thermally treated P3HT:PCBM sample. This is caused by the accelerated oxidation of P3HT by thermal annealing, which underlines the challenge and importance of enhancing the thermal stability of P3HT:PCBM in air. Additionally, detailing the spectra (not shown), it is found that the bandwidth is changed in the absorption range of 1565-1470 cm⁻¹, and that the 1269 cm⁻¹ band is shifted to 1261 cm⁻¹. These results indicate a structural change during thermal annealing. However, in the presence of QD networks, the chemical degradation under thermal annealing is prevented, as evidenced by the lack of change of the FTIR spectrum.

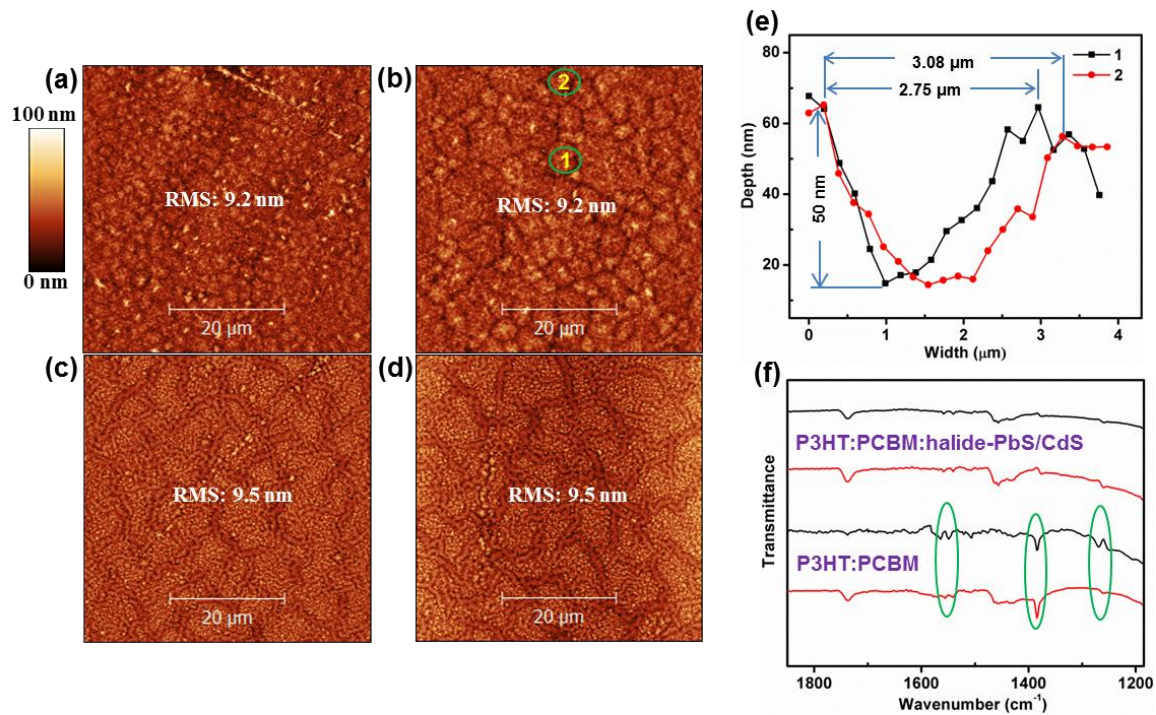


Figure 6. AFM topography images of P3HT:PCBM before (a) and after (b) thermal treatment; Images of P3HT:PCBM:halide-QDs film before (c) and after (d) thermal treatment; (e) Geometries details extracted from cracks 1 and 2 highlighted in (b); (f) FTIR spectra of different films before (black) and after (red) thermal annealing at 85 °C for 30 min under high humidity of 50-60%.

The effect of thermal treatment on the device PV performance was investigated by exposing the solar cell devices based on the P3HT:PCBM and P3HT:PCBM:halide-QDs films at the same temperature under a relatively high humidity rate of 50-60%. The PCE, V_{oc} , J_{sc} and FF are plotted in Figure 7(a,b) as a function of the thermal annealing duration. For the device based on P3HT:PCBM, over 50% of the pristine PCE is lost in the first 30 min, which could be attributed to the occurrence of cracks in the P3HT:PCBM film under thermal stress and to P3HT oxidation, consistently with the R_s and R_{sh} changes observed from the J-V curves. Recall that R_s drastically increases from 9.5 to 18.5 $\Omega\text{ cm}^2$, while R_{sh} varies at the opposite. Pursuing the thermal treatment to 12 h, only about 25% of the pristine PCE is retained. For the device with QD networks, the performance degradation is strongly slowed down. About 85.2% and 60% of pristine PCE are retained after 30 min and 12 h of thermal treatment, respectively. The greatly improved thermal stability of the device can be attributed to the remarkably reduced oxidation and improved immobilization of the organic materials owing to the presence of QD networks as

confirmed by the FTIR and AFM characterizations. The pristine R_s of $10 \Omega \text{ cm}^2$ did not change in the first 30 min, which well confirms the enhanced thermal stability of the device. The thermal stability of devices based on P3HT:PCBM:OA-PbS/CdS has also been recorded, and the results are shown in Figure S2. Briefly, around 31.5% of the pristine PCE was retained after 12 h thermal treatment, which is much worse than that of P3HT:PCBM:halide-PbS/CdS based device. Taking both of the long-term and thermal stability results into consideration, we confirm the significant role of QD networks on enhancing the device stability.

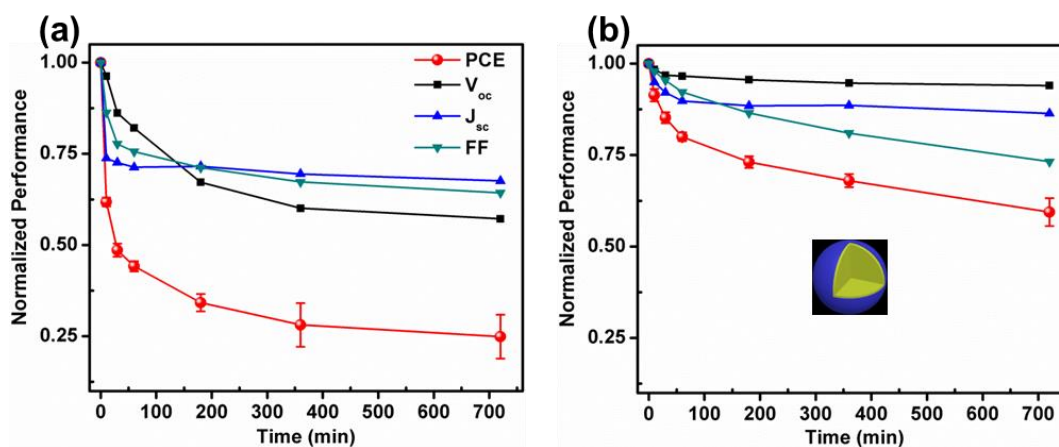


Figure 7. Thermal stability performance of devices based on P3HT:PCBM (a) and P3HT:PCBM:halide-PbS/CdS (b).

4. Conclusions

In summary, a significant improvement of the stability of P3HT:PCBM PSCs was accomplished at a relatively high humidity rate of 50-60% and a high temperature of $85 \text{ }^\circ\text{C}$. QDs with appropriate surface ligands were integrated to effectively stabilize the active layer of PSCs by forming unusual, continuous QD networks (for the first time) in the film. The presence of QD networks impedes the oxidative degradation of P3HT by serving as an effective diffusion barrier to $\text{O}_2/\text{H}_2\text{O}$ and reduces the formation of PCBM aggregates with time, which leads to excellent long-term stability of unencapsulated devices in highly humid air. Furthermore, the QD networks were discovered to suppress the morphology change of the active layer under thermal stress and the chemical degradation of P3HT at $85 \text{ }^\circ\text{C}$, again under high humidity of 50-60%. Therefore, the thermal stability of PSCs based on P3HT:PCBM in air is significantly enhanced. The work clearly underpins the importance of QD surface chemistry in forming QD networks, which play a

dominant role in enhancing the PCE stability. This new strategy could be further extended to other PSCs, such as high efficiency PSCs involving lower bandgap polymers, and hold high promise toward achieving air-processed, high-efficiency and stable PSCs. Further optimization of QDs and organic materials may also allow us to take advantage of the attractive features of QDs in enhancing photon absorption and thereby leading to the simultaneous increase of PCE. In addition, such stabilization strategy can also be applied to other kinds of polymer-based devices, such as light-emitting diodes, and therefore could contribute to the development of a broader field of polymers.

ASSOCIATED CONTENT

Supporting Information

Determination of QD concentration in the solution; topography images of P3HT:PCBM:halide-PbS/CdS film before and after thermal treatment; thermal stability performance of the solar cell device based on P3HT:PCBM:OA-PbS/CdS film.

AUTHOR INFORMATION

Corresponding Author

*E-mail: ma@emt.inrs.ca. Website: <http://www.inrs.ca/dongling-ma/>.

ACKNOWLEDGMENT

The authors thank Mr. Chamoulaud Gwenaél for helpful discussions on the AFM results. The financial support from the Natural Sciences and Engineering Research Council (NSREC) of Canada, in the context of a NSREC Discovery Grant, a NSERC Strategic Grant (industry partner: Canadian Solar Inc.) and an Engage Grant (industry partner: 1-Material Inc.) is greatly appreciated. D. Ma is also grateful for the financial support from Fonds de recherche du Québec-Nature et technologies (FRQNT) and from the Quebec Center for Functional Materials (CQMF), Canada.

References

- (1) Yu, K.; Ouyang, J. Y.; Zhang, Y. G.; Tung, H. T.; Lin, S. Q.; Nagelkerke, R. A. L.; Kingston, D.; Wu, X. H.; Leek, D. M.; Wilkinson, D.; Li, C. S.; Chen, I. G.; Tao, Y. Low-Temperature Noninjection Approach to Homogeneously-Alloyed $\text{PbSe}_x\text{S}_{1-x}$ Colloidal Nanocrystals for Photovoltaic Applications. *ACS Appl. Mater. Interfaces* **2011**, *3*, 1511-1520.
- (2) Zhao, N.; Osedach, T. P.; Chang, L. Y.; Geyer, S. M.; Wanger, D.; Binda, M. T.; Arango, A. C.; Bawendi, M. G.; Bulovic, V. Colloidal PbS Quantum Dot Solar Cells with High Fill Factor. *ACS Nano* **2010**, *4*, 3743-3752.
- (3) Yip, H. L.; Jen, A. K. Y. Recent Advances in Solution-Processed Interfacial Materials for Efficient and Stable Polymer Solar Cells. *Energy Environ. Sci.* **2012**, *5*, 5994-6011.
- (4) Zhao, J.; Li, Y.; Yang, G.; Jiang, K.; Lin, H.; Ade, H.; Ma, W.; Yan, H. Efficient Organic Solar Cells Processed from Hydrocarbon Solvents. *Nat. Energy* **2016**, *1*, 15027.
- (5) Lou, Y. H.; Wang, Z. K.; Naka, S.; Okada, H. Enhanced Short-Circuit Current Density in Poly(3-hexylthiophene) and 1-(3-methoxycarbonyl)-propyl-1-phenyl-(6,6)C61 Based Organic Solar Cells by Doping Small Molecular Perylene. *Appl. Phys. Lett.* **2011**, *99*, 033305.
- (6) Li, M.; Chao, Y. H.; Kang, T.; Wang, Z. K.; Yang, Y. G.; Feng, S. L.; Hu, Y.; Gao, X. Y.; Liao, L. S.; Hsu, C. S. Enhanced Crystallization and Stability of Perovskites by a Cross-Linkable Fullerene for High-Performance Solar Cells. *J. Mater. Chem. A* **2016**, *4*, 15088-15094.
- (7) Zhang, C. C.; Li, M.; Wang, Z. K.; Jiang, Y. R.; Liu, H. R.; Yang, Y. G.; Gao, X. Y.; Ma, H. Passivated Perovskite Crystallization and Stability in Organic-Inorganic Halide Solar Cells by Doping a Donor Polymer. *J. Mater. Chem. A* **2017**, *5*, 2572-2579.
- (8) Jorgensen, M.; Norrman, K.; Krebs, F. C. Stability/Degradation of Polymer Solar Cells. *Sol. Energy Mater. Sol. Cells* **2008**, *92*, 686-714.
- (9) Chang, L. L.; Lademann, H. W. A.; Bonekamp, J. B.; Meerholz, K.; Moule, A. J. Effect of Trace Solvent on the Morphology of P3HT:PCBM Bulk Heterojunction Solar Cells. *Adv. Funct. Mater.* **2011**, *21*, 1779-1787.

- (10) Chen, D. A.; Nakahara, A.; Wei, D. G.; Nordlund, D.; Russell, T. P. P3HT/PCBM Bulk Heterojunction Organic Photovoltaics: Correlating Efficiency and Morphology. *Nano Lett.* **2011**, *11*, 561-567.
- (11) Wu, Q.; Bhattacharya, M.; Moore, L. M. J.; Morgan, S. E. Air Processed P3HT:PCBM Photovoltaic Cells: Morphology Correlation to Annealing, Degradation, and Recovery. *J. Polym. Sci., Part B: Polym. Phys.* **2014**, *52*, 1511-1520.
- (12) Sun, Q.; Zhang, F.; An, Q.; Zhang, M.; Ma, X.; Zhang, J. Simultaneously Enhanced Efficiency and Stability of Polymer Solar Cells by Employing Solvent Additive and Upside-down Drying Method. *ACS Appl. Mater. Interfaces* **2017**, *9*, 8863-8871.
- (13) Li, Z.; Chiu, K. H.; Ashraf, R. S.; Fearn, S.; Dattani, R.; Wong, H. C.; Tan, C. H.; Wu, J. Y.; Cabral, J. T.; Durrant, J. R. Toward Improved Lifetimes of Organic Solar Cells under Thermal Stress: Substrate-Dependent Morphological Stability of PCDTBT:PCBM Films and Devices. *Sci. Rep.* **2015**, *5*, 15149.
- (14) Wong, H. C.; Li, Z.; Tan, C. H.; Zhong, H. L.; Huang, Z. G.; Bronstein, H.; McCulloch, I.; Cabral, J. T.; Durrant, J. R. Morphological Stability and Performance of Polymer-Fullerene Solar Cells under Thermal Stress: The Impact of Photoinduced PC₆₀BM Oligomerization. *ACS Nano* **2014**, *8*, 1297-1308.
- (15) Schroeder, B. C.; Li, Z.; Brady, M. A.; Faria, G. C.; Ashraf, R. S.; Takacs, C. J.; Cowart, J. S.; Duong, D. T.; Chiu, K. H.; Tan, C. H.; Cabral, J. T.; Salleo, A.; Chabinyc, M. L.; Durrant, J. R.; McCulloch, I. Enhancing Fullerene-Based Solar Cell Lifetimes by Addition of a Fullerene Dumbbell. *Angew. Chem., Int. Ed.* **2014**, *53*, 12870-12875.
- (16) Cheng, Y. J.; Hsieh, C. H.; Li, P. J.; Hsu, C. S. Morphological Stabilization by In Situ Polymerization of Fullerene Derivatives Leading to Efficient, Thermally Stable Organic Photovoltaics. *Adv. Funct. Mater.* **2011**, *21*, 1723-1732.
- (17) Li, Z.; Wong, H. C.; Huang, Z. G.; Zhong, H. L.; Tan, C. H.; Tsoi, W. C.; Kim, J. S.; Durrant, J. R.; Cabral, J. T. Performance Enhancement of Fullerene-Based Solar Cells by Light Processing. *Nat. Commun.* **2013**, *4*, 2227.

- (18) Ko, E. Y.; Park, G. E.; Lee, J. H.; Kim, H. J.; Lee, D. H.; Ahn, H.; Uddin, M. A.; Woo, H. Y.; Cho, M. J.; Choi, D. H. Excellent Long-Term Stability of Power Conversion Efficiency in Non-Fullerene-Based Polymer Solar Cells Bearing Tricyanovinylene-Functionalized n-Type Small Molecules. *ACS Appl. Mater. Interfaces* **2017**, *9*, 8838-8847.
- (19) Lira-Cantu, M.; Krebs, F. C. Hybrid Solar Cells Based on MEH-PPV and Thin Film Semiconductor Oxides (TiO₂, Nb₂O₅, ZnO, CeO₂ and CeO₂-TiO₂): Performance Improvement during Long-Time Irradiation. *Sol. Energy Mater. Sol. Cells* **2006**, *90*, 2076-2086.
- (20) Lee, K.; Kim, J. Y.; Park, S. H.; Kim, S. H.; Cho, S.; Heeger, A. J. Air-Stable Polymer Electronic Devices. *Adv. Mater.* **2007**, *19*, 2445-2449.
- (21) Li, J. G.; Kim, S.; Edington, S.; Nedy, J.; Cho, S.; Lee, K.; Heeger, A. J.; Gupta, M. C.; Yates, J. T. A Study of Stabilization of P3HT/PCBM Organic Solar Cells by Photochemical Active TiO_x Layer. *Sol. Energy Mater. Sol. Cells* **2011**, *95*, 1123-1130.
- (22) Hau, S. K.; Yip, H. L.; Baek, N. S.; Zou, J. Y.; O'Malley, K.; Jen, A. K. Y. Air-Stable Inverted Flexible Polymer Solar Cells Using Zinc Oxide Nanoparticles as an Electron Selective Layer. *Appl. Phys. Lett.* **2008**, *92*, 253301.
- (23) Sahin, Y.; Alem, S.; de Bettignies, R.; Nunzi, J. M. Development of Air Stable Polymer Solar Cells Using an Inverted Gold on Top Anode Structure. *Thin Solid Films* **2005**, *476*, 340-343.
- (24) Worfolk, B. J.; Hauger, T. C.; Harris, K. D.; Rider, D. A.; Fordyce, J. A. M.; Beaupre, S.; Leclerc, M.; Buriak, J. M. Work Function Control of Interfacial Buffer Layers for Efficient and Air-Stable Inverted Low-Bandgap Organic Photovoltaics. *Adv. Energy Mater.* **2012**, *2*, 361-368.
- (25) He, Z. R.; Xiao, K.; Durant, W.; Hensley, D. K.; Anthony, J. E.; Hong, K. L.; Kilbey, S. M.; Chen, J. H.; Li, D. W. Enhanced Performance Consistency in Nanoparticle/TIPS Pentacene-Based Organic Thin Film Transistors. *Adv. Funct. Mater.* **2011**, *21*, 3617-3623.
- (26) Ip, A. H.; Thon, S. M.; Hoogland, S.; Voznyy, O.; Zhitomirsky, D.; Debnath, R.; Levina, L.; Rollny, L. R.; Carey, G. H.; Fischer, A.; Kemp, K. W.; Kramer, I. J.; Ning, Z. J.; Labelle, A. J.;

Chou, K. W.; Amassian, A.; Sargent, E. H. Hybrid Passivated Colloidal Quantum Dot Solids. *Nat. Nanotechnol.* **2012**, *7*, 577-582.

(27) Chuang, C. H. M.; Brown, P. R.; Bulovic, V.; Bawendi, M. G. Improved Performance and Stability in Quantum Dot Solar Cells through Band Alignment Engineering. *Nat. Mater.* **2014**, *13*, 796-801.

(28) Tan, L.; Li, P. D.; Sun, B. Q.; Chaker, M.; Ma, D. L. Development of Photovoltaic Devices Based on Near Infrared Quantum Dots and Conjugated Polymers. *ChemNanoMat* **2016**, *2*, 601-615.

(29) Strein, E.; Colbert, A.; Subramaniyan, S.; Nagaoka, H.; Schlenker, C. W.; Janke, E.; Jenekhe, S. A.; Ginger, D. S. Charge Generation and Energy Transfer in Hybrid Polymer/Infrared Quantum Dot Solar Cells. *Energy Environ. Sci.* **2013**, *6*, 769-775.

(30) Jarzab, D.; Szendrei, K.; Yarema, M.; Pichler, S.; Heiss, W.; Loi, M. A. Charge-Separation Dynamics in Inorganic-Organic Ternary Blends for Efficient Infrared Photodiodes. *Adv. Funct. Mater.* **2011**, *21*, 1988-1992.

(31) Itskos, G.; Othonos, A.; Rauch, T.; Tedde, S. F.; Hayden, O.; Kovalenko, M. V.; Heiss, W.; Choulis, S. A. Optical Properties of Organic Semiconductor Blends with Near-Infrared Quantum-Dot Sensitizers for Light Harvesting Applications. *Adv. Energy Mater.* **2011**, *1*, 802-812.

(32) Zhang, Y. G.; Li, Z.; Ouyang, J. Y.; Tsang, S. W.; Lu, J. P.; Yu, K.; Ding, J. F.; Tao, Y. Hole Transfer from PbS Nanocrystal Quantum Dots to Polymers and Efficient Hybrid Solar Cells Utilizing Infrared Photons. *Org. Electron.* **2012**, *13*, 2773-2780.

(33) Zhou, R. J.; Stalder, R.; Xie, D. P.; Cao, W. R.; Zheng, Y.; Yang, Y. X.; Plaisant, M.; Holloway, P. H.; Schanze, K. S.; Reynolds, J. R.; Xue, J. G. Enhancing the Efficiency of Solution-Processed Polymer:Colloidal Nanocrystal Hybrid Photovoltaic Cells Using Ethanedithiol Treatment. *ACS Nano* **2013**, *7*, 4846-4854.

- (34) Ren, S. Q.; Chang, L. Y.; Lim, S. K.; Zhao, J.; Smith, M.; Zhao, N.; Bulovic, V.; Bawendi, M.; Gradecak, S. Inorganic-Organic Hybrid Solar Cell: Bridging Quantum Dots to Conjugated Polymer Nanowires. *Nano Lett.* **2011**, *11*, 3998-4002.
- (35) Dang, M. T.; Hirsch, L.; Wantz, G. P3HT:PCBM, Best Seller in Polymer Photovoltaic Research. *Adv. Mater.* **2011**, *23*, 3597-3602.
- (36) Zhao, J.; Swinnen, A.; Van Assche, G.; Manca, J.; Vanderzande, D.; Van Mele, B. Phase Diagram of P3HT/PCBM Blends and Its Implication for the Stability of Morphology. *J. Phys. Chem. B* **2009**, *113*, 1587-1591.
- (37) Gonfa, B. A.; Zhao, H. G.; Li, J. T.; Qiu, J. X.; Saidani, M.; Zhang, S. Q.; Izquierdo, R.; Wu, N. Q.; El Khakani, M. A.; Ma, D. L. Air-processed Depleted Bulk Heterojunction Solar Cells Based on PbS/CdS Core-shell Quantum Dots and TiO₂ Nanorod Arrays. *Sol. Energy Mater. Sol. Cells* **2014**, *124*, 67-74.
- (38) Yuan, M. J.; Kemp, K. W.; Thon, S. M.; Kim, J. Y.; Chou, K. W.; Amassian, A.; Sargent, E. H. High-Performance Quantum-Dot Solids via Elemental Sulfur Synthesis. *Adv. Mater.* **2014**, *26*, 3513-3519.
- (39) Pietryga, J. M.; Werder, D. J.; Williams, D. J.; Casson, J. L.; Schaller, R. D.; Klimov, V. I.; Hollingsworth, J. A. Utilizing the Lability of Lead Selenide to Produce Heterostructured Nanocrystals with Bright, Stable Infrared Emission. *J. Am. Chem. Soc.* **2008**, *130*, 4879-4885.
- (40) Zhao, H. G.; Chaker, M.; Ma, D. L. Effect of CdS Shell Thickness on the Optical Properties of Water-Soluble, Amphiphilic Polymer-Encapsulated PbS/CdS Core/Shell Quantum Dots. *J. Mater. Chem.* **2011**, *21*, 17483-17491.
- (41) Moreels, I.; Lambert, K.; Smeets, D.; De Muynck, D.; Nollet, T.; Martins, J. C.; Vanhaecke, F.; Vantomme, A.; Delerue, C.; Allan, G.; Hens, Z. Size-Dependent Optical Properties of Colloidal PbS Quantum Dots. *ACS Nano* **2009**, *3*, 3023-3030.
- (42) Neo, D. C. J.; Cheng, C.; Stranks, S. D.; Fairclough, S. M.; Kim, J. S.; Kirkland, A. I.; Smith, J. M.; Snaith, H. J.; Assender, H. E.; Watt, A. A. R. Influence of Shell Thickness and

Surface Passivation on PbS/CdS Core/Shell Colloidal Quantum Dot Solar Cells. *Chem. Mater.* **2014**, *26*, 4004-4013.

(43) Zhao, H.; Chaker, M.; Wu, N.; Ma, D. Towards Controlled Synthesis and Better Understanding of Highly Luminescent PbS/CdS Core/shell Quantum Dots. *J. Mater. Chem.* **2011**, *21*, 8898-8904.

(44) Brisdon, B. J.; Mialki, W. S.; Walton, R. A. X-Ray Photoelectron-Spectra of Inorganic Molecules XXVI Complexes of Molybdenum(0) and Molybdenum(II) Containing the Dicarbonyl Molybdenum Moiety. *J. Organomet. Chem.* **1980**, *187*, 341-347.

(45) Kim, M. R.; Ma, D. Quantum-Dot-Based Solar Cells: Recent Advances, Strategies, and Challenges. *J. Phys. Chem. Lett.* **2015**, *6*, 85–99.

(46) Sygletou, M.; Kakavelakis, G.; Paci, B.; Generosi, A.; Kymakis, E.; Stratakis, E. Enhanced Stability of Aluminum Nanoparticle-Doped Organic Solar Cells. *ACS Appl. Mater. Interfaces* **2015**, *7*, 17756-17764.

(47) Chander, N.; Singh, S.; Iyer, S. S. K. Stability and Reliability of P3HT:PC₆₁BM Inverted Organic Solar Cells. *Sol. Energy Mater. Sol. Cells* **2017**, *161*, 407-415.

(48) Ma, W. L.; Yang, C. Y.; Gong, X.; Lee, K.; Heeger, A. J. Thermally Stable, Efficient Polymer Solar Cells with Nanoscale Control of the Interpenetrating Network Morphology. *Adv. Funct. Mater.* **2005**, *15*, 1617-1622.

(49) Erb, T.; Zhokhavets, U.; Gobsch, G.; Raleva, S.; Stuhn, B.; Schilinsky, P.; Waldauf, C.; Brabec, C. J. Correlation between Structural and Optical Properties of Composite Polymer/Fullerene Films for Organic Solar Cells. *Adv. Funct. Mater.* **2005**, *15*, 1193-1196.

(50) Voroshazi, E.; Verreet, B.; Aernouts, T.; Heremans, P. Long-Term Operational Lifetime and Degradation Analysis of P3HT:PCBM Photovoltaic Cells. *Sol. Energy Mater. Sol. Cells* **2011**, *95*, 1303-1307.

(51) Oh, J. Y.; Shin, M.; Lee, H. W.; Lee, Y. J.; Baik, H. K.; Jeong, U. Enhanced Air Stability of Polymer Solar Cells with a Nanofibril-Based Photoactive Layer. *ACS Appl. Mater. Interfaces* **2014**, *6*, 7759-7765.

- (52) Gopalan, S. A.; Seo, M. H.; Anantha-Iyengar, G.; Han, B.; Lee, S. W.; Kwon, D. H.; Lee, S. H.; Kang, S. W. Mild Wetting Poor Solvent Induced Hydrogen Bonding Interactions for Improved Performance in Bulk Heterojunction Solar Cells. *J. Mater. Chem. A* **2014**, *2*, 2174-2186.
- (53) Taukeer Khan, M.; Kaur, A.; Dhawan, S. K.; Chand, S. In-Situ Growth of Cadmium Telluride Nanocrystals in Poly(3-hexylthiophene) Matrix for Photovoltaic Application. *J. Appl. Phys.* **2011**, *110*, 044509.
- (54) Sai, N.; Leung, K.; Zador, J.; Henkelman, G. First Principles Study of Photo-Oxidation Degradation Mechanisms in P3HT for Organic Solar Cells. *Phys. Chem. Chem. Phys.* **2014**, *16*, 8092-8099.
- (55) Manceau, M.; Rivaton, A.; Gardette, J.-L.; Guillerez, S.; Lemaître, N. The Mechanism of Photo- and Thermooxidation of Poly(3-hexylthiophene) (P3HT) Reconsidered. *Polym. Degrad. Stab.* **2009**, *94*, 898-907.
- (56) Lee, J. U.; Jung, J. W.; Emrick, T.; Russell, T. P.; Jo, W. H., Synthesis of C₆₀-end Capped P3HT and Its Application for High Performance of P3HT/PCBM Bulk Heterojunction Solar Cells. *J. Mater. Chem.* **2010**, *20*, 3287-3294.
- (57) Giansante, C.; Mastria, R.; Lerario, G.; Moretti, L.; Kriegel, I.; Scotognella, F.; Lanzani, G.; Carallo, S.; Esposito, M.; Biasiucci, M.; Rizzo, A.; Gigli, G. Molecular-Level Switching of Polymer/Nanocrystal Non-Covalent Interactions and Application in Hybrid Solar Cells. *Adv. Funct. Mater.* **2015**, *25*, 111-119.

Supporting Information

Enhanced Long-term and Thermal Stability of Polymer Solar Cells in Air at High Humidity with the Formation of Unusual Quantum Dot Networks

*Long Tan,^a Fan Yang,^a Mee Rahn Kim,^a Pandeng Li,^a Deepak Thrithamarassery Gangadharan,^{a,b}
Jo ële Margot,^c Ricardo Izquierdo,^b Mohamed Chaker,^a Dongling Ma^{a,*}*

^a Énergie, Matériaux et Télécommunications, Institut National de la Recherche Scientifique (INRS), 1650 Boul. Lionel-Boulet, Varennes, Quebec J3X 1S2, Canada

^b Département d'informatique, University du Québec à Montréal (UQAM), Case postale 8888, succursale Centre-ville, Montreal, Quebec, H3C 3P8, Canada

^c Département de physique, Université de Montréal, 2900 Edouard Montpetit Blvd, Montreal, Quebec, H3T 1J4, Canada

Email: ma@emt.inrs.ca

Determination of PbS/CdS quantum dots (QDs) mass concentration

Since the core/shell PbS/CdS QDs have very thin shell thickness (~ 0.1 nm, assuming uniform coating), the mass of PbS/CdS QDs in solution was assumed to approximately equal to that of the plain PbS QDs. Then, the Beer-Lambert's law: $A = \epsilon CL$ was used to first calculate the molar concentration of pure PbS QDs in solution, where A is the absorbance at the position of the first-excitonic absorption peak for a given sample, ϵ is the extinction coefficient per mole of PbS QDs, C is the molar concentration of QDs, and L is the light path length depending on the cuvette. ϵ can be determined following the equation: $\epsilon = 19600 (d/2)^{2.32}$,¹ where d is the diameter of QDs. d can be calculated by the following formula: $E = 0.41 + 1/(0.0252d^2 + 0.283d)$, where E and d are the bandgap and diameter of obtained QDs, respectively.² Finally, the molar concentration C was converted to mass concentration,² and the quantity of QDs being added to the organic materials solution can be determined by multiplying the mass concentration and the QD solution volume.

Figure S1 Topography images of P3HT:PCBM:halide-PbS/CdS film before (a) and after thermal annealing (b). By comparing these two images, we conclude that the QD networks were preliminarily formed during the spin-coating deposition, and the thermal annealing treatment helped the crystallization of P3HT and further “solidified” the QD networks. The formation of the QD networks is mainly attributed to the interface property (i.e., incompatibility) between the halide-PbS/CdS (capped by Cl⁻) and organic components.

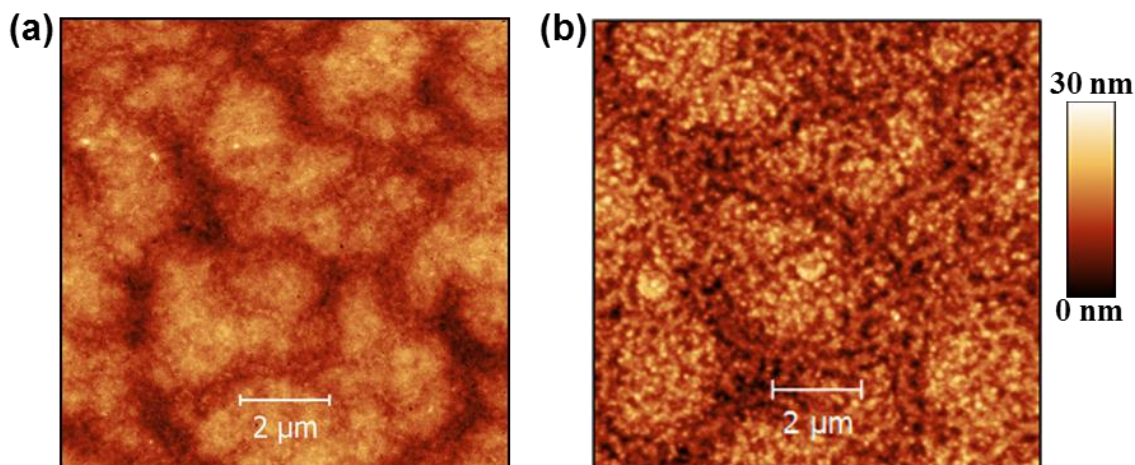
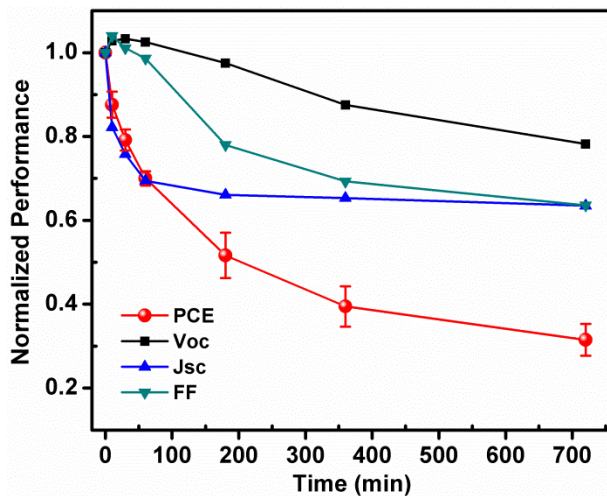


Figure S2 Thermal stability of the solar cell device based on P3HT:PCBM:OA-PbS/CdS film.



Reference

- 1) Cademartiri, L.; Montanari, E.; Calestani, G.; Migliori, A.; Guagliardi, A.; Ozin, G. A. Size-Dependent Extinction Coefficients of PbS Quantum Dots. *J. Am. Chem. Soc.* **2006**, *128*, 10337–10346.
- 2) Moreels, I.; Lambert, K.; Smeets, D.; Muynck, D. D.; Nollet, T.; Martins, J. C.; Vanhaecke, F.; Vantomme, A.; Delerue, C.; Zeger Hens, G. A. Size-Dependent Optical Properties of Colloidal PbS Quantum Dots. *ACS Nano* **2009**, *3*, 3023–3030.

4.3 Towards Enhancing Solar Cell Performance: An Effective and “Green” Additive

Long Tan, Pandeng Li, Ricardo Izquierdo, Mohamed Chaker and Dongling Ma

To be submitted

Manipulation of the active layer morphology via solvent additives represents an important way to effectively increase the PCE of PSCs. Although many additives have been explored for this kind of application, most of them belong to the groups of alkane dithiols and halogen chemicals, which are very toxic.

In this section, butylamine, which is much “greener”, was for the first time introduced as an additive to the P3HT:PCBM film and discovered to change the morphology of the P3HT:PCBM film. Its effects on the morphology, structure and performance have been investigated. A relatively high PCE of ~4.61% of P3HT:PCBM-based solar cells was achieved, owing to the butylamine induced morphology change of the active layer.

All of the experimental work was completed by me except for the thickness measurement of the active film, which was done by Pandeng. I also wrote the draft of the manuscript.

Towards enhancing solar cell performance: an effective and “green” additive

Long Tan,^a Pandeng Li,^a Ricardo Izquierdo,^b Mohamed Chaker,^a Dongling Ma^{a,*}

^a Énergie, Matériaux et Télécommunications, Institut National de la Recherche Scientifique (INRS), 1650 Boul. Lionel-Boulet, Varennes, Quebec J3X 1S2, Canada

^b Département d’informatique, University du Québec à Montréal (UQAM), Case postale 8888, succursale Centre-ville, Montreal, Quebec, H3C 3P8, Canada

Abstract: Performance of bulk heterojunction polymer solar cells (PSCs) highly relies on the morphology of the photoactive layer involving conjugated polymers and fullerene derivatives as donors and acceptors, respectively. Herein, butylamine was found to be able to optimize the morphology of the donor/acceptor (D/A) film composed of blend of poly(3-hexylthiophene-2,5-diyl) (P3HT) and phenyl-C₆₁-butyric acid methyl ester (PCBM). Compared to the commonly used alkane dithiols and halogen additives with high boiling points, butylamine has a much lower boiling point between 77-79 °C, and it is also much “greener”. A specific interaction between butylamine and PCBM was demonstrated to account for the morphology improvement. Essentially, butylamine can selectively dissolve PCBM in the P3HT:PCBM blend and facilitate the diffusion of PCBM in the film fabrication processes. Atomic force microscopy and X-ray photoelectron spectroscopy investigations confirmed the formation of the P3HT-enriched top surface and the abundance of PCBM at the bottom side, *i.e.*, the formation of vertical phase segregation, as a consequence of the specific PCBM-butylamine interaction. The D/A film with inhomogeneously distributed D and A components in the vertical film direction, with more P3HT at the hole extraction side and more PCBM at the electron extraction side, enables more efficient charge extraction in the D/A film, reflected by the largely enhanced fill factor. Power conversion efficiency of devices reached 4.03% and 4.61%, respectively, depending on the thickness of the D/A film, among the best values reported for P3HT:PCBM-based devices. As compared to the devices fabricated without the introduction of butylamine under otherwise the same processing conditions, they represented 19.6% and 21.6% improvement in the efficiency, respectively. The discovery of butylamine as a new, effective additive in enhancing the performance of PSCs strongly suggests that the differential affinity of additives towards donors

and acceptors likely plays a more important role in morphology optimization than their boiling point, different from what was reported previously. The finding provides useful information for realizing large-area PSCs fabrication, where a “greener” additive is always preferred.

Keywords: Photovoltaic; Polymer solar cells; Morphology; Vertical phase segregation; P3HT:PCBM; Additive engineering

1. Introduction

Polymer solar cells (PSCs), regarded as one type of the third-generation solar cells, have attracted significant attentions in the field of photovoltaics, owing to their advantages of excellent flexibility, low-cost processing, and free of heavy metals. Over the past decades, substantial progress has been made, thanks to intense research efforts made on the design and synthesis of new low bandgap polymeric materials, optimization of morphology/device architecture, interface engineering, *etc.*^[1-2] The bulk heterojunction (BHJ) structure consisting of conjugated polymers (donor) / fullerene derivatives (acceptor) (D/A) was discovered to overcome the compromise between light absorption and exciton diffusion, representing a milestone in the path of PSC development. This structure led to a breakthrough in power conversion efficiency (PCE), which is still the main research direction for PSC investigations.^[3] Importantly, the morphology control of the D/A film is highly crucial for achieving the superior PCE of BHJ solar cells, and worthwhile to be further investigated in order to attain the PCE (on a relatively large area) appropriate for practical application.

For the typical blend of poly(3-hexylthiophene-2,5-diyl) (P3HT)/phenyl-C₆₁-butyric acid methyl ester (PCBM), solvent annealing and thermal annealing are the two most commonly used routes for optimizing the morphology of the D/A film. In principle, solvent annealing can slow down the drying speed of the deposited, wet D/A film, while thermal annealing is able to improve the diffusion of PCBM in the entire film.^[1,4] Both processes assist the P3HT crystallization and the formation of a preferable bi-continuous interpenetrating phase structure within the blend film, which can efficiently enhance the PCE of PSCs. In addition to the solvent and thermal annealing, solvent additives have also been extensively explored in BHJ to improve the performance of PSCs.^[3,5-9] It was found that the morphology and thereby the PCE of PSCs is highly relevant to the boiling point of additives and the solubility of the polymer and fullerene derivative in

additives.^[6,8,10] Normally, the additives with high boiling points and good solubility of the fullerene derivatives, such as alkane dithiols and halogen, are preferred.^[3,5,11] They can be directly correlated to the intermixing of components in the D/A blend by manipulating the mobility of component(s). To date, additive engineering becomes one of the most efficient and convenient routes to enhance the performance of PSCs, thus attracting increasingly intense attention.^[12]

Herein, a new additive, butylamine, is employed to largely enhance the performance of P3HT:PCBM based PSCs. Compared with the commonly used alkane dithiols and halogen additives with a high boiling point, butylamine has a considerably lower boiling point of 77-79 °C and appears much “greener” free of halogen ions and without malodorous smell. Absorption spectroscopy, X-ray photoelectron spectroscopy (XPS), nuclear magnetic spectroscopy (NMR), X-ray diffraction (XRD) and atomic force microscopy (AFM) were used to analyze and understand the interaction between butylamine and each component, the surface morphology and the crystalline structure of the film. It was found that the formation of a vertical phase segregation (VPS) in the active film, which was reported to favor the exciton dissociation and charge transport,^[4] is responsible for the enhanced performance. It is noteworthy that the device based on butylamine induced VPS led to an impressively high fill factor (FF: ~70%) and PCE (4.03%) at commonly used concentrations of P3HT:PCBM, reflecting largely suppressed charge carrier recombination in the active film. It strongly indicates the beneficial morphology modification of the photoactive layer with the addition of butylamine. Further increasing the thickness of the photoactive film by simply doubling the concentrations of P3HT and PCBM in solution yielded an even higher PCE of 4.61%, among the best values reported for this system (4-5%).

2. Experimental

2.1 Chemicals and materials

Regio-regular P3HT (RR93-95) and PCBM (>99.5%) were purchased from Solaris Chem. Incorporation. N-butylamine (95%), zinc acetate dihydrate ($\text{Zn}(\text{CH}_3\text{COO})_2 \cdot 2\text{H}_2\text{O}$, 99.9%), ethanolamine ($\text{NH}_2\text{CH}_2\text{CH}_2\text{OH}$, 99.5%) and 2-methoxyethanol ($\text{CH}_3\text{OCH}_2\text{CH}_2\text{OH}$, 99.8%) were obtained from Sigma Aldrich Ltd.

2.2 Preparation of ZnO precursor solution

ZnO precursor was prepared by dissolving $\text{Zn}(\text{CH}_3\text{COO})_2 \cdot 2\text{H}_2\text{O}$ and $\text{NH}_2\text{CH}_2\text{CH}_2\text{OH}$ in $\text{CH}_3\text{OCH}_2\text{CH}_2\text{OH}$ under vigorous stirring for 12 h for the hydrolysis reaction in air.

2.3 Fabrication of solar cell devices

Indium tin oxide (ITO) glass substrates (2.5 cm×2.5 cm) were sequentially washed in water, acetone and isopropanol for 20 min each. The clean substrates were then patterned by optical lithography. The patterned ITO glass substrates with photoresist were removed by acetone, followed by isopropanol cleaning for 10 min and oxygen plasma treatment for 2 min, respectively. The ZnO film, acting as an electron transport/hole blocking layer was fabricated by spin-coating the precursor solution onto the patterned ITO glass and annealed at 200 °C for 30 minutes in air. P3HT:PCBM (1:0.8 by weight) solution in 1,2-dichlorobenzene with/without the addition of butylamine (3% by volume) was spin-coated onto the ZnO layer to form the photoactive film and kept in a petri dish for 30 min for solvent annealing before the thermal annealing step at 140 °C for 10 min. These processes were carried out under inert atmosphere in a glove box. Finally, the fabrication of the solar cell device was completed by depositing 20 nm thick MoO_3 on the photoactive film followed by the deposition of 80 nm thick Ag through a shadow mask, which makes the photoactive area of about 6 mm².

2.4 Characterization

The P3HT:PCBM blend solution and film with/without the introduction of butylamine were characterized by a Cary 5000 UV-Vis-NIR spectrophotometer (Varian) with a scan speed of 600 nm/min. XPS was performed using a VG Escalab 220i-XL equipped with an Al Ka source. The obtained XPS data were analyzed by using the Casa software. An X-ray diffractometer (Panalytical X-Pert PRO MRD, Bruker Corporation) was employed to investigate the crystallized film samples. Nuclear magnetic resonance (Bruker, Avance III HD, 600 MHz) was applied to examine the presence of butylamine in the film by dissolving the film in deuterated chloroform. A profilometer (Bruker, Dektak XT) was applied to measure the thickness of the active layer. The morphology of the film was detected by atomic force microscopy (Bruker Corporation). Large-area (50 × 50 μm) topography images were obtained by the ScanAsyst

mode with a silicon tip on a nitride lever, and the phase images ($1 \times 1 \mu\text{m}$) were obtained by tapping mode. Current-voltage (J-V) measurements of solar cells were recorded by a Keithley 2400 SourceMeter SMU instrument under AM 1.5 solar illumination. External quantum efficiency (EQE) measurements were also conducted using an IQE200B system (Newport Corporation).

3. Results and discussion

Figure 1(a) shows the absorption spectra of P3HT:PCBM blend solutions with and without the addition of butylamine. Two absorption peaks located at ~ 470 and ~ 330 nm were observed for both samples, corresponding to the photo-response from P3HT and PCBM, respectively. It indicates that the presence of butylamine didn't affect the photo-response range of the organic material. However, we noticed that the intensity of the 330 nm peak for the butylamine-involved sample slightly decreased compared to that of the standard one without the introduction of butylamine (both absorption spectra were normalized with the P3HT absorption peak at 470 nm). This phenomenon may be related with a special interaction between PCBM and butylamine. The P3HT:PCBM film deposited from the butylamine-containing solution was also characterized by absorption spectroscopy as seen in Figure 1 (b). The photo-response range of the P3HT:PCBM film was red-shifted to over 650 nm compared to the blend solution before the deposition, due to the enhanced structure ordering and crystallization of P3HT.^[13] Three characteristic peaks appeared at ~ 520 nm, 555 nm and 606 nm, indicating strong interactions among P3HT chains (π - π stacking) and high ordering of the polymer chains in the film.^[13] In addition to increasing the absorption of P3HT:PCBM at longer wavelengths, the well crystallized P3HT can improve the hole transport from chain to chain in the P3HT domain. Film samples with such absorption characters were reported to be promising for the PSC application.^[14]

The solubility difference of P3HT and PCBM in butylamine, which can significantly affect the eventual morphology of the active layer,^[6] was further tested by rinsing the P3HT:PCBM film with butylamine continuously for several seconds. The treated film was dried and re-measured using absorption spectroscopy. As displayed in Figure 1(b) (blue), the absorption pattern was obviously changed after butylamine rinsing, similar to that of the pure P3HT film (black), due to the easy removal of PCBM by butylamine. It indicates the big difference in the solubility of P3HT and PCBM in butylamine. The poor solubility of P3HT was further confirmed by keeping

P3HT in butylamine for 5 days, where the solid state of P3HT did not show any obvious change. We further examined the “special” interaction between PCBM and butylamine. The color of butylamine gradually changed with the addition and dissolution of PCBM from colorless to yellow, in line with absorption results. The absence of the PCBM characteristic absorption peak is considered to be due to the formation of a complex between PCBM and butylamine. Such an interaction can affect the morphology of the photoactive layer, which will be discussed in the later text.

We further checked the presence of butylamine in the film (after thermal annealing) by conducting NMR and XPS measurements. As seen in Figure 1(c), a strong peak around the chemical shift of 1.57 ppm, ascribed to the $-\text{CH}_2-$ group from both P3HT and PCBM, is clearly shown, whereas the response from $-\text{NH}_2$ (1.77 ppm) can't be found^[15], indicating the presence of butylamine is negligible. This result was further confirmed by XPS measurements as shown in Figure 1(d), where no N1s signal can be detected. Highly likely, butylamine completely evaporated during the film fabrication process, due to its low boiling point.

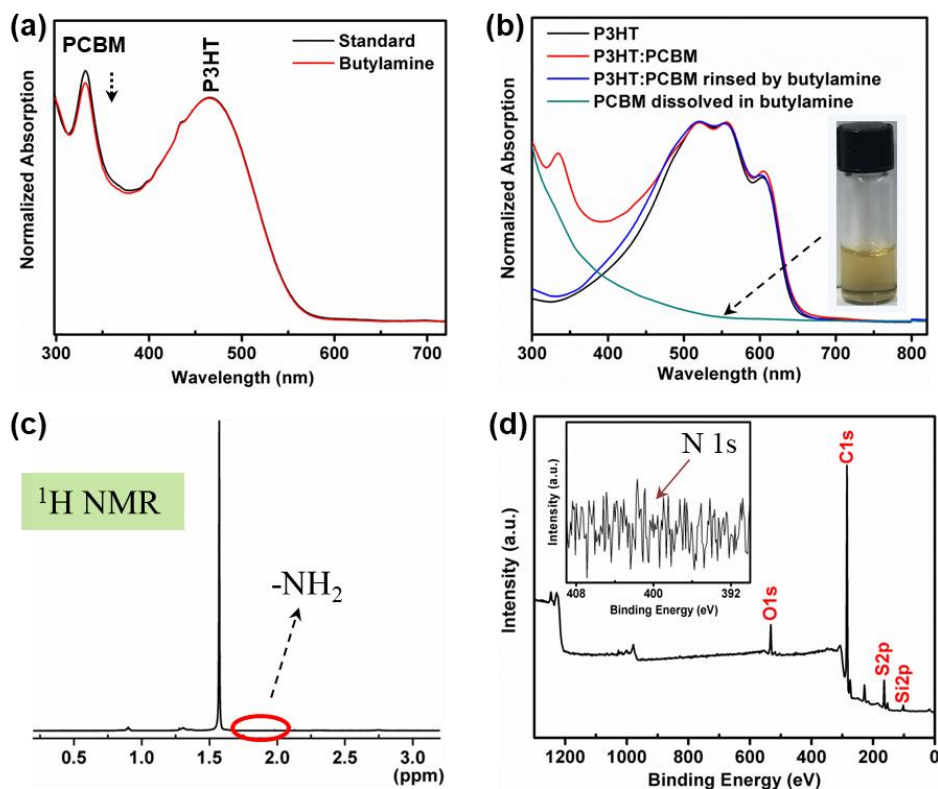


Figure 1 (a) Absorption spectra of P3HT:PCBM solution with and without butylamine; (b) absorption spectra of pure P3HT film (black), P3HT:PCBM film (red), rinsed P3HT:PCBM film (blue) and PCBM-in-butylamine solution; (c) NMR spectrum of the dissolved P3HT:PCBM film spin-coated from the solution containing butylamine; (d) XPS of the P3HT:PCBM film prepared from butylamine-containing solution.

The surface morphology of the photoactive films processed with and without butylamine was examined by AFM. Topography images ($50\ \mu\text{m} \times 50\ \mu\text{m}$) of the films were obtained by the Scanasynt mode, and are shown in Figure 2 (a,b). For the butylamine-involved sample, the film surface was relatively smooth with root-mean-square roughness (RMS) around 5.6 nm (Figure 2 (a)). However, the standard sample showed quite different surface character with largely increased RMS around 9.5 nm. Obviously, a finer structure was formed with the addition of butylamine, although it did not seem to be retained in the film. Such changes may be attributed to the alteration of composition distribution in the active layer, resulting in the formation of different domains. Similar result was obtained by using 1-chloronaphthalene as an additive in the blend of poly[2,3-bis-(3-octyloxyphenyl)quinoxaline-5,8-diyl-altthiophene-2,5-diyl] and [6,6]-phenyl C₇₁-butyric acid methyl ester.^[12] Phase images of both samples were collected in a tapping mode at a smaller scale ($1\ \mu\text{m} \times 1\ \mu\text{m}$) to detect the phase separation of P3HT and PCBM, which is believed to significantly affect the performance of devices. As for the standard sample, fiber-like P3HT domains were clearly identified by forming a bicontinuous structure with PCBM (Figure 2(d)), in line with previously published results.^[16] With addition of the butylamine additive, it seems that the morphology of the P3HT:PCBM film was thoroughly altered, even though it was not detectable in the final film sample.

XPS spectroscopy was employed to evaluate the uniformity of distribution of P3HT and PCBM in both butylamine-involved and standard films by estimating sulfur-to-carbon (S/C) ratios, since S is only present in P3HT.^[17] By integrating the areas of high resolution C and S spectra obtained from the top side (i.e., the surface in contact with MoO₃) of both samples, S/C ratios of ~0.13 and ~0.10 were obtained for butylamine-involved and standard samples, respectively. Clearly, the top side of the butylamine-involved sample contained more P3HT than that of standard sample; the evaporation of butylamine may carry some PCBM with it and thus cause the loss of PCBM close to the surface. A step further, these films were lifted-off from the substrate, and the S/C ratio of the bottom side of the films was also detected. S/C ratios around 0.067 and 0.080 were obtained for butylamine-involved and standard films, respectively.

Although the ratio was close for the top and bottom sides of the standard sample, it dropped nearly half for the butylamine-involved sample (Figure 2(e)). Such analysis results underline the composition inhomogeneity, and possibly the phase separation, in the vertical film direction for the latter sample.

The morphology formation of the photoactive layer depends on the P3HT crystallization and PCBM diffusion processes, which are closely correlated, during the film preparation process. To make a favorable VPS morphology, several aspects should be taken into consideration, especially solvent selection and the surface energy of the substrates.^[4,17-18] For instance, the *o*-xylene solvent can assist the formation of a VPS morphology, and the hydrophilic surface is preferable for the PCBM accumulation and hydrophobic surface the P3HT accumulation. Herein, the solution processed ZnO layer should be responsible for the formation of slightly more PCBM at the bottom side compared to that of top side for the standard sample. Thermal annealing can enhance the transformation by increasing the component mobility. As for butylamine-involved sample, the additive must have performed an important role in improving the mobility of PCBM by the special interaction mentioned above, which enhances the degree of VPS morphology, favoring the P3HT accumulation at the top side. We also applied XPS measurement to detect the presence of butylamine in the P3HT:PCBM film immediately after the film deposition, but before thermal annealing. The result (not presented) also shows the absence of butylamine in the film, which indicates that, quite likely, butylamine took its role during the process of solvent annealing and completely disappeared even before thermal annealing started. This effect slowed down the speed of P3HT self-organization, evidenced by the slower color change (from yellow to purple), which can benefit the performance of the devices.^[19]

The crystalline structure of the standard and butylamine-involved samples was examined by XRD. As seen in Figure 2(f), both samples show a single diffraction peak at $2\theta = 5.3^\circ$, corresponding to the (100) plane diffraction of crystallized P3HT.^[20] It originates from the P3HT crystallites with *a*-axis orientation, where the P3HT main chains are parallel to the substrate and side chains perpendicular.^[21] The mean size of P3HT crystallites (L) can be evaluated following the Scherrer's relation: $L = 0.9\lambda/\Delta_{2\theta}\cos\theta$, where $\Delta_{2\theta}$ is the full-width at half-maximum of the diffraction peak; λ and 2θ are the wavelength of incident beam (0.154 nm) and the angle between the incident and scattered X-rays, respectively. Via this equation, the size of P3HT crystallites

was found to be ~14-15 nm for both the butylamine-involved and standard samples. The introduction of butylamine does not seem affecting the size of P3HT crystallites.

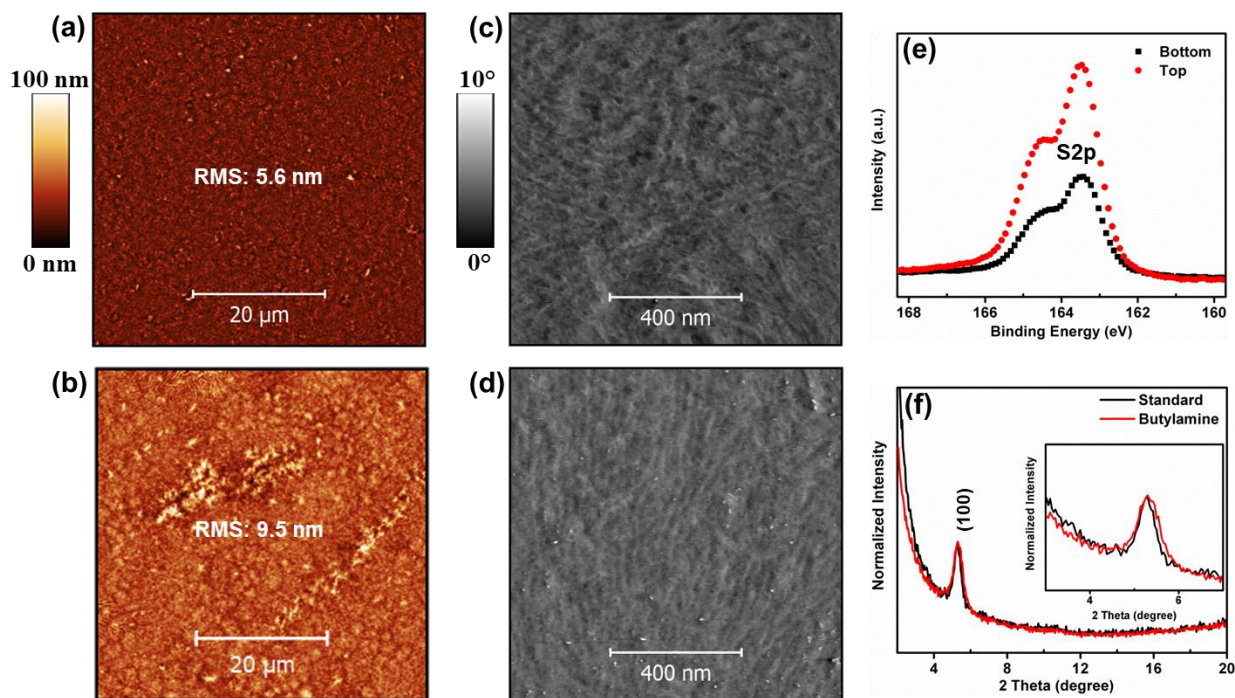


Figure 2. Topography images (a,b) and phase images (c,d) of butylamine-involved (a,c) and standard (b,d) samples. High resolution XPS S2p spectra of butylamine-involved sample at the top (red) and bottom (black) sides (e); XRD spectra of butylamine-involved and standard samples (f).

PSCs with an inverted structure of ITO/ZnO/P3HT:PCBM/MoO₃/Ag were fabricated and their J-V and EQE were characterized. Figure 3(a) shows the typical J-V curves of the devices with and without the introduction of butylamine fabricated using typical P3HT/PCBM concentration (24 mg/mL). The average PCE was enhanced by ~20% from 3.37% to 4.03% with the addition of butylamine. Analysis of the photovoltaic (PV) parameters reveals that short-circuit current (J_{sc}) and FF were increased by ~6.9% (from 8.62 to 9.21 mA cm⁻²) and ~12% (from 62.4 to 69.9%) with the introduction of butylamine, respectively, while the average open-circuit voltage (V_{oc}) was comparable (Table 1). The largely increased FF should be attributed to the reduced charge recombination benefiting from the increased degree of VPS, which improved the exciton dissociation, charge transport and charge collection at electrodes.^[4] J_{sc} was increased simultaneously for the same reason. Series resistance (R_s) was further extracted from the J-V curves of both devices, and values of ~4.6 Ω cm² and ~9.5 Ω cm² were obtained for butylamine-

involved and standard devices, respectively, according well with the above results. Consistently, EQE spectra shown in Figure 3(b) display that the quantum efficiency of the butylamine-involved device was increased in the range of 300-600 nm, owing to the suppressed charge recombination, although the photo-response range did not change. J_{sc} values derived from the EQE data were 8.9 and 8.3 mA cm^{-2} for butylamine-involved and standard devices, respectively, close to the values gained from J-V measurements.

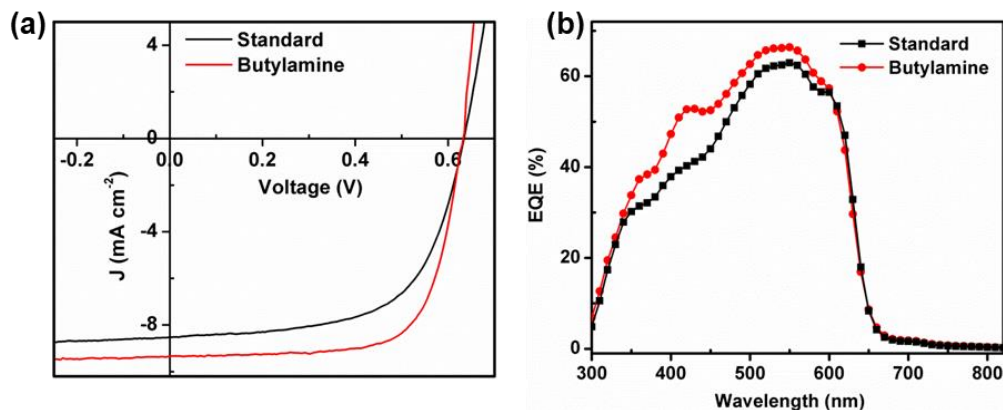


Figure 3. J-V curves (a) and EQE spectra (b) of PV devices.

Table 1. PV parameters of standard and butylamine-involved devices fabricated at different P3HT:PCBM concentrations.

Sample	P3HT+PCBM (mg ml^{-1})	Butylamine (vol %)	V_{oc} (V)	J_{sc} (mA cm^{-2})	FF (%)	R_s ($\Omega \text{ cm}^2$)	PCE (%)
Standard	24	0	0.63	8.62	62.4	9.5	3.37 ± 0.24
Butylamine	24	3	0.63	9.21	69.9	4.6	4.03 ± 0.08
Standard	48	0	0.58	11.52	56.5	9.5	3.79 ± 0.18
Butylamine	48	6	0.61	12.02	63.3	6.0	4.61 ± 0.15

The beneficial “butylamine effect” on morphology provides an opportunity to increase the thickness of the active layer in order to absorb more light, yet still allow efficient charge transport and collection. In other words, it is possible to further enhance the PCE by increasing the photocurrent without significantly sacrificing FF, if a preferable bi-continuous interpenetrating morphology can be achieved in a thicker film with the use of butylamine. With such consideration, we further made efforts to attain higher PCE by simply doubling the

concentration of P3HT:PCBM in the spin-coating solution, which increased the thickness of the photo-active film from ~80 nm to ~125 nm as measured by a profilometer. Butylamine concentration was also doubled (6 vol%). Figure 4(a,b) show the topography images of butylamine-involved and standard films, respectively, prepared at higher concentration. Both samples showed largely increased RMS compared to the low-concentration samples. Obviously, the butylamine additive led to a finer surface structure, although the RMS values for both samples were comparable.

PV devices were fabricated based on these thicker films, and J-V measurements were carried out. Typical J-V curves and PV parameters are presented in Figure 4(c) and Table 1, respectively. With increased film thickness, J_{sc} was increased to 11.52 and 12.02 mA cm^{-2} for standard and butylamine-involved devices, respectively, while V_{oc} and FF were decreased. It is known that increased photoactive film thickness is able to enhance light absorption, whereas prolong the transport distance for generated electrons and holes to respective electrodes. The interplay of these two factors yielded improved PCE for both samples. In addition, the butylamine-involved device was superior to the standard one in all aspects: J_{sc} , V_{oc} and FF, leading to the enhancement of the overall efficiency by ~21.6%. The average PCE of the butylamine-involved device reached 4.61%, among the best values reported for the P3HT:PCBM system. This enhancement should be attributed to the decreased charge transport resistance in the active layer of butylamine involved device which has a smaller R_s (Table 1) compared to the standard one. Overall, the important role of butylamine was once again clearly revealed.

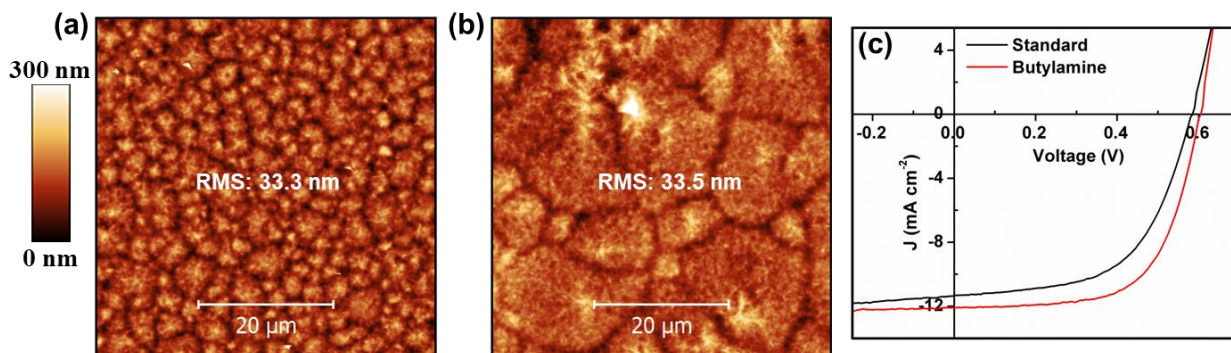


Figure 4. Topography images of butylamine-involved (a) and standard (b) samples fabricated from high P3HT:PCBM concentration solution, and J-V curves of corresponding devices (c).

4. Conclusion

In brief, for the first time butylamine was explored as an effective solution additive and found to have profound effects on the morphology and PV performance of P3HT:PCBM solar cells, although it is not detected in the final P3HT:PCBM film. Butylamine is capable of inducing the formation of a vertical phase segregation morphology in the P3HT:PCBM film, which can effectively suppress the exciton and charge recombination. As a consequence, excellent performance was achieved, with an impressively high FF (nearly 70%) at typical P3HT:PCBM concentration and a PCE of ~4.61% at higher P3HT:PCBM concentration, among the best efficiencies of P3HT:PCBM-based devices.

Reference

- (1) Dou, L. T.; You, J. B.; Hong, Z. R.; Xu, Z.; Li, G.; Street, R. A.; Yang, Y., 25th Anniversary Article: A Decade of Organic/Polymeric Photovoltaic Research. *Adv. Mater.* **2013**, *25*, 6642-6671.
- (2) Cai, C. S.; Zhang, Y. D.; Song, R. Y.; Peng, Z. S.; Xia, L. P.; Wu, M. X.; Xiong, K.; Wang, B. A.; Lin, Y. B.; Xu, X. F.; Liang, Q. B.; Wu, H. B.; Wang, E. G.; Hou, L. T., Polymer solar cells spray coated with non-halogenated solvents. *Sol. Energy Mater. Sol. Cells* **2017**, *161*, 52-61.
- (3) Collins, B. A.; Li, Z.; Tumbleston, J. R.; Gann, E.; McNeill, C. R.; Ade, H., Absolute Measurement of Domain Composition and Nanoscale Size Distribution Explains Performance in PTB7:PC71BM Solar Cells. *Adv. Energy Mater.* **2013**, *3*, 65-74.
- (4) Campoy-Quiles, M.; Ferenczi, T.; Agostinelli, T.; Etchegoin, P. G.; Kim, Y.; Anthopoulos, T. D.; Stavrinou, P. N.; Bradley, D. D. C.; Nelson, J., Morphology evolution via self-organization and lateral and vertical diffusion in polymer: fullerene solar cell blends. *Nat. Mater.* **2008**, *7*, 158-164.
- (5) Yao, Y.; Hou, J. H.; Xu, Z.; Li, G.; Yang, Y., Effect of solvent mixture on the nanoscale phase separation in polymer solar cells. *Adv. Funct. Mater.* **2008**, *18*, 1783-1789.

- (6) Dang, M. T.; Wuest, J. D., Using volatile additives to alter the morphology and performance of active layers in thin-film molecular photovoltaic devices incorporating bulk heterojunctions. *Chem. Soc. Rev.* **2013**, *42*, 9105-9126.
- (7) Guo, X.; Cui, C. H.; Zhang, M. J.; Huo, L. J.; Huang, Y.; Hou, J. H.; Li, Y., High efficiency polymer solar cells based on poly(3-hexylthiophene)/indene-C-70 bisadduct with solvent additive. *Energy Environ. Sci.* **2012**, *5*, 7943-7949.
- (8) Shi, G. Z.; Yuan, J. Y.; Huang, X. D.; Lu, Y.; Liu, Z. K.; Peng, J.; Ding, G. Q.; Shi, S. H.; Sun, J. X.; Lu, K. Y.; Wang, H. Q.; Ma, W. L., Combinative Effect of Additive and Thermal Annealing Processes Delivers High Efficiency All-Polymer Solar Cells. *J. Phys. Chem. C* **2015**, *119*, 25298-25306.
- (9) Choi, H.; Tamilavan, V.; Lee, D. Y.; Kim, S.; Lee, J.; Jung, Y. K.; Oh, S. H.; Jeong, J.; Hyun, M. H.; Park, S. H.; Kim, K., Successful incorporation of optical spacer and additive solvent for enhancing the photocurrent of polymer solar cell. *Sol. Energy Mater. Sol. Cells* **2016**, *153*, 131-137.
- (10) Cheng, P.; Li, Y.; Zhan, X., A DMF-assisted solution process boosts the efficiency in P3HT:PCBM solar cells up to 5.31%. *Nanotechnol.* **2013**, *24*, 484008.
- (11) Peet, J.; Kim, J. Y.; Coates, N. E.; Ma, W. L.; Moses, D.; Heeger, A. J.; Bazan, G. C., Efficiency enhancement in low-bandgap polymer solar cells by processing with alkane dithiols. *Nat. Mater.* **2007**, *6*, 497-500.
- (12) Hansson, R.; Ericsson, L. K. E.; Holmes, N. P.; Rysz, J.; Opitz, A.; Campoy-Quiles, M.; Wang, E.; Barr, M. G.; Kilcoyne, A. L. D.; Zhou, X.; Dastoor, P.; Moons, E., Vertical and lateral morphology effects on solar cell performance for a thiophene–quinoxaline copolymer:PC70BM blend. *J. Mater. Chem. A* **2015**, *3*, 6970-6979.
- (13) Li, L. G.; Lu, G. H.; Yang, X. N., Improving performance of polymer photovoltaic devices using an annealing-free approach via construction of ordered aggregates in solution. *J. Mater. Chem.* **2008**, *18*, 1984-1990.

- (14) Li, G.; Shrotriya, V.; Huang, J. S.; Yao, Y.; Moriarty, T.; Emery, K.; Yang, Y., High-efficiency solution processable polymer photovoltaic cells by self-organization of polymer blends. *Nat. Mater.* **2005**, *4*, 864-868.
- (15) SDBSWeb: <http://riodb01.ibase.aist.go.jp/sdbs/> (National Institute of Advanced Industrial Science and Technology)
- (16) Yan, H.; Li, D. H.; Lu, K.; Zhu, X. W.; Zhang, Y. J.; Yang, Y. L.; Wei, Z. X., Evolution of polymer photovoltaic performances from subtle chemical structure variations. *Phys. Chem. Chem. Phys.* **2012**, *14*, 15127-15134.
- (17) Xu, Z.; Chen, L. M.; Yang, G. W.; Huang, C. H.; Hou, J. H.; Wu, Y.; Li, G.; Hsu, C. S.; Yang, Y., Vertical Phase Separation in Poly(3-hexylthiophene): Fullerene Derivative Blends and its Advantage for Inverted Structure Solar Cells. *Adv. Funct. Mater.* **2009**, *19*, 1227-1234.
- (18) Waldauf, C.; Morana, M.; Denk, P.; Schilinsky, P.; Coakley, K.; Choulis, S. A.; Brabec, C. J., Highly efficient inverted organic photovoltaics using solution based titanium oxide as electron selective contact. *Appl. Phys. Lett.* **2006**, *89*, 233517.
- (19) Nagai, M.; Gao, W.; Huang, W.; Yamamoto, H.; Yoshida, Y., Effect of Drying Time on Morphology and Photovoltaic Characteristics of Polymer Solar Cells of Bis-PCBM/P3HT Composites. *ECS J. Solid State Sci. Technol.*, **2016**, *5*, Q244-Q252.
- (20) Ma, W. L.; Yang, C. Y.; Gong, X.; Lee, K.; Heeger, A. J., Thermally stable, efficient polymer solar cells with nanoscale control of the interpenetrating network morphology. *Adv. Funct. Mater.* **2005**, *15*, 1617-1622.
- (21) Zhokhavets, U.; Erb, T.; Gobsch, G.; Al-Ibrahim, M.; Ambacher, O., Relation between absorption and crystallinity of poly(3-hexylthiophene)/fullerene films for plastic solar cells. *Chem. Phys. Lett.* **2006**, *418*, 347-350.

CHAPTER 5 CONCLUSIONS AND PERSPECTIVES

5.1 Conclusions

Part I PbS QDs with size-tunable optical properties are promising for optoelectronic, biological imaging and sensor applications in the NIR range. It is well-known that the hot-injection method is an efficient route to synthesize high quality PbS QDs. In this route, TMS is the most widely used S precursor, which usually reacts with Pb-OA, yielding PbS QDs. However, it is inconvenient to handle the TMS which has very high reactivity and is malodorous. Elemental S has been proposed as a replacement for TMS, whereas the tunable photo-response range of PbS QDs based on elemental S involved reaction is limited compared to that of TMS involved route.

In this work, we focused on extending the tunable photo-response range of PbS QDs based on the synthesis involving elemental S and PbCl₂ as the S and Pb precursors, respectively. It has been proved that PbS QDs with the first-excitonic peak as short as 705 nm can be achieved by introducing TBP into the S precursor solution, whereas the TBP free reaction can only yield QDs with absorption ≥ 1056 nm. As characterized by PL spectroscopy, the TBP-assisted synthesized PbS QDs samples show high PL QY in the range of 60-90%, depending on the QD size. The TEM results indicate that such QDs have relatively narrower size distribution than TBP-free sample without any aggregation. Altogether, these results confirmed the high quality of QDs from TBP-assisted synthesis. As further evidenced by NMR results, TBP was revealed to act as surface ligands of QDs, which could impede the QDs growth and benefit the PL QY of QDs by forming stable bond with S atoms to better passivate the QD surface.

We further demonstrated that TBP can react with the PbCl₂-OLA complex, if 1:1 molar ratio (TBP:PbCl₂) of TBP was directly injected. As a result, the Pb(OH)Cl was formed as characterized by XRD, which is a promising new precursor for synthesizing high quality ultrasmall PbS QDs. This synthetic route is highly reproducible and easily controllable. The newly discovered Pb(OH)Cl precursor is also promising for conveniently synthesizing other lead-containing QDs.

Considering practical application, the scale-up reaction of this TBP-assisted synthesis was performed. It was confirmed that the synthesis of PbS QDs with different photo-response ranges

(corresponding to different sizes) can be successfully scaled up, which is promising for the real-world application. Additionally, LSC devices were fabricated using QDs synthesized via this route as fluorophore. In order to balance the PL QY, separation of absorption/emission spectra and photo-stability of these QDs, CdS shell of different thicknesses were performed based on the size of plain PbS QDs, and all devices showed promising performance. For instance, a record-high optical efficiency of ~1.2% has been achieved at a G factor of 50 (10 cm in length) for device based on ~2.5 nm QDs with a ~0.1 nm CdS shell.

Overall, we developed a facile and “greener” way to synthesize small-size and high quality PbS QDs for the first time. These synthesized QDs are potentially interesting in other NIR-related applications in addition to the LSC application.

Part II PSCs are considered as one of the candidates for the next generation solar cells due to their advantages of good flexibility, low-cost processing, and free of heavy metal. Polymer/fullerene based BHJ solar cell devices with high PCE are still the main research direction in this field. For this kind of solar cells, it is highly important to control the morphology of the polymer/fullerene blends film, which determines the PCE and stability of the devices.

In section I, we developed a new strategy to largely improve the long-term and thermal stability of PSCs by incorporating relative small amounts of QDs in the organic matrix. It is discovered that the surface ligands of QDs played a significant role in affecting the morphology of the active layer, which determines the final performance of corresponding devices. For PbS/CdS-OA QDs, they were homogeneously distributed inside the P3HT:PCBM film as characterized by AFM, due to high compatibility between OA ligands and organic components. When most of the OA ligands were replaced by inorganic Cl⁻ ions, the resulting QDs formed continuous networks in the P3HT:PCBM film. As a matter of fact, the device based on the active layer with QD networks showed the best long-term and thermal stability compared to that based on OA-PbS/CdS QDs incorporated film and QD-free P3HT:PCBM film. We conclude that the QD networks efficiently stabilize the active layer from chemical and physical (morphology) degradation, then resulting in improved stability of the devices. This strategy can be potentially applied to other polymer/fullerene based PSCs. Therefore, our work provides a new avenue to solve the stability issue of PSCs, which has significant meaning to their commercialization.

In section II, butylamine, for the first-time, was employed as an additive in the P3HT:PCBM blend solution, to manipulate the morphology of P3HT:PCBM film. It is much “greener” compared to commonly used alkane dithiols and halogenated additives. The PCBM can be well dissolved in butylamine by forming a complexity with it. As a result, the PCBM mobility during the solvent annealing process was changed, which optimized the morphology of the P3HT:PCBM film. Specifically, it made the P3HT and PCBM accumulating at the top and bottom of film, respectively. The film with this morphology is suitable for electron and hole transportation in opposite directions to the cathode and anode, respectively, and also benefit the exciton dissociation. As evidenced from the results of J-V measurements, the FF was largely increased due to the suppressed exciton and charge recombination. Thus, the PCE of devices was increased to ~4.03%, which stimulated us to further optimize the thickness of the active layer. The best average PCE of ~4.61% was achieved in this work among the best value of P3HT:PCBM-based devices. This new additive can be potentially used in other polymer/fullerene systems.

5.2 Perspectives

TBP route was first developed in our work to synthesize high quality small PbS QDs, which is facile and greener than the TMS involved method. Although we have achieved record-high optical efficiency at a G factor of 50 by applying synthesized QDs into the LSC devices, higher efficiency can be further targeted via improving the surface passivation of QDs. For instance, metal halide treatment can help to terminate the un-passivated dangling bonds on the surface of QDs and to fill unreachable midgap trap states owing to the smaller steric effect of Cl⁻ ions than that of OA ligands. It can directly improve the PL QY and stability of QDs, then leading to better performance of the devices. However, the surface treatment should not sacrifice the colloid stability of QDs. Additionally, the TBP route synthesized QDs can be explored for more applications, such as PV devices and light emitting diodes. Compared to the commonly used QDs obtained from TMS involved synthesis, TBP ligands can provide additional passivation on the S sites of QDs. Different from the role of QDs in LSC devices, where they act as light absorbers and emitters, QDs also play an important role in the charge transfer process in PV devices and light emitting diodes. Therefore, the surface chemistry of QDs can be more important than that in LSC devices.

The discovery of synthesizing ultrasmall PbS QDs via mixing elemental S solution with Pb(OH)Cl in our work gives a hint to explore a new, convenient way for PbS QDs synthesis in the future. Since the Pb(OH)Cl can act as the lead precursor for small PbS QDs synthesis, more efforts can be made for developing a more facile and greener way towards synthesizing Pb(OH)Cl. Then, these Pb(OH)Cl can be conveniently converted into PbS QDs at a low temperature (less than 100 °C) by reacting with the stable S precursor. In this case, it is able to save the energy consumption in the synthesis and avoid the usage of large amounts of toxic, unstable and expensive precursors, which will effectively realize the low-cost and “green” synthesis of PbS QDs. It has significant meaning to scale up the QDs synthesis into the industrialization scale. The crucial point for this route can possibly be the introduction of appropriate ligands in situ for Pb(OH)Cl, which is important to the optical properties and stability of final QDs.

To improve the stability of PSCs, incorporation of inorganic materials into the active layer is one of the research directions. The addition of NIR QDs into the P3HT:PCBM film in our work aimed to enhance the stability of the device and extend the photo-response range of the device to the NIR range. Although we have achieved good stabilities as expected, there is still large space to further increase the photocurrent induced from the NIR photons. One of the challenges is the trade-off between complete substitution of long-chain OA ligands on the surface of QDs with shorter ones and the QD colloid stability in solution. The ligand-exchange treatment is necessary for electron transport, while the colloid stability is crucial for the fabrication process. One strategy is to directly graft electron acceptor molecules, such as functionalized carbon nanotubes and fullerenes, on the QD surface as passivation ligands. Moreover, the reaction details between O₂/H₂O and the component in the ternary system need to be revealed. These investigations can guide the future work on designing and manipulating the active layer morphology. In performing them, the interface properties between each component and between the active layer and electrodes should also be taken into consideration.

Recently, polymer materials with lower band gap than that of traditional P3HT emerged as hot topics in this field. These materials with red-shifted absorption spectra are able to utilize more sun light compared to P3HT, and show better hole mobility simultaneously. The strategy of using QDs to largely improve the stability of devices is expected to work in low band gap

polymer based system, which normally suffer more severe degradations than that of P3HT:PCBM. Considering the environmental issue, the PbS-based QDs shall be replaced by heavy-metal free NIR QDs, depending on the development of materials chemistry. Overall, the ligand effect, band alignment, film morphology and the interface effect should be taken into consideration in order to fabricate PSCs with both high PCE and good stability.

State-of-the-art, halogenated solvents and additives such as chlorobenzene/dichlorobenzene and 1,8-diiodoctane are commonly used to fabricate PSCs with high PCE. However, these halogenated chemicals can cause environmental and human health problems. Moving forward toward real application of PSCs, it is time to develop new solvent/co-solvent/additives for the “green fabrication” of high performance PSCs. To achieve this goal, the key point is to control the nanoscale morphology of the D/A film, which is correlated with the solvent usage. Using mixed solvent with synergistic effect on the morphology of D/A film can be an effective way. Additionally, it is very promising to design novel water/alcohol-soluble photoactive materials for PSC application.

Reference

- [1] July 25, 2017; available from: <https://yearbook.enerdata.net/electricity/electricity-domestic-consumption-data.htm>.
- [2] July 25, 2017; available from: <http://sustainnovate.ae/en/industry-news/detail/solar-energy-is-taking-over-the-world-graph>.
- [3] Fritts, C.E., *On A New Form of Selenium Cell, And Some Electrical Discoveries Made By Its Use*. *AJS*, 1883. **26**(156):465-472.
- [4] Emin, S.; Singh, S. P.; Han, L. Y.; Satoh, N.; Islam, A., Colloidal quantum dot solar cells. *Solar Energy* **2011**, *85*, 1264-1282.
- [5] Szlufcik, J.; Sivothythaman, S.; Nijs, J. F.; Mertens, R. P.; VanOverstraeten, R., Low cost industrial technologies of crystalline silicon solar cells. *Proceedings of the IEEE* **1997**, *85*, 711-730.
- [6] Habas, S. E.; Platt, H. A. S.; van Hest, M. F. A. M.; Ginley, D. S., Low-Cost Inorganic Solar Cells: From Ink To Printed Device. *Chemical Reviews* **2010**, *110*, 6571-6594.
- [7] July 25, 2017; available from: <http://plasticphotovoltaics.org/lc/lc-solarcells/lc-introduction.html>.
- [8] Gratzel, M., Dye-sensitized solar cells. *Journal of Photochemistry and Photobiology C-Photochemistry Reviews* **2003**, *4*, 145-153.
- [9] Carey, G. H.; Abdelhady, A. L.; Ning, Z. J.; Thon, S. M.; Bakr, O. M.; Sargent, E. H., Colloidal Quantum Dot Solar Cells. *Chemical Reviews* **2015**, *115*, 12732-12763.
- [10] Dou, L. T.; You, J. B.; Hong, Z. R.; Xu, Z.; Li, G.; Street, R. A.; Yang, Y., 25th Anniversary Article: A Decade of Organic/Polymeric Photovoltaic Research. *Advanced Materials* **2013**, *25*, 6642-6671.
- [11] Yang, S. D.; Fu, W. F.; Zhang, Z. Q.; Chen, H. Z.; Li, C. Z., Recent advances in perovskite solar cells: efficiency, stability and lead-free perovskite. *Journal of Materials Chemistry A* **2017**, *5*, 11462-11482.
- [12] Giustino, F.; Snaith, H. J., Toward Lead-Free Perovskite Solar Cells. *ACS Energy Letters* **2016**, *1*, 1233-1240.
- [13] Liu, M. X.; Voznyy, O.; Sabatini, R.; de Arquer, F. P. G.; Munir, R.; Balawi, A. H.; Lan, X. Z.; Fan, F. J.; Walters, G.; Kirmani, A. R.; Hoogland, S.; Laquai, F.; Amassian, A.; Sargent, E.

H., Hybrid organic-inorganic inks flatten the energy landscape in colloidal quantum dot solids. *Nature Materials* **2017**, *16*, 258-263.

[14] Hagfeldt, A.; Boschloo, G.; Sun, L. C.; Kloo, L.; Pettersson, H., Dye-Sensitized Solar Cells. *Chemical Reviews* **2010**, *110*, 6595-6663.

[15] Wang, P.; Zakeeruddin, S. M.; Moser, J. E.; Nazeeruddin, M. K.; Sekiguchi, T.; Gratzel, M., A stable quasi-solid-state dye-sensitized solar cell with an amphiphilic ruthenium sensitizer and polymer gel electrolyte. *Nature Materials* **2003**, *2*, 402-407.

[16] Boatman, E. M.; Lisensky, G. C.; Nordell, K. J., A safer, easier, faster synthesis for CdSe quantum dot nanocrystals. *Journal of Chemical Education* **2005**, *82*, 1697-1699.

[17] Keuleyan, S.; Lhuillier, E.; Brajuskovic, V.; Guyot-Sionnest, P., Mid-infrared HgTe colloidal quantum dot photodetectors. *Nature Photonics* **2011**, *5*, 489-493.

[18] Bansal, A. K.; Antolin, F.; Zhang, S.; Stroea, L.; Ortolani, L.; Lanzi, M.; Serra, E.; Allard, S.; Scherf, U.; Samuel, I. D. W., Highly Luminescent Colloidal CdS Quantum Dots with Efficient Near Infrared Electroluminescence in Light-Emitting Diodes. *Journal of Physical Chemistry C* **2016**, *120*, 1871-1880.

[19] Stein, J. L.; Mader, E. A.; Cossairt, B. M., Luminescent InP Quantum Dots with Tunable Emission by Post-Synthetic Modification with Lewis Acids. *Journal of Physical Chemistry Letters* **2016**, *7*, 1315-1320.

[20] Yamaguchi, K.; Yujobo, K.; Kaizu, T., Stranski-Krastanov growth of InAs quantum dots with narrow size distribution. *Japanese Journal of Applied Physics Part 2-Letters* **2000**, *39*, L1245-L1248.

[21] Moreels, I.; Justo, Y.; De Geyter, B.; Haustraete, K.; Martins, J. C.; Hens, Z., Size-Tunable, Bright, and Stable PbS Quantum Dots: A Surface Chemistry Study. *ACS Nano* **2011**, *5*, 2004-2012.

[22] Cademartiri, L.; Bertolotti, J.; Sapienza, R.; Wiersma, D. S.; von Freymann, G.; Ozin, G. A., Multigram scale, solventless, and diffusion-controlled route to highly monodisperse PbS nanocrystals. *Journal of Physical Chemistry B* **2006**, *110*, 671-673.

[23] Padilha, L. A.; Stewart, J. T.; Sandberg, R. L.; Bae, W. K.; Koh, W. K.; Pietryga, J. M.; Klimov, V. I., Carrier Multiplication in Semiconductor Nanocrystals: Influence of Size, Shape, and Composition. *Accounts of Chemical Research* **2013**, *46*, 1261-1269.

- [24] Urban, J. J.; Talapin, D. V.; Shevchenko, E. V.; Murray, C. B., Self-assembly of PbTe quantum dots into nanocrystal superlattices and glassy films. *Journal of the American Chemical Society* **2006**, *128*, 3248-3255.
- [25] Zang, H. D.; Li, H. B.; Makarov, N. S.; Velizhanin, K. A.; Wu, K. F.; Park, Y. S.; Klimov, V. I., Thick-Shell CuInS₂/ZnS Quantum Dots with Suppressed "Blinking" and Narrow Single-Particle Emission Line Widths. *Nano Letters* **2017**, *17*, 1787-1795.
- [26] Xie, R. G.; Zhang, J. X.; Zhao, F.; Yang, W. S.; Peng, X. G., Synthesis of Monodisperse, Highly Emissive, and Size-Tunable Cd₃P₂ Nanocrystals. *Chemistry of Materials* **2010**, *22*, 3820-3822.
- [27] Harris, D. K.; Allen, P. M.; Han, H. S.; Walker, B. J.; Lee, J. M.; Bawendi, M. G., Synthesis of Cadmium Arsenide Quantum Dots Luminescent in the Infrared. *Journal of the American Chemical Society* **2011**, *133*, 4676-4679.
- [28] Liu, L. P.; Peng, Q.; Li, Y. D., Preparation of CdSe quantum dots with full color emission based on a room temperature injection technique. *Inorganic Chemistry* **2008**, *47*, 5022-5028.
- [29] Choi, H.; Ko, J. H.; Kim, Y. H.; Jeong, S., Steric-Hindrance-Driven Shape Transition in PbS Quantum Dots: Understanding Size-Dependent Stability. *Journal of the American Chemical Society* **2013**, *135*, 5278-5281.
- [30] Ellingson, R. J.; Beard, M. C.; Johnson, J. C.; Yu, P. R.; Micic, O. I.; Nozik, A. J.; Shabaev, A.; Efros, A. L., Highly efficient multiple exciton generation in colloidal PbSe and PbS quantum dots. *Nano Letters* **2005**, *5*, 865-871.
- [31] Hanna, M. C.; Beard, M. C.; Nozik, A. J., Effect of Solar Concentration on the Thermodynamic Power Conversion Efficiency of Quantum-Dot Solar Cells Exhibiting Multiple Exciton Generation. *Journal of Physical Chemistry Letters* **2012**, *3*, 2857-2862.
- [32] Semonin, O. E.; Luther, J. M.; Choi, S.; Chen, H. Y.; Gao, J. B.; Nozik, A. J.; Beard, M. C., Peak External Photocurrent Quantum Efficiency Exceeding 100% via MEG in a Quantum Dot Solar Cell. *Science* **2011**, *334*, 1530-1533.
- [33] Du, J.; Du, Z. L.; Hu, J. S.; Pan, Z. X.; Shen, Q.; Sung, J. K.; Long, D. H.; Dong, H.; Sun, L. T.; Zhong, X. H.; Wan, L. J., Zn-Cu-In-Se Quantum Dot Solar Cells with a Certified Power Conversion Efficiency of 11.6%. *Journal of the American Chemical Society* **2016**, *138*, 4201-4209.

- [34] Selopal, G. S.; Zhao, H.; Tong, X.; Benetti, D.; Navarro-Pardo, F.; Zhou, Y.; Barba, D.; Vidal, F.; Wang, Z. M.; Rosei, F., Highly Stable Colloidal “Giant” Quantum Dots Sensitized Solar Cells. *Advanced Functional Materials* **2017**, *27*, 1701468.
- [35] Lan, X. Z.; Bai, J.; Masala, S.; Thon, S. M.; Ren, Y.; Kramer, I. J.; Hoogland, S.; Simchi, A.; Koleilat, G. I.; Paz-Soldan, D.; Ning, Z. J.; Labelle, A. J.; Kim, J. Y.; Jabbour, G.; Sargent, E. H., Self-Assembled, Nanowire Network Electrodes for Depleted Bulk Heterojunction Solar Cells. *Advanced Materials* **2013**, *25*, 1769-1773.
- [36] Eames, C.; Frost, J. M.; Barnes, P. R. F.; O'Regan, B. C.; Walsh, A.; Islam, M. S., Ionic transport in hybrid lead iodide perovskite solar cells. *Nature Communications* **2015**, *6*, 7497.
- [37] Do Kim, H.; Ohkita, H.; Benten, H.; Ito, S., Photovoltaic Performance of Perovskite Solar Cells with Different Grain Sizes. *Advanced Materials* **2016**, *28*, 917-922.
- [38] Saliba, M.; Matsui, T.; Domanski, K.; Seo, J. Y.; Ummadisingu, A.; Zakeeruddin, S. M.; Correa-Baena, J. P.; Tress, W. R.; Abate, A.; Hagfeldt, A.; Gratzel, M., Incorporation of rubidium cations into perovskite solar cells improves photovoltaic performance. *Science* **2016**, *354*, 206-209.
- [39] Brittman, S.; Adhyaksa, G. W. P.; Garnett, E. C., The expanding world of hybrid perovskites: materials properties and emerging applications. *MRS Communications* **2015**, *5*, 7-26.
- [40] Seki, K.; Furube, A.; Yoshida, Y., Theoretical limit of power conversion efficiency for organic and hybrid halide perovskite photovoltaics. *Japanese Journal of Applied Physics* **2015**, *54*, 08KF04.
- [41] Huang, A. B.; Lei, L.; Zhu, J. T.; Yu, Y.; Liu, Y.; Yang, S. W.; Bao, S. H.; Cao, X.; Jin, P., Achieving High Current Density of Perovskite Solar Cells by Modulating the Dominated Facets of Room-Temperature DC Magnetron Sputtered TiO₂ Electron Extraction Layer. *ACS Applied Materials & Interfaces* **2017**, *9*, 2016-2022.
- [42] I, M.; Heeney, M.; Bailey, C.; Genevicius, K.; I, M.; Shkunov, M.; Sparrowe, D.; Tierney, S.; Wagner, R.; Zhang, W. M.; Chabynyc, M. L.; Kline, R. J.; McGehee, M. D.; Toney, M. F., Liquid-crystalline semiconducting polymers with high charge-carrier mobility. *Nature Materials* **2006**, *5*, 328-333.
- [43] Li, G.; Zhu, R.; Yang, Y., Polymer solar cells. *Nature Photonics* **2012**, *6*, 153-161.

- [44] Madogni, V. I.; Kounouhewa, B.; Akpo, A.; Agbomahena, M.; Hounkpatin, S. A.; Awanou, C. N., Comparison of degradation mechanisms in organic photovoltaic devices upon exposure to a temperate and a subequatorial climate. *Chemical Physics Letters* **2015**, *640*, 201-214.
- [45] Tan, L.; Li, P. D.; Sun, B. Q.; Chaker, M.; Ma, D. L., Development of Photovoltaic Devices Based on Near Infrared Quantum Dots and Conjugated Polymers. *ChemNanoMat* **2016**, *2*, 601-615.
- [46] Strein, E.; Colbert, A.; Subramaniyan, S.; Nagaoka, H.; Schlenker, C. W.; Janke, E.; Jenekhe, S. A.; Ginger, D. S., Charge generation and energy transfer in hybrid polymer/infrared quantum dot solar cells. *Energy & Environmental Science* **2013**, *6*, 769-775.
- [47] Nam, M.; Park, J.; Kim, S. W.; Lee, K., Broadband-absorbing hybrid solar cells with efficiency greater than 3% based on a bulk heterojunction of PbS quantum dots and a low-bandgap polymer. *Journal of Materials Chemistry A* **2014**, *2*, 3978-3985.
- [48] Tabachnyk, M.; Ehrlér, B.; Gelinas, S.; Bohm, M. L.; Walker, B. J.; Musselman, K. P.; Greenham, N. C.; Friend, R. H.; Rao, A., Resonant energy transfer of triplet excitons from pentacene to PbSe nanocrystals. *Nature Materials* **2014**, *13*, 1033-1038.
- [49] Thompson, N. J.; Wilson, M. W. B.; Congreve, D. N.; Brown, P. R.; Scherer, J. M.; Bischof, T. S.; Wu, M. F.; Geva, N.; Welborn, M.; Van Voorhis, T.; Bulovic, V.; Bawendi, M. G.; Baldo, M. A., Energy harvesting of non-emissive triplet excitons in tetracene by emissive PbS nanocrystals. *Nature Materials* **2014**, *13*, 1039-1043.
- [50] Kubin, R. F.; Fletcher, A. N., Fluorescence Quantum Yields of Some Rhodamine Dyes. *Journal of Luminescence* **1982**, *27*, 455-462.
- [51] Hermann, A. M., Luminescent Solar Concentrators - a Review. *Solar Energy* **1982**, *29*, 323-329.
- [52] Kinderman, R.; Slooff, L. H.; Burgers, A. R.; Bakker, N. J.; Buchtemann, A.; Danz, R.; van Roosmalen, J. A. M., I-V performance and stability study of dyes for luminescent plate concentrators. *Journal of Solar Energy Engineering-Transactions of the ASME* **2007**, *129*, 277-282.
- [53] Zhao, Y. M.; Meek, G. A.; Levine, B. G.; Lunt, R. R., Near-Infrared Harvesting Transparent Luminescent Solar Concentrators. *Advanced Optical Materials* **2014**, *2*, 606-611.

- [54] Sanguineti, A.; Sassi, M.; Turrisi, R.; Ruffo, R.; Vaccaro, G.; Meinardi, F.; Beverina, L., High Stokes shift perylene dyes for luminescent solar concentrators. *Chemical Communications* **2013**, *49*, 1618-1620.
- [55] Debije, M. G.; Verbunt, P. P. C.; Nadkarni, P. J.; Velate, S.; Bhaumik, K.; Nedumbamana, S.; Rowan, B. C.; Richards, B. S.; Hoeks, T. L., Promising fluorescent dye for solar energy conversion based on a perylene perinone. *Applied Optics* **2011**, *50*, 163-169.
- [56] Coropceanu, I.; Bawendi, M. G., Core/Shell Quantum Dot Based Luminescent Solar Concentrators with Reduced Reabsorption and Enhanced Efficiency. *Nano Letters* **2014**, *14*, 4097-4101.
- [57] Zhou, Y. F.; Benetti, D.; Fan, Z. Y.; Zhao, H. G.; Ma, D. L.; Govorov, A. O.; Vomiero, A.; Rosei, F., Near Infrared, Highly Efficient Luminescent Solar Concentrators. *Advanced Energy Materials* **2016**, *6*, 1501913.
- [58] Erickson, C. S.; Bradshaw, L. R.; McDowall, S.; Gilbertson, J. D.; Gamelin, D. R.; Patrick, D. L., Zero-Reabsorption Doped-Nanocrystal Luminescent Solar Concentrators. *ACS Nano* **2014**, *8*, 3461-3467.
- [59] Aeberhard, U.; Vaxenburg, R.; Lifshitz, E.; Tomic, S., Fluorescence of colloidal PbSe/PbS QDs in NIR luminescent solar concentrators. *Physical Chemistry Chemical Physics* **2012**, *14*, 16223-16228.
- [60] Zhao, H. G.; Benetti, D.; Jin, L.; Zhou, Y. F.; Rosei, F.; Vomiero, A., Absorption Enhancement in "Giant" Core/Alloyed-Shell Quantum Dots for Luminescent Solar Concentrator. *Small* **2016**, *12*, 5354-5365.
- [61] Meinardi, F.; Colombo, A.; Velizhanin, K. A.; Simonutti, R.; Lorenzon, M.; Beverina, L.; Viswanatha, R.; Klimov, V. I.; Brovelli, S., Large-area luminescent solar concentrators based on 'Stokes-shift-engineered' nanocrystals in a mass-polymerized PMMA matrix. *Nature Photonics* **2014**, *8*, 392-399.
- [62] Yang, C. C.; Lunt, R. R., Limits of Visibly Transparent Luminescent Solar Concentrators. *Advanced Optical Materials* **2017**, *5*, 1600851.
- [63] Bradshaw, L. R.; Knowles, K. E.; McDowall, S.; Gamelin, D. R., Nanocrystals for Luminescent Solar Concentrators. *Nano Letters* **2015**, *15*, 1315-1323.

- [64] Tan, L.; Li, P.; Sun, B.; Chaker, M.; Ma, D., Stabilities Related to Near-Infrared Quantum Dot-Based Solar Cells: The Role of Surface Engineering. *ACS Energy Letters* **2017**, *2*, 1573-1585.
- [65] Benjamin, W. E.; Veit, D. R.; Perkins, M. J.; Bain, E.; Scharnhorst, K.; McDowall, S.; Patrick, D. L.; Gilbertson, J. D., Sterically Engineered Perylene Dyes for High Efficiency Oriented Fluorophore Luminescent Solar Concentrators. *Chemistry of Materials* **2014**, *26*, 1291-1293.
- [66] Liu, C.; Li, B., Multiple dyes containing luminescent solar concentrators with enhanced absorption and efficiency. *Journal of Optics* **2015**, *17*, 025901.
- [67] Earp, A. A.; Smith, G. B.; Swift, P. D.; Franklin, J., Maximising the light output of a Luminescent Solar Concentrator. *Solar Energy* **2004**, *76*, 655-667.
- [68] Thomson, J. W.; Nagashima, K.; Macdonald, P. M.; Ozin, G. A., From Sulfur-Amine Solutions to Metal Sulfide Nanocrystals: Peering into the Oleylamine-Sulfur Black Box. *Journal of the American Chemical Society* **2011**, *133*, 5036-5041.
- [69] Ka, I.; Ma, D.; El Khakani, M. A., Tailoring the photoluminescence of PbS-nanoparticles layers deposited by means of the pulsed laser ablation technique. *Journal of Nanoparticle Research* **2011**, *13*, 2269-2274.
- [70] Kumar, S.; Nann, T., Shape control of II-VI semiconductor nanomaterials. *Small* **2006**, *2*, 316-329.
- [71] De Smet, Y.; Deriemaeker, L.; Finsy, R., A simple computer simulation of Ostwald ripening. *Langmuir* **1997**, *13*, 6884-6888.
- [72] Reiss, H., The Growth of Uniform Colloidal Dispersions. *The Journal of Chemical Physics* **1951**, *19*, 482-487.
- [73] Zhao, H. G.; Chaker, M.; Wu, N. Q.; Ma, D. L., Towards controlled synthesis and better understanding of highly luminescent PbS/CdS core/shell quantum dots. *Journal of Materials Chemistry* **2011**, *21*, 8898-8904.
- [74] Hines, M. A.; Scholes, G. D., Colloidal PbS nanocrystals with size-tunable near-infrared emission: Observation of post-synthesis self-narrowing of the particle size distribution. *Advanced Materials* **2003**, *15*, 1844-1849.

- [75] Hendricks, M. P.; Campos, M. P.; Cleveland, G. T.; Jen-La Plante, I.; Owen, J. S., A tunable library of substituted thiourea precursors to metal sulfide nanocrystals. *Science* **2015**, *348*, 1226-1230.
- [76] Campoy-Quiles, M.; Ferenczi, T.; Agostinelli, T.; Etchegoin, P. G.; Kim, Y.; Anthopoulos, T. D.; Stavrinou, P. N.; Bradley, D. D. C.; Nelson, J., Morphology evolution via self-organization and lateral and vertical diffusion in polymer: fullerene solar cell blends. *Nature Materials* **2008**, *7*, 158-164.
- [77] Kim, M.; Kim, J. H.; Choi, H. H.; Park, J. H.; Jo, S. B.; Sim, M.; Kim, J. S.; Jinnai, H.; Park, Y. D.; Cho, K., Electrical Performance of Organic Solar Cells with Additive-Assisted Vertical Phase Separation in the Photoactive Layer. *Advanced Energy Materials* **2014**, *4*, 1300612.
- [78] Sun, Q. Q.; Zhang, F. J.; An, Q. S.; Zhang, M.; Ma, X. L.; Zhang, J., Simultaneously Enhanced Efficiency and Stability of Polymer Solar Cells by Employing Solvent Additive and Upside-down Drying Method. *ACS Applied Materials & Interfaces* **2017**, *9*, 8863-8871.
- [79] Kokubu, R.; Yang, Y., Vertical phase separation of conjugated polymer and fullerene bulk heterojunction films induced by high pressure carbon dioxide treatment at ambient temperature. *Physical Chemistry Chemical Physics* **2012**, *14*, 8313-8318.
- [80] Dang, M. T.; Wantz, G.; Bejbouji, H.; Urien, M.; Dautel, O. J.; Vignau, L.; Hirsch, L., Polymeric solar cells based on P3HT:PCBM: Role of the casting solvent. *Solar Energy Materials and Solar Cells* **2011**, *95*, 3408-3418.
- [81] Savenije, T. J.; Kroeze, J. E.; Yang, X. N.; Loos, J., The effect of thermal treatment on the morphology and charge carrier dynamics in a polythiophene-fullerene bulk heterojunction. *Advanced Functional Materials* **2005**, *15*, 1260-1266.
- [82] Zheng, Y. F.; Li, S. G.; Zheng, D.; Yu, J. S., Effects of different polar solvents for solvent vapor annealing treatment on the performance of polymer solar cells. *Organic Electronics* **2014**, *15*, 2647-2653.
- [83] Dang, M. T.; Wuest, J. D., Using volatile additives to alter the morphology and performance of active layers in thin-film molecular photovoltaic devices incorporating bulk heterojunctions. *Chemical Society Reviews* **2013**, *42*, 9105-9126.
- [84] Li, Z.; Chiu, K. H.; Ashraf, R. S.; Fearn, S.; Dattani, R.; Wong, H. C.; Tan, C. H.; Wu, J. Y.; Cabral, J. T.; Durrant, J. R., Toward Improved Lifetimes of Organic Solar Cells under Thermal

Stress: Substrate-Dependent Morphological Stability of PCDTBT:PCBM Films and Devices. *Scientific Reports* **2015**, *5*, 15149.

[85] Li, G.; Yao, Y.; Yang, H.; Shrotriya, V.; Yang, G.; Yang, Y., "Solvent annealing" effect in polymer solar cells based on poly(3-hexylthiophene) and methanofullerenes. *Advanced Functional Materials* **2007**, *17*, 1636-1644.

[86] Chang, L. L.; Lademann, H. W. A.; Bonekamp, J. B.; Meerholz, K.; Moule, A. J., Effect of Trace Solvent on the Morphology of P3HT:PCBM Bulk Heterojunction Solar Cells. *Advanced Functional Materials* **2011**, *21*, 1779-1787.

[87] Hu, S.; Dyck, O.; Chen, H. P.; Hsiao, Y. C.; Hu, B.; Duscher, G.; Dadmun, M.; Khomami, B., The impact of selective solvents on the evolution of structure and function in solvent annealed organic photovoltaics. *RSC Advances* **2014**, *4*, 27931-27938.

[88] Tang, H. W.; Lu, G. H.; Li, L. G.; Li, J.; Wang, Y. Z.; Yang, X. N., Precise construction of PCBM aggregates for polymer solar cells via multi-step controlled solvent vapor annealing. *Journal of Materials Chemistry* **2010**, *20*, 683-688.

[89] Shi, G. Z.; Yuan, J. Y.; Huang, X. D.; Lu, Y.; Liu, Z. K.; Peng, J.; Ding, G. Q.; Shi, S. H.; Sun, J. X.; Lu, K. Y.; Wang, H. Q.; Ma, W. L., Combinative Effect of Additive and Thermal Annealing Processes Delivers High Efficiency All-Polymer Solar Cells. *Journal of Physical Chemistry C* **2015**, *119*, 25298-25306.

[90] Chirvase, D.; Parisi, J.; Hummelen, J. C.; Dyakonov, V., Influence of nanomorphology on the photovoltaic action of polymer-fullerene composites. *Nanotechnology* **2004**, *15*, 1317-1323.

[91] Klimov, E.; Li, W.; Yang, X.; Hoffmann, G. G.; Loos, J., Scanning near-field and confocal Raman microscopic investigation of P3HT-PCBM systems for solar cell applications. *Macromolecules* **2006**, *39*, 4493-4496.

[92] Vanlaeke, P.; Swinnen, A.; Haeldermans, I.; Vanhoyland, G.; Aernouts, T.; Cheyns, D.; Deibel, C.; D'Haen, J.; Heremans, P.; Poortmans, J.; Manca, J. V., P3HT/PCBM bulk heterojunction solar cells: Relation between morphology and electro-optical characteristics. *Solar Energy Materials and Solar Cells* **2006**, *90*, 2150-2158.

[93] Swinnen, A.; Haeldermans, I.; vande Ven, M.; D'Haen, J.; Vanhoyland, G.; Aresu, S.; D'Olieslaeger, M.; Manca, J., Tuning the dimensions of C-60-based needlelike crystals in blended thin films. *Advanced Functional Materials* **2006**, *16*, 760-765.

- [94] Guo, X.; Cui, C. H.; Zhang, M. J.; Huo, L. J.; Huang, Y.; Hou, J. H.; Li, Y., High efficiency polymer solar cells based on poly(3-hexylthiophene)/indene-C-70 bisadduct with solvent additive. *Energy & Environmental Science* **2012**, *5*, 7943-7949.
- [95] Yao, Y.; Hou, J. H.; Xu, Z.; Li, G.; Yang, Y., Effect of solvent mixture on the nanoscale phase separation in polymer solar cells. *Advanced Functional Materials* **2008**, *18*, 1783-1789.
- [96] Salim, T.; Wong, L. H.; Brauer, B.; Kukreja, R.; Foo, Y. L.; Bao, Z. N.; Lam, Y. M., Solvent additives and their effects on blend morphologies of bulk heterojunctions. *Journal of Materials Chemistry* **2011**, *21*, 242-250.
- [97] Cheng, P.; Li, Y. F.; Zhan, X. W., A DMF-assisted solution process boosts the efficiency in P3HT:PCBM solar cells up to 5.31%. *Nanotechnology* **2013**, *24*, 484008.
- [98] Das, S.; Keum, J. K.; Browning, J. F.; Gu, G.; Yang, B.; Dyck, O.; Do, C.; Chen, W.; Chen, J.; Ivanov, I. N.; Hong, K.; Rondinone, A. J.; Joshi, P. C.; Geohagan, D. B.; Duscher, G.; Xiao, K., Correlating high power conversion efficiency of PTB7:PC71BM inverted organic solar cells with nanoscale structures. *Nanoscale* **2015**, *7*, 15576-15583.
- [99] Murray, C. B.; Kagan, C. R.; Bawendi, M. G., Synthesis and characterization of monodisperse nanocrystals and close-packed nanocrystal assemblies. *Annual Review of Materials Science* **2000**, *30*, 545-610.
- [100] Gonfa, B. A.; Zhao, H. G.; Li, J. T.; Qiu, J. X.; Saidani, M.; Zhang, S. Q.; Izquierdo, R.; Wu, N. Q.; El Khakani, M. A.; Ma, D. L., Air-processed depleted bulk heterojunction solar cells based on PbS/CdS core-shell quantum dots and TiO₂ nanorod arrays. *Solar Energy Materials and Solar Cells* **2014**, *124*, 67-74.
- [101] Ren, F. Q.; Zhao, H. G.; Vetrone, F.; Ma, D. L., Microwave-assisted cation exchange toward synthesis of near-infrared emitting PbS/CdS core/shell quantum dots with significantly improved quantum yields through a uniform growth path. *Nanoscale* **2013**, *5*, 7800-7804.
- [102] Yuan, M. J.; Kemp, K. W.; Thon, S. M.; Kim, J. Y.; Chou, K. W.; Amassian, A.; Sargent, E. H., High-Performance Quantum-Dot Solids via Elemental Sulfur Synthesis. *Advanced Materials* **2014**, *26*, 3513-3519.
- [103] Cademartiri, L.; Montanari, E.; Calestani, G.; Migliori, A.; Guagliardi, A.; Ozin, G. A., Size-dependent extinction coefficients of PbS quantum dots. *Journal of the American Chemical Society* **2006**, *128*, 10337-10346.

- [104] Moreels, I.; Lambert, K.; Smeets, D.; De Muynck, D.; Nollet, T.; Martins, J. C.; Vanhaecke, F.; Vantomme, A.; Delerue, C.; Allan, G.; Hens, Z., Size-Dependent Optical Properties of Colloidal PbS Quantum Dots. *ACS Nano* **2009**, *3*, 3023-3030.
- [105] Tan, L.; Zhou, Y. F.; Ren, F. Q.; Benetti, D.; Yang, F.; Zhao, H. G.; Rosei, F.; Chaker, M.; Ma, D. L., Ultrasmall PbS quantum dots: a facile and greener synthetic route and their high performance in luminescent solar concentrators. *Journal of Materials Chemistry A* **2017**, *5*, 10250-10260.
- [106] Tan, L.; Yang, F.; Kim, M. R.; Li, P. D.; Gangadharan, D. T.; Margot, J.; Izquierdo, R.; Chaker, M.; Ma, D. L., Enhanced Long-term and Thermal Stability of Polymer Solar Cells in Air at High Humidity with the Formation of Unusual Quantum Dot Networks. *ACS Applied Materials & Interfaces* **2017**, *9*, 26257-26267.

RÉSUMÉ

L'introduction

Dans notre vie moderne, l'être humain dépend de plus en plus de l'électricité qui rend la vie de plus confortable et pratique. Ceci a entraîné une augmentation rapide de la consommation d'électricité dans le monde : selon les statistiques un accroissement de 60,9% (13,174 à 21,191 TeraWatt Hour) a été identifié entre 2000 et 2016.[1] Cependant, la production d'électricité repose principalement sur l'utilisation de combustibles fossiles tels que le charbon, le gaz naturel, *etc.* En plus de leur manque de réserves, le brûlage des combustibles fossiles est associé à l'émission de CO₂ et de SO₂ dans l'atmosphère, entraînant un réchauffement climatique et des pluies acides. Par conséquent, il est nécessaire et urgent de développer des ressources alternatives, propres et durables. Parmi les différents types de sources d'énergie renouvelables (comme l'énergie solaire, le vent, la biomasse, la géo-électricité, *etc.*), l'énergie solaire présente l'avantage d'une abondance quasi infinie et sa facilité d'utilisation est attrayante. La cellule solaire est un dispositif qui convertit directement l'énergie solaire en énergie électrique par effet photovoltaïque. Elle représente l'un des moyens les plus efficaces, les moins coûteux, les plus propres et les plus renouvelables pour fournir de l'électricité à l'être humain dans l'avenir, ce qui a attiré l'attention pour la recherche et les applications pratiques.

Classiquement, les technologies des cellules solaires peuvent être classées en trois générations. Les cellules solaires de première génération sont principalement à base de silicium (simple / multi-cristallines) et dominent toujours le marché en raison de leur efficacité de conversion de puissance (ECP) élevée (généralement: 15-20%) et de leur bonne stabilité[5,6] Cependant, nous avons besoin d'une technologie très coûteuse en coût et en énergie afin de pouvoir obtenir des

matériaux de silicium purs et sans défauts, ce qui entraîne des coûts de production élevés. La cellule solaire de deuxième génération (appelée aussi cellule solaire à couche mince) possède un coût de fabrication inférieur à celle de première génération (si on évite d'utiliser du silicium). Néanmoins, l'ECP est également diminuée. Par exemple, les cellules solaires amorphes basées sur le silicium sous forme de couche mince, le CuInGaSe_2 et le CdTe présentent des performances typiques de 10 à 15%. [7] En tenant compte du coût en énergie de leur fabrication, il est très peu probable que les cellules solaires de deuxième génération remplacent complètement celles de première génération.

En se basant sur les techniques de chimie des matériaux et d'ingénierie des dispositifs, la cellule solaire de troisième génération a été inventée il y a une décennie, dans le but de réduire le coût de fabrication et d'atteindre en même temps une ECP élevée. La cellule solaire de troisième génération peut être divisée en plusieurs catégories, selon les matériaux actifs utilisés dans leur fabrication, tels que des colorants, des points quantiques (PQ), des polymères conjugués, des perovskites et des mélanges de PQ et de polymères. [8-11] Les films actifs basés sur ces matériaux peuvent être fabriqués par une technique en solution (p. Ex. Processus de roulage à rouleau, *etc.*), qui est rentable et pratique pour la préparation d'un dispositif de grande surface. En outre, le traitement à haute température et sous vide couramment appliqué dans les cellules solaires de première et deuxième génération peut être évité ce qui réduit la consommation d'énergie lors du processus de fabrication. La performance de ces cellules solaires a été largement améliorée d'un modèle à l'autre en se concentrant principalement sur l'optimisation de la configuration des appareils et l'innovation du matérielle. À ce stade, chacune de ces cellules solaires présente ses propres avantages. Par exemple, la cellule solaire de perovskite tridimensionnelle (jonction unique) a montré la meilleure ECP de $\sim 22,1\%$ [12] sous

rayonnement solaire, tandis que l'appareil à base de PQ présente à la fois une stabilité dans l'air et une ECP raisonnable (11,28%) [13]. En revanche, l'amélioration des performances de ces cellules solaires et la réduction de leur coût nécessite davantage de temps pour pouvoir les rendre applicables.

Le dispositif concentrateur solaire luminescent (CSL), permettant de convertir des photons de large spectre en lumière concentrée dans une gamme spécifique, est un autre choix potentiel pour atteindre ces objectifs en réduisant l'utilisation de matériaux photovoltaïques coûteux. Il contient principalement un fluorophore (absorbeur / émetteur de lumière) et une matrice polymère agissant comme guide d'ondes des photons réémis. En comparaison aux dispositifs photovoltaïques, les CSL peuvent être produits à faible coût à cause de leurs matériaux composites et de leur procédé de fabrication. Ils permettent la mise en œuvre de technologies solaires à grande échelle en combinant le périphérique CSL (bon marché dans une large zone) avec un dispositif PV coûteux (dans une petite zone). Par conséquent, le coût total des technologies solaires peut être réduit sans diminuer l'ECP. Dans ce concept, le dispositif CSL doit être fabriqué avec un grand rapport entre la surface supérieure et celle du bord en vue du dispositif de la cellule solaire (Figure 1.9), afin de maximiser l'absorption et l'extraction de la lumière.

Dans un appareil CSL, le matériau fluorophore est le facteur le plus important pour la performance de l'appareil. Les progrès récents dans la synthèse des PQ inorganiques avec une photoluminescence à haut rendement quantique (RQ PL), des propriétés optiques ajustables selon leur taille, une bonne qualité chimique et une bonne photostabilité, en font d'excellents candidats pour les technologies CSL. Dans le cas des PQ de PbS par exemple, une RQ PL allant jusqu'à 90% a été atteinte lorsque le diamètre du PQ a été réduit à ~3,0 nm. De plus, le dopage et

le revêtement des ions métalliques ont été identifiés comme des stratégies efficaces pour séparer le spectre d'absorption et d'émission des PQ et améliorer leur stabilité. Selon les types de PQ, leur traitement peut résulter en une RQ PL raisonnable voire supérieure. Ces PQ incluent ZnSe dopé au Mn, CdSe / CdS, PbS / CdS, PbSe / PbS et ainsi de suite. [56-63]

Jusqu'à présent, des progrès substantiels ont été réalisés pour les cellules solaires de troisième génération, grâce au développement de la chimie des matériaux et de l'ingénierie des dispositifs. À l'exception des cellules solaires hybrides, l'ECP record pour chaque type de cellules solaires de troisième génération atteint le seuil du critère de commercialisation (environ ou plus de 15%). Pour les CSL, le développement de la chimie des matériaux fournit également plus de latitude pour concevoir de nouveaux dispositifs avec une stabilité de performance améliorée, une gamme d'utilisation de lumière élargie et une gamme de photons d'émission ajustable, par rapport au dispositif le plus répandu avec des colorants comme luminophores. [64-66] Autrement dit, la chimie des matériaux et l'ingénierie des dispositifs ont joué un rôle important dans le développement des technologies solaires, qui sont les deux voies de recherche pour continuer à améliorer les performances des technologies solaires vers une application réelle.

Objectif de la thèse

Partie I: Etudes sur la synthèse, la caractérisation, le mécanisme et l'application de PQs

Les PQ à base de PbS sont prometteurs pour diverses applications dans la gamme du proche infrarouge (PIR), en raison de leurs propriétés optiques qui relèvent principalement de leur méthode de synthèse. Parmi les diverses voies de synthèse, l'utilisation PbCl₂ et de S élémentaire comme précurseurs est un moyen facile, sûr et propre (environnement) de synthétiser des PQ de haute qualité. Cependant, cette méthode produit normalement des PQ possédant une gamme de

spectre d'absorption limité de 1200 à 1600 nm, ce qui correspond à une taille de 4,2 à 6,4 nm. [22] Selon ces travaux, bien que le trioctylphosphine ait été utilisé comme additif pour élargir la gamme accordable de des PQ synthétisés, le rendement du produit de la réaction est limité [21]. De plus, ces travaux ont principalement porté sur la synthèse de PQ de grande taille avec le premier pic excitonique à 1600 nm. Par conséquent, il est encore difficile de synthétiser des PQ de PbS de très petite taille. Comme nous le savons, les petits PQ possèdent généralement une RQ plus élevée, une meilleure constante optique et une meilleure stabilité que les grands. Par conséquent, nous avons comme objectif de réaliser la synthèse de très petits PQ de PbS par cette voie en introduisant un nouvel additif dans la réaction. En outre, les propriétés de surface des PQ seront examinées, ce qui est corrélé avec leurs performances optiques. Le mécanisme de réaction, la réaction de mise à l'échelle et l'application des PQ sont également étudiés.

Partie II: Amélioration de la performance des cellules solaires à base polymère (CSP)

Bien que des ECP supérieures à 10% aient été atteintes pour les CSP, les recherches sur la stabilité du dispositif et la fabrication via des "solvants verts" sont limitées, ce qui entrave leur commercialisation. Pour résoudre les problèmes de stabilité des dispositifs, deux facteurs principaux doivent être pris en compte [4]: 1) la dégradation chimique des polymères et des électrodes par réaction avec O_2 / H_2O ; 2) la dégradation physique due au changement de morphologie de la couche active. Sur la base de ces considérations, nous visons à améliorer la stabilité thermique et à long terme des CSP en insérant des points quantiques inorganiques dans la couche active en tant que stabilisant du film et en même temps pour empêcher O_2 / H_2O d'attaquer le polymère. La sensibilité des PQs à O_2/H_2O et l'effet morphologique sont deux points sur lesquels focaliser les travaux.

L'étude du remplacement de solvants halogénés par des "solvants verts" est une des autres futures directions de recherche sur les CSP. Pour obtenir des CSP avec des performances élevées à l'aide de «solvants verts», il est intéressant d'utiliser un mélange solvant / cosolvant ou solvant / additif pour préparer une solution dérivée de polymère/fullerène afin de contrôler la morphologie et la structure de la couche active. Dans ce cas, l'utilisation à la fois du solvant et de l'additif devraient permettre d'éviter l'utilisation de produits chimiques halogénés. A cette fin, nous cherchons à étudier les effets d'un nouvel additif (butylamine) vert sur la morphologie et la structure du film P3HT:PCBM. Après avoir compris l'effet de cet additif, il sera possible de combiner la couche avec des PQs pour fabriquer un polymère stable et à haute performance et obtenir des dispositifs photovoltaïques dérivés du fullerène à base de PQs en jouant à la fois sur les additifs et le ligand de surface des PQs.

Dans la première partie de notre travail, nous avons synthétisé des PQs de PbS absorbant dans le PIR de très petite taille de haute qualité en utilisant respectivement $PbCl_2$ ainsi que le soufre élémentaire (S) comme précurseur de plomb et de soufre, et en introduisant de la tributylphosphine (TBP) dans la réaction. Cette voie est beaucoup plus propre et aisée par rapport à la méthode utilisant du sulfate de bis (triméthylsilyle) toxique comme précurseur de soufre et qui exige le recours à une boîte à gants. Par la suite, le mécanisme de réaction de la synthèse de petits PQs et l'examen de leurs propriétés optiques, de leur morphologie, de la dispersité de leurs propriétés de surface et de leur application aux CSL ont été systématiquement étudiés. De manière détaillée, ce travail peut être divisé en trois sections: deux sont liées à la synthèse de PQs de PbS, et la dernière section concerne l'application aux CSL à base des PQs synthétisés.

Dans la section 1, la solution S-oléylamine (OLA) a été mélangée avec différentes concentrations de TBP avant son injection dans la solution préchauffée de PbCl₂-OLA. Pour la réaction sans TBP, la longueur d'onde d'absorption la plus courte des PQs de PbS est limitée à ~ 1056 nm. En augmentant le contenu de TBP à 40 µL, le premier pic d'absorption excitonique des PQs obtenus a été progressivement décalé vers le bleu à ~ 705 nm, en raison de la diminution de la taille des PQs (Figure R1- (a)). En augmentant encore la concentration de TBP, aucun PQ ne peut être collecté. Le facteur clé qui mène au pic d'absorption excitonique décalé vers le bleu et à la disparition finale des PQs quand la quantité de TBP augmente est la formation d'une forte liaison entre S et TBP. Le S-TBP aurait pu participer au processus de croissance de PQ, ce qui aurait empêché les PQs de continuer à grossir avec le TBP comme un type de ligand rigide à la surface. Cependant, le S-TBP stable n'a pas pu démarrer la réaction de nucléation avec le précurseur de plomb, puis il n'a pas réussi à former le PQ une fois que la concentration de S-OLA est devenue inférieure au point critique de la réaction de nucléation après avoir ajouté certaines quantités de TBP. En plus de diminuer la taille des PQs, le TBP en tant que ligands supplémentaires situés sur les sites S sur une surface PQ autre que celle des ligands OLA sur le site Pb aurait pu modifier la composition de la surface, la morphologie, la dispersion et la distribution des tailles et bénéficier de ces propriétés optiques. En bref, la synthèse assistée par TBP des PQ de PbS montre des distributions de taille étroite sans agrégation et démontre une PL RQ élevée dans la gamme de 60-90% (Figure R1-b), selon la taille du PQ. Tous ces résultats ont révélé que cette voie est applicable pour la synthèse de PQs de PbS de très petite taille et de haute qualité.

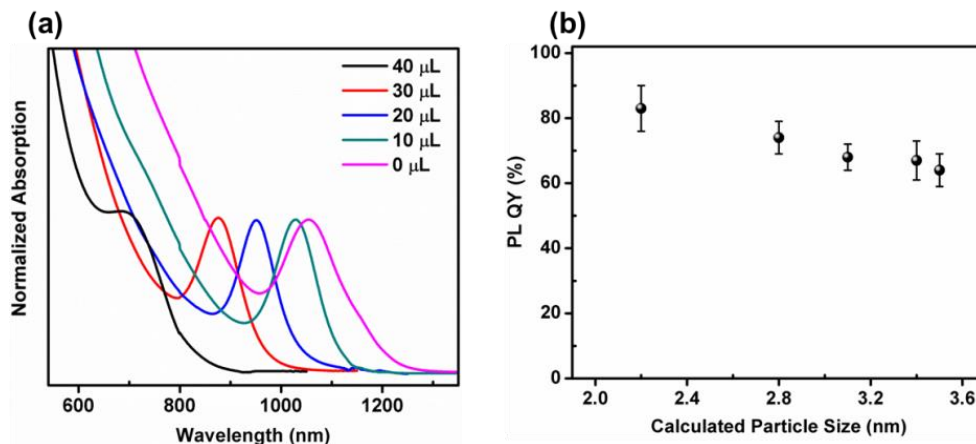


Figure R1. Les spectres d'absorption (a) et RQ PL (b) des PQ synthétisés sans TBP et par la voie TBP.

Contrairement à la section 1, un processus de synthèse par injection en deux étapes est utilisé dans la section 2. Par exemple, de grandes quantités de TBP ont d'abord été injectées dans le précurseur de plomb préchauffé, suivi de la solution de précurseur de soufre. (Figure R2) Sur la base de cette synthèse, le premier pic excitonique des QP de PbS peut être étendu à ~ 780 nm (correspondant au diamètre ~ 2,5 nm) par rapport à celui de la réaction sans TBP. Les PQ de PbS résultants montrent une excellente dispersité sans agrégation et une PL RQ d'environ 80%. De plus, le TBP s'est révélé aider la transformation de $\text{PbCl}_2\text{-OLA}$ (précurseur de plomb) en Pb(OH)Cl plus réactif sans changer sa structure propre, ce qui participe directement au processus de nucléation, conduisant à des PQs ultrapetits. Ceci indique que le Pb(OH)Cl peut être potentiellement appliqué pour la synthèse d'autres PQs de petite taille basés sur le plomb en tant que nouveau précurseur.

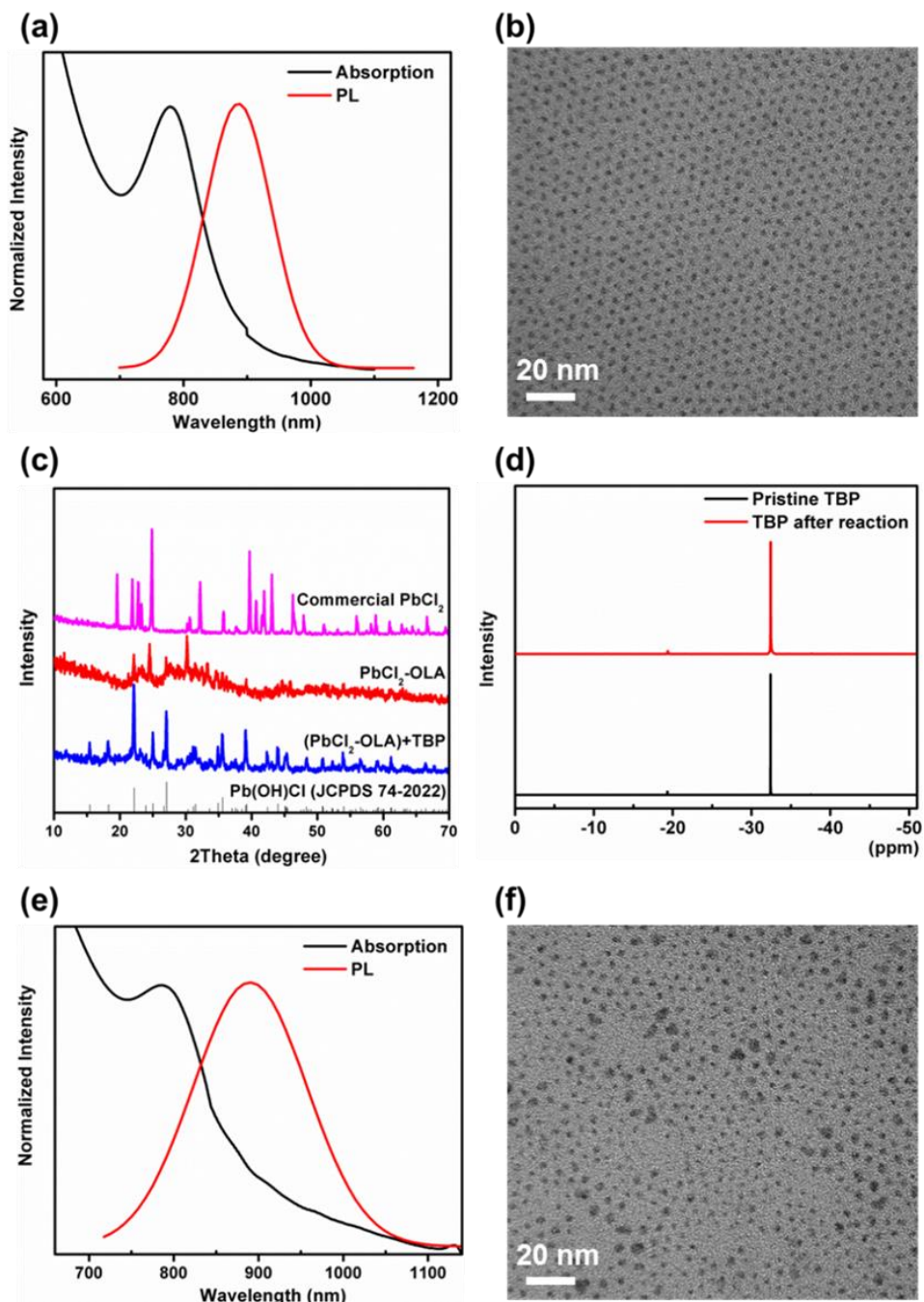


Figure R2. (A) Absorption et spectromètres PL des PQ PbS obtenus par injection en deux étapes de grandes quantités de TBP puis de S-OLA. (B) image TEM de PbS PQ obtenues par injection en deux étapes. (C) spectres XRD de précurseurs de plomb et de PbCl₂ commercial. (D) spectres de RMN 31P précédés à partir de la solution de DLP vierge et qu'après réaction. (E) Absorption et spectre PL et (f) image TEM de PbS PQ synthétisé par Pb(OH)Cl et S-OLA.

Dans la section 3, les CSL utilisant des PQs de PbS ou de PbS / CdS à mesure que le phosphore ont été fabriqués, et leur performance pour concentrer les photons de large bande dans une gamme spécifique ont également été testés, ce qui est principalement corrélé au RQ de leur PL, à la séparation d'absorption, au spectre de PL et à la photo-stabilité (Figure R3-(a, b)) Par conséquent, des PQs ultrapetits présentant les avantages des grands dans tous ces aspects sont prometteurs pour l'application aux CSL. En fait, le CSL a montré une efficacité optique d'environ 1,2% à un facteur géométrique de 50 (10 cm de longueur) en utilisant des PQs de 2,5 nm avec une coque de CdS de 0,1 nm, ce qui constitue un record par rapport à d'autres CSL basés sur des PQs. La figure R3-(c) montre que le dispositif CSL tel que préparé présente une très bonne transparence, ce qui est attribué aux PQ de PbS dispersés de manière homogène dans la matrice de polymère. En outre, une caméra dans le PIR avec un filtre passe-bas de 780 nm a été utilisée pour photographier un CSL excité par une source laser à 636 nm (Figure R3-(d, e)). Une grande partie des photons générés a été guidée avec succès au bord du dispositif CSL avec une luminosité comparable à la zone excitée sous éclairage direct, ce qui indique la bonne qualité du CSL. Des dispositifs utilisant des PQ de pur PbS et de PbS/CdS avec une coquille épaisse ont également été fabriqués et testés, et tous ont montré des résultats prometteurs. Au total, ces résultats ont confirmé la qualité de nos PQ synthétisés via la voie de synthèse impliquant le TBP.

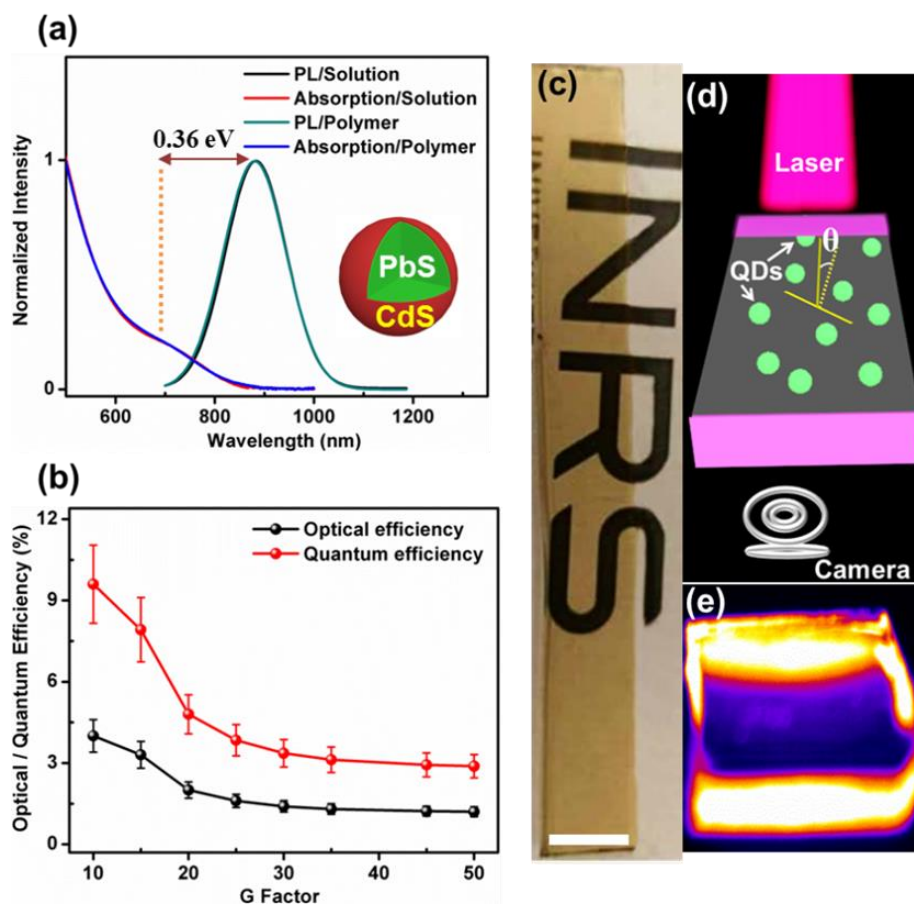


Figure R3. (A) Absorption et spectromètres PL de PbS / CdS en solution et une matrice polymère. (B) Efficacité optique / quantique des CSL intégrés de PbS / CdS PQ avec des facteurs G différents. (C) Photographie d'un appareil CSL (barre d'échelle: 1 cm). (D) Schéma de la configuration expérimentale pour exciter et prendre la photographie d'un dispositif CSL éclairant (l'angle de la région θ est le cône d'échappement de la lumière émettrice). (E) Photographie d'un CSL éclairé capturé par une caméra PI avec un filtre passe-longue de 780 nm.

Les résultats correspondants de cette section sont présentés dans la publication [105]:

[105] L. Tan, Y. Zhou, F. Ren, D. Benetti, F. Yang, H. Zhao, F. Rosei, M. Chaker and D. Ma, J. Mater. Chem. A, 2017, 10250-10260.

Dans la première section de la deuxième partie, nous nous sommes concentrés sur l'amélioration de la stabilité dans l'air des cellules solaires polymères (CSP) en utilisant un mélange de poly (3-hexylthiophène-2,5-diyle) (P3HT) et d'acide phényl-C₆₁-butyrique Méthyl ester (PCBM). Pour ce faire, des PQ inorganiques absorbant dans le PIR ont été sélectionnés comme stabilisateur, ce qui a permis en même temps de prolonger la photoréponse du dispositif dans la plage PIR. Compte tenu de la proximité des niveaux d'énergie de P3HT et de PCBM, un échantillon de PQ de PbS avec un diamètre ~3,3 nm a été sélectionné ce qui peut faciliter les processus de transfert de charge dans le dispositif. En outre, d'autres traitements de surface des PQ ont été effectués avant de les appliquer aux applications PV. Tout d'abord, une fine couche de CdS (0,1 nm) a été formée à la surface des PQs par une réaction d'échange de cations. Cela peut améliorer considérablement la stabilité de l'air des PQs eux-mêmes ainsi que leur stabilité thermique et photo, sans bloquer le transport du porteur de charge et changer leur diamètre global. Deuxièmement, une grande quantité de ligands d'oléate isolés par de longues chaînes sur la surface du PQ a été remplacée par de plus petits ligands atomiques de Cl⁻ en utilisant un traitement par des halogénures métalliques. Les ligands atomiques de Cl⁻ peuvent former une "coquille de ligand" dense sur la surface et atteindre les états piégés intermédiaires ce que ne peuvent faire les longs ligands, en raison de l'effet stérique. Par conséquent, la stabilité des PQs peut être encore améliorée et la densité des états piégés efficacement réduite, ce qui rend les PQs appropriés pour les applications PV. Il convient de mentionner que la manipulation du ligand de surface a également affecté la morphologie du film P3HT: PCBM: PQs, qui joue un rôle important dans la stabilité du dispositif. Comme en témoignent les images obtenues par microscopie atomique (MA), les PQs avec ligands Cl forment des réseaux continus de PQ dans le film P3HT: PCBM (Figure R4), tandis que ceux sans ligands Cl sont répartis de manière

homogène dans le film. Il est important de noter que les dispositifs CSP basés sur des films contenant des réseaux inhabituels de PQs présente une excellente stabilité à long terme sous une humidité relativement élevée (50-60%), tout en fournissant simultanément plus de 3% de ECP. (Figure R5-(a, b)) Après 30 jours de stockage sans encapsulation, environ 91% des ECP vierges peuvent être conservés. C'est une amélioration remarquable par rapport à celle des dispositifs basés sur le P3HT pur: film PCBM (~ 53%). Nous avons vérifié qu'une telle amélioration est due à l'absence d'agrégation des PCBM et à l'oxydation du cycle thiophène dans P3HT.

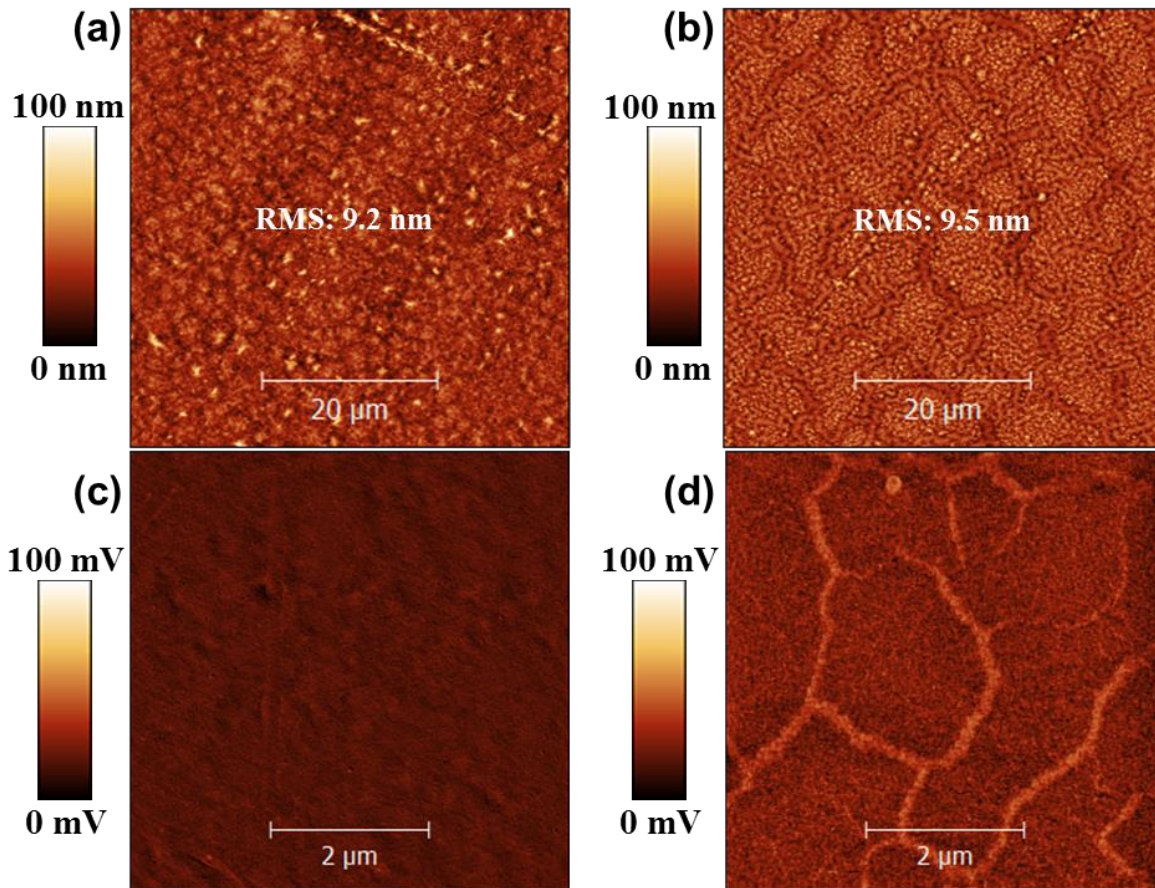


Figure R4. Images topographiques MA de P3HT: PCBM (a) et P3HT: PCBM: films halogénure-PbS/CdS (b) par balayage en mode ScanAsyst; Images de force latérale de P3HT: PCBM (c) et P3HT: PCBM: halde-PbS/CdS (d) films par balayage en mode contact.

En outre, la présence de réseaux de PQs améliore efficacement la stabilité thermique du dispositif tout en supprimant le stress thermique / l'oxydation sous une humidité relativement élevée. (Figure R5- (c, d)) Environ 60% des ECP vierges sont préservés après 12 h de traitement thermique à 85 °C, soit plus de deux fois que pour le dispositif sans réseaux de PQs. À notre connaissance, ce travail représente la première démonstration sans équivoque de la formation de réseaux de PQs dans la couche photoactive et de leur contribution à la stabilité des CSP. Cette stratégie est très prometteuse pour les autres CSP basés sur les fullerènes et ouvre une voie vers la réalisation de CSP avec une ECP élevée et une excellente stabilité.

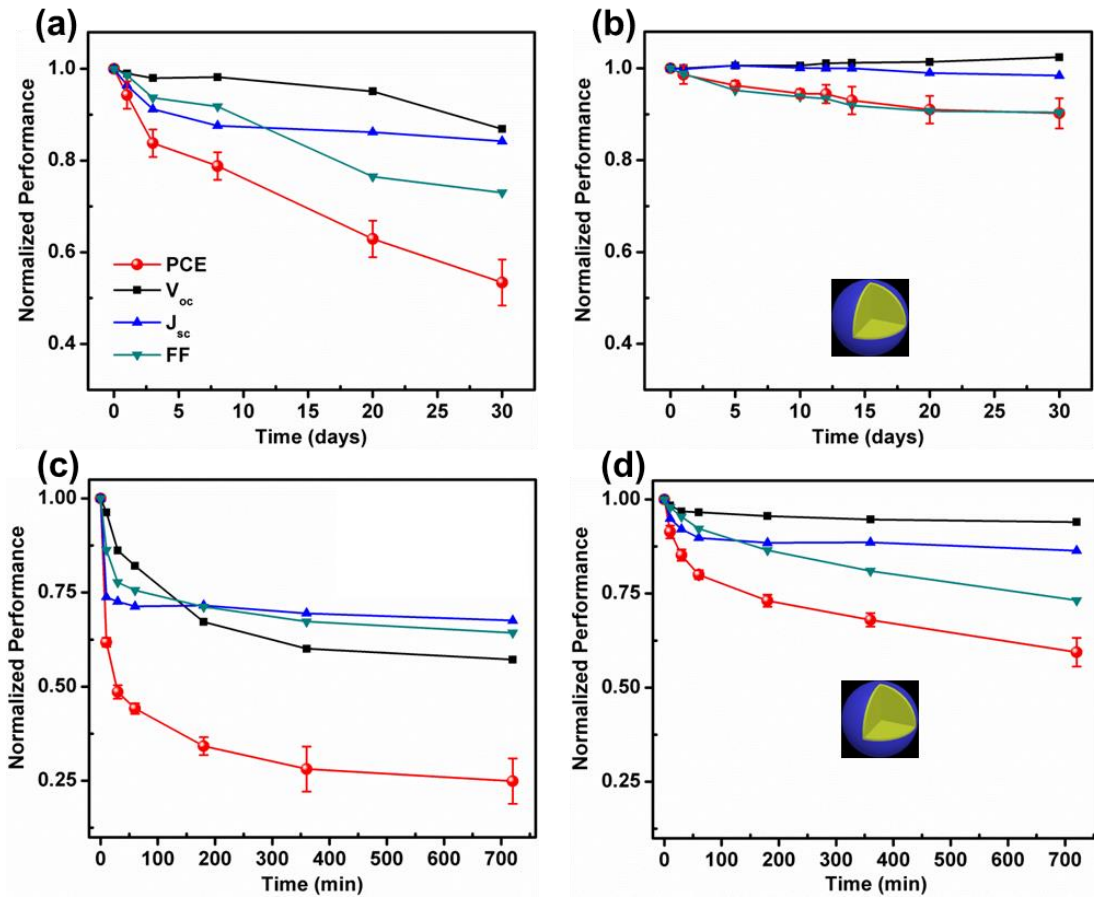


Figure R5. Performance de stabilité à long terme des dispositifs non encapsulés dans l'air sous haute humidité de 50 à 60% selon le film de P3HT: PCBM (a), P3HT: PCBM: halogénure-PbS / CdS (b), stabilité thermique des dispositifs basés sur P3HT: PCBM (c) et P3HT: PCBM: halogénure-PbS / CdS (d).

Les résultats correspondants de cette section sont présentés dans la publication [106]:

[106] L. Tan, F. Yang, M. R. Kim, P. Li, D. T. Gangadharan, J. Margot, R. Izquierdo, M. Chaker, and D. Ma, ACS Appl. Mater. Interfaces, 2017, 9, 26257–26267.

La seconde section de la deuxième partie était centrée sur la manipulation de la morphologie du mélange P3HT: PCBM, afin d'améliorer l'ECP des CSP. Le point essentiel est de contrôler la mobilité des composants du film lors du processus de fabrication. Pour ce faire, la butylamine a été introduite comme additif dans la solution P3HT: PCBM avec du dichlorobenzène comme solvant. Il a été confirmé que la butylamine présente une bonne solubilité pour PCBM, alors qu'elle est insoluble pour P3HT. (Figure R6) En conséquence, l'addition de butylamine améliore l'accumulation de P3HT dans la partie supérieure et PCBM dans la partie inférieure du film, cela qui conduit à un enrichissement en P3HT sur la surface supérieure et une abondance (déficit) de PCBM. Nous montrons le résultat sur la figure AFM et la caractérisation XPS dans la figure ci-dessous.

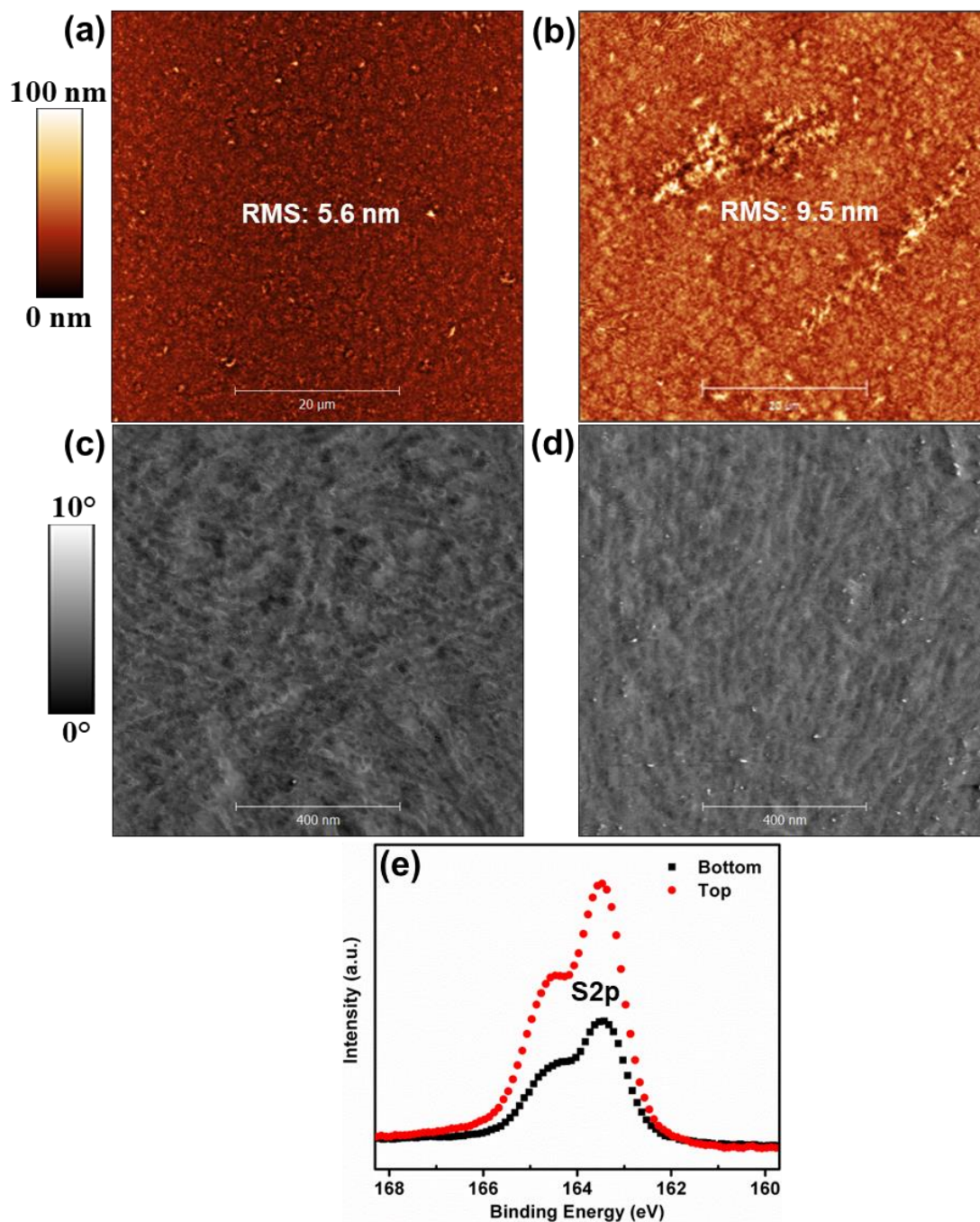


Figure R6. Les images topographiques des échantillons standard (a) et de la butylamine (b); Images en phase de l'échantillon (c) et de l'échantillon standard (d) de l'addition de butylamine; Spectres XPS S 2p à haute résolution de l'échantillon impliqué dans la butylamine sur les côtés supérieur (rouge) et inférieur (noir) (e).

Par la suite, des cellules solaires possédant la configuration ITO / ZnO / P3HT:PCBM / MoO₃ / Ag ont été fabriquées pour évaluer l'effet du changement de morphologie résultant de la butylamine sur la performance du dispositif. L'étude a révélé que le dispositif soumis à la butylamine présente un facteur de remplissage largement amélioré (FR: ~ 70%) et un meilleur ECP (~ 4,03%) que le dispositif standard (Figure R7- (a), Tableau 1), ce qui peut être attribué à l'amélioration du transport de charge dans le film P3HT:PCBM et à une sélectivité accrue des électrodes. Ces résultats fournissent un moyen d'optimiser l'épaisseur de la couche active afin d'absorber plus de lumière. En d'autres termes, il est possible d'améliorer encore l'ECP en augmentant le courant de court-circuit (J_{sc}) sans sacrifier de manière significative le FR, si une morphologie bicontinue préférable et interpenétrée existe, elle va pouvoir être observée dans un film épais. Par conséquent, nous avons fabriqué des dispositifs à base de film épais P3HT:PCBM en doublant la concentration des matériaux en solution. Les mesures courant-tension indiquent qu'une valeur de FR d'environ 63% est obtenue pour le dispositif affecté par la butylamine, ce qui est encore plus élevé que celui du dispositif standard basé sur un film relativement mince. Dans le même temps, J_{sc} a également été largement amélioré grâce à l'augmentation d'épaisseur de la couche active, ce qui a entraîné une ECP de 4,61% (figure R7- (b), tableau 1). Au final, ces résultats confirment bien que la butylamine en tant qu'additif peut efficacement améliorer les performances du dispositif P3HT:PCBM. En outre, l'avantage est l'absence d'ions malodorants et d'halogènes par rapport aux dithiols d'alcane et aux additifs halogènes couramment utilisés, ce qui rend cet additif prometteur pour l'application aux CSP.

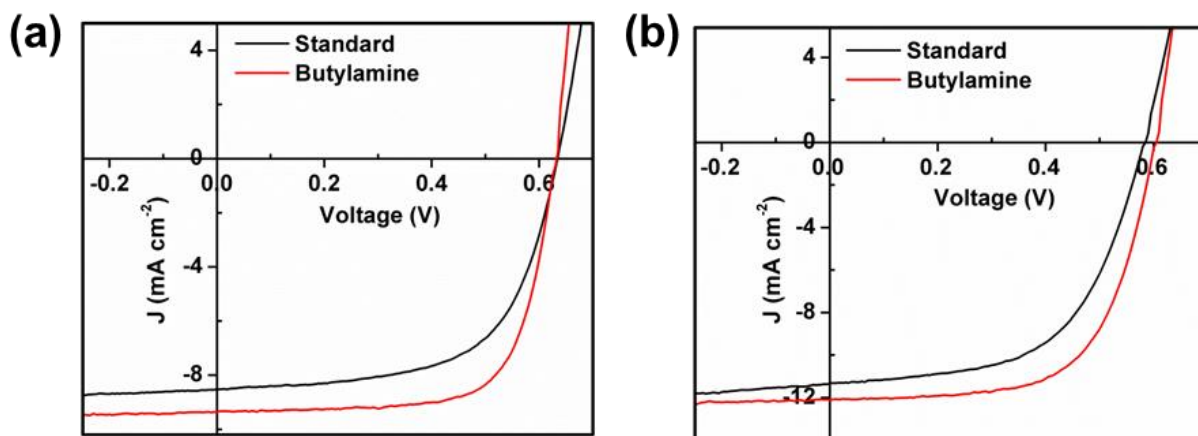


Figure R7. Courbes J-V des appareils photovoltaïques basés sur le film relatif (a) et épais (c) P3HT: PCBM.

Tableau 1. Paramètres photovoltaïques de dispositifs normaux et liés à la butylamine fabriqués à différentes concentrations de P3HT: PCBM.

Sample	P3HT+PCBM (mg ml ⁻¹)	Butylamine (vol %)	V _{oc} (V)	J _{sc} (mA cm ⁻²)	FR (%)	ECP (%)
Standard	24	0	0.63	8.62	62.4	3.37
Butylamine	24	3	0.63	9.21	69.9	4.03
Standard	48	0	0.58	11.52	56.51	3.79
Butylamine	48	6	0.61	12.02	63.34	4.61

Ce travail est décrit dans l'article ci-dessous:

Towards enhancing solar cell performance: an effective and “green” additive, L. Tan, P. Li, R. Izquierdo, M. Chaker and D. Ma. être soumis.